INVESTIGATING THE MECHANISMS UNDERLYING THE PATHOGENESIS OF ALOPECIA AREATA

Fatma Nagy Hamed

Submitted for the degree of Doctor of Philosophy

The University of Sheffield

Faculty of Medicine, Dentistry and Health

Department of Infection, Immunity and Cardiovascular Disease

Abstract

Alopecia areata (AA) is an autoimmune disease of hair follicles (HFs). The exact pathogenesis is unclear, but it is believed to result from T-cell mediated destruction of anagen HF due to the collapse of immune privilege (IP). In this study, we hypothesised that IP collapse is a consequence of an imbalance between regulatory T-cells (Treg) and inflammatory T-cells (Teff), which leads to the upregulation of the expression of Major Histocompatibility Complex (MHC) class I and class II molecules in HF, resulting in IFN-γ mediated attack of Teffs against HFs.

To test this hypothesis, we compared circulating lymphocytes from AA patients and healthy controls (HCs), using a flow-cytomteric technique. Data analysis showed that CD39 and HLA-DR+ suppressive Tregs were significantly reduced in AA patients indicating impaired function of circulating Tregs. This reduction was accompanied by a marked increase in the circulating Teff proportion, particularly in activated CD8+ T-cells (NKG2D+CD8+ T-cells), Th17 and Th1. These findings were supported by immunofluorescence (IF) staining of AA skin sections, showing a marked reduction of CD39+ Tregs in diseased HF. To further characterise circulating lymphocytes, next generation sequencing (NGS) was performed to analyse T-cell receptors chain β (TCRβ) in patients and controls. Sequencing analysis revealed a predominance of two unique TCRβ clones in the total lymphocyte population shared by many AA patients suggesting clonal expansion in response to a specific antigen during the disease process. Interestingly, database searches found that these clones have over 80% amino acid identity to TCR clones from CD8+ T-cells isolated from diseased subjects, and therefore could be pathogenic. There was also predominance of

two public TCR clones within the Treg population in the HC group; suggesting that these clones have a protective effect. Our data support the hypothesis of a potential Treg role in preventing AA as their impairment leads to Teff predominance in peripheral blood, therefore specific Treg clones might be used for therapeutic purposes.

Epigallocatechin gallate (EGCG) was proposed as a treatment to re-establish Teff-Treg balance, due to its inhibitory effect on the Teff signalling pathway (IFN-γ-JAK-STAT) and its stimulatory effect on Treg differentiation. EGCG showed an inhibitory effect on the JAK-STAT pathway by reducing the levels of p-STAT-1 protein *in vitro* in the Keratinocyte cell line (HaCat) and in the lymphocyte cell line (Jurkat); as well as *ex vivo* in PBMCs isolated from patient blood. The reduction of p-STAT1 was accompanied by a significant decrease in the expression of MHC class I and II genes in HaCat cells as well as a decrease in the proportion of activated CD8+ T-cells and Th1 cells in peripheral blood of AA patients. This data would support the development of a clinical pilot study to measure the efficacy of EGCG in enhancing hair re-growth in AA patients.

To sum up, it has been demonstrated that Teff-Treg imbalance could have a role in IP collapse. Our data brings a new insight into the current understanding of the immunological basis for AA pathogenesis and could be used to facilitate the development of an effective therapeutic intervention.

Acknowledgment

First and foremost, I would like to thank God Almighty for giving me the strength, knowledge and opportunity to undertake this research study and complete it satisfactorily. I would like to express my sincere gratitude to my supervisor Dr. Rachid Tazi-Ahnini for his continuous support throughout my PhD, for his patience, motivation and guidance. I sincerely thank Dr.Andrew McDonagh for sparing his valuable time reading this work and being around whenever I approached him and showing me the way ahead. I have great pleasure in expressing my gratitude to my colleagues at IICD being there at times when I required motivation and propelling me on the course of this research with special thanks goes to Dr. Thomas Lovewell and my friend Sarah Almaghrabi. Her support, encouragement and credible ideas have been great contributors in the completion of the thesis. I would also like to express my gratitude to technicians at flowcyomtery, histology core facility and SiTran, who have been so helpful and cooperative in giving their support whenever needed. I express my sincere thanks to my beloved my parents, without their loving upbringing and nurturing; I would not have been where I am today. Thanks to my brothers and sisters, your prayers and support was what sustained me this far. At the end, I would like to express tremendous appreciation to my beloved husband for his continuous and unfailing love, support and understanding during my pursuit of PhD degree that made the completion of this thesis possible. You were always around at times I thought that it is impossible to continue. Words would never say how grateful I am to my cherished little girls Mayar and Menatallah for abiding my ignorance and the patience they showed during hard times throughout my PhD.

This thesis is dedicated to my beloved husband (Eiman)

& my dear parents (Nagy and Gharieba)

Table of Contents

List of Figures

List of Tables

List of abbreviations

AA	Alopecia Areata
APM	Arrector Pili Muscle
AT	Alopecia Totalise
AU	Alopecia Universalis
CDR3	Complementarity-Determining Regions
DC	Dendritic Cells
EAE	Experimental Autoimmune Encephalomyelitis
HC	Healthy Control
HF	Hair follicle
ICAM	Intercellular Adhesion Molecule
ICOS	Inducible T-cells Co-stimulatory molecules
IDO	Indoleamine 2,3-Dioxygenase
IFN	Interferon
IGF	Insulin Like Growth Factor
IL	Interleukin
IP	Immune Privilege
IRF-1	Interferon Regulatory Factor-1
JAK	Janus Kinase
IRS	Inner Root Sheath
LC	Langerhans Cells
MHC	Major Histo-Compatibility molecules
MW	Molecular weight
NGS	Next generation sequencing
NK	Natural Killer Cells
ORS	Outer Root Sheath
RT	Room Temperature
TCR	T-Cell Receptor
Teff	Effector (inflammatory) T-cells
TGF	Transforming Growth Factor
Th	T Helper cells
TNF	Tumour Necrosis Factor
Treg	Regulatory T-cells
SCID	Severe combined immune deficiency

Chapter 1 . Introduction

1.1 Hair follicle structure and cycle

The hair follicle (HF) is one of the skin appendages with many important functions, which range from biological processes such as thermoregulation, wound healing and sensory function to social function where hair is an important part of an individual's self-image. HFs grow in cycles; anagen (growth phase), catagen (regression phase) and telogen (rest phase) before the hair is shed and the anagen phase starts again. Alopecia areata (AA) is non-scarring hair loss resulting from T-cell attack on anagen HF causing damage and hair cycle arrest with substantial changes in the HF histology. Therefore, an overview of HF structure, histology and growth cycle is crucial to the understanding of AA pathogenesis.

1.1.1 Anatomy, histology and function

The hair can be defined as a slender, thread-like outgrowth from a follicle in the skin of mammals (Paus et al., 1999b). The HF is located in the dermis and consists of concentric layers of keratinocytes, which are organised in three compartments in the horizontal cross section (Figure1.1) including the hair shaft, the inner root sheath (IRS), which is composed of the cuticle, Huxley and Henle layers, and the outer root sheath (ORS) (Stenn and Paus, 2001). The hair bulb is a reservoir of rapidly dividing epithelial cells, which are responsible for the formation of hair shaft and IRS (Paus et al., 1999b). Heterogeneous adult stem cells are housed in the bulge area, which is encircled by the arrector pili muscle (APM), which offers a specialised microenvironment or niche (Wang et al.,

2012b). Stem cells in the bulge have a central role in hair follicle cycling and skin wound healing (Ito et al., 2005, Ansell et al., 2010).

Longitudinally, the HF is divided into three zones (Figure1.1) including the lower zone (bulb and suprabulb), also called the lower cycling region, which extends from the base to the APM insertion. The middle zone (isthmus) extends from the muscle insertion to the sebaceous gland opening. The upper zone (infundibulum) extends from the opening of the sebaceous gland to the hair orifice (Sperling, 1991).

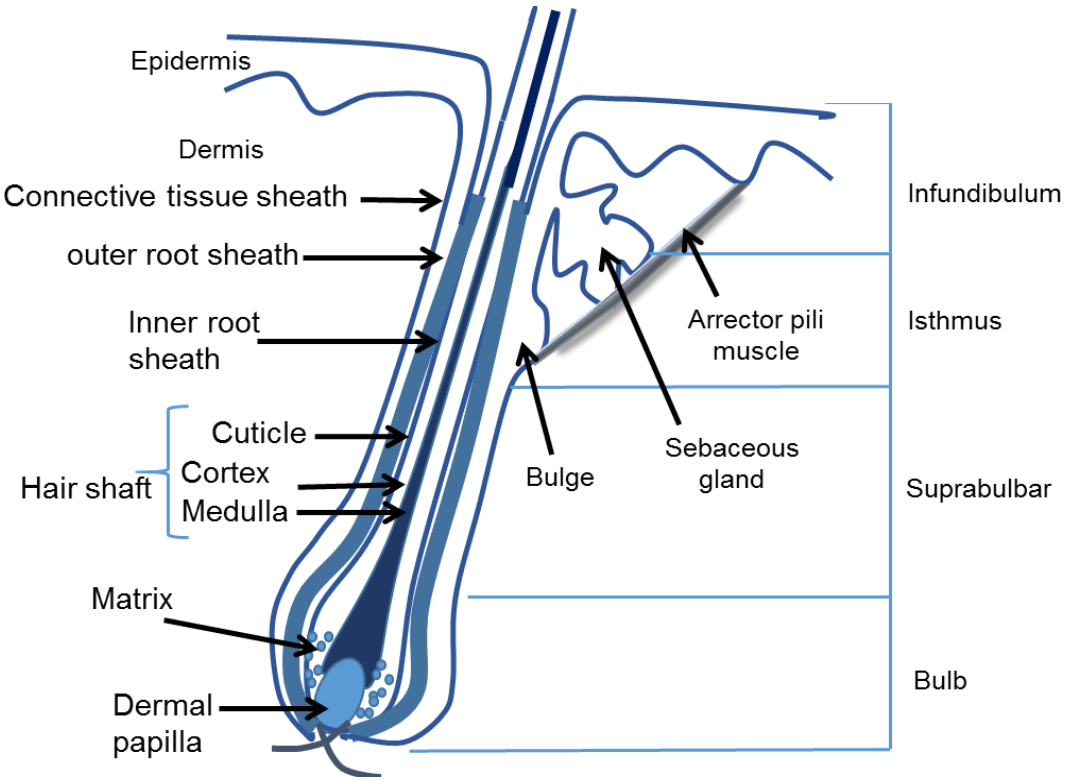

Figure 1.1. Anagen hair follicle structure.

The anagen hair follicle is composed of concentric layers of keratinocytes arranged horizontally as outer root sheet (ORS), inner root sheet (IRS) and shaft, which has three layers cuticle, cortex and medulla (from out to in). The ORS is surrounded by connective tissue sheath (CTS) containing hyaline membrane, fibroblasts and collagen bundles. The three main anatomical zones longitudinally are: Lower (suprabulbar and bulb), middle (isthmus) and upper (infundibulum). The bulb region contains the dermal papilla surrounded by matrix. The isthmus and infundibulum region are associated with hair appendages, namely, sebaceous gland and arrector pili muscle.

Histologically, keratinocytes are the main cell population forming the HF while melanocytes are interspersed among the bulb matrix cells and give rise to hair pigmentation. The ORS contains melanocytes, Langerhans' cells (dendritic antigen-presenting cells), and Merkel cells (specialised neurosecretory cells) (Paus et al., 1999b). Outside the ORS, there is a connective tissue sheath (CTS) composed of a thin basal lamina, elongated fibroblasts and collagen bundles running in different direction to the ORS (Ito and Sato, 1990). The dermal papilla, which is composed of specialised fibroblasts located at the base of HF, plays a central role in hair growth and cycling (Matsuzaki and Yoshizato, 1998).

In addition to its role in hair growth, the HF has other functions. For example, the HF is a reservoir of Langerhans cells (LCs) that repopulate the epidermis after injury (Gilliam et al., 1998). LCs play the role of the sensor arm of skin immune system by detecting any skin intruder and activating the effector arm including perifollicular macrophages, mast cells and other immunocytes (Jimbow et al., 1969). However, the lower part of the HF has a very low number of natural killer cells (NK) and LCs giving a complex immunological profile to HF, which will be discussed in details in section 1.3.

1.1.2 Hair cycle

The hair follicle is a dynamic mini-organ, which undergoes cyclic changes (Figure 1.2) from the active growth phase (anagen) through the regression phase (catagen) and the quiescent phase (telogen) (Dry, 1926), to eventual shedding (exogen) (Stenn and Paus, 2001, Milner et al., 2002). Transition between these phases is controlled by many local and systemic factors, such as cytokines and hormones, as reviewed by Stenn and Paus (2001).

Anagen

The active growth phase of the hair cycle extends from the termination of telogen to the beginning of catagen (Muller-Rover et al., 2001). Anagen involves six stages that recapitulate the HF morphogenesis to some extent. In stage I, epithelial cells at the base of the telogen follicle (secondary hair germ) show mitotic activity (Oshima et al., 2001). In stage II, the hair germ cells grow downward into the dermis and enclose the dermal papilla. At this stage, the IRS starts to appear as keratinised plates overlying the matrix. At stage III, the cortex starts to differentiate as a conical structure inside the IRS slender and the hair follicle elongates further in stage IV (Oshima et al., 2001, Muller-Rover et al., 2001). Stage V is characterised by commencing melanogenesis and keratinization of the cortex, which in turn penetrates the IRS at the level of the sebaceous gland during stage VI. Finally, stage VI shows the fully developed hair as depicted in Figure 1.1. As suggested by observational studies, AA is primarily a disease of anagen follicles where the inflammatory infiltrate is concentrated on anagen hair bulbs (Messenger et al., 1986), in addition to observing high levels of autoantibodies directed to multiple structures of anagen hair (Madani and Shapiro, 2000) This predominance of AA in anagen stage has been attributed by some researchers to the melanogenesis that takes place in this phase, and melanocyte-associated proteins are believed to be a possible target of the autoimmune attack (Paus et al., 1993).

In addition to the morphological characterisation of the anagen HF with the fully concentric layers IRS, ORS and hair shaft, immunohistochemical staining of anagen HF is characterised by positive staining for TFG-β receptors 1 and 2 (Muller-Rover et al., 2001) and higher levels of telomerase activity in the bulb area compared to catagen HF indicating active mitosis in this phase

(Ramirez et al., 1997). Many morphogenic gene families regulate HF cycling, such as homeobox, sonic hedgehog, fibroblast growth factor (FGF) and transforming growth factor beta (TGF-β) gene families providing another indication of the HF cycle as a highly regulated process (Stenn and Paus, 2001), particularly during the anagen-catagen transition. For example, fibroblast growth factor 5 (FGF5) expression is normally increased in late anagen exerting a catagen inducing effect (Hébert et al., 1994) while insulin like growth factor 1 (IGF1) induces anagen prolongation and catagen inhibition (Philpott et al., 1994).

Catagen

At this stage of the hair cycle, the growth phase ends and a highly controlled process of apoptosis starts (Stenn and Paus, 2001). The first sign of regression is detachment of dermal papilla fibroblasts from the basement membrane (Figure 1.2) (Parakkal, 1970). This is followed by papilla shrinking, which eventually results in the release of papilla from the bulb. The lower cycling portion of the follicle ceases growth and cell division, which is accompanied by massive apoptosis in the bulb matrix causing shrinkage and involution of the lower two thirds of the follicle to form the epithelial column (Parakkal, 1970, Stenn and Paus, 2001).

Immunostaining of this phase is characterised by a high positive TUNEL score indicating massive apoptosis has taken place (Muller-Rover et al., 2001). Moreover, there is perifollicular infiltration of mast cells and mononuclear inflammatory cells, particularly macrophages, along with increased expression of major histocompatibility molecules class I and II (MHC I and II) (Westgate et al., 1991).

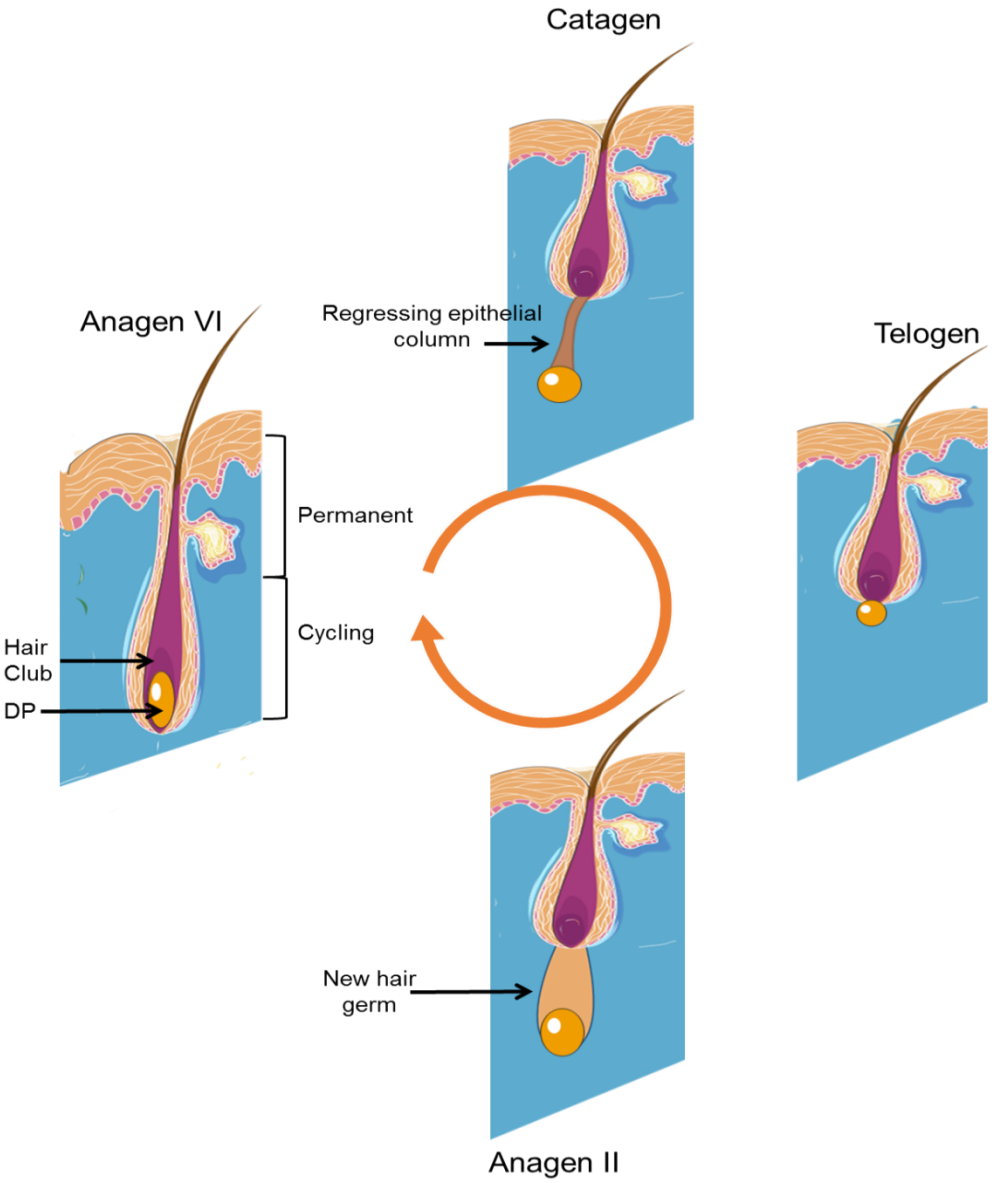

Figure 1.2. Representation of the hair growth cycle.
In the hair cycle, the DP shrinks to form an epithelial column in the catagen phase. Telogen is the resting stage followed by renewed anagen, starting by formation of new hair germ and the events of the HF morphogenesis ensues to give rise to mature HF in anagen VI. Figure was created using Servier medical art.

Telogen

This is the resting phase where follicles lie in the dermis as an epithelial sac overlying the dermal papilla, which appears as a condensed cluster of fibroblasts (Stenn and Paus, 2001). Inside the epithelial sac, the club hair is seen as a brush-like base attached to ORS. The hair germ, which is a specified region

of the epithelial sac at the very base of hair club, is composed of a cluster of small, densely packed cells that are developed from the stem cells of the bulge (Stenn and Paus, 2001). This phase is characterised by low level of DNA synthesis in telogen epithelial cells (Silver and Chase, 1970) and an absence of anagen HF protein synthesis, such as trichohyalin and the hair cortical keratins (Milner et al., 2002).

Hair cycle changes in AA

AA is likely to target anagen HF, and the pathology causes range of abnormalities from miniaturizing the anagen hair to a complete cessation of hair cycling according the severity of the disease. In the acute phase, infiltration of inflammatory cells interrupts the production of healthy hair fibre minimizing the hair size and affecting its integrity resulting in a breakage of hair fibres. Miniaturised or dystrophic anagen follicles are seen histologically which may continue producing an abnormal hair fibre (Whiting, 1987). In more severe cases, HF may be follow a truncated cycle with rapid progression from anagen to telogen resulting in the state known as nanogen, which has mixed features of anagen, telogen and catagen (Whiting, 2001). Another abnormality of hair cycle observed in AA is the high number of HFs pushed into the catagen phase (about 50% of HFs) as the disease progresses, and they subsequently proceed to telogen ending in hair shedding. In chronic disease, the hair cycle seems to be distorted with more HF pushed into a prolonged telogen phase and some can be forced into telogen permanently and no new hair fibres are produced, and during that stage the inflammatory infiltrate decreases markedly (Whiting, 2003).

1.2 Alopecia areata

Alopecia areata (AA) is an autoimmune disease of the hair and nails resulting in non-cicatricial hair loss (Gilhar and Krueger, 1987, McDonagh and

Messenger, 1996, Gilhar et al., 1998). It can be a psychologically devastating disease often with no effective therapy available. An inadequate understanding of the disease pathogenesis is the main restriction of the therapeutics targeting of this disease. It is believed to be caused by T-cell mediated destruction of anagen HF associated with of the collapse of immune privilege (Safavi et al., 1995, Gilhar and Kalish, 2006).

1.2.1 Features

AA presents typically with a well-demarcated patch of complete hair loss with no sign of inflammation (Gilhar et al., 2007). Characteristic short hairs tapered toward their base (exclamation mark hairs) may be present at the edge of lesional skin, and re-growing white hairs are seen in some cases (Tobin et al., 1990).

Based on the extent of hair loss, AA is classified clinically into three main patterns: patchy AA with partial scalp hair loss appears as either single or many discrete areas of total hair loss that may coalesce to form larger patches (Figure 1.3.A); alopecia totalis (AT), which is characterised by total loss of scalp hair (Figure 1.3.B); and alopecia universalis (AU) with 100% loss of scalp and body hair. Other less common patterns of AA have been reported; for example, ophiasis and ophiasis inversus, which is characterised by band-like hair loss in the parieto-temporo-occipital and frontal temporo-occipital region of the scalp respectively (Figure 1.3.C and D) (Alkhalifah et al., 2010a). Nail abnormalities such as trachyonychia, longitudinal ridging and pitting, thinning or thickening can be observed in AA patients. Their reported incidence in association with AA ranges from 10% to 60% (Madani and Shapiro, 2000).

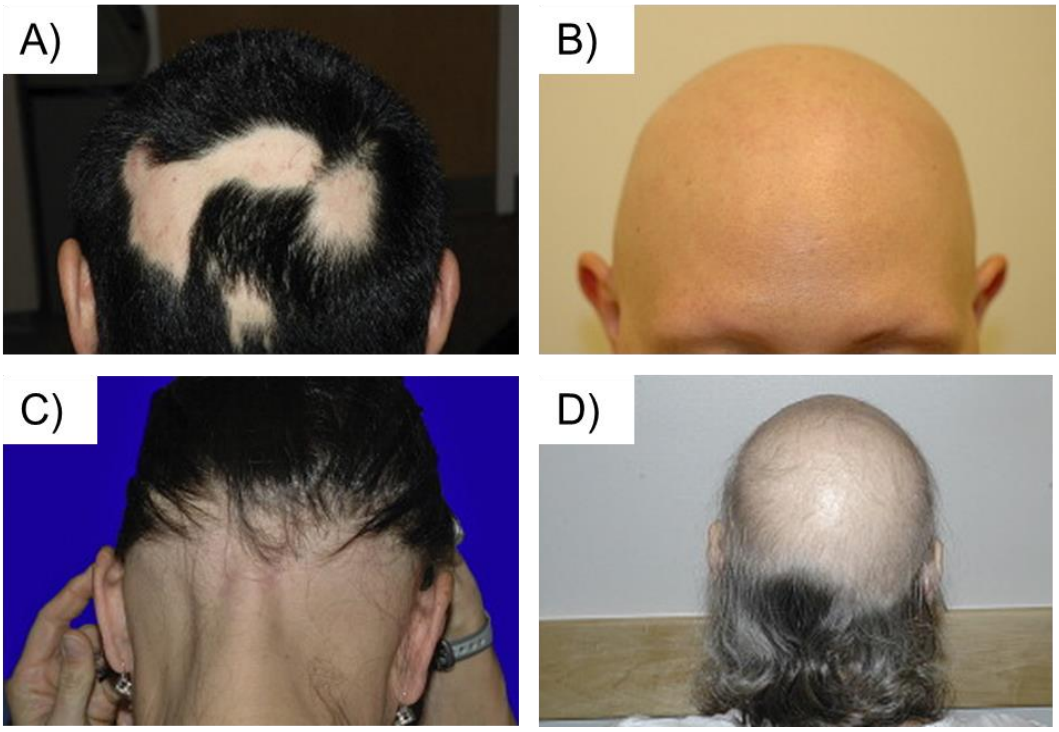

Figure 1.3. Clinical types of AA.
A) Patchy AA with well-demarcated patches of total hair loss. B) AA totalis with 100% scalp hair loss. C) Ophiasis pattern of AA and D) Ophiasis inversus pattern of AA. The images were adopted from Alkhalifah et al. 2010 with permission.

The main histopathologic feature of AA is the dense intra-follicular and peri-follicular lymphocytic infiltrate giving rise to what is called the “swarm of bees” appearance in skin biopsies particularly in the acute stage of the disease (Todes-Taylor et al., 1984, Perret et al., 1984). The infiltrate is mainly T-lymphocytes both CD4+ and CD8+, in addition to LCs and macrophages (Zhang and Oliver, 1994). The expression of inflammatory markers, such as Intercellular Adhesion Molecule 1 (ICAM) (Zhang and Oliver, 1994) and MHC class I and II, is elevated in lesional skin (Messenger and Bleehen, 1985, Bröcker et al., 1987). Another characteristic is a reduced number of anagen HFs and more telogen and catagen HFs found in the affected areas, in addition to an increased number

of miniaturised hairs and decreased terminal hairs in chronic cases (Peckham et al., 2011).

1.2.2 Epidemiology

AA affects about 0.1% of the general population (Alzolibani, 2011) with lifetime risk approximately 1.7% -2.1% making it one of the most common autoimmune diseases (Safavi et al., 1995, Mirzoyev et al., 2014). In the UK, it affects 0.15% of the population (Delamere et al., 2008). Male and female individuals are equally affected (Safavi et al., 1995) with peak incidence between 20-25 years of age and higher incidence is seen in patients with a family history of the condition (Alzolibani, 2011). Although AA remains patchy in most cases and spontaneous remission is expected in a considerable proportion of cases, 7% -25% progress to AT and AU according to data from tertiary and secondary centres (Walker and Rothman, 1950, Safavi et al., 1995). The percentage of cases progressing to more severe types reaches up to 43% in children (Tosti et al., 2006), and the cure rate of AT/AU is very limited. Although these studies have limitations, mainly in terms of the number of patients involved, variability of the figures and lack of up to date studies, these figures, especially in children, are striking because the cure rate from AT and AU is unfavourable with only 10% of these patients experiencing full hair regrowth (Safavi et al., 1995).

The morbidity of AA is not attributed to hair loss alone, but also to its psychologically distressing nature as most of the patients experience psychological problems in the longer term (Aghaei et al., 2014). The cosmetic impact of hair loss affects self-confidence negatively with consequent psychiatric comorbidity, such as anxiety, social phobia, and paranoid disorder (Colón et al., 1991, Chu et al., 2012), and AA patients have a higher incidence of depression

and neuroticism (Aghaei et al., 2014). Furthermore, AA has a negative impact on the quality of life (Dubois et al., 2010). Based on a systemic review performed in 2016, AA patients experience significant impairment in health-related quality of life, and mainly in the area of mental health (Rencz et al., 2016).

1.2.3 Treatment

To date, there is no FDA approved treatment of AA. This is mainly because none of the available treatments can alter the natural history of the disease nor do they have a significant long-term effect (Messenger et al., 2012, Alkhalifah et al., 2010b).

The drugs that are the most commonly used in clinical practice (Table 1.1) have many limitations. In addition to their adverse effects, the relapse rate after treatment is high. For example, after systemic corticosteroid therapy, the relapse rate has been observed in 25% of patients within three months (Winter et al., 1976), which does not outweigh the side effects. The relapse rate is even higher with topical immunotherapy estimated up to 60% with diphencyprone (Wiseman et al., 2001). Furthermore, the response rate is highly variable between the studies. For instance, the response rate to topical sensitizer Diphencyprone (DPCP) was 15% in one study and as high as 85% in another (Happle et al., 1983, Orecchia and Rabbiosi, 1985). Most importantly, AT and AU are highly resistant to all the current treatments with the best response rate of 20% (Alkhalifah et al., 2010b).

Many biological drugs have either been proposed or trialled in AA patients, however, the results were not in general encouraging. For example, anti-TNF–α antibodies such as alefacept or etanercept (Strober et al., 2009, Strober et al., 2005), and efalizumab, a CD11A antagonist and inhibitor of T-cell activation, were shown to be ineffective in AA (Price et al., 2008). IFN-γ is a main player in

AA pathogenesis where it mediates its inflammatory effect via the JAK-STAT pathway. Targeting the JAK-STAT pathway by a chemical inhibitor has shown promising results in AA. Three JAK inhibitors have been used in AA including ruxolitinib, tofacitinib and baricitinib. Oral administration of 20 mg twice daily ruxolitinib resulted in a complete hair regrowth in 9 patients in a small pilot study of 12 AA patients after 3-5 months of therapy (Xing et al., 2014). Tofacitinib is a JAK 1 and 3 inhibitor that was initially approved for the treatment of rheumatoid arthritis (Liu et al., 2016) and used in clinical trials for psoriasis (Hsu and Armstrong, 2014). Daily administration of 10 mg of Tofacitinib for at least 4 months in a cohort of 90 AA patients showed >50% improvement in 42% of the patients (Liu et al., 2016). Treatment with baricitinib, a JAK1 and 2 inhibitor was reported in 1 patient, showing full scalp hair regrowth after 9 months (Jabbari et al., 2015). JAK inhibitors are efficient but they are known for relapse that occurred within a few weeks after cessation of treatment (Kennedy Crispin et al., 2016).

JAK inhibitors have a range of potential side-effects (Shreberk-Hassidim et al., 2017). For instance, ruxolitinib is a broad JAK (1 and 2) inhibitor with potential to modulate the signalling pathway of cytokines including IL-17, IL-21, IL-22 (Fridman et al., 2010), IL-6 and TNF (Verstovsek et al., 2010). Ruxolitinib adverse-effects include reactivation of tuberculosis, thrombocytopenia, anaemia and there is a risk of other unknown long-term adverse-effects (Tefferi and Pardanani, 2011). Furthermore, JAK inhibitors are relatively of high cost; Ruxolitinib cost is £3600 for a 60-tablet pack of 15 mg or 20 mg tablets excluding the VAT, according to British National Formulary [BNF] online, which corresponds to approximately £43,200 per patient per annum.

Table 1-1. Drugs most commonly used in treatment of AA as reviewed by Messenger et al. (2012) with their mechanism of action and side effects.

Treatment	Mechanism of action	Side-effects
Intralesional/Topical Corticosteroids	Anti-inflammatory	Topical atrophy, telangiectasia and folliculitis
Systemic corticosteroids	Anti-inflammatory	Hypertension, obesity, Acne impaired adrenocorticotropic hormone (ACTH)
Contact immunotherapy	Topical sensitizer, inducing lymphocyte apoptosis	Bullous/vesicular reaction, urticaria, cervical lymphadenopathy, facial and scalp oedema
Minoxidil	Vasodilation, angiogenesis, proliferation and opening k^+ channels	Contact dermatitis and hypertrichosis
Anthralin	Inhibitory effect on the cytokines TFG–α	Irritation and folliculitis

1.2.4 Aetiology and pathogenesis

Many components are believed to play a role in the pathogenesis of AA, such as genetic factors, which mostly reflect immunological involvement, atopy, trauma, infection and stress (McDonagh and Messenger, 1996).

Genetic factors

The role of genetic factors in AA pathogenesis was first suggested due to the increased frequency of the disease in individuals with a positive family history varying between 10-42% in different studies (Duvic et al., 2001, Colombe et al., 1995, Shellow et al., 1992, Alzolibani, 2011), and a concordance rate in monozygotic twins of about 55% (Alzolibani, 2011) . In addition, a higher incidence of the disease compared to the general population has been seen in association with genetic disorders, such as Down syndrome and autoimmune poly-glandular syndrome 1 (APS1) at about 8.8% (Carter and Jegasothy, 1976) and 30% (Tazi-Ahnini et al., 2002).

A number of genes encoding for immune system components have been found to be involved in AA pathogenesis (Table 1.2). Association studies have

revealed well-established genetic association of AA to the MHC/ Human Leukocyte Antigen (HLA) complex, a region located at chromosome 6 p21.3 region (Gilhar et al., 2007). Many studies have supported the links of AA with HLA- class II loci namely HLA-DR and HLA-DQB (Colombe et al., 1995, Colombe et al., 1999, de Andrade et al., 1999, Duvic et al., 1991, Megiorni et al., 2011). HLA-DQB1*03 is a general common susceptibility allele for AA in many populations (Colombe et al., 1999, Gilhar et al., 2007). Strikingly, Colombe et al. (1999) found HLA-DQB1*03 in 80% of all AA patients enrolled in the study while DRB1*0401 (DR4) and DQB1*0301(DQ7) was detected only in patients with AT/AU, which implicates the role of HLA alleles not only in the aetiology of AA but also with its severity.

Although, the association to HLA class I was less extensively studied, HLA-B18 and HLA-B12 have found as possible susceptibility loci in the Israeli and Finnish populations respectively (Kianto et al., 1977, Hacham-Zadeh et al., 1981, Haida et al., 2013). Xiao and colleagues (2006) have found higher frequencies of HLA- class I alleles namely HLA-A*02, A*03, B*18, B*27, B*52 and Cw*0704 in Chinese patients (Xiao et al., 2006). All these findings support the notion of AA as a polygenic disease with MHC class I and II as the most commonly involved genes in AA pathogenesis. As HLA-B and HLA-DR genes encode for proteins of antigen presentation, their intimate association with AA indicates the key role of the immune system in AA pathogenesis.

Table 1-2. Some genes involved in AA pathogenesis and their function.

Gene	Genomic locus	Function	References
AIRE	21q22.3	Central tolerance	(Tazi-Ahnini et al., 2002)
NOTCH4	6p21.3	T-cell maturation/ keratinocyte differentiation	(Tazi-Ahnini et al., 2003)
MIF	22q11.23	Pro-inflammatory cytokine	(Shimizu et al., 2005)
PTPN22	1p13.2	Control T-cell activation	(Kemp et al., 2006)
CLTA-4	2q33.2	Inhibitor of T-cell activation	(Petukhova et al., 2010)
ULBP3-6	6q25.1	NKG2D ligands	(Martinez-Mir et al., 2007)
MICA	6p21.3	NKG2D ligand resulting in activation of NK cells	(Barahmani et al., 2006)
HLA-DQB1	6p21.32	Antigen presentation	(Betz et al., 2015)

NOTCH4-Neurogenic Locus Notch Homolog 4. MIF-Macrophage Inhibitory Factor. ULBP-Cytomegalovirus UL16-Binding Protein. PTPN22-Protein Tyrosine Phosphatase, Non-receptor type 22. CTLA-cytotoxic T-cell lymphocyte-associated protein. MICA-MHC class I chain related gene A.

Many other genes of the immune system have been found to be associated with AA in the genome wide association study (GWAS) conducted by Petukhova and colleagues (2010), which identified a large number of genes involved in AA that had not been identified before because of the bias of gene selection in the association studies. In Petukhova's GWAS, 1054 AA patients and 3278 healthy controls were studied and 139 single nucleotide polymorphisms were found to be associated with AA (Petukhova et al., 2010). In addition to HLA genes, genomic regions of association contain genes controlling regulatory T-cell function and proliferation, such as Cytotoxic T-lymphocyte-Associated protein 4 (*CTLA-4)*, IL-2RA and IL-2 (Petukhova et al., 2010). Moreover, genes encoding NKG2D ligands namely ULBPs showed a strong association with these ligands, considered as a danger signal that can activate NK and CD8 cells upon antigenic stimulation (Barahmani et al., 2006).

Immunological factors

The autoimmune aetiology of AA was questioned for many years, but with accumulating evidence, the status of AA as autoimmune disease has been confirmed. As early as 1984, Perret and Todes-Taylor observed a dense intrafollicular and perifollicular infiltration of T-lymphocytes both CD4+ and CD8+ T-cells into the affected areas of the skin of AA patients (Todes-Taylor et al., 1984, Perret et al., 1984). Furthermore, inflammatory markers, such as; ICAM-1, which is essential for the keratinocyte-leukocyte interaction that is followed by lymphocytic infiltrate (Zhang and Oliver, 1994), and MHC class I and II are elevated in lesional skin (Messenger and Bleehen, 1985, Bröcker et al., 1987). The disease association with other autoimmune disorders, such as vitiligo and autoimmune thyroiditis has always been proposed as a marker of autoimmunity in the origin of AA (Cunliffe et al., 1969, Milgraum et al., 1987).

Additionally, autoantibodies to anagen HFs have been found in 100% AA patient serum (Tobin et al., 1994). However, these antibodies are heterogeneous and target different hair structures including cuticle, cortex and IRS and ORS. The antibodies are directed to one or more HF antigens such as hair-specific keratins (52, 50, 46 and 44KD) (Tobin et al., 1994), trichohyalin (Tobin, 2003), melanocyte-associated proteins (Bystryn and Tobin, 1994, Paus et al., 1993). Contradictory to the theory of the humoral immune system's involvement in AA, antibodies to different HF structures fail to inhibit hair growth in human AA scalp tissue grafted onto nude mice that had regrown hair (Gilhar et al., 1992). As a result, it has been suggested that humoral immune system involvement is late and non-specific (Carroll et al., 2002).

The theory of AA as a T-cell mediated tissue restricted autoimmune disease has become more established as evidence has confirmed the failure to develop

the disease when the immune system is inhibited as in the case of nude mice that were devoid of T lymphocytes (Gilhar and Krueger, 1987). Additionally, AA can be transferred by T-cells. For instance, bald human skin can re-grow hair when grafted onto SCID mice, however, injecting autologous T-cells isolated from AA patients into the same human skin graft resulted in hair loss with upregulation of antigen presenting molecules including HLA-DR indicating that auto-reactive T-cells can be an inducer of AA and their absence reverses the disease (Gilhar et al., 1998).

Another widely proposed hypothesis of AA pathogenesis is immune privilege collapse. HF is an immune privileged site due to the absence of antigen presenting protein MHC class I and II on the surface of keratinocytes and very scant lymphocytes in normal HF under the effect of immunosuppressive factors. Collapse of the immunosuppressive microenvironment of the HF bulb results in HF attack by auto-reactive T-cells, particularly CD8+ T-cells, and subsequent HF damage along with infiltration of CD4+ T-cells and NK cells, more details of immune privilege hypothesis will be discussed in section 3. The key elements of AA pathogenesis, such as autoantibodies, T-cells, NK cells and IP have been elucidated better in animal models, which have contributed significantly toward our knowledge of AA pathogenesis.

Animal models

There are several animal models for AA, among the most extensively used ones are the spontaneous adult onset C3H/HeJ mouse and DEBR rat models. That is due to their marked similarities both phenotypically and histologically to human AA (Sundberg et al., 2015). AA in C3H/HeJ mouse was first described by Sundberg et al. (1994) and in the Dundee Experimental Bald

Rat (DEBR) model was described by Michie et al. (1991) (Michie et al., 1991, Sundberg et al., 1994).

Animal models are of great value in studying AA pathogenesis by elucidating the role of key players in AA pathogenesis such as auto-antibodies, IFN-γ, T-cells and NK cells. For instance, IFN-γ as a key cytokine in AA pathogenesis was demonstrated by the resistance of IFN-γ deficient C3H/HeJ mice to AA development (Freyschmidt-paul et al., 2006). T-cell involvement has been demonstrated in the nude mouse model (Figure 1.4), which is an athymic mouse devoid of T-cells. Hair regrowth was noticed on the affected scalp from AA patients grafted onto nude mice (Gilhar and Krueger, 1987) whilst injecting T-cells re-induced hair loss in human AA scalp with regrown hair that had been grafted onto SCID mice (Gilhar et al., 1999).

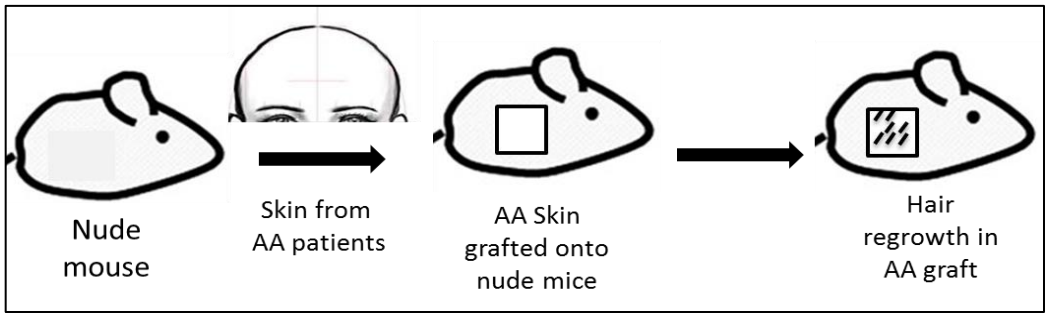

Figure 1.4. An example of animal study in AA.
The nude mouse model contributes to the current understanding of AA pathogenesis. Grafting AA patient's affected skin onto the nude mouse resulting in hair regrowth in the graft on these T-cell devoid mice.

The contribution of auto-antibodies has been investigated in C3H/HeJ mice (Tobin et al., 1997) and DEBR rat (McElwee et al., 1996). McElwee and colleagues had measured the autoantibodies in sera of DEBR rat. Serum from the affected rat was reactive to various components of HF including cuticle, cortex and IRS using indirect immunofluorescence staining of cryosections of

HF from normal and affected rats (McElwee et al., 1996). That has been reproduced in C3H/HeJ mice by Tobin and colleagues (1997) where autoantibodies have found in 100% of the affected mice. An induced AA model has also been developed which offers better understanding of disease kinetics; a graft from affected C3H/HeJ was transplanted onto normal mice resulting in hair loss 8-10 weeks later (McElwee et al., 1998), and serial changes in the cellular infiltrate and HF morphology was studied.

The limitations of these two models are the late onset and low penetrance of the disease. The hair loss is observed in ≤1% of C3H/HeJ mice by age of 4-6 months, which increases to 20% at 18 months (McElwee and Hoffmann, 2002). In DEBR rat, the penetrance is higher (30% in male and 70% in female) but at later onset about 5-8months, which renders it a more expensive model compared to C3H/HeJ mice (Michie et al., 1991, Oliver et al., 1991).

A new animal model with 100% incidence by age of 4months was developed by Alli et al. (2012) in C57BL/6J mice, which overcomes the penetrance limitation of C3H/HeJ and DEBR. The model was developed in retroviral transgenic mice that express monoclonal TCR, which induces development of CD8+ cells directed to HF that is followed by activation and expansion of CD8+ cells and their infiltration into HFs. The striking observation in this model is the ability to induce human AA analogous disease changes by CD8+ lymphocytes independently, which supports the notion of AA as CD8+ dependent autoimmune disease as discussed earlier (Alli et al., 2012).

In addition to the limitation of disease penetrance in some of the previously discussed animal models, researchers have been debating whether they are the best models for studying human AA. There are differences in the location of lymphocytic infiltrate while it extends from sebaceous gland to the

bulb of affected HFs in humans and DEBR rat, it extends from supra-bulbar to sebaceous gland in affected HFs of C3H/HeJ mice (Sun et al., 2008). More significantly, there are differences in some molecular aspects of the disease; For example, AA in C3H/HeJ mice is characterised by a major defect in toll-like receptor 4 (TLR4) signalling which is not a feature of human AA (Gosemann et al., 2010, Gilhar et al., 2013). Furthermore, the animals are maintained in highly controlled conditions compared to human subjects where the environmental factors and stress might have a contribution in the disease induction (Sun et al., 2008).

A humanised mouse model of AA has been recently introduced by Gilhar et al. (2013). Healthy human scalp skin was transplanted onto Immune-compromised SCID mice. Intradermal injection of mononuclear cells enriched with NKG2D+ and CD56+ cells supplemented by IL-2 resulted in hair loss associated with dense infiltrate of CD4+ and CD8+ cells (Gilhar et al., 2013). This model is more powerful in studying the disease kinetics in the context of human pathogenesis. Furthermore, it highlighted the role of NKG2D+ cells in AA pathogenesis (Gilhar et al., 2013).

Animal models have also contributed in elucidating the mechanisms of IP collapse. For instance, the molecular mechanism underlying the high expression of antigen presenting molecules MHC I and II was explained using the nude mouse model where injecting INF–γ in the nude mouse with regrown hair resulted in hair loss associated with up-regulation of MHC class I and II and ICAM-1 (Gilhar et al., 1993).

1.3 Immune privilege

Immune Privilege (IP) is a tissue characteristic enabling the relative protection of allograft against immune attack (Head and Billingham, 1985, Paus

et al., 2003). A number of sites in the body enjoy IP, such as the anterior eye chamber, parts of the testis and ovary, the adrenal cortex, segments of the central nervous system behind the blood–brain barrier, the feto-maternal placental unit and the proximal third of the hair bulb and hair bulge regions of HF (Medawar, 1948, Niederkorn, 2003). Collapse of IP results in autoimmune attack of the originally privileged sites and subsequently autoimmune diseases such as autoimmune uveitis (Wilbanks and Streilein, 1991), autoimmune orchitis (Zhao et al., 2014), foetal rejection (Kanellopoulos-Langevin et al., 2003) and AA (Westgate et al., 1991). The collapse of anagen HF privilege is proposed as an initiating event in AA pathogenesis (Paus et al., 2003) where many molecular and cellular elements are involved in maintaining and establishing hair follicle IP.

HF was first suggested as an immune privileged site by Billingham and Silvers in 1971, when the black guinea pig skin graft was accepted by the albino guinea pig. Black hair shafts were observed in the graft, which suggested that some of the donor melanocytes escape the immune rejection and grow in the recipient's hair bulb (Billingham and Silvers, 1971).

In the normal IP state (Figure 1.5), the anagen HF is characterised by lack of expression of MHC class I and class II in the proximal part of the HF (Westgate et al., 1991, Christoph et al., 2000), and the entire lower two-thirds of the anagen HF is devoid of APCs (Moresi and Horn, 1997, Paus et al., 1999a). Only scant numbers of NK cells, CD4+ are found in the lower portions of the proximal hair follicle (Christoph et al., 2000). All these features are thought to be mediated by immunosuppressive factors, such as TGF-β, α- MSH, IL-10, adrenocorticotrophic hormone and immune-inhibitory signal (CD200) secreted by HF cells (Gruschwitz et al., 1990, Paus et al., 1993, Grabbe et al., 1996, Rosenblum et al., 2004, Ito et al., 2004).

In the aberrant IP state, cellular and molecular elements of normal HF are altered where expression MHC class I and class II is upregulated in AA compared to normal control skin (Ito et al., 2004) resulting in presentation of auto-antigen to cytotoxic T-cells and subsequent infiltration of $CD4^+$ T-cells, NK and APC (Khoury et al., 1988). The expression of the main inducer of MHC class I (IFN–γ), which is a Th1 cytokine, is increased in the affected skin (Ito et al., 2004). Opposite to the normal state, IP guardians, such as TGF-β and α-MSH are downregulated in AA affected areas (Taylor et al., 1992, Paus et al., 2003).

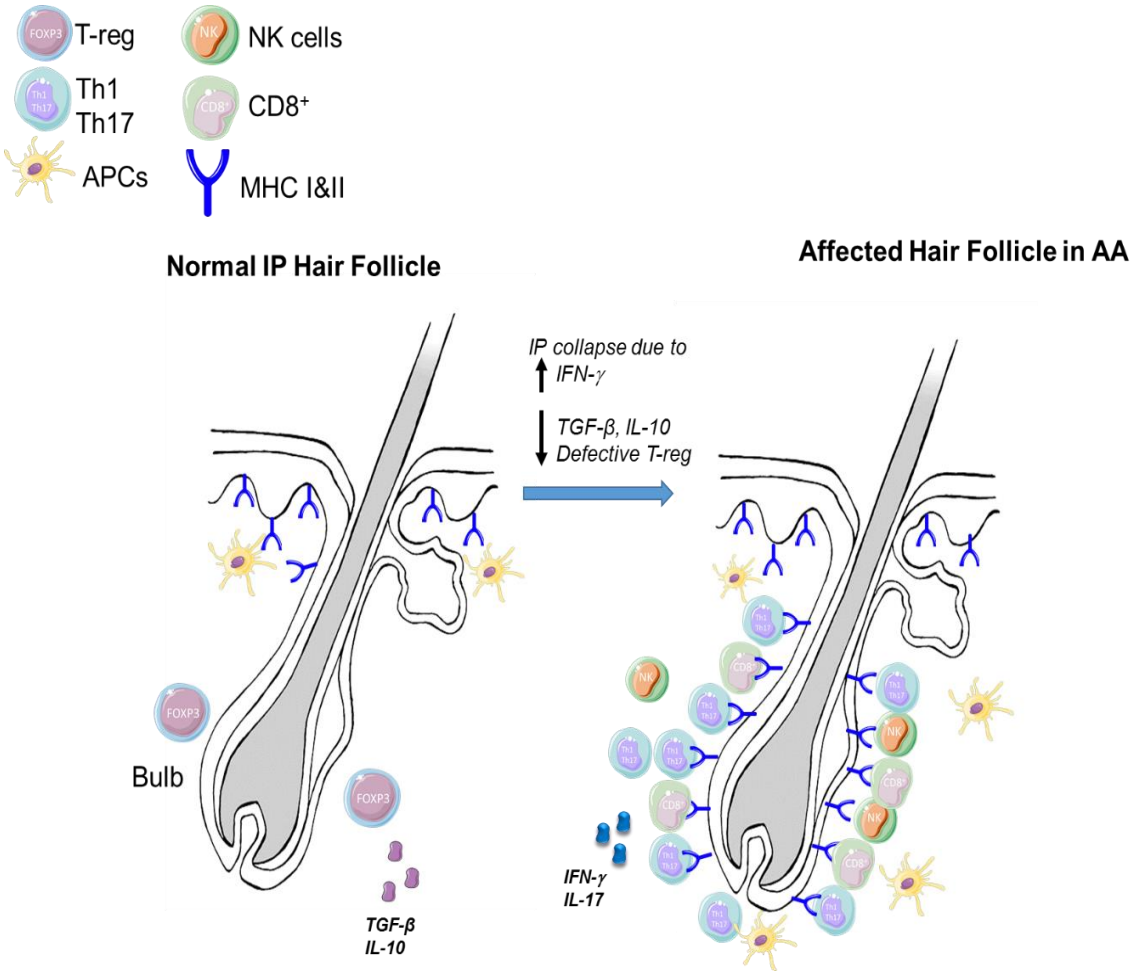

Figure 1.5. IP theory of AA pathogenesis.

Normal HF with no APCs and scant CD4+ T-cells in the bulbar and supra-bulbar region, which are proposed to be mostly Tregs secreting IL-10 and TGF–β maintaining the normal IP state of HF. Lesional HF is infiltrated with APCS, NK, CD8+ (Tc) and Th1 and Th17 cells. We propose that antigen identification and processing by APCs results in IFN-γ production, which in turn upregulates MHC class I with subsequent sequestration of Tc cells and further production of IFN-γ, upregulation of MHC class II and sequestration of Th1 and Th17 resulting in HF damage. Figure was created using Servier medical art.

1.3.1 Molecular elements of IP

1.3.1.1 Major histocompatibility complex (MHC) classes I and II

MHC class I molecules are expressed on the surface of all nucleated cells, and act as a sensory arm of the immune system by presenting antigens to the CD8+ cytotoxic T-cells (Qazi and Hamrah, 2013). MHC class II molecules are expressed on the surface APCs and present antigens to CD4+ T-cells (Bröcker et al., 1987).

In this thesis, MHC antigens will be considered as the main representative of IP collapse since their absence is a unique feature of IP sites. No detectable MHC class I and II expression is found in the anagen HF particularly in the sub-infundibular and matrix keratinocytes (Harrist et al., 1983, Bröcker et al., 1987, Ito et al., 2004). Absence of these molecules in the privileged sites plays an important role in preventing the immune attack (Christoph et al., 2000). In the aberrant IP state, MHC class I expression is up-regulated (Figure1.5) resulting in recruitment of CD8+ T-cells to the HF (Ito et al., 2004). Similarly, the expression of MHC class II was increased in AA affected skin as demonstrated by Messenger et al. (1985), however, it is thought to be a consequence of lymphocyte infiltration not a primary event in the pathogenesis (Khoury et al., 1988, Messenger and Bleehen, 1985). Therefore, decreasing the expression of MHC molecules is a key target in any AA treatment to reduce presentation of hair autoantigens to T-cells, and this feature could be employed as a marker to assess the success of any potential treatment of AA in experimental models.

1.3.1.2 IP collapse inducers

The main inducer of MHC class I expression and thereby IP collapse is INF-γ (Figure 1.5), and its role as a key cytokine in AA pathogenesis was

demonstrated by the resistance of INF–γ deficient C3H/HeJ mice to AA development (Freyschmidt-paul et al., 2006). In agreement with its role as an AA inducer, injecting high dose IFN-γ increased the rate of AA incidence in the C3H/HeJ mouse model (Gilhar et al., 2005). In human AA, ectopic expression of MHC class I and II can be induced by INF-γ as demonstrated in the *ex vivo* HF model by Ito's group (Ito et al., 2004). Moreover, IFN-γ is considered as a catagen inducer, which interferes with hair growth. This role replicates the AA nature as a disorder of HF growth cycling where increase in the number of catagen HF is one of histopathological characteristics of AA affected skin (Sato-Kawamura et al., 2003). It is thought that environmental factors such as viral or bacterial infection induce IFN-γ production resulting in upregulation of chemokine expression, such as CXCL-9 (Gilhar et al., 2003) and CXCL-10 (Kuwano et al., 2007) in the hair bulb. These chemokines in turn stimulate T-cell accumulation in and around the hair bulb (Ito et al., 2012).

It is well known that IFN-γ mediates its action via the JAK-STAT pathway (Horvath, 2004). INF–γ binds to its receptors, INFGR1 and 2, followed by their dimerization and activation of Janus kinase enzymes JAK1 and 2 accordingly (Figure1.6). JAK enzymes phosphorylate signal transducer and activator of transcription proteins (STAT1), which translocates into the nucleus and binds to IFN-**g**amma **a**ctivated **s**equence (GAS). GAS is a specific DNA sequence that responds to INF–γ binding by subsequent activation of INF–γ dependent genes expression, which mediates the inflammation (Darnell et al., 1994).

IFN–γ activates a large number of genes, up to 500, where the transcription factor, interferon regulatory factor (IRF-1), is among the key genes regulated by IFN–γ (White et al., 1996). IRF-1 activates a group of genes such

as those involved in transcription of antigen presenting molecules namely MHC class I and class II, transporter associated with antigen processing (TAP) (White et al., 1996), the cellular adhesion molecules such as ICAM-1 and VCAM-1 (Lechleitner et al., 1998) and Th1 and Tc cells development and function (Matsuyama et al., 1993). IRF-1 is also considered a key negative regulator of Treg through repressing FOXP3 expression (Fragale et al., 2008).

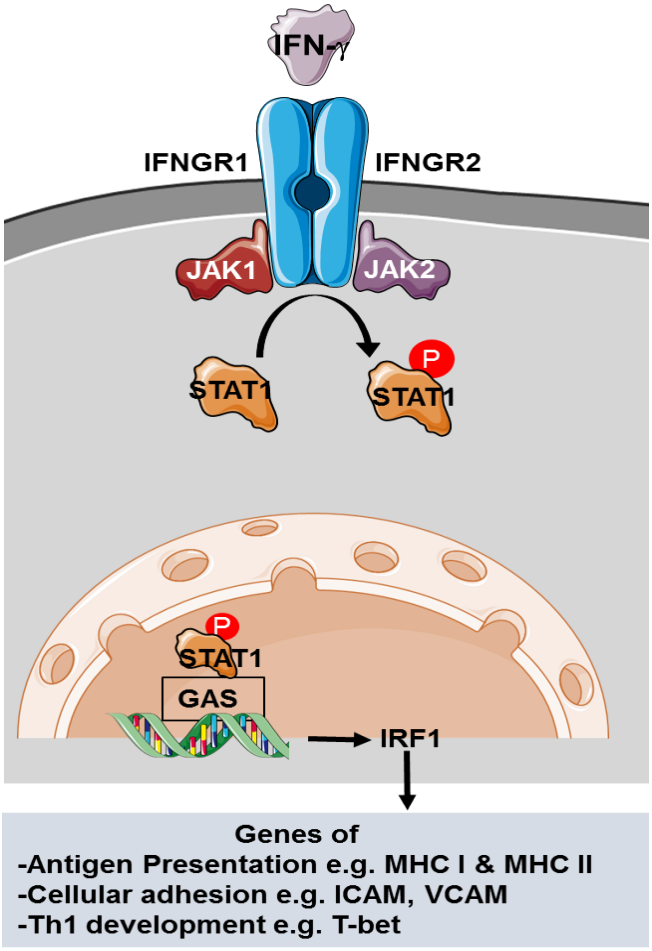

Figure 1.6. Schematic simplification of IFN-γ signalling pathway.

IFN-γ binds to its receptors INFGR1 and 2, which upon dimerization bind to their prospective JAKs. JAK enzyme phosphorylates STAT-1 signal transducer that translocate to the nucleus where it activates IFN-**g**amma **a**ctivated **s**equence (GAS) resulting in activation of transcription factors such as IRF-1 with subsequent activation of many genes involved in inflammation and autoimmunity such as genes of Th1 development, antigen presentation and adhesion molecules.

1.3.1.3 IP guardians

Immune suppressive factors (IP guardians), such as indoleamine-2,3-dioxygenase (IDO), IK/Red, transforming growth factor β (TGF-β), α-melanocyte-stimulating hormone (α-MSH) and interleukin 10 (IL-10) are elaborated by anagen HF (Kang et al., 2010). They mediate IP maintenance by different mechanisms. For example, IK cytokine is expressed on ORS and acts as an antagonist of IFN-γ induced MHC II expression (Muraoka et al., 2006). IDO mediates immunological tolerance by inhibiting lymphocyte proliferation (Hou et al., 2009). α-MSH, TFG-β and IL-10 are important in peripheral immunological tolerance by inducing differentiation of naïve $CD4^+$ cells into the regulatory phenotype (Taylor et al., 2000). Expression of these immunosuppressive molecules is decreased in AA (Kang et al., 2010). IP guardians are promising candidate targets for AA treatment where α-MSH, IGF-1 and TGF-β have shown to decrease IFN-γ induced MHC I expression in HF (Ito et al., 2004), and α-MSH has demonstrated therapeutic potential in experimental uveitis (Edling et al., 2011).

Some studies suggest that blocking lymphocyte activity in immune-privileged HFs is mediated through an inhibitory molecule expressed on the outer connective tissue sheath known as Programmed Death-Ligand 1 (PD-L1) that induces T-cell anergy (Wang et al., 2013b, Guo et al., 2015). The same molecule plays a key role in feto-maternal tolerance (Guleria et al., 2005). Treg cells are postulated as IP guardian cells based on the ability to block disease onset in the mouse model (McElwee et al., 2005a), and their abundance around the normal HF as studied by Rosenblum' group (Sanchez Rodriguez et al., 2014) . Treg involvement in maintaining IP will be discussed in details in cellular mechanism of IP.

1.3.2 Cellular elements of IP

1.3.2.1 Natural killer (NK) cells

NK cells exert direct cytotoxic effects on tumour cells or infected cells lacking MHC I expression (Eric et al., 2008, Joncker and Raulet, 2008). Despite being MHC negative, the hair bulb is protected from perifollicular NK cell-mediated attack (Christoph et al., 2000). This can be explained in the eye and HF by the presence of NK cell inhibitory cytokines, such as TGF-β and MIF (Rook et al., 1986, Apte and Niederkorn, 1996, Ito et al., 2008). Moreover, NK cell activating receptor ligands such as MICA are not expressed on the ORS of anagen HF, thus boosting the protection against NK attack in normal IP state (Ito et al., 2008). NK receptors (NKG2D) that recognize MICA ligand are also weakly expressed on NK cells from healthy controls compared to AA patients (Ito et al., 2008). NKG2D also recognizes surface glycoproteins that bind human cytomegalovirus UL16 proteins (ULBPs), which stimulates immune cells to attack target cells, and genes encoding for ULBP have been found to be associated with AA (Petukhova et al., 2010). In the aberrant IP state, CD56+ NK cells contribute to the perifollicular infiltrate, which is accompanied by massive immune reactivity of HF to MICA, and increased expression of NKG2D on NK cells (Ito et al., 2008). Therefore some researchers conclude that maintaining the HF IP state is closely linked to blocking NK cell attack.

1.3.2.2 Antigen presenting cells (APC)

Langerhans cells (LCs), which are the skin resident dendritic cells (DCs), are normally very scant in the lower two-thirds of human HF (Moresi and Horn, 1997). Additionally, they are non-functional as they lack MHC class II expression (Christoph et al., 2000). However, their role as the initiator of skin immune responses put this cell population at the centre of AA research. They have a

dual role where LCs recognise antigen, migrate to lymph nodes, display MHC class I or II and activate CD8+ or CD4+ cells respectively resulting in destruction of antigen-bearing infected cells or tumour cells (Mutyambizi et al., 2009). LCs also mediate the self-tolerance role where during the catagen phase of the hair cycle, LCs phagocytose apoptotic keratinocytes and melanocytes without inducing an immune attack (Mutyambizi et al., 2009). The tolerogenic phenotype of LCs is thought to be mediated by immunosuppressive molecules secreted by keratinocytes such as TGF–β or/and α–MSH (Grabbe et al., 1996) inducing IL-10 secretion by LCs and thereby Treg development. Similar changes have been seen in melanoma where IL-10 secreted by tumour cells induced tolerizing LCs and mediated tumour evasion (Enk et al., 1997).

In the eye, APCs' tolerogenic effect has been demonstrated to have a central role in maintaining IP (Wilbanks and Streilein, 1991). Upon antigen inoculation, APCs induce differentiation of naïve $CD4^+$ T-cells into regulatory T-cells instead of inflammatory (Th1) cells under the effect of TGF-β in aqueous humour (Wilbanks and Streilein, 1991, Orazio and Niederkorn, 1998). In the HF, this mechanism has not been studied and it is not known if APCs have a role in maintaining or collapsing the IP state. However, APCs expressing CD1a, CD40, CD54 and HLA-DR are detected in lymphocytic infiltrates in AA (Sato-Kawamura et al., 2003). Specifically, CD1a+ cells have been detected in high numbers in perivascular and peribulbar regions of affected HF in the acute phase of AA while they are scant in the chronic phase, which may suggest a primary role of APCs in the early phases of AA (Ghersetich et al., 1996).

1.3.2.3 T-cells

Although the exact aetiology of AA is not known, T-cells and their cytokines play a pivotal role in the disease process. Normally, the hair bulb is

devoid of intra-epithelial T-lymphocytes (Christoph et al., 2000). IP collapse results in dense Infiltration of T-lymphocytes of both CD4+ and CD8+ phenotype, which is one of the histopathological hallmarks of the disease.

1.3.2.3.1 CD8+ T-cells

CD8+ cytotoxic T (Tc) lymphocytes constitute 20-40% of the lymphocytic infiltrate in AA affected skin (Todes-Taylor et al., 1984). While CD4+ cells infiltrate around the HF, CD8+ cells invade and infiltrate inside the bulb. They dominate the lymphocytic infiltrate in chronic cases of the disease indicating their destructive role in HF damage (Ito et al., 2012). CD8+ T-cells infiltration is believed to be downstream to IP collapse due to upregulation of MHC I by INF–γ (Figure1.5). AA is considered to be mainly a CD8+ cell-mediated disease, which was demonstrated in many animal models. For instance, CD8+ T-cells cultivated with human HF homogenate induced hair loss in grafts of human AA scalp where the hair had initially regrown following grafting onto SCID mice (Gilhar et al., 2001). Additionally, Alli's mouse model described earlier showed development of AA in 100% of C57BL/6J mice by inducing the development of clonal CD8+ T-cells (Alli et al., 2012).

NKG2D receptors, which are expressed on the surface of activated CD8+ T-cells, have attracted more attention when their ligands, namely ULBP3 and MICA, were showed to have a strong association with AA in GWAS, and up-regulated in dermal papilla and dermal sheath of HFs of AA patients compared to normal subjects (Ito et al., 2008, Petukhova et al., 2010). NKG2D ligands activate cytotoxic activity of CD8+ T-cells (Petukhova et al., 2010, Xing et al., 2014). This is followed by IFN-γ production by cytotoxic CD8+ NKG2D+ T-cells mediating inflammation and HF damage. These findings have been confirmed when the signalling pathway downstream of CD8+ cell activation, namely the

JAK-STAT pathway, has been targeted by a small molecule and shown to result in a complete hair regrowth in some AA patients (Xing et al., 2014).

CD8+ T-cells mediate their cytotoxic effect through secreting granyzyme B and Fas/FasL cytotoxic mechanisms (Bodemer et al., 2000) and C3H/HeJ mice deficient in Fas or Fas L do not develop AA. Nonetheless, McElwee et al. (2005) showed that injection of CD8+ cells alone resulted in limited disease while injecting $CD4^+$ $CD25^-$ cells alone induced a more extensive disease phenotype (McElwee et al., 2005a), which indicates probable interaction between CD8+ and CD4+ cells is a key element in AA pathogenesis (Gilhar et al., 2002).

1.3.2.3.2 CD4+ T-cells

It is well known that CD4+ and CD8+ T-cells constitute the main components of the cellular infiltrate around affected HF in AA; however, the question of how they interact to cause the disease is still not answered. Strikingly, CD4+ cells constitute 60-80% of the lymphocytic infiltrate in AA affected skin (Todes-Taylor et al., 1984). However, there are many questions that recent researches have been attempting to elucidate. Importantly, which CD4+ cell subset has the key role in AA pathogenesis and whether they mediate their effect by collapsing IP and how. Naïve $CD4^+$ can differentiate into effector inflammatory conventional T helper cells (Teff) such as Th1, Th2, Th17 or into CD4+ $CD25^+$ regulatory T-cells (Tregs), which functionally inhibit any deleterious activity of Teff (Zhu et al., 2010). Each sub-population of CD4+ T-cells is characterised by their cytokine profile as well as cell surface or intra-cellular markers summarised in Table 1.3.

Table 1-3. Main subsets of CD4+ cells and profile of secreted cytokines.

CD4+ subsets	Surface/Intracellular Markers	Cytokines secretion	References
Th1	CD4, CD119	IFN-γ, TNF-β, IL-2	(Romagnani et al., 2000)
Th17	CD4	IL-17, IL-21, IL-22, IL-23, IL-6	(Ghoreschi et al., 2011)
Th2	CD4 CRTH2	IL-4, IL-5, IL-10, IL-13	(Noble et al., 1993)
Treg	CD4 CD25 FOXP3	TGF-β, IL-10	(Levings et al., 2002)

Inflammatory effector T-cells (Teffs)

Inflammatory T-cells (Teff) include CD8+ T-cells (discussed previously in section 3.2.3.1.) and inflammatory cells differentiating from CD4+ T-cells such as Th1 Th2 and Th17. In this section, some evidence of Th1, Th2 and Th17 association with AA pathogenesis will be discussed. The role of Th1 in AA pathogenesis is supported by INF–γ role (section 3.1.2) as it is the main cytokine secreted by this population (Farrar and Schreiber, 1993). Furthermore, expression of Th1 chemokines such as CXCL-9, CXCL-10 and their receptor CXCR3 were up-regulated and this was correlated with disease activity (Kuwano et al., 2007). IL-2, which is another Th1 cytokine, was found to be elevated in peripheral blood of patients with severe AA (Teraki et al., 1996). Although the role of Th2 cells has not been studied thoroughly, IL-13 levels were found to be higher in AA patients compared to controls without specifying the type of AA (Tembhre and Sharma, 2013). Moreover, Th2 cytokines, such as IL-4 and IL-10, were found to dominate in sera of patients with localised disease while Th1 cytokines, INF–γ and IL-2, were elevated in patients with extensive disease (Teraki et al., 1996).

Th17 is another CD4+ cell population that has been suggested to be involved in AA pathogenesis. Th17 cytokines, particularly IL-17, are increased in AA patients' blood, and IL-17 expression was found to be significantly higher in AA affected skin compared to control (Atwa et al., 2016). Additionally, infiltration of Th17 cells was detected around lesional HF (Tanemura et al., 2013). Involvement of Th17 cells in AA might be explained by their role in reducing Treg recruitment as suggested in one study by Katayama's group (Tanemura et al., 2013) which probably resulted in inducing the inflammatory micro-environment of HF as proposed in Figure 1.5. Nonetheless, better understanding of Treg function and development is required to elucidate their role in AA.

Regulatory T-cells (Treg)

Naturally occurring Treg (nTregs) develop in the thymus and constitute 4-10% of CD4+ T-cells population in peripheral blood. They play a central role in peripheral immune tolerance where they have an anergic effect on Teffs (Peterson, 2012). nTregs differentiate from CD4+ CD8- T-cells in the thymus where the transcription factor (FOXP3) plays a pivotal role in their differentiation and function. Mutation in FOXP3 in scurfy mice abrogates Treg development resulting in lethal autoimmune disease (Fontenot et al., 2003). Similarly, IL-2 is an essential element in nTreg development and function where mice deficient in IL-2 or its receptor CD25 have a profound reduction in the number of FOXP3+ Treg, Therefore nTreg are also named FOXP3+ CD25+ CD4+ T-cells (Jonuleit and Schmitt, 2003). Other subtypes of Tregs also develop from naïve CD4+ T-cells in peripheral tissue up on antigenic stimulation and are called induced/adaptive Treg (iTreg) (Schmitt and Williams, 2013).

iTreg are subdivided according to their cytokine profile and FOXP3 expression into; IL-10-Producing Treg Cells (Tr1), TGF-β producing Treg cells (Th3) and FOXP3+ CD25+ CD4+ Treg (Figure 1.7). However, categorization of Treg population is a complicated topic as many other subtypes have been described in the literature, and Shevach made an analogy of Treg repertoire discoveries by developments in the ice cream industry from one original vanilla flavour to the huge number of flavours available today. For instance, subtypes such as γδ T-cells , CD8+ Treg and CD4−CD8−double-negative (DN) Treg, NK Treg and more have been described (Shevach, 2006). Despite the fact that many T-cells exert immune suppression effects as explained, the discussion in this thesis will be confined to CD4+CD25+FOXP3, which is the main population of Treg that have been extensively studied and characterised. Nonetheless, phenotypic differentiation between natural or induced CD4+CD25+FOXP3+ Treg cells is not attainable (Shevach, 2006, Lan et al., 2012) due to lack of specific markers. Therefore, CD4+CD25+FOXP3+ T-cells in the thesis are referred to as Treg population either developed in thymus or periphery.

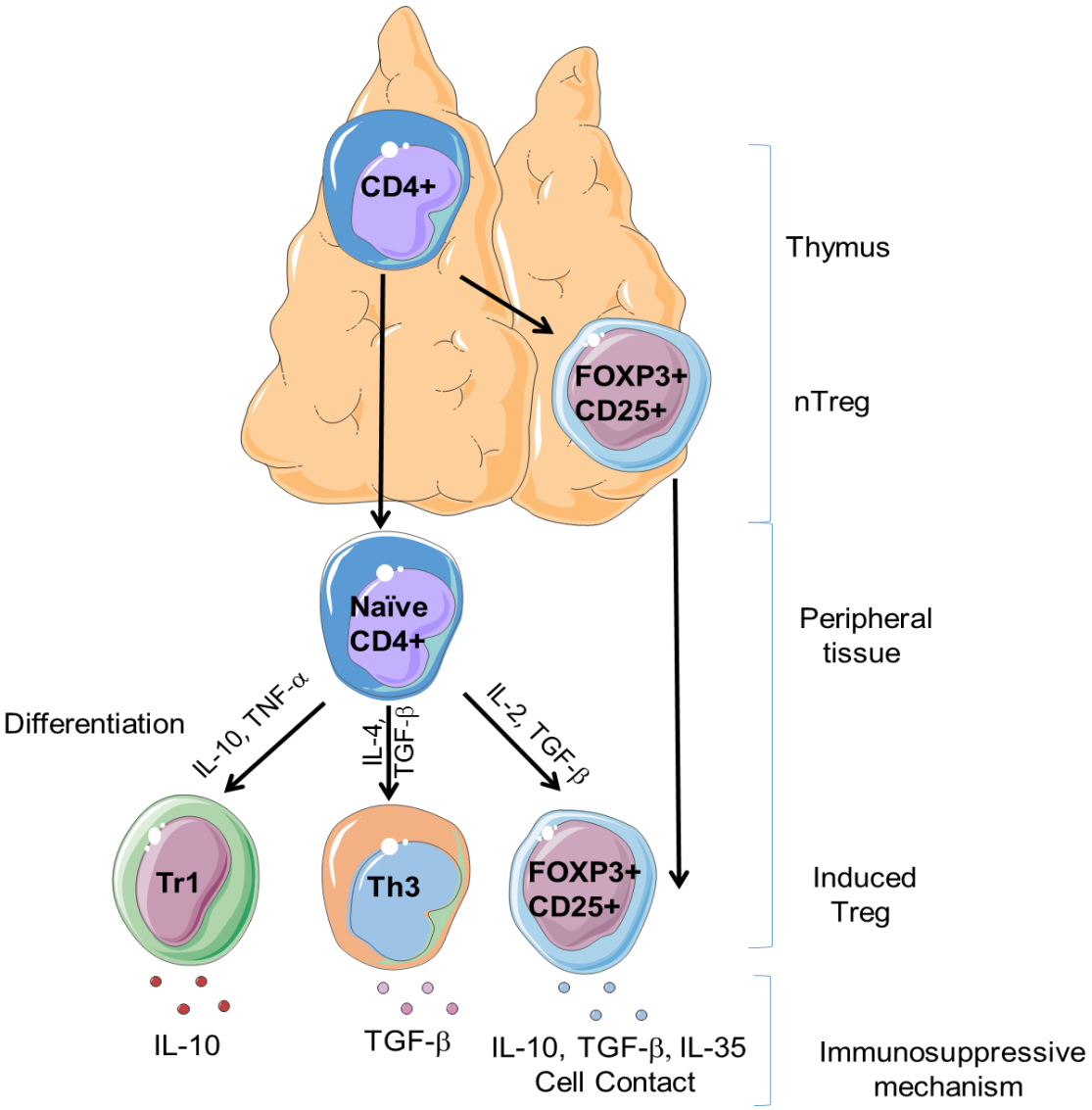

Figure 1.7. Differentiation and immunosuppressive mechanisms of natural and induced Treg.

CD4+ T-cells develop into FOXP3+CD25+CD4+ Treg in thymus giving rise to natural Treg (nTreg). Induced Treg cells develop in the periphery from naïve CD4+ T-cells, which differentiate to a distinct subtype of Treg according to the inducing cytokine. IL-10 and TNF–α induces differentiation of Tr1, TGF–β and IL-4 induces Th3 development while induced FOXP3+ CD25+CD4+ Tregs develop under the effect of TGF-β and IL-2. Each Treg subtype is characterised by a specific immunosuppressive mechanism; Tr1 and Th3 exert immunosuppression via IL-10 and TGF-β secretion respectively. Induced and natural FOXP3+CD25+CD4+ share their immunosuppressive mechanism including both cell contact and secretion of immunosuppressive molecules such as TGF–β, IL-10 and IL-35. Figure was created using Servier medical art.

Tregs can be classified into phenotypically and functionally distinct subpopulations based on CD45RA (Miyara et al., 2009) or CD45RO cell surface markers (Ye et al., 2015). Expression of CD45RO and CD45RA is usually regulated in a reciprocal manner where positively selected T-cells express CD45RO in the thymus, convert to CD45RA at the time of emigration to the periphery, and then switch back to CD45RO after antigen recognition (Vanhecke et al., 1995, Fukuhara et al., 2002). Therefore Tregs expressing CD45RA but not CD45RO (CD45RA+CD45RO-) are naïve cells that haven't encountered antigen before (Rosenblum et al., 2016). Naïve CD4+CD25+FOXP3 Treg cells acquire CD45RO+ upon antigen presentation and proliferate, however, they need activation molecules to exert their immune-suppressive function such as CD39 (Ye et al., 2015), and named suppressive Tregs (Figure 1.8). Once inflammation subsides, effector Treg lose their activation markers and maintain only CD45RO+ markers and rest in lymph nodes or peripheral tissues as memory Treg (Rosenblum et al., 2016).

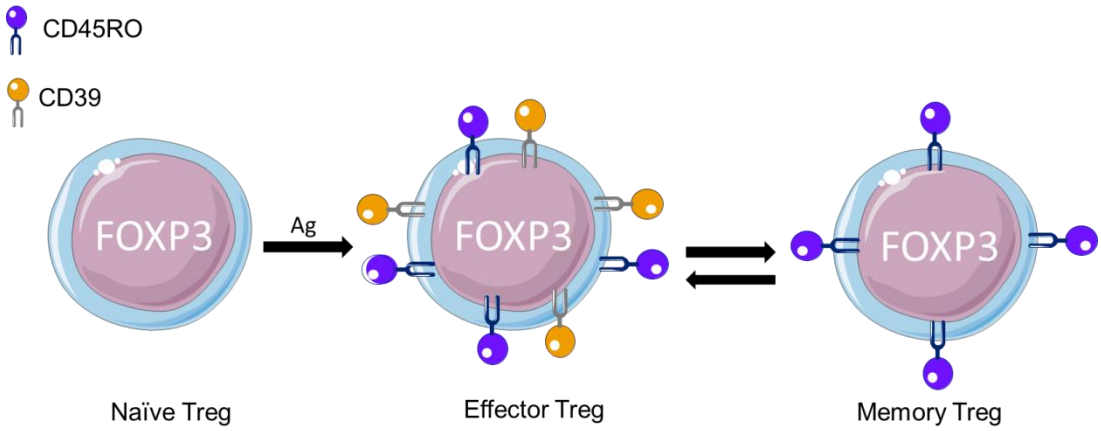

Figure 1.8. Treg classification according to their development.
Naïve Treg express CD25+FOXP3+ are converted into effector Treg upon antigen presentation acquiring CD45RO+ and CD39+, the latter will be lost once the inflammation subsides and cells will maintain CD45RO+ to be memory Treg. Figure was created using Servier medical art.

However, how Tregs mediate their suppressive function is more complicated and cannot be confined to CD39-mediated suppression. Tregs' primary function is controlling expansion and activation of autoreactive Teff, which is mediated by many different suppressive mechanisms. Schmidt and colleagues (2012) postulated that Treg uses one or more of these mechanisms depending on the antigen, target cell type, activation status and cytokine microenvironment (Schmidt et al., 2012). Among the most known mechanisms are:

1- Secreting immune-modulatory molecules such as IL-10, TGF-β (Von Boehmer, 2005), IL-35 (Collison et al., 2007) and galactin-1 that result in cell cycle arrest, apoptosis and inhibiting pro-inflammatory cytokine secretion (Garín et al., 2007).

2- IL-2 consumption where Tregs compete with Teffs for IL-2 required for Teff proliferation resulting in their deprivation and apoptosis (Pandiyan et al., 2007) .

3- Direct cell-to-cell contact with Teff cells and resultant cytolysis mediated by the granzyme /perforin pathway (Grossman et al., 2004). Interestingly expression of MHC-II (HLA-DR) on Tregs identifies a distinct suppressive population that mediates an early cell-contact dependent mechanism to inhibit T-cell proliferation and induce FOXP3 expression (Ashley and Baecher-Allan, 2009, Baecher-Allan et al., 2006).

4- Modulating dendritic cell function is another suppressive machinery of Treg. That is mediated by engagement of CD223 (Lymphocyte-activation gene 3, LAG-3) molecules on the surface of Treg with MHC class II on DC inhibiting activation of Teffs (Liang et al., 2008).

5- Modulating T-cell response and inhibiting Teff proliferation via A2 adenosine receptor. CD39 and CD73 are ecto-enzymes expressed on Treg cells, and they

are considered key components in Treg suppressive machinery. CD39, ecto-nucleoside triphosphate diphosphohydrolase 1, ENTPDase1, is an enzyme of the ATPase family that hydrolyses ATP into AMP, which is subsequently hydrolysed by CD73, an ecto-5-nucleotidase, into adenosine (Antonioli et al., 2013). Adenosine modulates the pro-inflammatory micro-environment induced by ATP into an anti-inflammatory milieu (Figure 1.9). Adenosine binds to receptors on the surface of T and B lymphocytes, DCs and NK cells inhibiting their development (Deaglio et al., 2007).

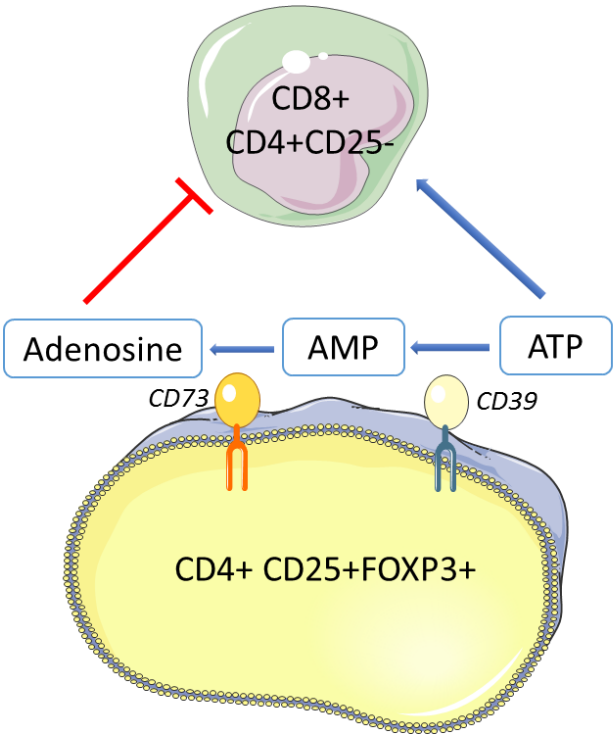

Figure 1.9. A schematic representation of CD39+ suppressive Treg function. CD39 induces the hydrolysis of the pro-inflammatory molecule ATP into AMP, which in turn will be hydrolysed by CD73 into adenosine. Adenosine is an anti-inflammatory molecule inhibiting activated T-cells proliferation. Figure was created using Servier medical art.

Based on a recent study by Sanchez Rodriguez et al., 2014, CD4+ CD25+ FOPX3+ cells are more predominant in skin than peripheral blood constituting 20% of CD4+ T-cells in the skin. CD45RO+ memory Tregs express

activation markers such as CD25, CTLA-4 and ICOS (Sanchez Rodriguez et al., 2014). These activated memory Treg are a considerable population of T-cells in the skin, particularly in hair bearing areas, which suggest their possible role in maintaining IP.

A potential role of Treg cells have been identified in many skin diseases such as psoriasis vulgaris, mycosis fungoides and eczematous dermatitis (Fujimura et al., 2008, Sakaguchi et al., 2011). Depletion of CD4+ CD25+ Treg induces autoimmune disease in animal models (Sakaguchi et al., 1995, McElwee et al., 2005a). In AA, Tregs have a central role in the pathogenesis. For instance, CD4+ CD25+ Tregs have found to be very low in AA affected skin of C3H/HeJ mice (Zoller et al., 2004), and injecting these cells significantly reduced the disease incidence in C3H/HeJ mice (McElwee et al., 2005a). Furthermore, In human AA, the Treg cytokine TGF-β was found to be significantly decreased in peripheral blood of AA patients compared to controls (Tembhre and Sharma, 2013). Moreover, peripheral Tregs were found to be functionally impaired in AA patients (Shin et al., 2013). The importance of Treg in AA pathogenesis has been recently supported by finding an association of novel regions containing genes important for Treg function such as IL-2RA, IL-2/IL-21 and CTLA4 in AA patients in GWAS (Betz et al., 2015).

It has been suggested that dysfunction of Tregs is one of the IP collapse mechanisms (Gilhar et al., 2007). In the eye, antigen specific Tregs have been found in spleen after experimental uveitis (Kitaichi et al., 2005), which clearly indicates Treg central role in maintaining IP in eye. Treg recruitment via IL-2 induced hair regrowth in five AA patients, which might have been achieved by restoring the IP (Castela et al., 2014). However, the mechanism by which Treg maintain the IP in the HF is not entirely understood. Therefore, investigating

Treg population in peripheral blood and skin of AA patients will be one of the aims of the current research.

Treg-Teff balance

Alterations in the balance between Teff (Th1, Th2 and Th17) and Treg populations of CD4+ T-cells is the cause of autoimmunity in many diseases (Almeida et al., 2002, Cai et al., 2013), however, this mechanism is not elucidated in AA. Here, as simplified in Figure 1.10, IP is proposed to be maintained under the effect of immune-suppressive molecules such as IL-10 and TGF-β resulting in a Treg infiltrate around the normal immune-privileged HF with lack of Teff infiltration, and Tregs are probably contributing to maintenance of the IP microenvironment by secreting immunomodulatory molecules (Figure 1.10 left panel). In the aberrant IP state (right panel), the balance between Teffs such as Th1 and Th17, and Tregs is reversed and more Teffs infiltrate the HF with low or non-functioning Treg, which could be a key event in the pathogenesis with more secretion of inflammatory cytokines such as IFN-γ and IL-17. The question, which has not been elucidated yet, is whether deficiency of Treg is the primary initiating event in IP collapse or it is secondary to the effect of inflammatory cytokines secreted by Teffs infiltrating the affected HF.

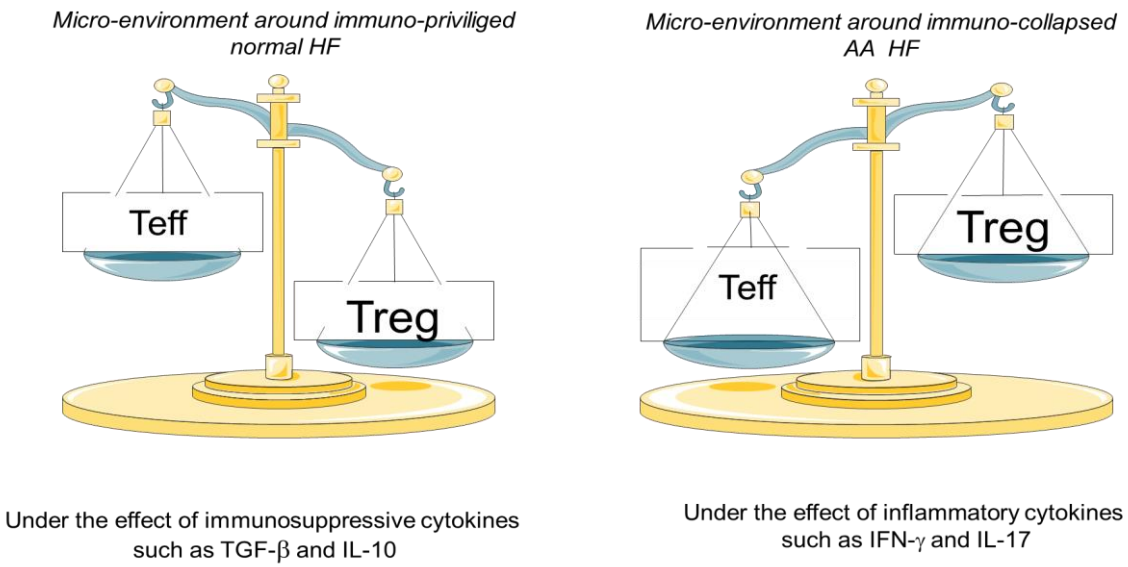

Figure 1.10. Proposed role of T-cells in IP collapse.
In normal IP state (left panel), Treg and other HF cells secret IP guardians such as TGF-β and IL-10 keeping MHC class I and II expression low, as a result, HF is devoid of inflammatory lymphocytes. In aberrant IP state (right panel), balance between inflammatory T-cells (Teff) such as Th1 and Th17 and Treg is a key event in the pathogenesis. Th1 and Th17 activation results in IFN-γ secretion leading to upregulation of MHC class I and II expression. Figure was created using Servier medical art.

One of the examples of the reciprocal correlations between inflammatory and regulatory arms of the immune system is Th17/Treg balance. Both populations differentiate under the effect of the same cytokine TGF-β, which up-regulates expression of FOXP3 and RORγt transcription factors in naïve CD4+ cells to develop Treg or Th17 cells respectively (Noack and Miossec, 2014). Although it has been found that the presence of IL-6 and IL-21 cytokines is essential to develop Th17 by TGF-β, the exact mechanism of developing Treg by TGF-β is not fully understood. Defective Th17/Treg balance has been proposed as a causative mechanism in the development several autoimmune diseases such as experimental autoimmune encephalomyelitis (Zhang et al., 2011), rheumatoid arthritis (Wang et al., 2012a) and experimental autoimmune

uveitis (Zhang et al., 2016). This correlation has not been studied in AA. Therefore, in this work, a comprehensive analysis of Teff and Treg populations in peripheral blood of AA patients will be performed.

1.4 TCR beta chain

1.4.1 Adaptive immunity

All multicellular organisms are equipped with many defence mechanisms against infectious agents such as viruses, bacteria, parasites and fungi. Innate immunity is the body's non-specific first line defence against pathogens, and is mediated by macrophages and neutrophils (Dempsey et al., 2003). This innate immunity is reliant on germline-encoded receptors to recognize microorganisms, therefore, it is not specific and can recognise a wide range of invaders that bear a common surface marker, which is conserved over the course of evolution (Janeway, 2001). In contrast, adaptive immunity is a more specialised defence mechanism mediated by lymphocytes, and is capable of specifically recognising foreign micro-organisms or molecules and selectively eliminating them from the body. The adaptive immune system relies on pathogen-specific receptors encoded by a unique genetic mechanism during lymphocyte development (Dempsey et al., 2003). The huge diversity of lymphocyte receptor molecules explains why the mammalian immune system has the ability to neutralise almost any antigen to which it is challenged. The adaptive system includes both humoral immunity mediated by B-lymphocytes and cellular immunity mediated by T-lymphocytes.

The main question in the field of immunity was how lymphocytes precisely recognise a specific antigen. Macfarlane Burnet first proposed the theory of clonal selection in 1950s to answer this question. Each naïve lymphocyte in the

blood stream has antigen receptors with a single specificity (Figure 1.11). The specificity is determined by unique genetic mechanism during their development in the thymus and bone marrow, which generates millions of different variants of the genes encoding the receptor molecules. Re-arrangements of multiple sets of profoundly similar genetic regions create numerous functional genes, which are main contributor to the huge diversity of B cell receptor (BCR) and T-cell receptor (TCR) repertoires (Jackson et al., 2013). This ensures that the millions of lymphocytes in the body collectively carry millions of different antigen receptor specificities, and that is what constitutes the lymphocyte receptor repertoire of the individual (Silverstein, 2002). Throughout an individual's lifetime these lymphocytes experience a process associated to clonal selection; those lymphocytes that encounter an antigen on which their receptor binds will be activated and differentiate into effector cells. Activation triggers a process called clonal expansion where these cells proliferate and produce many identical progeny, known as a clone (Silverstein, 2002). T-cells have a central involvement in AA pathogenesis as discussed in section 1.3.2.3, therefore, studying their receptor's (TCR) repertoire will be in the center of focus in this research.

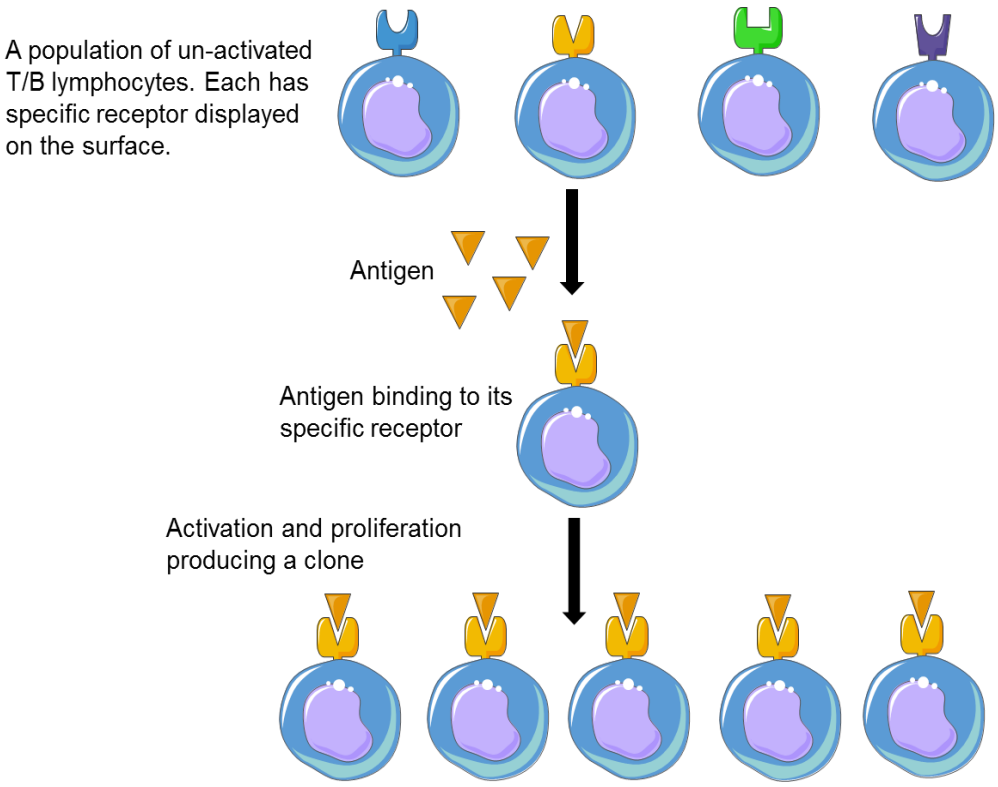

Figure 1.11. A theory of clonal selection.

Naïve lymphocytes differ in their antigen specificity based on somatic rearrangement of their receptors. Upon encountering antigen, the antigen binds to its specific receptor on the naïve cell resulting in its activation and proliferation of a single cell producing more lymphocytes expressing identical surface markers (clonotype) in a process called clonal expansion. Figure was created using Servier medical art.

1.4.2 Structure of T-cell receptor (TCR)

Unlike B-cells that mature in the bone marrow, naïve T-cells migrate to the thymus where they mature by expressing a unique antigen-binding receptor on their cell membrane called the T-cell receptor (TCR) (Tonegawa, 1983). While B-cells produce membrane-bound antibodies that recognise the antigen alone, the TCR recognises the antigen only when it is associated to cell-membrane proteins (MHC class I and class II). These molecules are expressed on the surface of antigen presenting cells (APC) such as macrophages, DCs, cancer cells, virus-infected cells or self-cells (Kuby, 1997).

First, it is important to understand the TCR structure and function (Figure 1.12). The TCR is a transmembrane glycoprotein, which consists of disulphide-linked heterodimer proteins. In most T-cells, the heterodimer is composed of α and β chains; while in small proportion of T-cells (about 5%), it is composed of γ and δ chains. The carboxyl terminal of each chain is characterised by a highly conserved sequence named constant region (C), while the amino domain exhibits high variability and is referred to as the variable region (V).

The C region includes constant domain (C), hinge domain (H) composed of a short connecting sequence containing cysteine residues involved in disulphide bonding of the two chains of TCR heterodimer, followed by a 21-22 amino acids sequence anchoring each chain into the plasma membrane and called the transmembrane region (T_m), and finally the cytoplasmic tail (C_t) of 5-12amino acids at the carboxyl-terminal of each TCR chain (Kuby, 1997) (Figure 1.13).

The amino acids of the C region are encoded by the C gene segment, which is comprised of four exons encoding for C and H domains as well as T_m and C_t regions. The V domain of the TCR is preceded by a signal sequence, which is also called the leader peptide (L) that attaches the nascent receptor polypeptide to the endoplasmic reticulum during the process of protein assembly (Kuby, 1997).

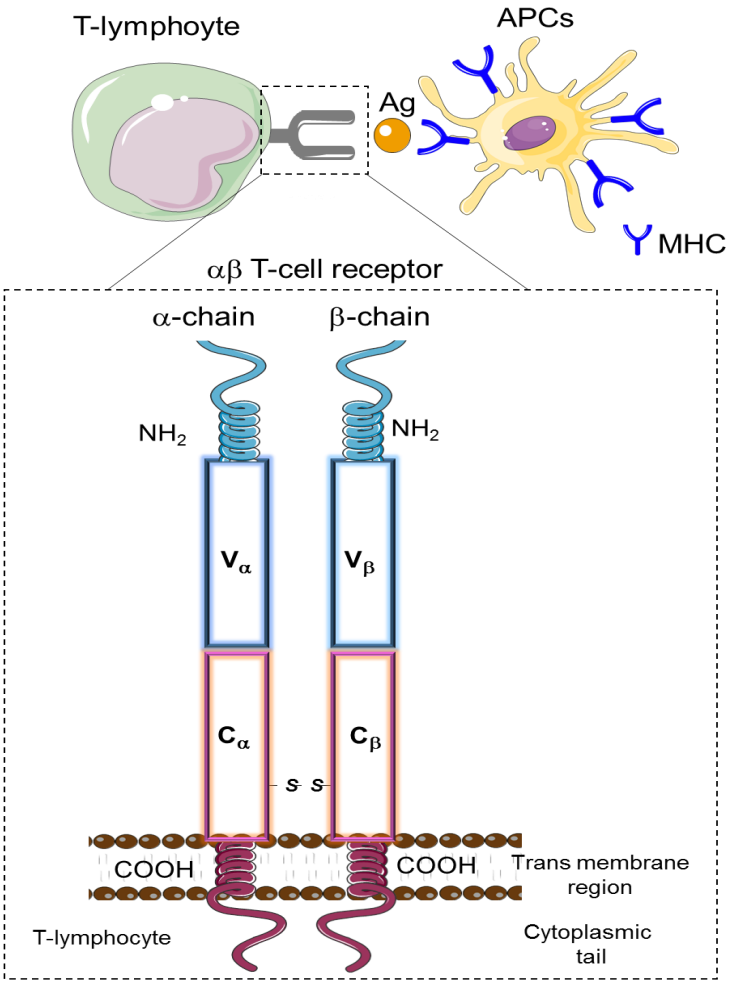

Figure 1.12. Schematic diagram illustrating TCR structure and function.
The TCR recognises antigen associated with MHC molecules on the surface of the cell. It consists of α and β chains connected by a disulphide bond, and each of them contains two domains. The amino-terminal domain (NH_2) exhibits sequence variation and referred to as V region while the sequence in the carboxyl domain (COOH) is conserved and known as C region. Figure was created using Servier medical art.

The V domain has three hyper-variable regions equivalent to Complementarity-Determining Regions (CDRs) in immunoglobulin chains, known as CDR1, CDR2 and CDR3. The antigenic specificity of the TCR is determined by these CDRs, while CDR1 and CDR2 (encoded by germline DNA) mainly fix the TCR to the MHC platform; CDR3 is the highly variable region,

which mainly engages the solvent-exposed chain of MHC bound peptides (Davis and Bjorkman, 1988, Kuby, 1997).

The V_α region is generated from rearrangement of two coding segments variable V and joining J segments while V_β is generated from rearrangement of three coding segments V, J and diversity D. Diversity of TCR repertoires is generated through processes of V(D)J recombination during lymphoid differentiation (Davis and Bjorkman, 1988). Interestingly, this diversity is focused in CDR3, which is the main contact domain that interacts with the MHC presented antigenic peptide while CDR1 and CDR2 attach to the MHC residues (Davis and Bjorkman, 1988) . As VDJ recombination is the main mechanism that mediates CDR domains diversity, it will be discussed in more detail in the next section.

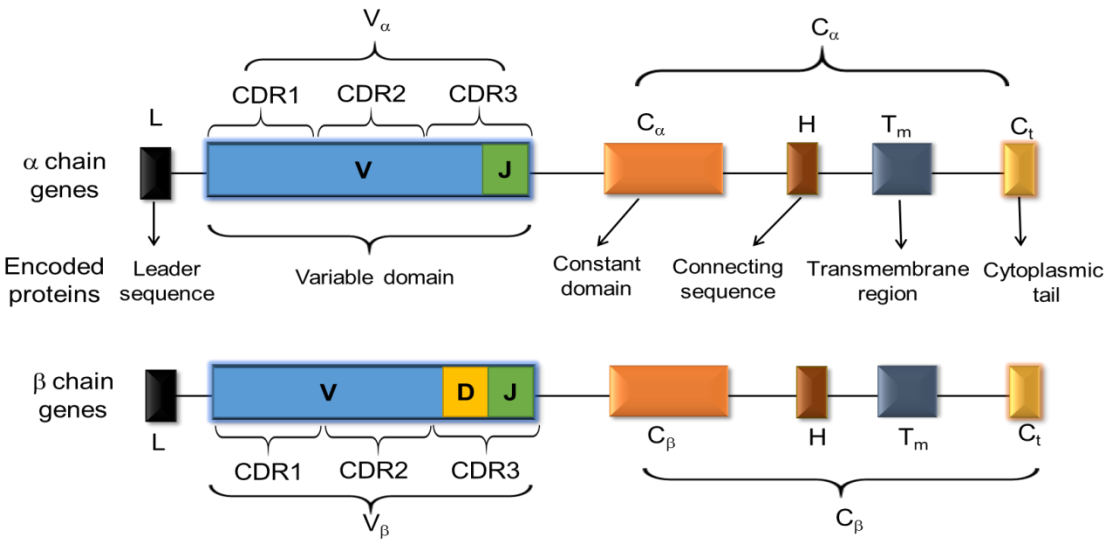

Figure 1.13. TCR proteins and genes.
The V domain is a highly variable peptide generated by somatic rearrangement of variable (V) diversity (D) and joining (J) genes in the β chain while it is generated by rearrangement of V and J segments in a chain. The C region in both α and β chains consists of C domain, connecting segment H, Transmembrane region T_m and Cytoplasmic tail C_t encoded by germline conserved genes. Figure was created using Servier medical art.

1.4.3 V(D)J recombination

V(D)J recombination is a vital process in the adaptive immune system to generate the diverse repertoire of T-cells required for antigen recognition. In the absence of this process, the immune system is compromised (Hodges et al., 2003). Each developing T-cell generates a novel pair of variable regions of their cell surface receptor by recombination between three gene segments V, D and J at the level of genomic DNA during early lymphoid differentiation in the thymus (Tonegawa, 1983). This results in a novel amino acid sequence in the TCR antigen-binding site accounting for the specificity of each T-cell (Janeway, 2001). The mechanism of gene assembly is almost similar in all peptide chains of TCR except that of α and γ chains lacking the D gene segment, however, the explanation in this section will be referred to the TCR β-chain for simplicity and because the CDR3 region of the β-chain accounts for most of the variation within an individual's T-cell repertoire (Laydon et al., 2015). The gene encoding the TCRB is located on chromosome 7 at the 7q32–35 locus (Caccia et al., 1984). The TCRB locus (Figure 1.14.A) comprises TCRBV families, which are grouped into 40-42 functional families with greater than 80% nucleotide sequence identity (Arden et al., 1995, Kuby, 1997). The TCRB locus also contains two C genes and two D gene segments. Each D gene segment is associated with upstream J genes consisting of 13 J segments, referred to as J_1S1 to J_1S6 and J_2S1 to J_2S7 (Arden et al., 1995).

The process of V(D)J recombination in the TCRB gene involves random rearrangement of three gene segments V, D and J in two separate steps. First, DJ segments are brought together, which is followed by recombining the V gene segment with the newly rearranged DJ block (Willerford et al., 1996) (Figure 1.14.B). Somatic recombination is directed to the appropriate site by recognition

of specific DNA sequence motifs called recombination signals sequences (RSSs) that flank TCR recombining genes. These motifs are formed of two blocks of conserved sequences of nonamer (ACAAAAACC or GGTTTTTGT) or heptamer (CACAGTG or GTGTCAC) found in the noncoding region flanking each V, D or J gene segment (Roth and Craig, 1998).

Recombination is catalysed by a set of enzymes that are also involved in DNA repair such as RAG1, RAG2, and TdT (Bassing et al., 2002). Recombinase enzymes known as recombination activity gene 1 and 2 (RAG1 and RAG2) recognize RSSs (McBlane et al., 1995). In the TCRB gene, RAG1 and RAG2 first form a complex with RSSs flanking D and J genes bringing them together and forming a hairpin loop of intervening nucleotides (McBlane et al., 1995, Roth and Craig, 1998) as illustrated in Figure 1.14.C. A 5nick is then introduced by RAG1 and RAG2 at the 5 end of RSS heptamer causing deletion of the intervening loop of DNA and generates a double strand break that is consequently repaired by V(D)J recombinase enzymes brining the D and J segments together (van Gent et al., 1996, Roth and Craig, 1998). The same process is repeated when joining the V gene segment to the newly rearranged DJ block (Hodges et al., 2003).

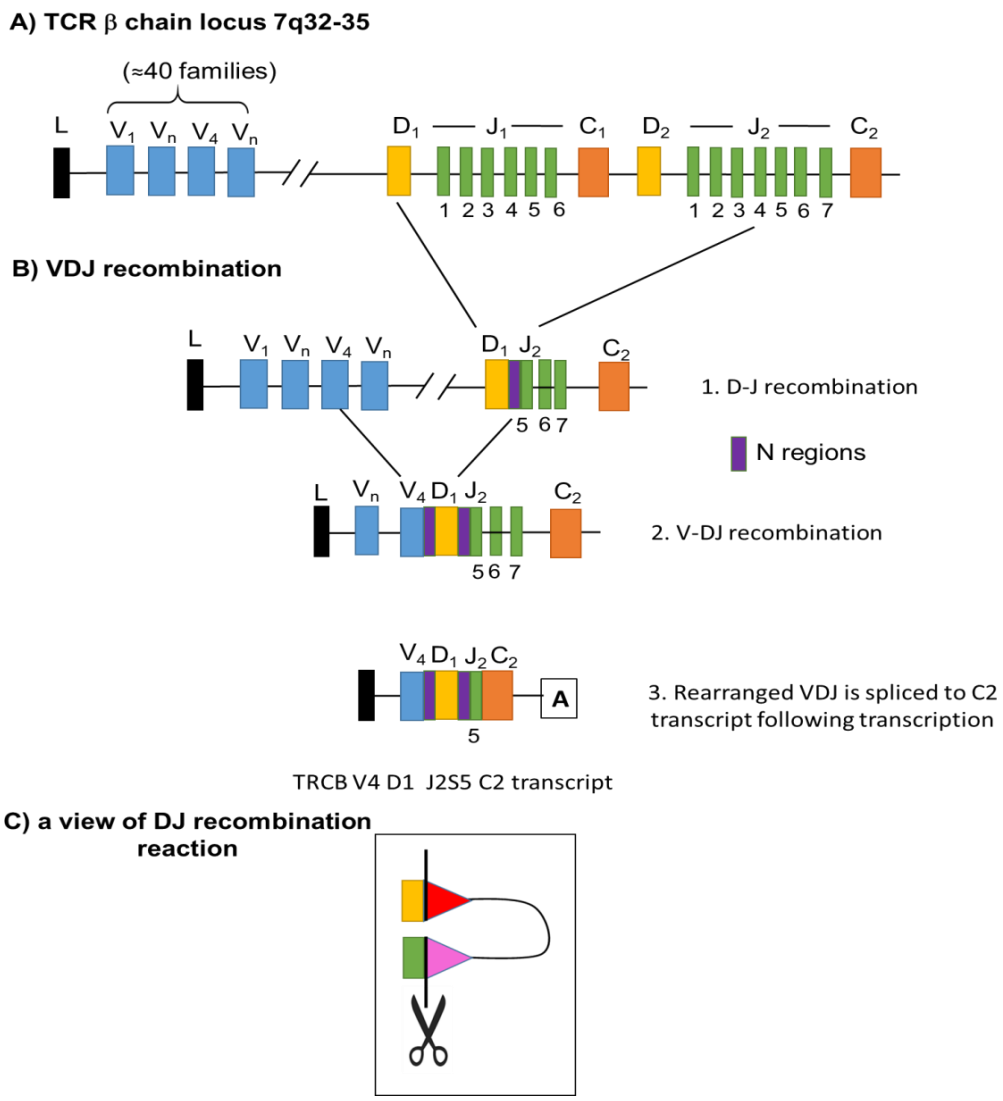

Figure 1.14. Germline organisation of the TCRB gene and explanatory example of its somatic rearrangement.

A) Schematic representation of TCRB locus including V gene families (blue) and 2 D genes (yellow), 2 C gene segments (orange) and 2 J gene segments with S1-6 in J1 and S1-7 in J2 (green). B) Schematic representation of VDJ recombination with explanatory example of one of the possible recombinations. The recombination in TCRB takes place into two steps. First, the D gene segment combines with the J segment then the V gene segment combines with the newly rearranged DJ gene. Secondly, the rearranged VDJ segment is then spliced post transcriptionally to the C transcript that contains poly A tail. N nucleotides (purple) are inserted during the recombination process. C) A cartoon view of a DJ recombination reaction. D segments (yellow) are flanked by RSSs with 12 bp-long spacers (red), while the J segments are flanked by RSS with 23 bp-long spacers (pink). Breaks are introduced directly between the heptamer and the coding sequence, and a DJ block is formed between a V and C segment (Market and Papavasiliou, 2003) leaving the intervening nucleotide including RSSs and their the spacers sequences.

Diversity is not only generated by the recombination but also by nucleotide addition and deletion that occurs at the junction sites during the recombination process such as incorporation of a short palindromic repeat (P-nucleotides) at the recombining edges (Janeway, 2001). Diversification is further increased by (N-diversity mechanisms), which include incorporation of template independent GC rich nucleotides called N-nucleotides via the action of terminal deoxynucleotidyl transferase (Tdt) (Gilfillan et al., 1993, Cabaniols et al., 2001) as well as exonuclease trimming of the recombining gene ends causing loss of some nucleotides (Pannetier et al., 1993). Furthermore, the combinatorial association of individual TCRA and TCRB chains in $\alpha\beta$ T-cells is adding to the diversity producing a vast number of unique TCRs that can recognise huge array of antigens in specific manner.

The small number of genes encoded for TCR have the potential to generate vast number of clonotypes estimated between 10^{15} to 10^{20} (Hodges et al., 2003). Although the process of recombination is thought to be random, there are some clonotypes that are common and shared between individuals more than others, known as public clonotypes (Laydon et al., 2015). Due to the difficulty in studying such huge numbers of rearrangements and the importance of CDR3 in antigen recognition, studies of TCR repertoire have focused strongly on the diversity of CDR3, which is the MHC-binding region. Furthermore, the CDR3 region of the β-chain accounts for most of the variation within a person's T-cell repertoire, which will be the focus of the next generation sequencing work in this thesis.

1.5. EGCG as potential treatment for AA

Green tea (*Camellia sinensis*), a commonly consumed beverage, has shown to have many health promoting effects. Catechins constitute about 40% of the dry weight of green tea. Epigallocatechin-3-gallate (EGCG) is the major catechin in green tea, constituting 60% of the total catechin (Yang et al., 2002). EGCG is a polyphenolic flavonoid ($C_{22}H_{18}O_{11}$ of average molecular mass 458 Da) (Figure 1.15) with anti-inflammatory, anti-oxidant and anti-tumour properties.

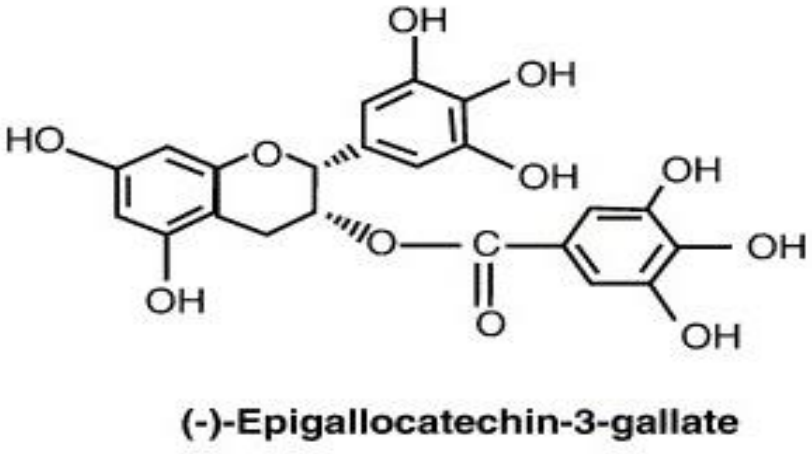

Figure 1.15. Chemical structure of EGCG.
A polyphenol with chemical formula: $C_{22}H_{18}O_{11}$ and average molecular mass: 458.372Da.

1.5.1 Anti-inflammatory effect of EGCG

EGCG has been proposed as an anti-inflammatory molecule for treatment of inflammatory and autoimmune conditions such as rheumatoid arthritis (Ahmed, 2010, Yang et al., 2014), diabetes (Wolfram et al., 2006), ocular inflammation (Cavet et al., 2011) and experimental autoimmune encephalomyelitis (EAE) (Aktas et al., 2004). EGCG was found to have an inhibitory effect on IFN-γ signalling via the JAK-STAT pathway. It reduces STAT-1 translocation into the nucleus through inhibiting its phosphorylation. Furthermore, down-regulation of JAK1 and JAK2 enzymes has been achieved

by EGCG in human oral cancer cell lines (Cheng, 2007). Similarly, a STAT-1 inhibitory effect of EGCG was reproducible in a study on colorectal cell lines (Ogawa et al., 2012).

EGCG was also shown to inhibit T-cell proliferation through impeding IL-2 utilisation (Pae et al., 2010). In Wu et al. study, EGCG at 2.5-10μM concentration inhibits T-cell proliferation in primary T-cells isolated from C57BL mouse spleen by inhibiting cell division and cycle and IL-2 signalling (Wu et al., 2009). A similar experiment in human subjects was performed by Katiyar (1999) by applying EGCG cream topically (3 mg EGCG on 2.5 cm^2) to normal volunteers' skin. The EGCG was applied 30 min before UVB exposure and an inhibitory effect of EGCG on UVB induced leukocyte infiltration (neutrophil, monocytes and macrophage) was observed (Katiyar et al., 1999).

EGCG also has shown a stimulatory effect on Treg differentiation from naïve CD4+ T-cells via inducing FOXP3 expression with subsequent upregulation of IL-10 (Wong et al., 2011) and enhancing the naïve CD4+ T-cell differentiation toward the regulatory pole was also attributed to its inhibitory effect on STAT-1 and STAT-3 (Wang et al., 2013a).

1.5.2 Safety profile of EGCG

No adverse effects have been recorded in human healthy volunteers after oral administration of 800mg daily of EGCG for 4 weeks, which is equivalent to EGCG content of 6-18 cups of tea daily giving EGCG a good dose safety margin (Chow et al., 2003). Additionally, EGCG is available in topical preparations with a good skin penetration index, to minimize any possible systemic side effects theoretically (Scalia et al., 2014), nonetheless, the evidence on its safety as topical application is limited. These features support EGCG as a potential AA therapeutic candidate to investigate.

A study on the safety and tolerability of systemic administration of ascending doses of pure EGCG has also reported that catechin was well tolerated in healthy human volunteers at doses of up to 1.6g/day (Ullmann et al., 2003). No changes in cardiovascular physical findings and clinical chemistry was observed in those volunteers. However, it is noteworthy that EGCG has poor bioviability as it is metabolised extensively in intestine and liver (Scalbert et al., 2002), so doses shown to have health promoting effect ranging (10-1000 μM) cannot be achieved by ingesting two to three 200 mg capsules or drinking green tea (Nagle et al., 2006).

1.5.3 Topical formulation of EGCG

Using EGCG topically is encouraged by its good dermal penetration characteristics mainly due to its low MW (458.372Da) (Bos and Meinardi, 2000). Also, EGCG binds to the lipid bilayer (Sun et al., 2009) and its keratin binding is mediated by a group of hydrogen bonding, hydrophobic and aromatic interactions (Marzinek et al., 2013) contributing its good intradermal permeation. However, the transdermal permeation is observed to be less than intradermal permeation when 10mg/cm^2 formulation containing 6% green tea extract emulsion was applied to human Caucasian skin for 24hrs. EGCG recovery was measured 0.54 and 0.38μg/cm2 by HPLC in the epidermis and dermis respectively (Dvorakova et al., 1999, Dal Belo et al., 2009). Improving the limited transdermal penetration was achieved by incorporating nano-particles; for instance, catechins loaded chitosan particles resulting in a significant improvement of skin permeation and reduced its enzymatic digestion (Wisuitiprot et al., 2011) indicating the potential use of topical EGCG for AA treatment in the future. EGCG stability was another major concern for further clinical use, which was addressed by Alberts's group. EGCG formulations

supplemented with 0.1 or 0.5% butylated hydroxytoluene (BHT) was highly stable when stored at 4°C as BHT prevents EGCG oxidation (Dvorakova et al., 1999).

In vivo, five different EGCG topical preparations (emulsion or gel) have been tested for their photo-stability and skin permeation. 1% o/w EGCG emulsion (containing 1.5% cetearyl alcohol, 1.5% glyceryl monostearate, 5% sweet almond oil, 5% cetearyl isononaoate, 0.5% dimethicone, 0.8% phenonip, 5% montanov, 5% propylene glycol, 0.1% EDTA, 0.1% sodium dehydroacetate) showed the least photo-degradation and best skin penetration. The percentage of EGCG permeated into stratum conreum particularly to the deeper layers was about 36% of the applied dose as measured *in vivo* by direct HPLC using a tape stripping method after 60mins of EGCG emulsion application (Scalia et al., 2014).

In skin conditions, EGCG has been applied topically with a significant UVB protective effect. EGCG cream (3mg EGCG in 100μl acetone on 2.5cm^2) was topically applied to normal volunteers' skin 30 min before UVB exposure (Katiyar et al., 1999). EGCG significantly reduced the UVB induced erythema as reflected by the chromometer readings, as well as leukocyte infiltration, which was observed as reduced myeloperoxidase MPO activity, compared to UVB only exposed skin. Yoon et al. (2013) have used 1% EGCG solution in 3% ethanol vehicle showing a significant improvement of acne vulgaris in an 8-weeks randomized split-face clinical trial (Yoon et al., 2013).

To sum up, the molecular targeting of key pathways and cells involved in AA pathogenesis and the availability of EGCG topical creams with a good penetration index and cost-efficiency make EGCG a promising therapeutic

candidate in AA, however, limited evidence on its safety as topical preparation should be considered.

1.6 Hypotheses and objectives

Hypothesis 1

Disrupted balance between regulatory and inflammatory T-cells is the main driver of IP collapse in HF.

Objectives

A- Determine the phenotypic profile of T-cells in AA patients' peripheral blood with detailed focus on regulatory T-cells.

B- Perform molecular analysis of the T-cell receptor to determine whether there is an expansion of a particular clone of T-cells in AA that would suggest antigen-dependent T-cell activation.

Hypothesis 2

Inhibiting inflammatory cells and enhancing Treg function can be mediated by blocking the JAK-STAT pathway with EGCG.

Objectives

A- Optimise the EGCG dosage *in vitro*.

B- Construct an IFN-γ–induced cellular model to induce JAK-STAT pathway.

C- Study the effect of EGCG on the IFN-γ signalling pathway (JAK-STAT) and regulatory molecules involved in AA pathogenesis.

Chapter 2 . Material and Methods

2.1 Reagents and buffers

2.1.1 Chemicals and reagents

Table 2-1. Chemical and reagents.

Material	Cat no./Source
Dimethyl sulfoxide (DMSO)	D8418, Sigma
Foetal bovine serum (FBS)	FB-1090, Biosera
Ethylene-Diamine-Tetra-Acetic acid (EDTA)	03701, Sigma
Trypsin-EDTA	T3924, Sigma
Tris base	T1503, Sigma
Bovine serum albumin (BSA)	A9418, Sigma
Analytic grade solvents Ethanol and Methanol	459836, 82762 Sigma
Iso-propranol	I9516, Sigma
Chloroform	372978, Sigma
Glycine	G8898, Sigma
Skimmed milk powder	70166, Sigma
Sodium dodecyl sulfate (SDS)	L4390, Sigma
Tween 20	P2287, Sigma
Serum-free blocking buffer	DAKO

2.1.2 Buffers

Media: purchased from Lonza: Roswell Park Memorial Institute (RPMI) 1640 medium supplemented with L-glutamine (BE-12-702F) and Dulbecco's modified Eagle's medium (DMEM) high glucose medium supplement with L-glutamine (BE-12-604F). The media was supplemented with 10% foetal bovine serum FBS unless stated otherwise. As all cell culture work was performed

under strict aseptic conditions, antibiotics were not required unless primary cells were used, when 1% Strep/Pen (Gibo) was added to the medium.

Phosphate buffered saline (PBS): Used as a wash solution throughout this work, PBS tablets (P4417) were purchased from Sigma where one tablet dissolved in 200 mL of deionized water to give 0.01M phosphate buffer, 0.0027 M potassium chloride and 0.137M sodium chloride, pH 7.4. For cell culture purposes, sterile BioWhittaker 1X PBS without Ca++ Mg++ or phenol red (BE-17-516F) was used.

PBS-EDTA: PBS supplemented with Ethylene-Diamine-Tetra-Acetic acid (EDTA) (BE02-017F) was purchased from Lonza to enhance HaCat cell detachment prior to trypsinisation.

Freezing media: Used for cell cryopreservation and prepared on ice from 40% FBS and 10% DMSO.

Phosphate buffered saline (TBS): 10X TBS was prepared for use in western blotting by dissolving 24.4 g Tris-HCl and 80 g NaCl in 1 litre of deionised water to obtain a buffer containing 50 mM Tris-Cl and 150 mM NaCl> The pH was adjusted to 7.5 with 1M HCl

Tris-buffered saline Tween 20 (TBST): 1X TBST used in western blot was prepared by diluting 100 ml 10 × TBS in 1 litre of deionised water and adding 1 ml of Tween 20.

FACS wash buffer: used in the flow-cytometry experiment washing steps was prepared by dissolving 1g bovine serum albumin (BSA) (A9418, Sigma) in 100ml PBS.

4% Paraformaldehyde: was used to fix the cells after flow-cytometry staining and was prepared by dissolving 4 g paraformaldehyde (P6148-500G, Sigma) in100ml of PBS pre-heated to 60^{o}C in ventilated hood. The pH was adjusted to

7 and the solution was then aliquoted and frozen or could be stored at 2-8 °C for up to one month.

Trypan Blue: (T6146, Sigma) was used to determine cell- viability.

PBS/0.3% Triton X-100: 100 ml of the buffer was prepared by adding 300 µl Triton™ X-100 to 100 ml 1X PBS.

PBS/0.15% Triton X-100: 100 ml of the buffer was prepared by adding 150 µl Triton™ X-100 to 100 ml 1X PBS.

2.2 Blood samples

2.2.1 Blood donors

The study was reviewed and approved by the Institutional Review Boards and ethics committees at the University of Sheffield (LREC reference number 002651) and Sheffield Teaching Hospitals (NHS permission reference number STH18941). Twenty patients with active hair loss and an established diagnosis of AA, were recruited and consented at the Department of Dermatology, Royal Hallamshire Hospital, Sheffield, UK. Patients diagnosed with other autoimmune diseases or receiving immunosuppressive drugs were excluded from the study. The cases recruited included 9 with patchy AA, 5 with alopecia totalis, and 6 with alopecia universalis. Ten healthy controls were recruited at the University of Sheffield. Patients and healthy controls were age-matched and were all female of Caucasian ancestry, 18 years or over.

2.2.2 Separation of peripheral blood mononuclear cell (PBMC)

Peripheral blood mononuclear cells (PBMCs) were isolated from heparinised venous blood by density gradient purification using Lymphoprep as described by the manufacturer (07801, Stem Cell). Briefly, 10ml of fresh whole heparinised blood was diluted with an equal amount of PBS supplemented with

2% FBS, and carefully overlaid on top of 15ml Lymphprep medium. Samples were then centrifuged at 800Xg for 20mins at room temperature (RT); mononuclear cells (the buffy coat layer) at the plasma-Lymphoprep interface (Figure 2.1) were then collected and washed once. Viable PBMCS were counted using Trypan blue and processed immediately for flow-cyometry or frozen for use in other applications.

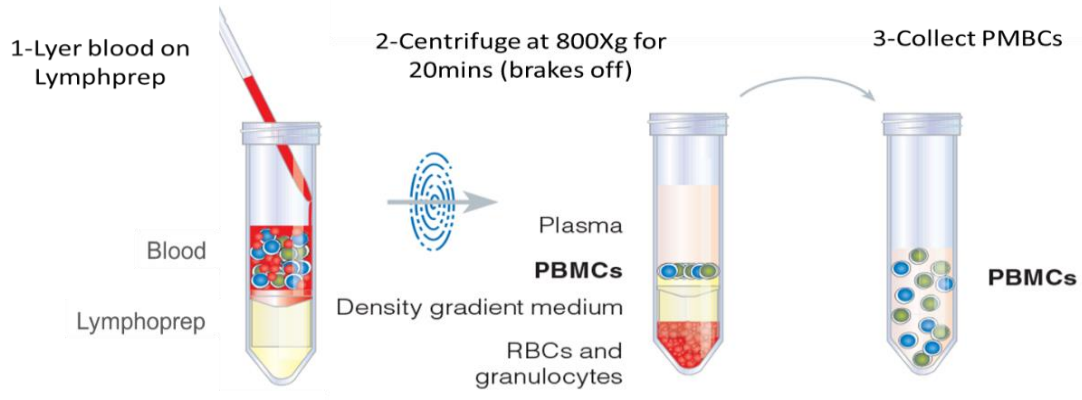

Figure 2.1. PBMCs separation protocol using Ficoll gradient protocol. (adapted from StemCell technologies Image with permission).

2.3 Cell culture

All cell culture work was performed under aseptic conditions in a laminar flow hood.

2.3.1 Cell lines

A human keratinocyte cell line (HaCat), derived from normal adult male skin, was kindly provided by Professor Sheila McNeil, Department of Materials Science and Engineering, University of Sheffield, and maintained in high glucose DMEM at 5-100% confluence. A human lymphocyte cell line (Jurkat), which was originally derived from T-cell leukaemia patient, was selected as a model of T-cells (Jurkat, Clone E6-1. ATCC TIB-152) and was kindly provided by Mrs Vanessa Singleton, Department of Infection and Immunity and

Cardiovascular Disease, University of Sheffield, and maintained in RPMI 1640 at a cell density of 2-10 $x10^5$. For both cell lines, the media was supplemented with 10% foetal bovine serum (FBS, Gibco- BRL) and cells were maintained at 37°C in an atmosphere of 5% CO_2. The cell culture work was performed under aseptic conditions in a laminar flow hood. The colony morphology of the cell lines demonstrated in Figure 2.2.

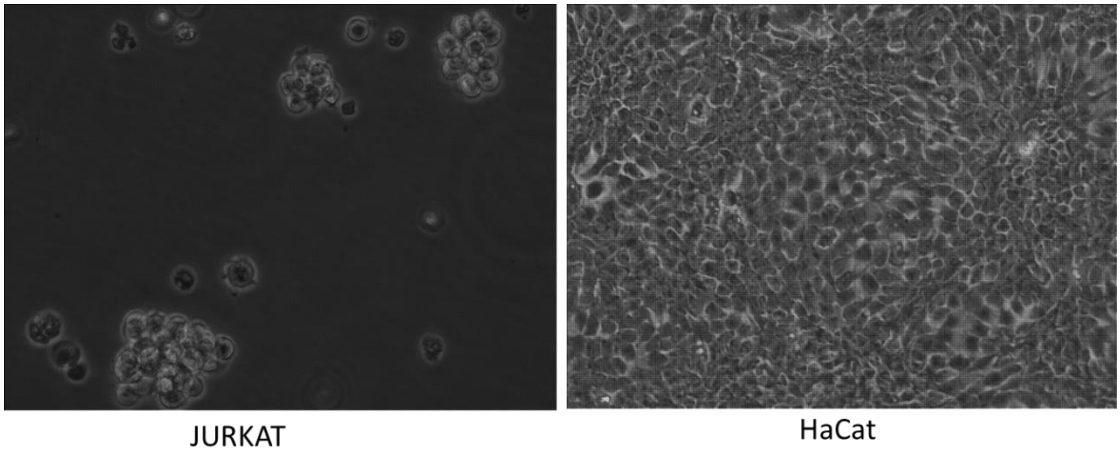

Figure 2.2. Jurkat and HaCat cells morphology.
On the left, Jurkat cells appeared as rounded cells and tend to clump forming grape-like colonies, image at x20 magnification. On the right, HaCat cells appeared with polygonal morphology and forming a confluent monolayer imaged at 10x magnification. Images were captured by digital inverted microscope Evos XI core (AMG, WA, U.S.A).

2.3.2 Freezing

For long-term storage, cells were cryopreserved in liquid nitrogen (≤-150°C). A generic freezing protocol was used to lower the temperature gradually. 1-5 x 10^6 cells were re-suspended in 500μl of the appropriate growth medium (DMEM for HaCat or RPMI-1640 for Jurkat/PBMCs) supplemented with 10% FBS. 500μl of freezing medium was prepared from 400μl (40% v/v) FBS and 100μl (10%v/v) dimethyl sulfoxide (DMSO) (D8418, Sigma). DMSO is a cryo-protective agent and is used in order to minimise cellular damage during the freezing process. Freezing medium was added slowly to the cell suspension on

ice. Cells were stored at -80°C overnight prior to transfer to liquid nitrogen (≤-150°C).

2.3.3 Thawing

A fast thawing procedure was followed in order to minimise any toxic effects of DMSO. First, cells were warmed briefly in a water bath heated to 37°C and then diluted with 5ml of pre-warmed growth media. The cell suspension was then centrifuged for 5mins at 1500rpm, the supernatant was discarded and an appropriate volume of growth medium was added to allow cell growth.

2.3.4 Cell maintenance

Cells were maintained so as not to exceed 90-100% confluence (for HaCat) or $1x10^6$ per ml (for Jurkat and PBMCs) and then harvested, or sub-cultured, according to the intended downstream application. For HaCat cells, cells were passaged twice a week. To detach these adherent cells, they were first washed once with PBS to remove any excess FBS, then incubated in PBS-EDTA for 10 mins at 37°C to facilitate detachment. The PBS-EDTA was then discarded and the cells were incubated with trypsin-EDTA for 3 to 5 mins at 37°C (Hoornstra et al., 2013). The cells were dislodged and the trypsin was deactivated by adding fresh media. Finally, the cell suspension was centrifuged and the pellet washed once with medium before being seeded at the desired density. For Jurkat passaging, the cell suspension was spun and the pellet was re-suspended in RPMI-1640 at the desired density. Unless otherwise stated, PBMCs were maintained in CD3/CD28 beads (Dynabeads human T-cell activator CD3/ CD28) at 1:1 bead-to-cell ratio as recommended by the supplier (111.61D, Invitrogen) in presence of 30U/ml rIL-2 (200-02, Peprotech). Cell density was assessed by automated cell counter (TC20, BioRad) for cell suspensions and by light optical microscopy (Olympus, U-PMTVC, 2D0843,

Japan) for adherent cells. Cell incubation was performed at 37°C and 5% CO_2 in humidified air.

2.3.5 Viability assay by Trypan Blue

Trypan blue dye identifies nonviable cells by penetrating the damaged cell membranes to change their colour to blue (Wiegand and Hipler, 2008). For the trypan blue analysis, HaCat cells were trypsinised as described previously and Jurkat or PBMCs were directly collected from the suspension. An aliquot of 10 µl of each sample was then mixed with 10 µl of trypan blue solution (T6146, Sigma) and incubated at RT for 1-2 mins. Nonviable and viable cells in a 10 µl aliquot of each sample were identified and counted in an automated cell counter (Automated Cell Counter TC10, BioRad, Hercules, CA, USA).

2.3.6 IFN-γ Induced model

In order to induce STAT-1 phosphorylation, cells were activated with IFN-γ .The cells were seeded at densities of $5x10^5$ per well in 6-well plate (HaCat), $2x10^5$ per ml in a T25 flask (Jurkat) or at $5x10^5$ per well in 6-well plate for PBMCs isolated from healthy control peripheral blood. After an overnight incubation, the cells were stimulated with 50 IU/ml (HaCat) or 100 IU/ml (Jurkat/ PBMCs) recombinant human IFN-γ (300-02, Peprotech) or left un-stimulated as a control for each batch. The optimal dosage that can induce STAT-1 phosphorylation without affecting cell viability and growth was selected based on an optimisation experiment where cells were incubated with a range of IFN-γ concentrations 10, 20, 50, 100, 200 IU/ml for 24, 48 or 72hrs.

2.3.7 Treatment with EGCG

EGCG (E4143, Sigma) was dissolved in distilled water to give a 10mM stock solution as recommended by the supplier. Cells, pre-activated with IFN-γ,

were treated with 20 or 40μM EGCG for 24 or 48hrs before being harvested for RNA or protein assays. For AA patient samples, PBMCs were seeded at a density $5x10^5$ per well in 6-well-plate plate and incubated with 40μM EGCG for 48hrs without any prior induction with IFN-γ. Before selecting the mentioned dosage, an optimisation experiment was performed to assess the toxicity of EGCG on the cells. After an overnight incubation of HaCat or Jurkat cells, they were treated with serial concentrations of ECGC 10, 20, 40, 60 and 100μM for 24 or 48hrs, and the toxicity of EGCG was assayed with trypan blue (Singh and Katiyar, 2013). At the end of incubation period, trypan blue was added to 10μl of the cell suspension (1:1) and the cell count and percentage of live cells were measured by automated haemocytometer. Each experiment was performed in triplicate and the cytotoxic effect of EGCG was presented as a mean and SD. Morphological changes were examined using a Leica AF6000LX inverted microscope.

2.4 Flow-cytometry

2.4.1 Flow-cytometry staining

A multicolour flow-cytometry technique was used to analyse the circulating inflammatory and regulatory T-cells. Freshly isolated PMBCs were stained with two panels of antibodies in two separate tubes: the first panel was to look at the subsets of effector/inflammatory T-cells (Teff panel), and the other was to investigate the Treg subtypes (Treg panel) (Tables 2.2 and 2.3). Briefly, 1-2 $x10^6$ PBMCs were incubated for 30mins at RT with viability stain (blue fixable live/ dead dye); the cells were then washed once with phosphate buffered saline (PBS) and incubated for 30mins at 4°C with antibodies targeting surface markers in each panel. The cells were washed and fixed and permeabilised in

1ml fix/ perm buffer (Transcription buffer set, 562725, BD) for 40-50 mins at 4°C. They were then transferred to fix/ wash buffer for a further wash and incubated with antibodies specific to intracellular antigens, FOXP-3, IL-10, TGF-β or IL-17, for 40-50 mins at 4°C. Extracellular and intracellular antibodies were added to the cells at a 1:100 dilution. Finally, the cells were fixed in 2% PFA and the staining was visualised by BD LSR II (Becton Dickinson, Heidelberg, Germany).

Table 2-2. Teff panel: Summary of the flurochrome-conjugated antibodies used to analyse the frequency of inflammatory T-cell subsets in PBMCs.

Flurochromes/ Antibodies	Purpose	Catalogue no	Supplier
Live/Dead Blue	Dead cell exclusion	L23105	Thermo-Fischer
BUV496-Anti-CD3	Generic lymphocyte marker	564809	BD
BV421- Anti-IL17	Th17 cells maker	562933	BD
BV510 –Anti-CD4	Generic T helper marker	562970	BD
BB515-Anti-NKG2D	Activated CD8	564566	BD
PE-Anti-CD119	Th1 marker	558937	BD
PE-CF594-Anti CD8	Cytotoxic T-cells	562282	BD
PECy7-Anti-CD25	Treg gating	557741	BD
AF647-Anti-FOXP3	Treg marker	560045	BD
APC-CY7-Anti-CRTH2	Th2 marker	303523	Biolegend

Table 2-3. Treg panel: Summary of the flurochrome conjugated antibodies used to analyse Treg subtypes in PBMCs.

Flurochromes/ Antibodies	Purpose	Catalogue no.	Supplier
Live/Dead Blue	Dead cell exclusion	L23105	Thermo-Fischer
BUV496-Anti-CD3	Generic lymphocyte marker	564809	BD
BV510 - Anti- CD4	Generic T helper marker	562743	BD
PECy7 Anti- CD25	T-cell activation/ Treg identification	557741	BD
AF647 Anti- FOXP-3	Treg identification	560045	BD
APC-H7-Anti-CD45RO	Maturation/Differentiation	561137	BD
PE Anti- LAG3	Treg suppressive marker	565616	BD
PE-CF594 Anti- IL-10	Immunosuppressive cytokine	562400	BD
PercP-5.5 Anti-TGF-β	Immunosuppressive cytokine	562423	BD
BB515- Anti- CD39	Treg suppressive marker	565469	BD
BV421-Anti-HLA-DR	Treg suppressive	562970	BD

2.4.2 Flow-cytometry analysis

On LSRII, about $5x10^5$ events were acquired for each sample, and further gating was performed to determine frequency of T-cell subpopulations. For analysis, first, lymphocytes were gated based on their scatter properties in terms of forward scatter (FSC) and side scatter (SSC), which represent cell size and granularity respectively (Figure 2.2.A), then doublet cells were excluded from the analysis based on the FSC and voltage pulse height and area (FSC-H/FSC-A) as cells with higher area represent double cells or clumps, which could be misinterpreted as false positives (Figure 2.2.B). Dead cells were excluded based on the live-dead dye signal on UV-450/50 (Figure 2.2.C). At this point, the population of live single lymphocytes was analysed and the positive population for each marker was gated based on florescence minus one control (FMO) (Roederer, 2002, Tung et al., 2007). The FMO control includes all antibodies

used in the panel apart from the one of interest (Figure 2.2.D). Unstained, single cell controls and compensation controls were used to set up the experiment and a detailed analysis of the samples was performed on Flow Jo software to calculate the percentage of targeted T-cell subpopulation out of the parent population.

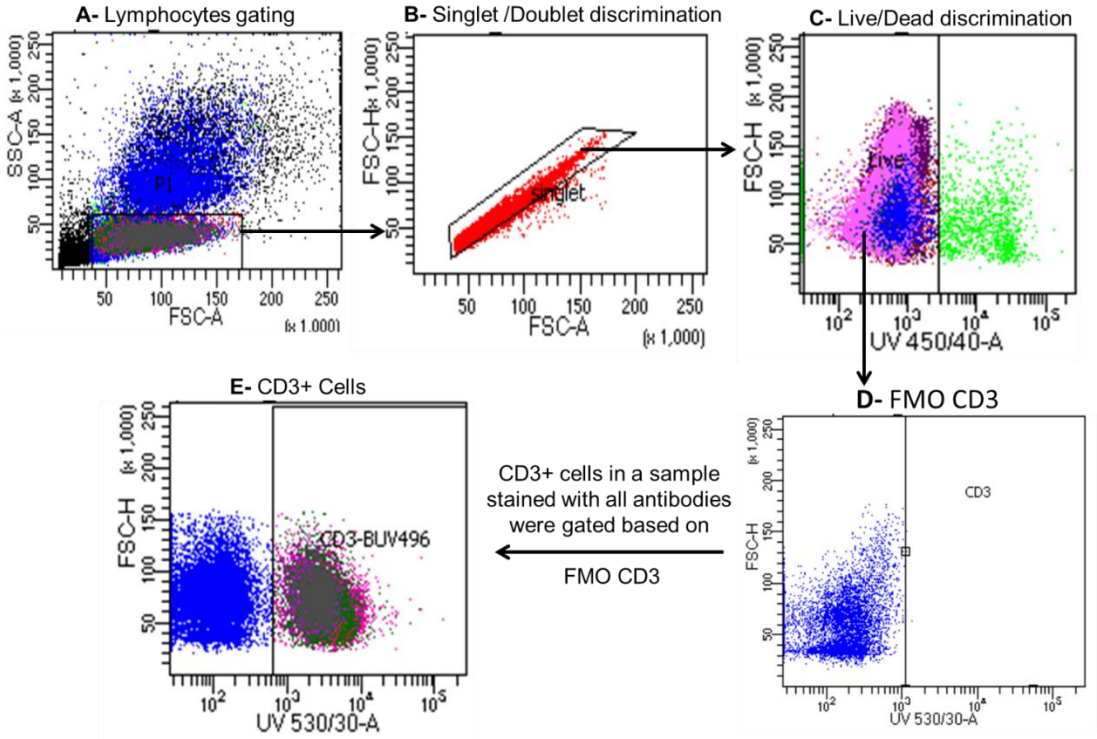

Figure 2.3. The flow-cytometry gating strategy for T-cell analysis.
PBMCs were labelled with a panel of antibodies and the signal produced was analysed as follows: A) Lymphocytes were gated based on SSC/FSC properties. B) SingleT-cells were gated based on FSC-H/A. C) Dead cells were excluded. D) An example of the FMO control where all antibodies were added to the tube of panel1 but no CD3 specific antibodies. E) An example of gating a population of interest where CD3+ cells situated in the area were gated based on the FMO CD3 sample.

2.4.3 FACS sorting for Treg cells

PBMCs were isolated by Ficoll gradient as described in section 2.2.2. Cells were then stained with CD4, CD25 and FOXP3 antibodies in concentration described in section 2.4.2. The cells were then fixed in 2% PFA before being sent to flow core facility to be sorted using BD FACS Aria. The cell count before and after sorting is shown in Table 2.4.

Table 2-4. The count of cells before and after FACS sorting.

Samples	PBMCs10^5	CD25+FOXP3+
HC-01	36	13000
HC-15	15	43454
HC-16	17	19000
AA26	10	52326
AA32	22	17746
AA33	11	2944
AA34	28	11531

2.5 Western blotting

2.5.1 Protein extraction protocol

Cell lysate was prepared by homogenisation in RIPA buffer (150mM sodium chloride, 50mM Tris-HCl, pH 7.4, 2mM ethylenediaminetetraacetic acid, 1% Triton X-100, 0.5% sodium deoxycholate, 0.1% sodium dodecylsulfate) containing halt protease inhibitor cocktail (P8340-5ML, Sigma) and halt phosphatase inhibitor cocktail (78420, ThermoFischer). First, cells were first washed with ice cold PBS, and incubated in 200µl RIPA buffer for 20mins. The lysate was then spun at 13rpm for 10 mins at 4°C to pellet the cell debris, and the supernatant (total protein) was collected into fresh tube, the lysate was stored in 50µl aliquots at -80◦C.

2.5.2 Protein quantification by BCA assay

The total protein in the cell lysate was quantified by a colorimetric method using a bicinchoninic acid assay (BCA) (Pierce™ BCA Protein Assay Kit, 23225, ThermoFischer). Standards were prepared from bovine serum albumin (BSA) in RIPA buffer, as described by the manufacturer, in order to obtain serial concentrations in µg/mL as follows: 2000, 1500,1000, 750, 500, 250, 125, 25 and 0 as a blank. 20µl of cell lysate (unknown samples) was diluted 1:3 in RIPA buffer. 25µL of each standard or unknown sample was loaded in duplicate to control for assay and sampling variance, and 200µL of the working reagent was added to each well. The plates were incubated at 37°C for 30mins. The absorbance (optical density, OD) was then measured at 562nm on a plate reader (VERSAMAX, Molecular Devices). The corrected OD was found by subtracting the average absorbance of the blank standard from that of other individual samples and standards (Table 2.5).

Table 2-5. A representative example of protein standard O.D readings.

Standards Conc.µg/ml	O.D1	O.D2	Average O.D	Corrected OD
2000	1.79	1.79	1.79	1.67
1500	1.40	1.29	1.34	1.22
1000	0.88	0.98	0.93	0.81
750	0.65	0.65	0.65	0.53
500	0.46	0.45	0.46	0.34
250	0.27	0.28	0.28	0.16
125	0.21	0.20	0.21	0.09
25	0.14	0.14	0.14	0.02
0	0.12	0.12	0.12	0.0

A standard curve was plotted using the corrected OD measurement for each BSA standard against its concentration in µg/mL. The standard curve equation

was used to determine the protein concentration of each unknown sample (Table2.6).

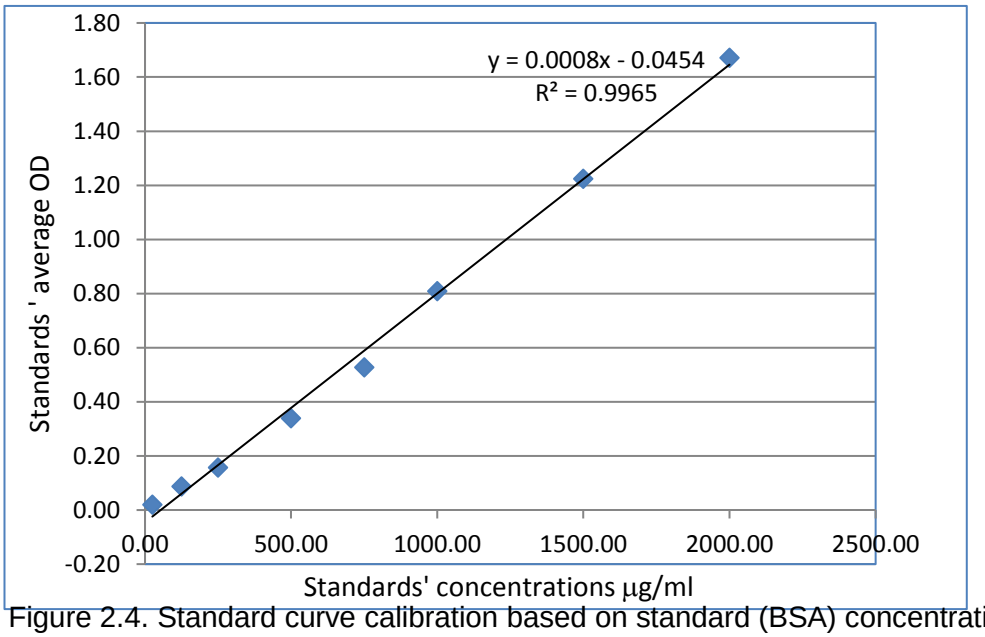

Figure 2.4. Standard curve calibration based on standard (BSA) concentrations and OD measurements.

Table 2-6. An example of protein quantification by BCA.

Unknown	O.D1	O.D2	Average O.D	Conc µg/ml	Conc X 3	µg/ul	Volume Loaded
Sample 1	0.95	0.98	0.96	1100	3300	3.3	12.1
Sample 2	0.54	0.53	0.54	568	1704	1.7	23.4
Sample 3	0.84	0.87	0.86	964	2893	2.8	13.8
Sample 4	0.87	0.91	0.89	1006	3019	3.0	13.2
Sample 5	0.72	0.73	0.72	798	2396	2.4	16.6
Sample 6	0.72	0.73	0.73	805	2415	2.4	16.5

2.5.3 SDS polyacrylamide gel electrophoresis

Protein samples were separated using SD-PAGE separating gel (Table 2.7). The gel percentage was selected based on the targeted protein size, a 10% gel was used for proteins larger than 30KDa, and a 15% gel was used for proteins lower than 30KDa. Stacking gel (Table 2.7) was poured on top of the separating gels to make up the well. 40µg of total protein, as measured by BCA

assay, were denatured at 95°C for 5 mins in 1 x SDS sample buffer (B31010, Lifetechnologies) prior to loading with pre-stained protein ladder (56-0024, Geneflow) to visualise the protein size. The gel was resolved at 80V for 20 min followed by 120 V for 1.5 hrs in running buffer (Table 2.8).

Table 2-7. SDS-PAGE Separating and stacking gels.

Buffers	Separating gel		Stacking gel
	10%	15%	4%
H2O	4 ml	3.8 ml	3.05 ml
30% Acrylamide	3.35 ml	7.9 ml	650 µl
1.5M Tris pH 8.8	2.5 ml	4 ml	-
0.5M Tris pH 6.8	-	-	1.75 ml
10% SDS	100 µl	160 µl	50 µl
10% APS	50 µl	160 µl	650 µl
TEMED	10 µl	16 µl	50 µl

Table 2-8. Running buffer

component	Quantity
Tris Base	30.2g
glycine	188g
10%SDS	100ml
dH20	Make up to 1litre

2.5.4 Western blotting

After electrophoresis, separated proteins were transferred to PVDF membrane using iBlot gel transfer stacks (IB401002, Invitrogen) following a dry blotting method, using a voltage of 23mA for 6min as described by iBlot Dry Blotting System (IB1001, Invitrogen). Membranes were then blocked in 5% milk in TBST for 45mins, washed 3x10mins in TBST and probed overnight at 4°C with primary antibody diluted in 5% milk in TBST according to the supplier's recommendation (Table 2.9). After 3x10mins washes in TBST to remove excess

antibody solution, goat anti-rabbit IgG or horse anti-mouse IgG horseradish peroxidase (HRP)-conjugated secondary antibodies were used in 1:10.000 dilutions for 45min at RT. When required, the membranes were stripped of bound antibodies using a stripping buffer (Table 2.10) 2x 10mins followed by 2x 10 minute washes with PBS and 2x5 min washes with TBST. They were then re-blocked, and re-probed with the appropriate antibody.

Table 2-9. Primary and secondary antibodies used for western blot analysis

Catalo no /supplier	Epitope	Host	MW kDa	dilution
Ab108248/Abcam	CD39	Rabbit	58	1:1000
NBP2-45314/ Novus Biologicals	HLA-DR	Mouse	28	1:1000
MAB3171-SP/R&D	IL-17	Mouse	17	1:1000
9167/ CST	STAT-1	Rabbit	91	1:1000
9167/ CST	p-STAT-1	Rabbit	91	1:1000
Ab128915/ Abcam	GAPDH	Rabbit	35	1:10,000
Ab20272/ Abcam	B-actin	Mouse-HRP conjugated	42	1:10,000
4050-05/ Southern-Biotech	Anti-rabbit IgG HRP	Goat	2ndry antibody	1:10,000
7076P2/CST	Anti-mouse IgG HRP	Horse	2ndry antibody	1:10,000

Table 2-10. Stripping buffer pH2.2.

component	Quantity (upto1L dH2O)
SDS	1g
Glycine	15g
Tween20	10ml

To detect target proteins, an enhanced chemiluminescence (ECL) reaction was performed using EZ-ECL chemiluminescent reagent (20-500-120, Biological Industries) and visualised on ChemiDoc XRS+ System (Bio-Rad). After visualising the protein of interest, membranes were probed with an internal

control (B-actin or GAPD) to normalise any variation in the amount of protein loaded. Densitometric analysis was carried out using ImageJ software 1.41 where the band density of each target protein was measured and normalised to the internal control.

2.6 Enzyme Linked-Immuno-Sorbent Assay (ELISA)

In order to assess the levels of the intracellular cytokines (IL-17 and IFN-γ) secreted by PBMCs, ELISA was performed to investigate the level of these cytokines in the media before and after induction. PBMCs were isolated from heparinised blood by density gradient purification over Lymphoprep as described previously, the cells were then stored at - 80°C. Samples were collected from 6 patients and 5 healthy controls. The cells were thawed as described previously and maintained in RPMI media supplemented with 10% FBS and 1% strep/ pen antibodies and incubated at 37°C for 12 hours to rest the cells before performing any experiments. After this, living PBMCs were counted using trypan blue staining, and about $1x10^6$ cells were activated with 5ng/ml phorbol 12-myristate 13-acetate (PMA) (P-8139, Sigma) and 0.1μg/ml ionomycin (I-0634, Sigma) for 3.5hrs or left un-stimulated. Supernatants were assayed for IL-17 or IFN-γ levels by IL-17 ELISA kit (KAC1591, Invitrogen) or IFN-γ ELISA kit (KHC4021, Invitrogen) according to the manufacturer's instructions.

The ELSA kits used in these experiments are solid phase Enzyme Amplified Sensitivity Immunoassays. A monoclonal antibody specific for IL-17 or IFN-γ was coated onto the wells. 50μl of samples, including standards, control specimens, and unknowns, were pipetted into these wells in duplicate, followed by the addition of a biotinylated polyclonal second antibody. The microtitre plate

was incubated for 2hrs at RT to allow the formation of a sandwich: coated cytokine-specific antibody/ cytokine/ secondary antibody-biotin, the plate was then washed to remove unbound biotinylated antibodies. 100μl of streptavidin-peroxidase was added to bind to the biotinylated antibody. After 45mins incubation at RT in the dark, the unbound enzyme was removed by washing and 100μl of chromogenic substrate solution was added. The reaction was stopped after 15-30mins with the addition of 100μl stop solution and the microtiter plate was then read at a wavelength of 450nm, which was subtracted from readings taken at 630nm. The amount of substrate turnover was determined colorimetrically by measuring absorbance that was proportional to the IL-17 or IFN-γ concentration. A standard curve was plotted and the cytokine concentration in unknown samples was determined by interpolation from the standard curve. As the un-stimulated samples showed undetectable levels of protein, the readings included in the analysis were from PMA/ ionomycin stimulated samples.

2.7 Immuno-fluorescence staining (IF)

An immuno-fluorescent detection technique was used to study CD3, CD39 and FOXP3 expression as markers of suppressive Treg in HF in formalin-fixed, paraffin-embedded (FFPE) skin tissue from AA and healthy subjects. Antigens were retrieved from deparaffinised sections by heating in a microwave set to full power for 10 mins. Non-specific binding sites were blocked using serum-free blocking buffer. The target antigens were initially labelled with primary antibodies to surface antigens (CD3 or CD39) overnight at 4^{o}C followed by labelling with the primary antibody against the intracellular marker (FOXP3) for 2hrs at RT in 0.2% Triton in PBS to enhance the membrane permeabilisation.

The sections were then incubated with fluorochrome-conjugated secondary antibodies for 1hr at RT, and the signal was detected using immunofluorescence-scanning microscopy (AF6000). The primary antibodies and the fluorochrome-conjugated secondary antibodies are listed in Table 2.11.

Table 2-11. List of antibodies used for IF staining.

Catalo no /supplier	Epitope	Host	dilution
ab178572 / Abcam	CD39	Mouse	1:100
ab54501 / Abcam	FOXP3	Rabbit	1:100
ab11089 / Abcam	CD3	Rat	1:100
A11008/ Lifetechnologies	Anti-Rabbit IgG, Alexa Fluor 488	Goat	1:500
A11004/ Lifetechnologies	Anti-Mouse IgG, Alexa Fluor 568	Goat	1:500
ab150159/ Abcam	Anti-Rat IgG, Alexa Fluor® 647	Goat	1:500

2.8 Gene expression analysis

2.8.1 Q-PCR analysis

2.8.1.1 RNA extraction and cDNA synthesis for q-PCR

Total RNA was extracted using the Trizol reagent method (T9424, Sigma Aldrich). Cells were lysed with Trizol and the aqueous phase was separated and collected. RNA was then precipitated by addition of 0.5ml of isopropanol per 1ml of Trizol washed with 75% ethanol and finally resuspended in 20μl RNase free water. RNA concentration was measured by Nanodrop (NanoDrop 1000 Spectrophotometer version3.8.1) and 5μg total RNA was reverse transcribed to a first strand cDNA using SuperScript® III First-Strand Synthesis System kit using random hexamer (18080-051, Life Technologies), following the manufacturer's protocol where cDNA synthesis mix contains 10X RTbuffer+

20mM MgCl2+ 0.1M DTT+ RnaseOUT+ SuperScript III RT as summarised in Table 2.12.

Table 2-12. Summary of cDNA synthesis protocol.

Reaction	Temperature◦C /duration	Aim
10µl RNA+Primers+dNTPs	65 for 5mins	Denaturation
10µl cDNA synthesis mix+ Random hexamer	50 for 50mins 85 for 5mins	cDNA synthesis Terminate reaction
1ml Rnase H	37 for 20mins	Remove RNA

2.8.1.2 Q-PCR analysis of gene expression

The relative expression of genes of interest was measured by q-PCR using power SYBER green fluorescence (4367659, Life Technologies) and specific primers for the target gene (Table 2.13). A 10µl final volume of real-time PCR reaction, containing 600nM of forward and reverse primers, was run in triplicate. The targeted sequence-specific amplification was detected using SYBER green detector and the thermal profile (Table 2.14). Glyceraldehyde-3-phosphate dehydrogenase (GAPDH) was run for each sample as an internal control to normalise any variation in the amount of RNA, and a NTC control was run to regulate any contamination. The PCR reaction was carried out in 384-well plates using the ABI Prism 7900HT Sequence Detection System (Applied Biosystems).

Table 2-13. Primer sequences (5' > 3') used in the q-PCR reactions.

Gene	Forward sequence	Reverse Sequence
STAT1	GCAGGTTCACCAGCTTTATGA	TGAAGATTACGCTTGCTTTTCCT
STAT3	CAGCAGCTTGACACACGGTA	AAACACCAAAGTGGCATGTGA
JAK-1	GCGGAGGGATCGACAAATGG	TGGGACATAGCTTAAAGAGGCA
JAK-2	CTCTTTGTCACAACCTCTTTGCC	TTGGAGCATACCAGAGCTTGG
IRF1	GCAGCTACACAGTTCCAGG	GTCCTCAGGTAATTTCCCTTCCT
IL-17A	AGATTACTACAACCGATCCACCT	GGGGACAGAGTTCATGTGGTA
CCL-5	CTCATTGCTACTGCCCTCTGCGCTCCTGC	GCTCATCTCCAAAGAGTTGATGTACTC
FOXP3	CGGACCATCTTCTGGATGAG	TTGTCGGATGATGCCACAG
HLA-DR	ATCATGACAAAGCGCTCCAACTAT	GATGCCCACCAGACCCACAG
HLA-B	CCGGACTCAGAATCTCCTCAG	AAACACAGGTCAGCATGGGAA
KRT14	CATGAGTGTGGAAGCCGACAT	GCCTCTCAGGGCATTCATCTC
KRT17	GGTGGGTGGTGAGATCAATGT	CGCGGTTCAGTTCCTCTGTC
TGF–β	CTAATGGTGGAAACCCACAACG	TATCGCCAGGAATTGTTGCTG
GAPDH	GGAGCGAGATCCCTCCAAAAT	GGCTGTTGTCATACTTCTCATGG
B2M	GAGGCTATCCAGCGTACTCCA	CGGCAGGCATACTCATCTTTT
β-Actin	TCCCCCAACTTGAGATGTATGAAG	AACTGGTCTCAAGTCAGTGTACAGG

Table 2-14. Thermal profile used in q-PCR reaction.

Reaction	Duration/Temperature	Cycle
Hot start activation of polymerase	10 mins at 95°C	1
Denaturation	15s at 95°C	40
Annealing and elongation	1min at 60°C	
Dissociation curve	15s at 95°C	1
	15s at 60°C	1
	15s at 95°C	1

2.8.2 Next generation sequencing (NGS)

There has been increasing demand for a sequencing tool able to read long fragments of the genome in one experiment. 454 Life Technologies brought the first next generation sequencing platform to the market in 2005, and that was a great advance in the sequencing technology as it can produce about 1 million

reads per run with reads up to 300-500 bases (Margulies et al., 2006), however, this platform has limitations including its inability to identify homopolymers, which are stretches of nucleotides where all bases are identical, and its high cost that is considered ineffective compared to the relatively low number of reads (Hodkinson and Grice, 2015). More advanced platforms followed to provide cost-effectiveness, high sequence yield per run and improved resolution such as Illumina, Ion Torrent and SOLiD (Morozova and Marra, 2008) that have brought unprecedented advances to the field of genomic research. Illumina, which was introduced in 2006, is the most widely used platform due to its ability to produce large number of reads per run in a cost-effective way, ranging from 500 million to 3 billion reads per run with maximum read length up to 300bp (Hodkinson and Grice, 2015).

Illumina sequencing, in principle, is based on the Sanger sequencing technique, which was developed in 1977 by Frederick Sanger and colleagues (Morozova and Marra, 2008). The Sanger technique is based on incorporation of dideoxynucleotide non-reversible terminator (ddNTP) to the sequencing reaction that contains DNA polymerase, primers and ordinary deoxynucleotides (dNTP). The reaction is terminated when the terminator ddNTP is incorporated as it lacks the 3'-OH end required for a phosphodiester bond formation between two nucleotides. The ddNTPs are radioactively or fluorescently labelled, which emit fluorescence after the addition of each base to reveal DNA sequence product based on size initially upon gel electrophoresis but subsequently using capillary separation and laser data collection (Sanger et al., 1977, Morozova and Marra, 2008).

The Illumina technique implements a similar principle to the Sanger technique except that the terminators are reversible (Bentley, 2006). gDNA was

extracted from total blood samples in this experiment and amplified by PCR reaction. Prior to sequencing, PCR product requires pre-library preparation, which includes incorporating an adaptor on either end of each DNA fragment followed by PCR amplification of adapter-ligated DNA molecules using specific primers to enhance binding to complementary oligonucleotides on the surface of the flow cell in the illumine chip (Bentley, 2006). During the sequencing, Illumina involves an approach called sequencing by synthesis where reversible terminators are incorporated into the elongating neucleotide chain, and after a given time, the excess un-incorporated nucleotides are washed away, and an image of fluorescently labelled nucleotides will be captured (Bentley, 2006). The terminators are labelled with fluorochromes of four different colours to distinguish among the different bases at the given sequence position (Morozova and Marra, 2008).

2.8.2.1 DNA extraction for NGS

10^6 PBMCs isolated from heparinized venous blood by density gradient purification as described in section 2.2.2, and $1X10^4$ CD4+CD25+FOXP3+ Treg sorted by FACS technique (as described in (section 2.4.3) underwent DNA extraction using two different kits. Genomic DNA (g-DNA) extraction from PBMCs was performed using Quick-gDNA extraction Miniprep (D-3006, Zymo research). Lysis step was performed by adding 500 µl of genomic lysis buffer to the cell pellet incubated 5-10mins at RT. The mixture was then transferred to a zymo-spin column in a collection tube and centrifuged at 10,000xg for 1min. DNA binding step was followed by adding 200µl of DNA pre-wash buffer and centrifuging at the same speed for one minute, which was followed by washing using 500µl of g-DNA wash buffer. After the wash step, DNA elution was

performed by adding 50μl elution buffer and incubated at RT for 2-5mins before centrifuging at top speed to elute the DNA. The eluted DNA was stored at -20ºC.

DNA extraction from FACs sorted Treg cells was performed using a kit that is suitable for paraffin fixed cells, Pico Pure DNA extraction kit (KIT0103, Applied Biosystems). 155μl of reconstitution buffer was added to one vial of proteinase K provided in the kit to construct the extraction solution. 150μl of extraction solution was added to the FACS sorted cell pellet and incubated at 65°C for 12hrs, and then incubated at 95°C for 10mins to deactivate the proteinase K and stored at -20°C. DNA samples were then stored at -80°C to be used for multiplex PCR reaction.

2.8.2.2 Multiplex- PCR amplification of the TRCβ CDR3 region

TCRβ CDR3 was defined according to International Immunogenetic collaboration (IMGT) (Monod et al., 2004), TCRβ CDR3 begins with the second conserved cysteine encoded by the 3′ position of the Vβ gene segment and ended with the conserved phenylalanine encoded by the 5′ position of the Jβ gene segment. Multiplex-PCR system was used to amplify the rearranged regions of TCRβ CDR3 from genomic DNA using 39 forward primers specific to TCR Vβ segments and 13 reverse primers each specific to a TCR Jβ segment (Primer sequences in appendix 1) to generate a template library for analyses using Genome Analyzer. 50μL PCR reaction was set at 0.8μM forward (F) primers pool (22nM for each unique TCR Vβ F primer), 1.0μM reverse (R) primers pool (77nM for each unique TCR Jβ primer), 200ng gDNA, 1 × QIAGEN Multiplex PCR master mix and 5% Q solution (QIAGEN). The PCR reaction was performed under thermal cycling conditions listed in table 2.15. A clean PCR

product using this protocol was obtained of about 500bp size as show in Figure 2.5.

Table 2-15. Summary of multiplex PCR thermal cycles

Reaction	Duration/Temperature	Cycle
Hot start activation of polymerase	15mins at 95◦C	1
Denaturation	30sec at 94◦C	40
Annealing	90sec at 59◦C	
Extension	1min at 72◦C	
Final extension	10mins at 72◦C	1

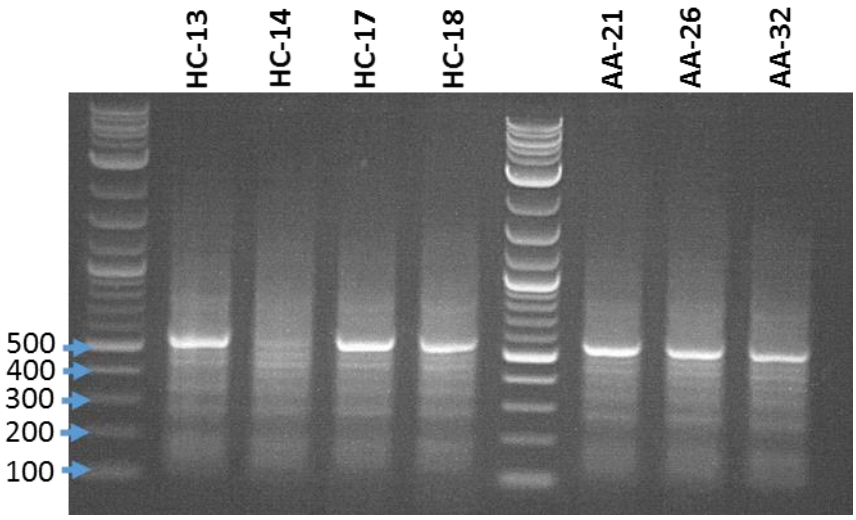

Figure 2.5. PCR product of multiplex PCR.
PCR products showed bands of about 500bps size.

2.8.2.3 Library preparation

All experiments in library preparation stage were performed by Mr Matt Wyles in the Sheffield Institute for Translational Neuroscience (SITraN) under supervision of Dr. Paul Heath.

DNA quantification

Prior to library construction, an accurate measurement of the concentration of PCR products was performed using Quibt ds DNAHS assay (Q32851, Invitrogen). The assay involves adding Quibt working buffer provided in the kit to the standards and the samples in volumes stated in the protocol and

incubated for 2mins at RT. The concentration of the samples was then calculated automatically using Qubit® Fluorometer.

DNA Fragmentation

The size of DNA fragments (multiplex PCR product of PBMCs samples) was around 500bps, which cannot be sequenced in full by Hiscan SQ Illumina sequencer as it performs paired-end sequencing, coupled with 2 × 100 bp read lengths. Therefore DNA was first digested using the NEB double stranded DNA fragmentase enzyme (M03485, NEB) into appropriate size following the manufacturer's protocol.

The digestion step was followed by an accurate determination of DNA fragments size using Agilent High sensitivity DNA assay (5067-4626, Agilent). The technique involves separating the samples based on their size by electrophoresis after loading them in Agilent chip. The travel time of samples through the micro-channels is based on their size where smaller fragments migrate faster. The chip was then read on an Aligent 2100 Bioanalyser involving two key metrics; fluorescent intensity units (FU) that depends on the sample concentration and migration time, which relates to the size of the nucleotides. The Agilent2100 bioanalyser software generated graphs representing migration time in seconds (S) on X axis against the fluorescent units (FU) in the Y axis for the ladder (Figure 2.6.A). The software then calculated the size of DNA fragments based on standard curve plotting the migration time against known ladder sizes, and the results depicted manually on each peak in bp (Figure 2.A), which is then used to measure the size of DNA fragments for each well from the migration time. The samples (Figure 2.6.B) were successfully fragmented into about 200-300bp size after 20mins incubation with fragmentase enzyme at 37°C.

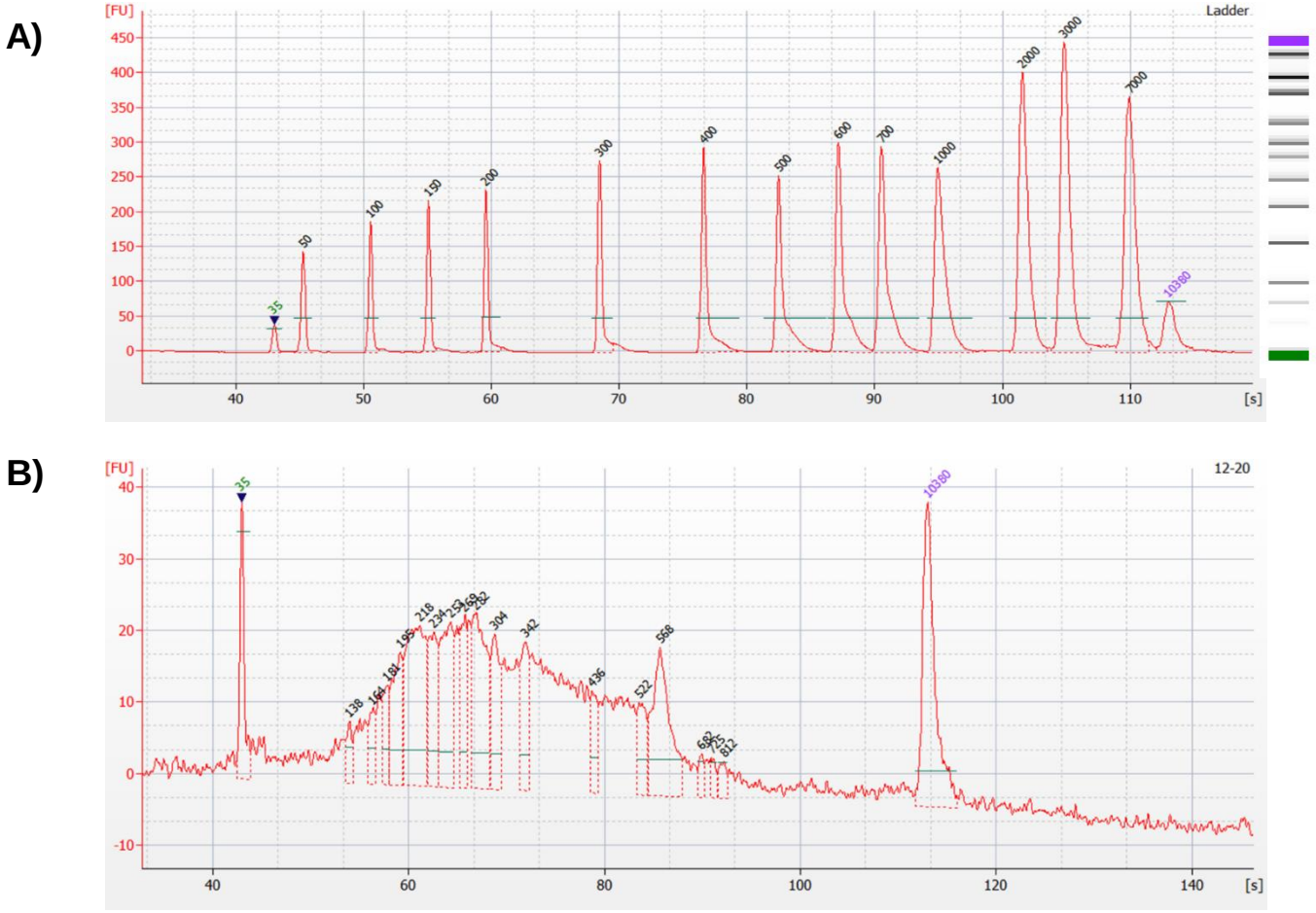

Figure 2.6. Agilent 2100 bioanalyser analysis of DNA library preparation.
A). Plot shows the migration time (seconds) against fluorescent intensity (FU) of the ladder with known size. B) Representative electropherogram of the DNA library after digestion where the peak point is at about 300bp.

DNA Purification

Bead purification of the PCR products was performed as described by supplier AgenCourt AMPure XP (A63881, Beckman Coulter) to remove excess enzymes, primers, salts and nucleotide. The Agencourt AMPure XP Purification systems utilize solid-phase paramagnetic bead technology for high-throughput purification of PCR amplicons where 1.8μl of AMPure XP buffer was added to 1.0μl of PCR product and incubated for 5mins at RT, the beads-containing buffer selectively bind to PCR amplicons. The plate was then placed onto the Agencourt magnetic rack for 2mins before aspirating the cleared supernatant. The bead-bound PCR product was then washed 2X with 200μl of 80% ethanol to remove contaminants and finally purified PCR was eluted from the beads by adding 40μl of elution buffer to each well and incubated for 2mins at RT after removing the plate from the magnet. The plate was then replaced onto the magnet for 1min before transferring the eluent (purified sample) into clean tubes to be used in final library preparation.

2.8.2.4 End library preparation

Sequencing libraries were generated using the standard protocol in the NEB Ultra II DNA library prep kit for Illumina (E7645S, NEB) summarised in Figure 2.7. First, end repair of the fragmented DNA was performed by adding dA tail at 3' end of the fragments and phosphorylation at 5' end. In this reaction, 50μl of fragmented DNA added to 3μl of the NEBNext Ultra II End Prep Enzyme Mix and 7μl of NEBNext Ultra II End Prep reaction buffer and mixed very well. The reaction was run in the thermocycler with the following setup: 30mins at 20°C, 30mins at 65°C and hold at 4°C.

That was followed by adaptor ligation; platform-specific adapters serve as a template for the PCR reaction for final library preparation. Adaptor, which is self-

complimentary oligonucleotides forming a stem-loop containing uracil, was added to the DNA fragments. The following buffers were added directly to end repair reaction; 30µl of NEBNext ultra II ligation master mix, 1µl of NEBNext Ligation Enhancer and 2.5µl NEBNext Adaptor for Illumina, mixed 10 times and incubated for 15mins at 20°C in the thermocylcer. That was followed by adding 3µl of USER™ (Uracil-Specific Excision Reagent) enzyme to the ligation mixture and incubated at 37°C for 15mins in order to generate a single nucleotide gap in the adaptor at the uracil residue to open the loops.

Finally clean-up was performed to remove excess enzymes using Agencourt AMPure XP beads as described previously and a high sensitivity DNA bioanalyser chip (Agilent) was performed to assess the size of the DNA fragments and the amount of the final library was quantified using the Qubit kit.

2.8.2.5 Library amplification

The adaptor-ligated DNA was amplified by PCR reaction (Table 2.16) where barcoding sequence identifying each sample was added to the DNA fragments, and indexed by forward and reverse primers for paired-end sequencing (P5 and P7 Primer) adding termini that bind to the oligonucleotides on the flow cell surface.

P5 PCR Primer: 5'AATGATACGGCGACCACCGAGATCTACACTCTTTCCCTACACGA3'

P7 PCR Primer: 5' CAAGCAGAAGACGGCATACGAGAT 3'.

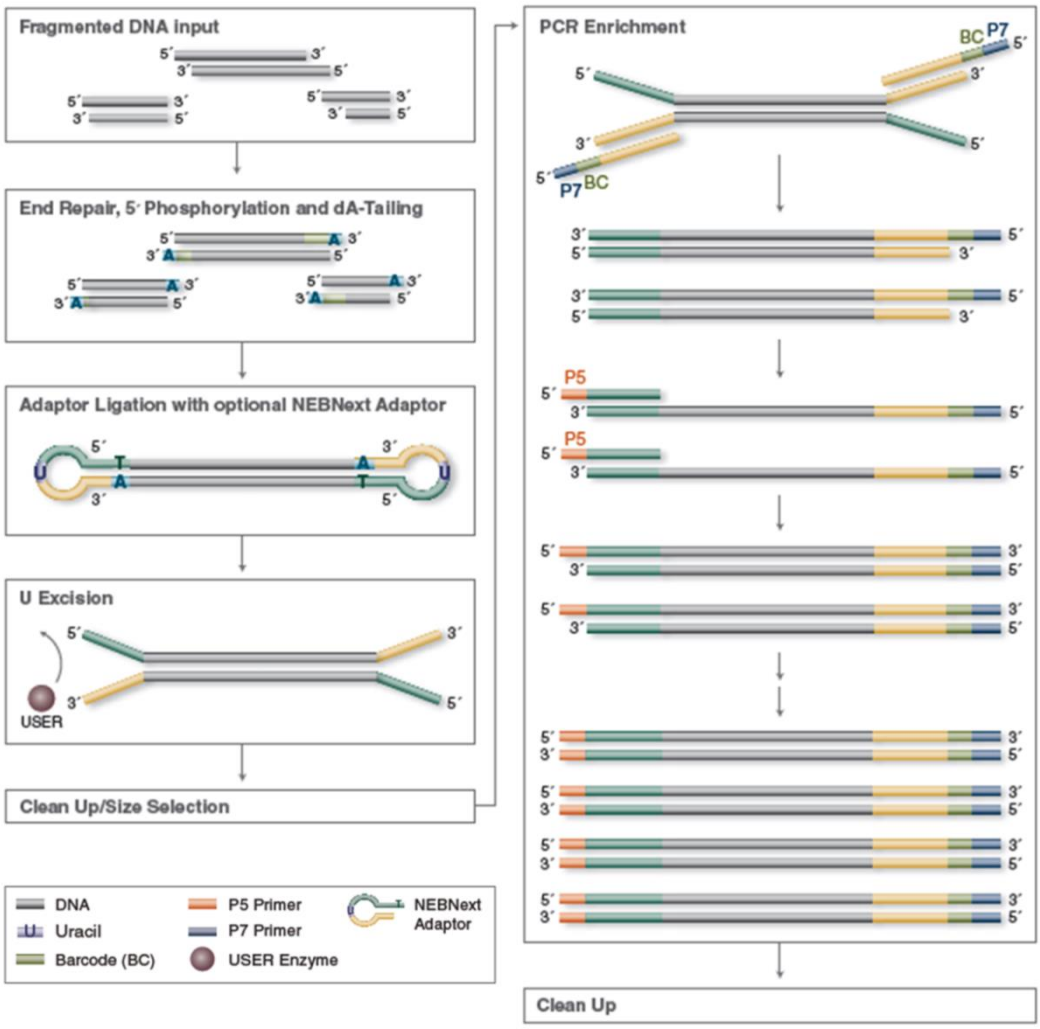

Figure 2.7. Work flow of NEB library preparation kit.
First, DNA fragments undergo end repair of the fragmented DNA by adding dA tail at 3' end of the fragments and phosphorylation at 5' end. Secondly, adapter ligation is performed. Thirdly, the adapter loop is cut by USER enzyme, and the library undergoes clean up step. Finally, PCR amplification is performed using P5 and P7 indexed primers and involves inserting barcode for each sample.

Table 2-16. PCR reaction used in library amplification.

Reagent	Volume
Adaptor-ligated DNA fragments	15 µl
NEBNext Ultra II Q5 Master Mix	25 µl
Index Primer/i7 Primer	5 µl
i5 Primer	5 µl
Total volume	50 µl

All samples were indexed uniquely so they could be pooled together and sequenced in one lane of a HiScan SQ using a 2x100bp high output run. The reaction was run in the thermocycler using thermal profile in Table 2.17.

Table 2-17. Thermal profile used in library amplification.

Reaction	Duration/Temperature	Cycle
Initial Denaturation	30s at 98◦C	1
Denaturation	10s at 98◦C	8
Annealing and elongation	75s at 65◦C	
Final extension	5mins at 65◦C	1

A final clean-up using beads as described before was performed and the library size was about 300bp. The total DNA concentration in the final library (Table 2.18) was calculated by Quibt.

Table 2-18. Concentration of DNA in final library as calculated by Quibt.

Sample ID	Fragment size	Qubit	nM
PAA29	326	33	155.7
PAA28	326	22.4	105.7
PAA27	326	15	70.7
PAA26	326	17.2	81.1
PAA24	326	34.6	163.2
PAA22	326	14.8	69.8
PAA21	326	41.8	197.2
PAA13	326	11.2	52.8
PAA10	326	10.7	50.4
PAA7	326	19.8	93.4
PHC18	326	8.45	39.8
PHC17	326	17.7	83.5
PHC16	326	44.9	211.8
PHC15	326	26.9	126.9
PHC13	326	11.5	54.2
PHC03	326	15.5	73.1
PHC01	326	26.2	123.6
FAA34	326	72.9	344.0
FAA33	326	43.8	206.7
FAA32	326	72.7	343.1
FHC16	326	8.51	40.1
FHC15	326	21.3	100.5
FAA26	326	14.4	67.9
FHC01	326	10.1	47.6

F=FACS sorted samples, P=PBMC

2.9 Statistical analysis

Q-PCR data was exported into an Excel file, Dct was calculated by subtracting Ct value of gene of interest (GOI) from housekeeping gene, then the mean was calculated for the triplicate Dct values for each gene in the experiment. Differential expression was determined by the ΔΔCt method where means and SD were determined for experimental repeats. For flow-cytometry data, the percentage of each T-lymphocyte sub-population was compared between patients and HC. Comparison of data between variables in each experiment was performed using a two-tailed independent t-test, and the corrected t-test was used whenever the homogeneity of variance was violated. The analysis was carried out using Graphprism software version 6 with $P \leq 0.05$ as the significance level. Descriptive statistics are presented as the mean ± SD.

Chapter 3 . T-cell role in AA pathogenesis

3.1 Introduction

As previously discussed in section 1.3, T-cells and their cytokines play a major role in the AA pathogenesis. The dense intrafollicular and perifollicular infiltration of T-lymphocytes into the affected HF is a histopathological hallmark of the disease (Todes-Taylor et al., 1984, Perret et al., 1984), where, $CD4^+$ and $CD8^+$ T-cells constitute the main components of the cellular infiltrate. Despite this, only a limited number of studies detailing changes in proportions of T-cell subsets in AA patients has been performed. Naïve $CD4^+$ can differentiate into Th1, Th2, Th17 or $CD4^+$ $CD25^+$ regulatory T-cells (Treg) (Zhu et al., 2010). $CD8^+$ cytotoxic T-cells (Tc) can be also further differentiated based on their activation marker (NKG2D) (Petukhova et al., 2010, Hu et al., 2016). In this study, representative groups of cytokines and cell surface markers have been selected to study different populations of inflammatory/effector T-cells (Teffs) (Table 3.1).

Table 3-1. Main subsets of Teff cells and profile of secreted cytokines.

T-cell subsets	Surface/intracellular marker	Additional markers
Th1	CD4, CD119	NA
Th17	CD4	IL-17
Th2	CD4 CRTH2	NA
Tc	CD8	NKG2D

NA- Not applicable as no additional marker was not used due to the restricted number of markers that can be used in this multi-colour flowcytometric panel.

Regulatory T (Treg) cells constitute 20% of CD4+ T-cells in human skin (Sanchez Rodriguez et al., 2014). Tregs play a central role in peripheral immune tolerance where they have an anergic effect on the effector T-cells (Peterson,

2012). Peripheral blood Tregs have shown to be functionally impaired in AA patients (Shin et al., 2013). However, none of the subsequent studies have characterised Treg subtypes and their activation status to determine the cause of their functional impairment. Therefore, the aim of the work in this chapter was to analyse T-cell subsets (Teff and Treg) and characterise Treg cell subtypes and their activation status in AA patients and HC.

3.2. Results

3.2.1. Inflammatory T-cell subsets (Teff) in peripheral blood

To determine T-cell subpopulations within the circulation, lymphocytes were isolated from peripheral blood, analysed using flow-cytometry and T-cell subtypes detected using flurochrome-conjugated antibodies for each population marker/s as listed in Table 3.1. Twenty AA patients, who were not on any treatment, and ten healthy controls (HC) were enrolled in the study. Changes in the proportions of different T-cell subsets were determined after gating around the total lymphocyte population and collecting about 500,000 cell events.

3.2.1.1. CD4+ T-cells and their subtypes

As a main component of diseased HF inflammatory infiltrate forming about 60-80% of perifollicular infiltrate (Todes-Taylor et al., 1984), the proportion of CD4+ T-cells and their subtypes in peripheral blood of patients and HC donors was investigated. Within the total CD3+ T-cells, there was a significantly higher proportion of circulating CD4+ T-cells (P=0.03) in the peripheral blood of AA patients when compared to the HC group by about 10% (Figure 3.1.A). The proportion of Th1, Th2 and Th17 subtypes as a percentage of the total CD4+ T-cells population was determined using CD119 cell surface marker, CRTH2 cell surface marker and IL-17 intracellular cytokine as representative markers of

each subpopulation respectively. The proportion of Th1 subpopulation was 3 times higher in patients (P=0.003), similarly, there was a higher proportion of Th2 cells where it significantly increased from 2% of CD4+ T-cells in healthy controls to 4% in patients (P=0.038). The proportion of the Th17 subset was significantly raised as well from only 3.3% of the total CD4+ T-cells pool in HC to about 12.4% in patients (P=0.001) (Figure 3.1.B).

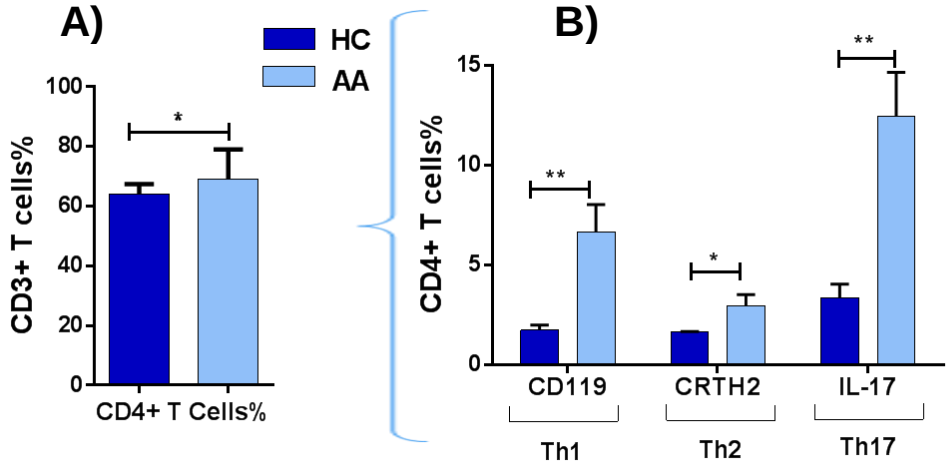

Figure 3.1. CD4+ T-cell subsets.

A) The frequency of CD4+ T-cells in the total lymphocyte population (CD3+). Data is shown as a percentage of total CD3+ T-cells. B) The frequencies of Th1, Th2 and Th17 in CD4+ population calculated as a percentage of total CD4+ T-cells. Data analysed by a two-tailed independent t-test, and the corrected t-test was used whenever the homogeneity of variance was violated. A 95% confidence interval was used where P≤ 0.05 is considered significant (*), P ≤ 0.01 (**). All bars plot depict mean with SEM in each study group. AA patients n=20, healthy controls (HC) n=10.

In view of the changes observed in Teff subset proportions, especially Th1 and Th17, an ELISA assay was performed to assess the level of the intracellular cytokines, IFN-γ and IL-17, produced by activated PBMCs. PBMCs isolated from patients and HC blood were activated with PMA/ ionomcyin, and the levels of IFN-γ and IL-17 in the supernatant were measured. It was found that patient PBMCs produced about seven times higher levels of IFN-γ (P≤0.01) compared to those of HC (Figure 3.2.A), and a significant increase in IL-17 production in patient PBMCs by about 150 times (P=0.006) was observed in patient when compared to HC samples (Figure 3.2.B).

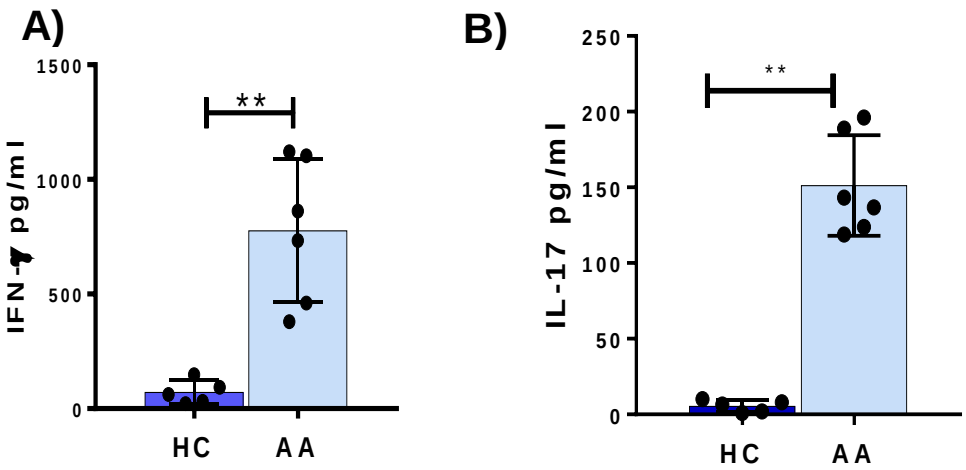

Figure 3.2 Production of IFN-y and IL-17 by PBMCs of patients and HCs.
ELISA analysis of IFN-γ (A) and IL-17 (B) production (pg/ml) by PBMCs of patients (n=6) and healthy control (n=5) stimulated by PMA/ ionomycin for 3.5hrs. Data analysed by a two-tailed independent t-test, and the corrected t-test was used whenever the homogeneity of variance was violated. Individual data points and mean ± SD are shown. A 95% confidence interval was used where (**) indicates significant difference P value≤0.01.

3.2.1.2. CD8+ T-cells and activation status

CD8+ T-cells (Tc) are another key Teff cell population in AA pathogenesis constituting 20-40% of the lymphocytic infiltrate around affected HF (Todes-Taylor et al., 1984). However, it is not known if that is a reflection of systemic

involvement of CD8+ T-cells, therefore, it was sought to investigate this in peripheral blood. As a percentage of total CD3+ T-cells, the frequency of CD8+ T-cells was found to be slightly less in AA patients' blood compared to HC, which was not statistically significant. However, looking at the activation status of these cells represented by expression of the NKG2D surface marker, the data demonstrated a significantly more activated Tc cell proportion in AA patients where there was about 12% increase in the expression of NKG2D+ marker on CD8+ T-cells isolated from patients' blood (P=0.015) when compared to HC (Figure 3.3).

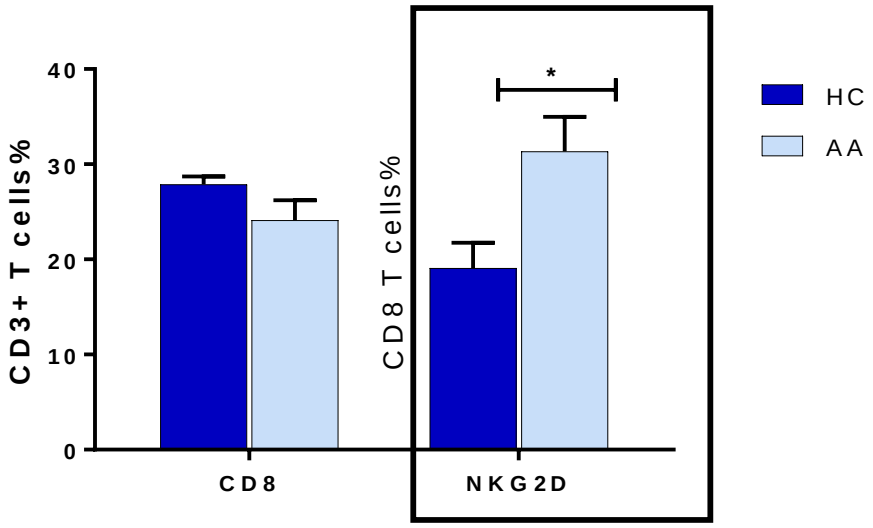

Figure 3.3. CD8+ T-cells and their activated subset in patients and HCs.
The frequency of CD8+ T-cells in the total lymphocyte population (CD3+) was slightly less in patients while the proportion of activated CD8+ T-cells subset ($NKG2D^+$ cells) was significantly higher. Data analysed by a two-tailed independent t-test, and the corrected t-test was used whenever the homogeneity of variance was violated. A 95% confidence interval was used where P≤ 0.05 is considered significant. All bars depict mean with SEM in each study group. AA patients n=20, healthy controls (HC) n=10.

3.2.1.3. CD4+: CD8+ ratio

The ratio of CD4+: CD8+ in peri-follicular lymphocytic infiltrates has been studied extensively, however, it is not known if this localised variation is a reflection of systemic derangement of these T-cell subsets. In this study, the

ratio of CD4+:CD8+ cells in the total CD3+ T-cell pool was investigated and a significantly higher CD4+:CD8+ ratio was observed in patients' peripheral blood (3:1± 0.3) compared to HC (2:1 ± 0.09) P=0.04 (Figure 3.4).

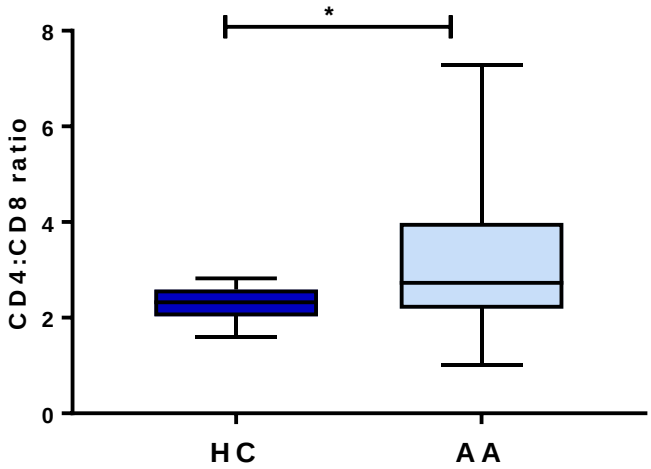

Figure 3.4. The ratio of CD4+:CD8+ T-cells in peripheral blood of AA patients and HCs.

Data was analysed by a two-tailed independent t-test with A 95% confidence interval where P≤ 0.05 is considered significant. The box and whisker plots depict median with minimum to maximum values in each study group, AA patients n=20 and healthy control (HC) n=10.

3.2.2. Regulatory T-cells (Tregs) in AA patients

Tregs infiltrate normal HF (Sanchez Rodriguez et al., 2014) and have a potential role in AA pathogenesis (Shin et al., 2013), therefore, detailed study of Tregs and their functional subsets in AA was performed. Circulating Tregs were identified by co-expression of CD25 and FOXP3 markers in the CD4+ T-cell pool, and detailed analysis of their subsets were performed based on the main functional subsets: naïve, memory or suppressive expressing a group of activation markers and immunosuppressive cytokines listed in Table 3.2.

Table 3-2. Main subsets of Treg cells.

Treg subsets	Generic Treg marker	Additional markers
Total Treg	CD25 FOXP3	
Memory Treg	CD25 FOXP3	CD45RO
Suppressive Treg	CD25 FOXP3	CD39, HLA-DR or LAG3
Suppressive cytokines producing Treg	CD25 FOXP3	TGF-β or IL1-0

3.2.2.1. Total Treg frequency in AA patients' peripheral blood

Within the CD4+ T-cell pool, total Tregs were found to be about 40% higher in peripheral blood of AA patients when compared to HCs (P=0.001). Interestingly, a higher proportion of CD45RO+ memory cells (about 15%) in the CD25+FOXP3+ Treg pool from patients was noted when compared to HC samples (10%) (Figure 3.5).

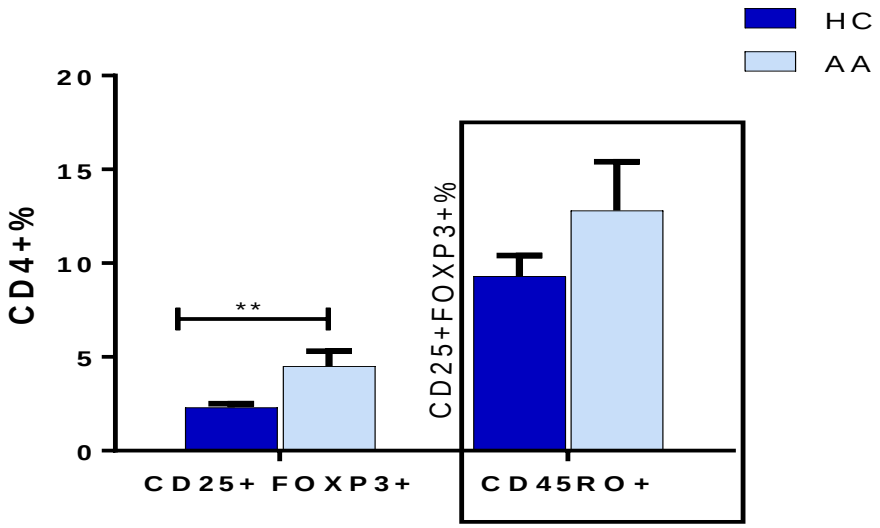

Figure 3.5. Percentages of CD25+FOXP3+ Tregs and their memory subset (CD45RO+) in peripheral blood of AA patients and HC.
Data analysed by a two-tailed independent t-test, and the corrected t-test was used whenever the homogeneity of variance was violated. A 95% confidence interval was used where P≤ 0.05 is considered significant (*), P≤0.01 (**), All bars depict mean with SEM in each study group. AA patients n=20, healthy controls (HC) n=10.

3.2.2.2. Suppressive Treg frequency in in AA patients' peripheral blood

Next, it was important to study the functionality of Treg cells by looking at some key immunosuppressive surface markers such as CD39, HLADR and LAG3. Interestingly, the mean frequency of suppressive Treg subset (CD39+ cells) was 43.5% of the CD25+FOXP3+ population in HC, however, this was significantly less in AA patients at 21.4% (P=0.001). There was also a concomitant reduction in the expression of the HLA-DR suppressive marker by Tregs with 38% of Tregs are HLA-DR positive in HC compared to 22% in AA patients (P≤0.0001). Contrarily, there was no change in the percentage of LAG-3+ cells in the Treg pool (Figure 3.6).

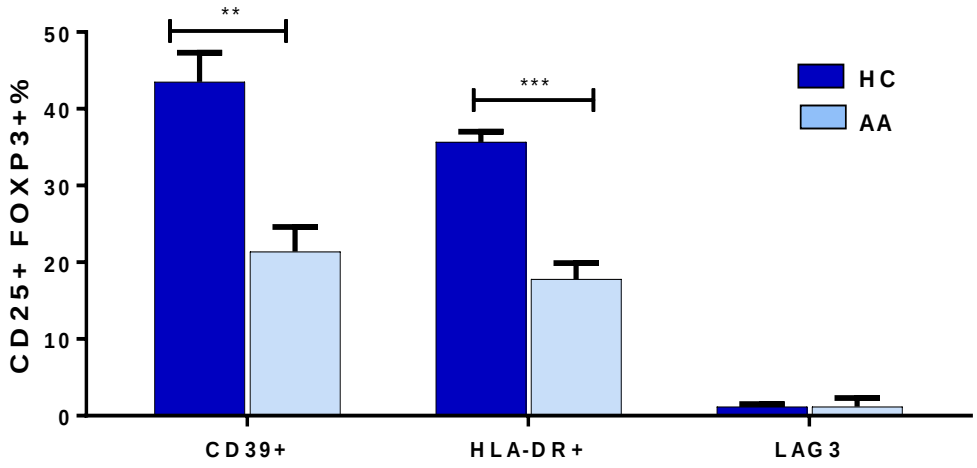

Figure 3.6. Suppressive subsets of CD25+FOXP-3+ Treg cells.
The frequency of suppressive subsets indicated by expression of CD39, HLA-DR or LAG3 surface makers was calculated out of the total Treg pool. Data analysed by a two-tailed independent t-test, and the corrected t-test was used whenever the homogeneity of variance was violated. A 95% confidence interval was used where P≤ 0.05 is considered significant (*) P≤0.01 (**), P≤0.001 (***). All bars depict mean with SEM in each study group. AA patients n=20, healthy controls (HC) n=10.

3.2.2.3. Immunosuppressive cytokine expression by Tregs

It was important to investigate the levels of intracellular cytokines produced by Tregs such as IL-10 and TGF-β to enable detailed dissection of Treg suppressive machinery, as secreting these cytokines is another key mechanism in Treg suppressive function. There was no significant difference in the percentage of cells expressing IL-10 (P=0.8) nor TGF-β cytokines (P=0.2) between patients and HC samples (Figure 3.7).

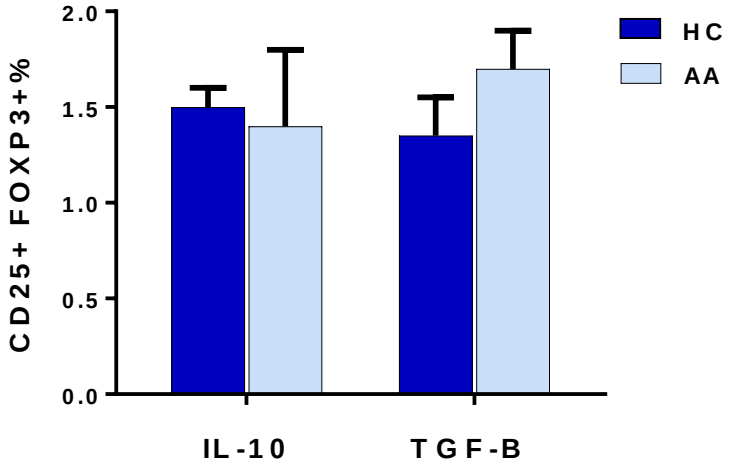

Figure 3.7. Suppresive cytokine expression by CD25+ FOXP3+ Treg cells.
The percentage of Treg cells expressing the intracellular markers IL-10 or TGF-β was calculated. There was no statistcally significant difference in both subsets between patients and HC. Data analysed by a two-tailed independent t-test, and the corrected t-test was used whenever the homogeneity of variance was violated. A 95% confidence interval was used where P≤ 0.05 is considered significant. All bars depict mean with SEM in each study group. AA patients n=20, healthy controls (HC) n=10.

3.2.2.4. Treg:Teff balance in AA patients' peripheral blood

To test the hypothesis of Treg:Teff balance disruption, a statistical correlation test was performed to see if there is any association between the changes observed in suppressive Treg populations and inflammatory T-cell subsets (Th1, Th17, Th2 and activated Tc). A two tailed, Pearson correlation

test was applied with a 95% confidence level. First, the correlation between the proportion of CD39+ suppressive Treg and Th17 was calculated. A significant negative correlation between the two T-cell subsets was found, Pearson's R= -0.46, P=0.006 (Figure 3.8). A high frequency of CD39+ Treg cells was associated with low frequency of Th17 cells in the peripheral blood, which was noticeably observed in HC samples. On the other hand, samples with reduced CD39+ Treg frequency tend to have high frequency of Th17 cells, which was evident in some patient samples, however; the heterogeneity of the patients recruited in this study may have limited the possibility to confirm the correlations.

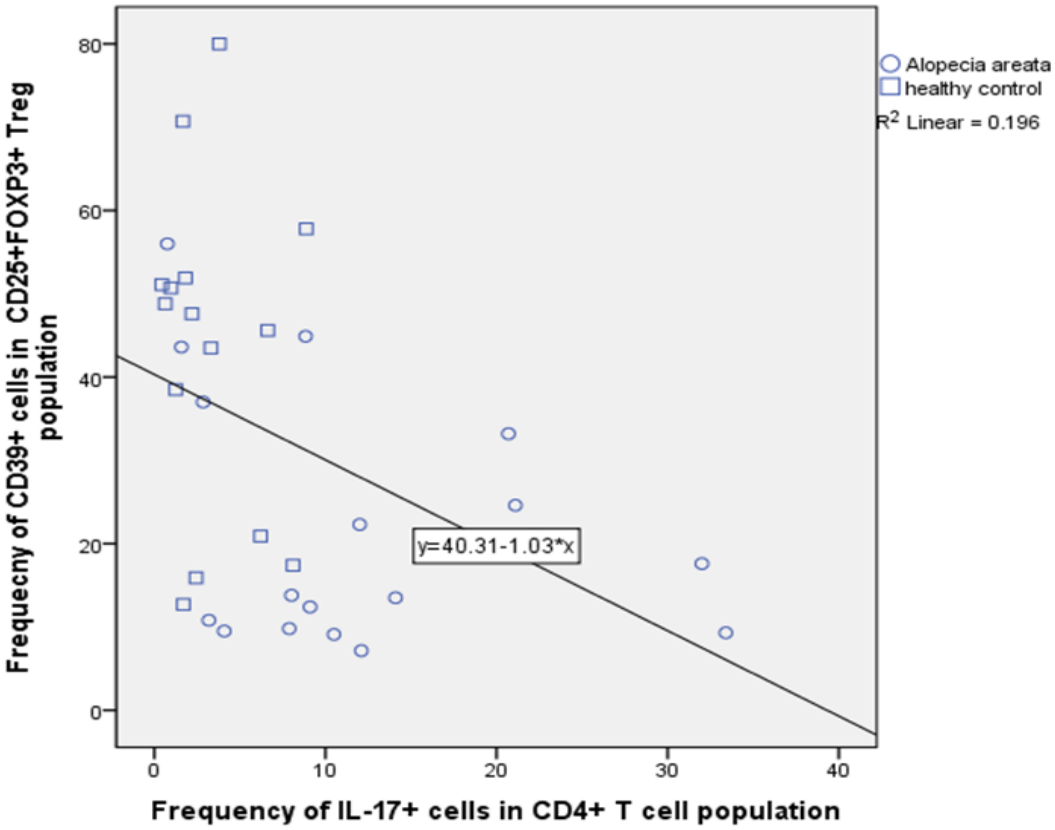

Figure 3.8. Correlation between Th17 and CD39+ suppressive Treg population (CD25+FOXP-3+CD39+).

The correlation was calculated by two-tailed Pearson's correlation coffiecient test on SPSS software. It indicates a negative correlation between the suppressive Treg expressing CD39 marker and Th17 CD4+ T-cell population. Data analsyed from 10 healthy control and 20 AA patients, Pearson's r= -0.46, P=0.006.

The HLA-DR+ Treg subset also showed significant negative correlation with Th17 cells, Pearson's R= -0.53, P=0.002. The correlation is more evident in HC blood samples where high frequency of HLA-DR+ Treg was associated with low frequency of Th17 cells (Figure 3.9).

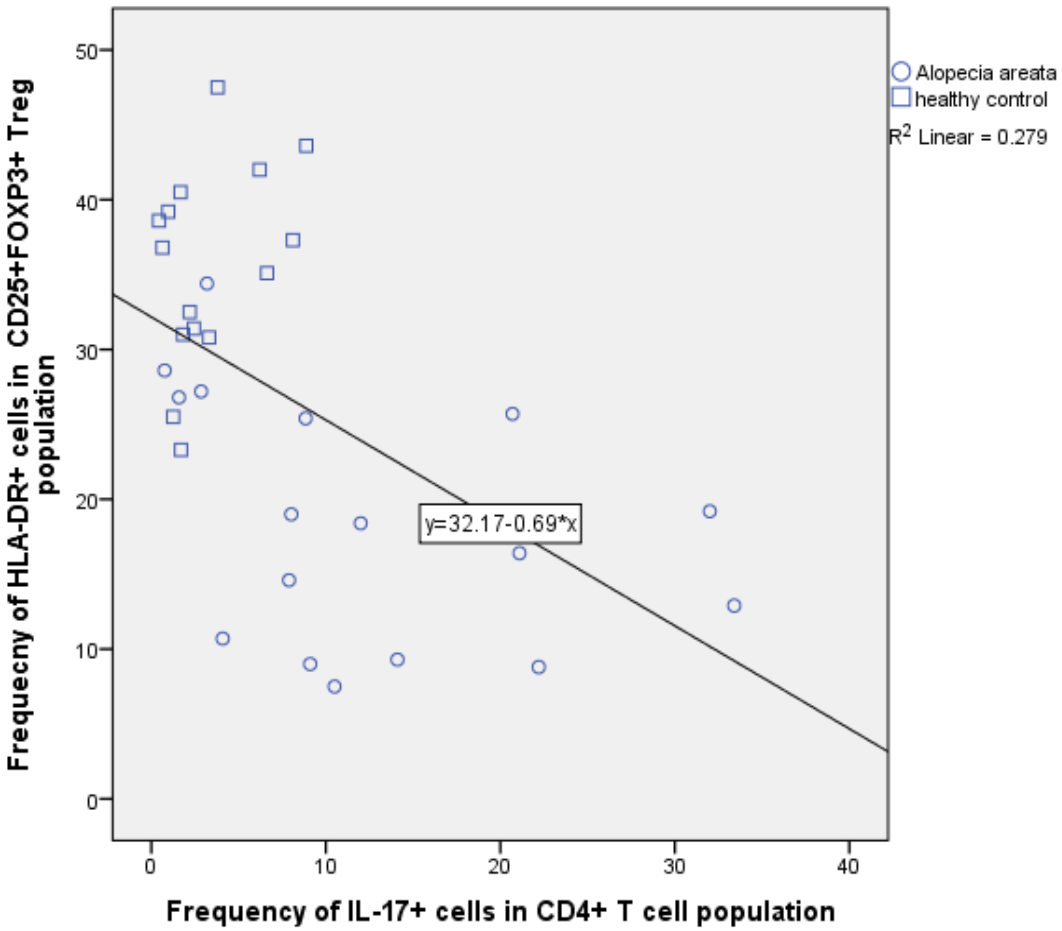

Figure 3.9. Correlation between Th17 and CD39+ suppressive Treg population (CD25+FOXP-3+HLA-DR+).

The correlation was calculated by two-tailed Pearson's correlation coffiecient t on SPSS software. It indicates a negative correlation between the suppressive Treg expressing HLA-DR marker and Th17 CD4+ T-cells population. Data analsyed from 10 healthy control and 20 AA patinets, Pearson's r= -0.46, P=0.006.

Interestingly, this negative correlation of suppressive Treg subsets (CD39+Treg and HLA-DR+Treg) was specific to Th17 cells. There is no significant correlation between the frequencies of CD39+ Treg or HLA-

DR+ Treg with any of the other Teff subpopulations including Th1 (CD119+ CD4+ T-cells), Th2 (CRTH2+ CD4+ T-cells), and activated cytotoxic T (Tc) cells (NKG2D+ CD8+ T-cells) (Table 3.3).

Table 3-3. Correlation data between suppressive Treg cells and inflammatory T-cell subsets.

Comparison		R value	P Value
HLA-DR + Treg	vs IL-17+ CD4+ T-cells (Th17)	-0.53,	0.002 **
	vs CD119+ CD4+ T-cells (Th1)	-0.33	0.06
	vs CRTH2+ CD4+ T-cells (Th2)	-0.30	0.09
	vs NKG2D+ CD8+ T-cells (activated Tc)	-0.18	0.31
CD39+ Treg	vs IL-17+ CD4+ T-cells (Th17)	-0.46	0.006 **
	vs CD119+ CD4+ T-cells (Th1)	-0.21	0.24
	vs CRTH2+ CD4+ T-cells (Th2)	-0.23	0.19
	vs NKG2D+ CD8+ T-cells (activated Tc)	-0.29	0.08

R and P values are shown to each pair of data.

3.2.2.5. CD39+ cell distribution in AA skin

The observations of a significant deficiency in the proportions of CD39+ Tregs in the peripheral blood of patients, and its negative correlation with Th17 suggested a need to investigate this marker further. Western blot analysis of the protein extracted from PBMCs of AA patients and HC was performed to look at CD39 protein expression. CD39 protein is found to be produced by PBMCs isolated from HC subjects but not by those of AA patients supporting the flow-cytometry findings (Figure 3.10).

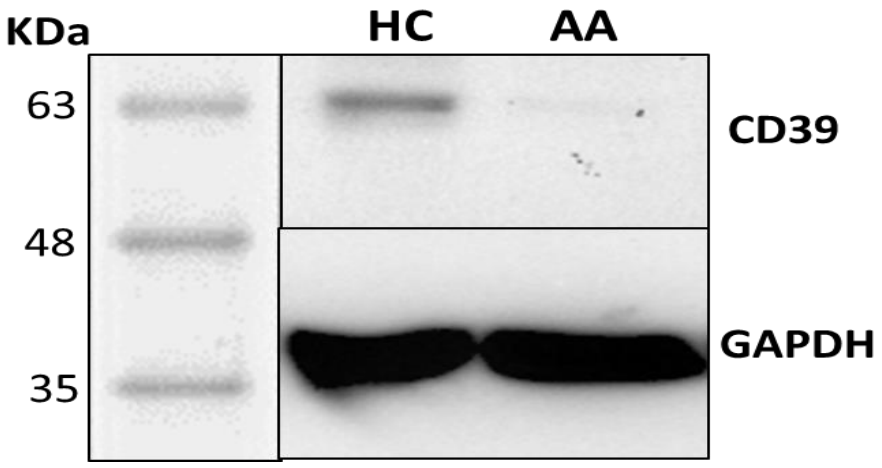

Figure 3.10. CD39 protein expression in AA and HC PBMCs.
PBMCs isolated from blood of AA and HC donors were lysed and loaded in SDS gel, CD39 protein was detected using rabbit monoclonal antibodies. CD39 protein ~(60KDa) was detected in HC but not AA samples.

A further analysis of total FOXP3+ Treg and CD39+ suppressive Treg populations within skin tissue was undertaken to define their distribution in normal and diseased skin. Treg-specific immunofluorescence microscopic analyses were performed on formalin-fixed, paraffin embedded, 5μm thick scalp skin sections obtained from HC, and lesional and non-lesional areas of AA patients. Antibodies against CD3 (generic T-cell marker), FOXP3 (Treg marker) and CD39 (suppressive Treg marker) were used. Three populations have been identified using this panel; CD3+FOXP3+CD39+ cells are suppressive Treg, CD3+FOXP3+CD39- Non-suppressive Treg that can be naïve or memory, and CD3+FOXP-CD39- are Teff cells. Suppressive Tregs were preferentially localized to normal skin (Figure 3.11.A) with lack of Teffs. Tregs infiltrate the outer connective tissue layer of HFs in close proximity to the follicular epithelium. The same distribution of suppressive Treg was seen in non-lesional skin of AA patients (Figure 3.11.B) in addition to an intra-follicular infiltrate of non-suppressive Treg (CD3+FOXP3+ CD39-Treg) and Teff (CD3+Foxp3- CD39-) in some sections. In contrast, diseased HFs lack these suppressive Treg, and they

are heavily infiltrated with Teff cells in presence of some non-suppressive Treg lacking CD39+ marker (Figure 3.11.C).

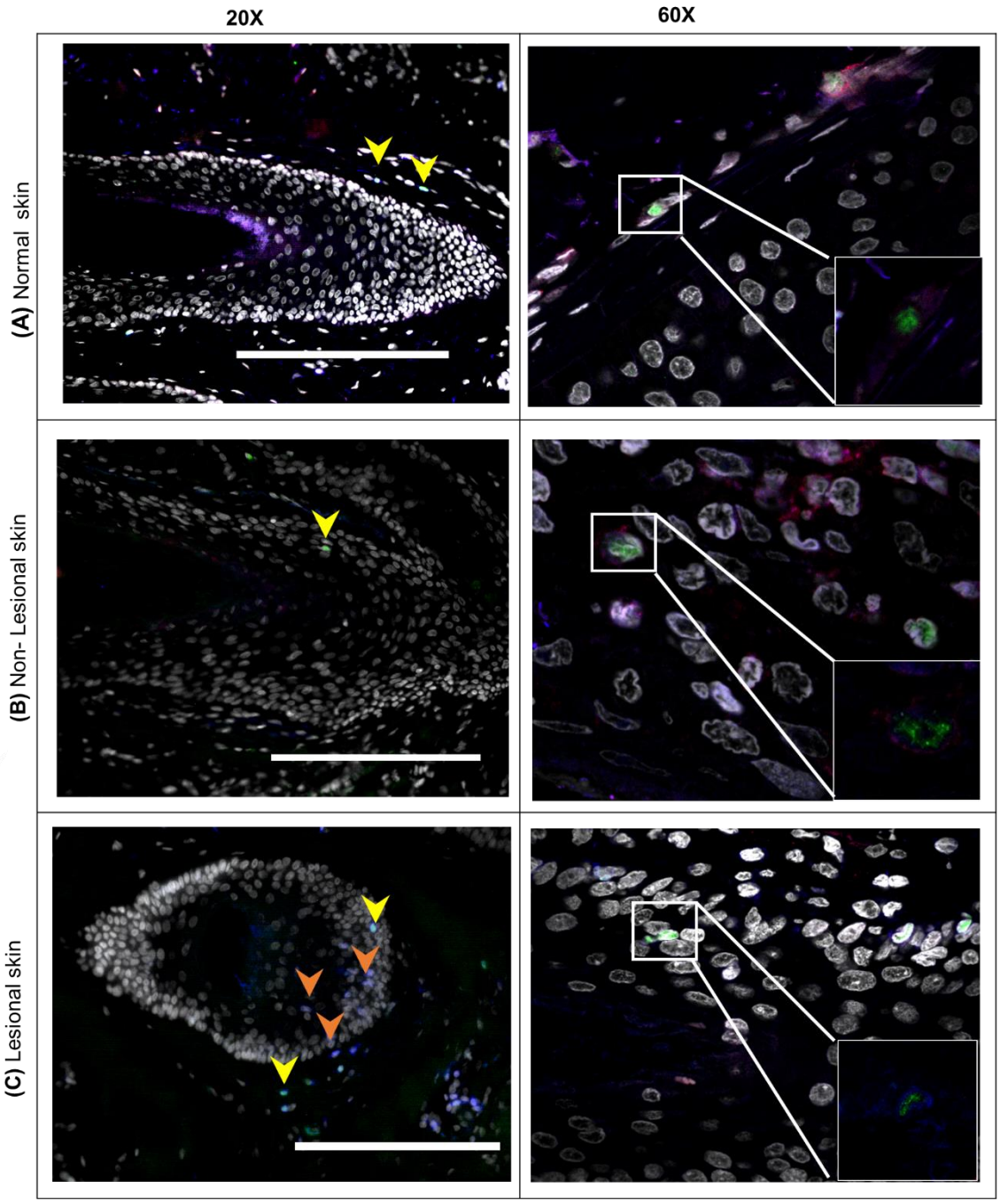

Figure 3.11. Suppressive Tregs localize to HFs in human skin.
Confocal microscopy of normal human skin, lesional and non-lesional skin of AA patients. Sections were stained for CD3 (blue), Foxp3 (green), CD39 (red), and DAPI (grey). Images taken at magnification X20 (left side) or X60 (right side). Small box is the zoom on 60X images without nuclei to clarify the triple staining. Scale bars: 100 μm. Arrows denote Treg (yellow) or Teff (orange).

Next, semi-quantitative analysis of IF images was performed to determine the frequency of Treg cells and their suppressive subtype in normal, non-lesional and lesional skin. The numbers of CD3+, FOXP3+ and CD39+ cells were counted per field, and the ratio of FOXP3+ cells to CD3+ T-cell pool in each field was calculated using FIJI cell counter software. The ratio of CD39+ cells in the FOXP3+ cell pool was calculated by the same method. Interestingly, the proportion of total FOXP3+ Treg cells was significantly reduced by about 80% in lesional skin compared to non-lesional skin ($P \leq 0.01$) and by about 90% when compared to normal skin ($P \leq 0.001$) (Figure 3.12). A similar trend was observed with suppressive Treg where the proportion was significantly less in AA affected skin compared to non-lesional ($P \leq 0.5$) and normal skin ($P \leq 0.001$). The data is representative of the skin sections of lesional areas from four AA patients and non-lesional skin sections of three patients and one healthy control. Only anagen HF were included in the analysis as AA is thought primarily to affect anagen HF, and to avoid the possibility that the variation observed in the sections were due to normal changes seen in the hair cycle stages. Due to that, data from two patients were excluded from the study as no anagen HFs were found as all HFs were in telogen phase.

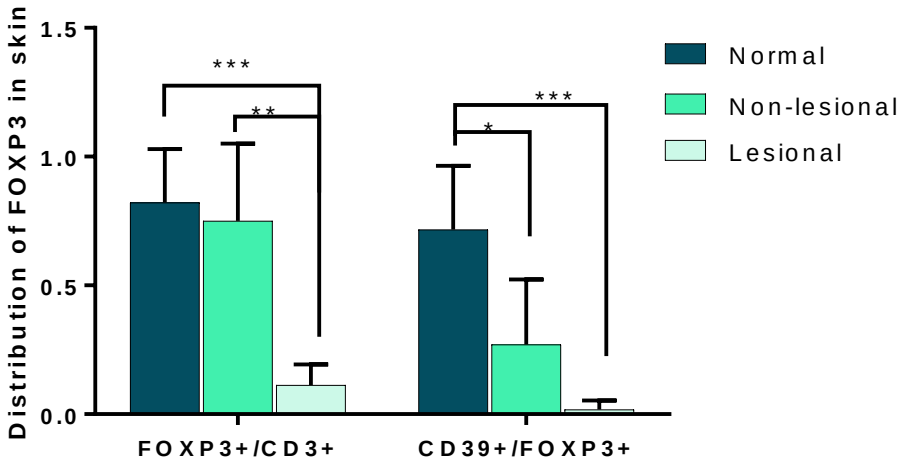

Figure 3.12. Treg distribution in normal and affected human skin.
The percentage of total and suppressive Treg indicated by expression of FOXP3 and CD39 makers was caluclated out of the total CD3+ or FOXP3+ T-cell pool respectively. Data analysed by ANOVA test with multiple comparison. A 95% confidence interval was used where P≤ 0.05 is considered significant (*),P≤0.01 (**). P≤0.001 (***). All bars depict mean with SEM of four fields in each study group.

3.3. Discussion

Autoimmunity is caused by defective balance of suppressive and pathogenic T-cells (Dejaco et al., 2006). This imbalance is proposed as the main mechanism in AA pathogenesis; however, despite the accumulating evidence on T-cells involvement, our understanding of the role of regulatory T-cells is very limited.

Tregs are key guardians of peripheral immune tolerance, and defects in their function can lead to fatal autoimmune diseases as seen in FOXP-3 null mice (Fontenot et al., 2003). Abnormality in lymphocyte function and numbers is not confined to the skin, as it can also be seen in spleen, skin draining lymph nodes (LN) and peripheral blood of affected subjects (McElwee et al., 2005b). For instance, CD4+CD25+ T-cells were found to be fewer in spleen and skin draining LN of affected C3H/HeJ mice compared to sham mice (Zoller et al,

2002). Zoller and et al. (2004b) investigated the frequency of CD4+CD25+ T-cells in the peripheral blood of AA patients, which showed an unexpected significant increase in this population. However, there was a decline in their suppressive activity particularly in progressive AA (Zoller et al., 2004, Shin et al., 2013). We think this reduction in Tregs' inhibitory function can explain the severity of the disease in these patients as this may enhance auto-reactivity, thereby stimulating the inflammation by activated T-cells. Defective Treg function has been observed in other autoimmune diseases such as thyroiditis and autoimmune diabetes in animal models (Sakaguchi, 2004).

In this study, flow-cytometery data showed a significant increase in CD4+CD25+FOXP3+ T-cells (Treg) by about 40% in patient's peripheral blood compared to HC in agreement with previous researchers' findings. This can in part be explained in the current study by the marked increase in CD4+FOXP3+ CD45RO+ T-cells (memory Treg), which is expected to be high as these cells encountered HF autoantigens previously. More importantly, the second question this study attempts to answer is whether these Treg cells are functionally suppressive. Different mechanisms are employed by Tregs to exert their suppressive function. The conversion of ATP to adenosine initiated by the ectonucleotidase CD39 (Antonioli et al., 2013); cell to cell contact mediated by HLA-DR+Tregs (Baecher-Allan et al., 2006); and suppressive cytokine secretion (Liberal et al., 2015) are among the most used suppressive mechanisms by Tregs. Therefore, it was important to elucidate which of these mechanisms if any is defective in AA?

These data showed for the first time which regulators mediate the impairment in Treg function. There was a significant reduction in CD39 and HLA-DR subsets of the Treg population by about 50% in AA subjects compared to

HCs. CD39 is ENTPDase1 that hydrolyses ATP into AMP, which is subsequently hydrolysed by CD73 into adenosine (Antonioli et al., 2013). Hence, CD39 plays a central role in modulating the pro-inflammatory micro-environment induced by ATP, into anti-inflammatory milieu driven by adenosine thereby inhibiting Teff development (Deaglio et al., 2007). In comparison to CD39- Treg, CD39+ Treg cells have higher suppressive capacity (Ye et al., 2015) and greater stability (Gu et al., 2017). That was supported in many studies where CD39+FOXP3+ cells show marked suppressive activity against Teff, particularly Th17 (Fletcher et al., 2009).

Our immunostaining data have demonstrated the presence of CD39+ suppressive Tregs around the normal HF in human skin, preferentially in the outer connective tissue layer of the lower two-thirds of HF, which supports the proposed role of these cells in maintaining IP. Interestingly, the proportion of total Tregs to the infiltrating lymphocyte pool (CD3+ T-cells) was reduced significantly in non-lesional HF by about 80% ($P \leq 0.01$), and more significant reduction was observed when compared to normal HF ($P \leq 0.001$), and that was accompanied by reduction in the proportion of suppressive CD39+Treg. Our flow-cytometry data also demonstrated significant reduction of HLA-DR+ Treg where it is known that HLA-DR on Tregs mediates cell-to-cell suppression of Teff. Interestingly, Rissiek et al 2015 showed that HLA-DR expressing Tregs are almost always CD39+, which could explain their containment reduction observed in the current study (Rissiek et al., 2015).

These findings provide a novel insight on the mechanism of IP maintenance. Thus IP collapse can be explained by two mechanisms; primary failure of Treg suppressive capacity, which is proposed in this study to be through CD39 molecule deficiency. Impaired Treg function has been proposed

as a key player in other autoimmune diseases such as rheumatoid arthritis (Ehrenstein et al., 2004) and psoriasis (Yang et al., 2016). Yang and colleagues showed Tregs isolated from psoriatic patients have impaired suppressive function being unable to inhibit proliferation of Teff in co-culture, and they produce inflammatory cytokines such IL-17 and IFN-γ attributing that to an activation of STAT-3 pathway in these cells. The second proposed mechanism of IP collapse is Treg functional failure secondary to the increase in Teff cell frequencies including CD8+ cells and inflammatory CD4+ cells. Due to Treg plasticity, production of inflammatory cytokines by Teffs such as IL-17 and IFN-γ probably results in Treg differentiation into Teff (Yang et al., 2008, Oldenhove et al., 2009).

The suppressive cytokine secretory capacity of Tregs was investigated and showed no significant changes in the frequency of IL-10+ nor TGF-β+ Tregs between patients and HC. This finding was also supported by LAG-3 expression, which showed no difference between the two groups. Activation gene (LAG3) was reported as a marker of IL-10 producing Tregs (Nakachi et al., 2017). These findings collectively suggest that Treg impaired function in AA is mainly due to defect in the cell-to-cell contact and CD39-mediated suppressive machinery and not in cytokine secretion. It is also suggested these two mechanisms are the main suppressive mechanisms via which Tregs mediate their inhibitory function around normal HF.

The defect in Treg function can be the drive to the increase in the inflammatory T-cells (Teff) that has been seen in this study. IL-17+ producing CD4+ T-cells (Th17) were four times higher in patients' PBMCs compared to HC. Increase in Th17 around HF of AA patients associated with reduction in FOXP3+ Treg was observed in other studies (Tojo et al., 2013, Tanemura et al., 2013,

Han et al., 2015). A significant negative correlation was observed in this study between Th17 cells and suppressive Tregs, CD39+ Treg (r= -0.46) and HLA-DR+ Treg (r= -0.53). Interestingly, this correlation was specific to Th17 cells with no significant correlation of suppressive Tregs with the other inflammatory T-cells subsets being found. This correlation can be explained by the competing fates (either Th17 or Treg) of naïve T cell differentiation where the lineage choice is determined by relative amounts of IL-6 and TGF-β (Bettelli et al., 2006, Zhou et al., 2008). Therefore, Tregs might limit Th17 differentiation by exhausting common precursors (Bettelli et al., 2006).

Previous studies reported involvement of Th17 in AA as suggested by Aytekin et al (2015) due to association of IL-17 gentotype with increased susceptibility for AA (Aytekin et al., 2015). Furthermore, serum IL-17 level measured by ELISA was found significantly increased in its production in patients compared to HC (El-Morsy et al., 2016), which agrees with our ELISA data showing significant increase (p=0.006) in IL-17 production by patients' PBMCs. CD4+ helper T cells differentiation into Th17 cells is mediated by STAT-3 activation under the effect of cytokines including transforming growth factor-β, IL-6, IL-1β, and tumor necrosis factor (TNF)-α, however, it is important to highlight that neuropeptides also control Th17-dependent pathways. This is supported by the fact that chronic stress can alter activated lymphocytes to a Th17 response in mouse model (Harpaz et al., 2013). Therefore, the increase in IL-17 reported in this study could support the neuroendocrine-immune hypothesis of AA pathogenesis. For instance, episodes of alopecia areata (AA) have occurred after severely stressful life events (Reinhold, 1960, Paus and Arck, 2009). Similarly, neuropeptides such as substance P have been demonstrated to mediate a collapse of MHC class I–based hair follicle immune

privilege in organ-cultured normal human scalp hair follicles resulting in hair follicle degeneration (Siebenhaar et al., 2007). Further studies are warranted to better delineate the exact role of IL-17 in AA pathogenesis.

Our data showed that CD8+ T-cells were less frequent in PBMCs of patients compared to HC in line with the increase in CD4:CD8 cells ratio in peripheral blood agreeing with Luckac and colleagues' study (Luckac et al., 1993). This is also in agreement with CD4:CD8 ratio around affected HF, in which the cellular infiltrate is composed of higher numbers of CD4+ T-lymphocytes than CD8+ T-lymphocytes, and the ratio has shown to be slightly higher in the acute phase in comparison to the chronic phase (Ghersetich et al., 1996). Interestingly, despite the observed reduction in CD8+ T-cell proportion, the NKG2D+ expression on CD8+ T-cells is significantly higher in patients compared to HC by about 12%. IFN–γ, a main inducer of ectopic MHC class I expression (René et al., 1998), was produced in higher proportion by patients' PBMCs ($P \leq 0.01$) that could be secreted by the activated CD8+ T-cells or Th1. NKG2D+ is closely associated with HF auto-reactivity in AA resulting in termination of the anagen phase of HF growth and precipitating catagen via binding to MICA molecules on target cells (Ito et al., 2008). The CD8+NKG2D+ T-cell subset has become an important measure in testing any response to a new treatment in AA.

To sum up (Figure 3.14), this novel work demonstrated Treg-Teff balance disruption as a major player in AA pathogenesis. Impaired Treg function is mainly due to lack of CD39+ and HLA-DR+ mediated suppressive mechanisms with unaffected immune-suppressive molecules secretion and LAG3 mediated suppression. Impaired Treg functionality is accompanied by increased frequency of Th1, Th17 and NKG2D+ CD8+ T-cells.

One of the limitations in this part of the study is the low number of participants; therefore, more time is required to recruit more participants in order to gain a larger statistical population. That would also allow stratification of the data according to disease severity, which would give more information about the role of Treg in disease progression. More skin tissue sections would allow analysis of infiltrating T-cell subsets such as CD4+, CD8+ and Treg cells as well as their activation status in HF. That also requires taking in consideration whether the tissue biopsy is taken from margin or the centre of the hair loss patch and the stage of the disease. The data could then be compared with peripheral blood samples to further elucidate the reason for changes in circulating peripheral T-cell subsets noted in this thesis.

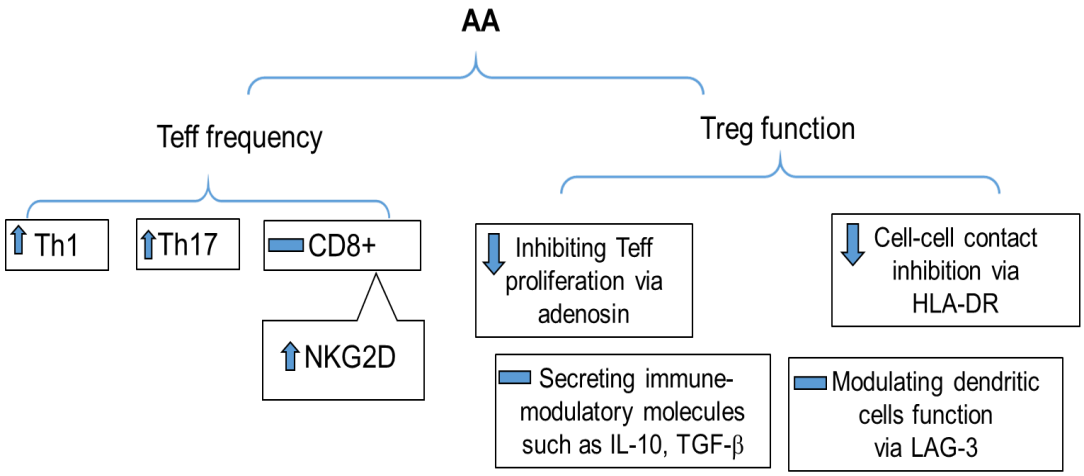

Figure 3.13. Proposed T-cell involvement in AA pathogenesis.
IP collapse in AA is mainly due to impairment of Treg function, which is mediated by lack of adenosine production via the CD39-mediated anti-inflammatory mechanism and cell-cell contact inhibition via HLA-DR while other mechanisms are not affected such as secreting immune-modulatory molecules such as IL-10, TGF-β and LAG-3-mediated suppressive function. This is associated with increased frequency of Th1, Th17 and NKG2D+ subsets of CD8+ cells.

Chapter 4 . TCR clonotyping in AA patients

4.1. Introduction

T-cells have a central role in AA pathogenesis indicated by the dense lymphocytic infiltrate of T-cells around HF along with their cytokines profile and genetic association to AA (Todes-Taylor et al., 1984, Xing et al., 2014, El-Morsy et al., 2016). In addition, flow-cytometry and IF findings shown in the previous chapter indicated a marked disruption of T-cell distribution in patients' blood and skin when compared to HC. However, there is a gap in current understanding of the molecular basis of immune cell involvement in AA. Recently, huge effort has been directed towards deciphering the TCR signature of T-cell clones involved in many autoimmune diseases. This provides novel insight on the disease mechanism; as TCRs are the main determinants of epitope specificity and phenotype predominance in a disease, (Acha-Orbea et al., 1988). One example is TCR-specific antibodies showed protective effect against experimental autoimmune encephalomyelitis (EAE) in Lewis rats (Stevens et al., 1992, Vandenbark et al., 1989).

The antigenic epitope is presented to the TCR in conjugation with major histocompatibility complex (MHC) molecules. Each unique TCR is generated by TCRα and TCRβ chain rearrangements, where the greatest amount of diversity is found in the TRCβ chain, in particular in CDR3 region as explained in section 1.4.3. CDR3 is generated by rearrangement of three genes V, D and J with the possibility of N nucleotide insertions into the VD and DJ junction increasing the region's diversity. Advances in sequencing technology, in particular NGS

techniques, allow in depth analyses to be performed on the CDR3 region of TCR chain of many subjects at the same time (Morozova and Marra, 2008).

Peripheral blood mononuclear cells (PBMCs) isolated from AA patients and HC represent total lymphocyte population. CD4+CD25+FOXP3+ T-cells were FACs sorted from PBMCs, and represented the regulatory T-cells pool (Treg). Multiplex PCR was performed on gDNA extracted from these samples using 39 V primers and 13 J primers to amplify the rearranged CDR3 region, and the PCR products were analysed by NGS using the Illumina platform. The aim was to determine the TCRβ signature of total lymphocytes and Tregs involved in AA pathogenesis to unveil the complexity of the T-cell response in AA.

4.2. Results

4.2.1. Clinical data

PBMCs were isolated from ten AA patients and seven healthy donors. Tregs were sorted from another four AA patients and three HCs. The clinical data on these patients is shown in Table 4.1.

Table 4-1. Clinical data of participants.

Patient ID	Clinical type	Age
AA32	AA	25
AA33	AA	65
AA34	AU	55
AA26	AU	58
AA07	AA	68
AA10	AU	69
AA13	AA	39
AA21	AT	52
AA22	AU	51
AA24	AU	68
AA26	AU	58
AA27	AA	49
AA28	AT	34
AA29	AA	66
HC01	NA	40
HC03	NA	34
HC13	NA	45
HC15	NA	35
HC16	NA	29
HC17	NA	25
HC18	NA	27

HC=Healthy control, AA=Alopecia areata,
AT=Alopecia totalis, AU=Alopecia universalis

4.2.2. Quality control

The quality of the NGS data can be affected by a series of steps involved the sequencing process such as library preparation, base calling and read alignment. Therefore, a number of quality metrics were applied to assess the effect of each step of the upstream workflow on the data output. The sequence analysis viewer of Illumina provides quality control charts during the run to monitor the run quality and reliability. The base calling accuracy is one of the main quality metrics; it refers to the accuracy of the sequencer to recall the right base. This is measured by the Phred quality score (Q score), which calculates the probability of calling the incorrect base using the formula ($Q=-10 \log_{10} P$) where P is the base calling error probability giving figures as shown in table 4.2 where the higher Q score means the higher probability of calling the right base

during the sequencing process. In this NGS experiment, 89% of the data was above Q30 indicating the probability of calling the right base was 99.9% (Figure 4.1).

Table 4-2. Quality score of NGS data.

Phred Q Score	Probability of incorrect base call	Accuracy of Base call
10	1 in 10	90%
20	1 in 100	99%
30	1 in 1000	99.9%
40	1 in 10,000	99.99%
50	1 in 100,000	99.999%

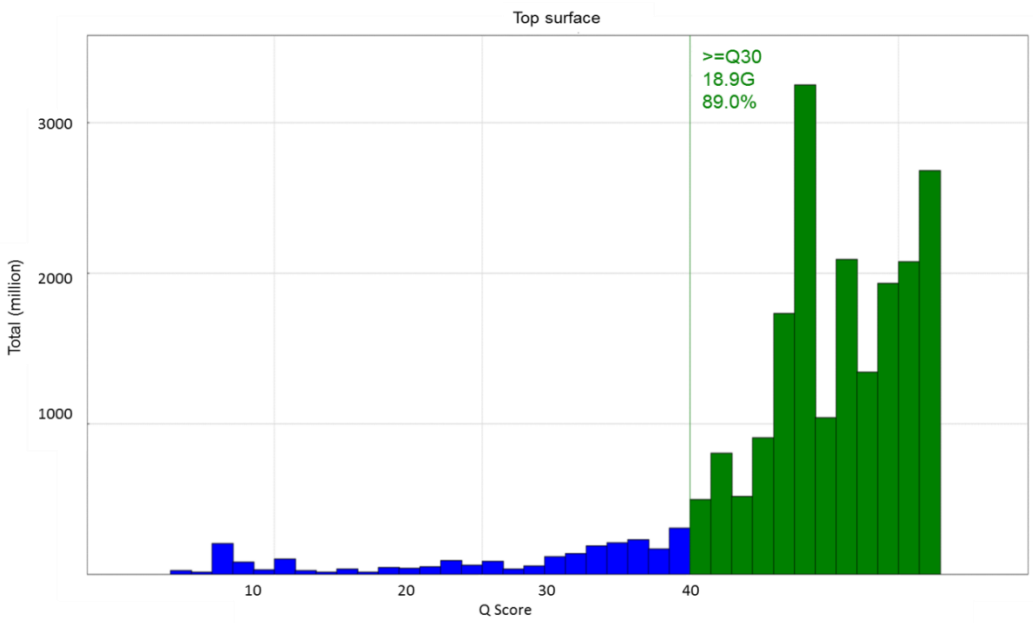

Figure 4.1. Quality score of NGS data.
About 89% of data has Q score above 30 indicating 99.9% probability of calling the right base during the sequencing process.

The distribution of quality metric throughout the 200 cycles run was calculated by Illumina software. The clusters became unstable over the length of a 200 cycle run as it took 11 days. Therefore, it was observed that the quality was high initially, and dropped off gradually, however, it remained above Q30. Note the decline in quality at cycle 50 and 150 and indexing step at about 100 cycle (Figure 4.2).

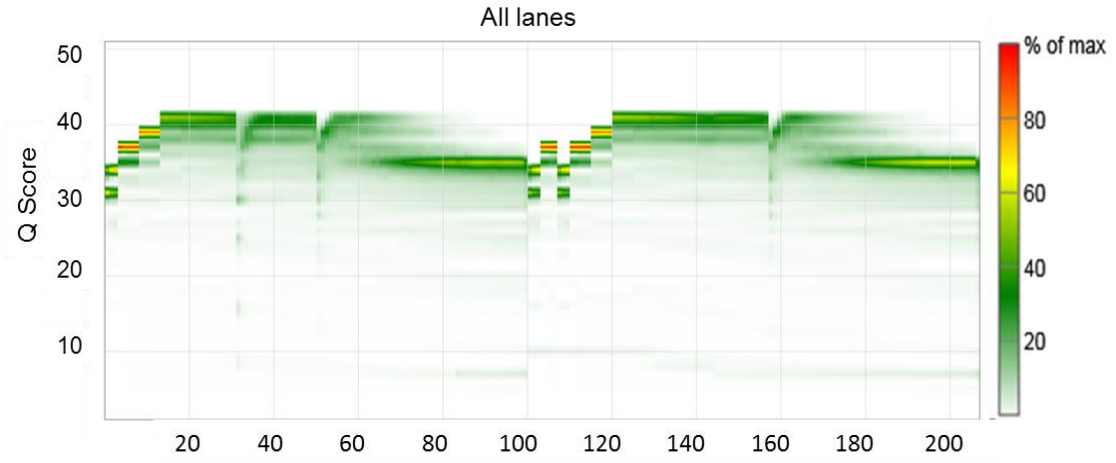

Figure 4.2. Quality score distribution of NGS data throughput the run.
Q score was above 30 thought the major time of the run, drops at about 50, 100 and 150 can be seen.

The drop in the quality at cycles 50, 100 and 150 can be explained by looking at signal intensity (Figure 4.3). This shows the signal intensity for each base (A, C, G, T) added to each cluster and imaged over the course of the entire 200 sequencing cycles. Cycles 50 and 150 show a spike in intensity where the laser receives a power boost. Finally, the change in intensity during the middle part of the run is due to the index read where the barcodes added during the library preparation were sequenced during that time.

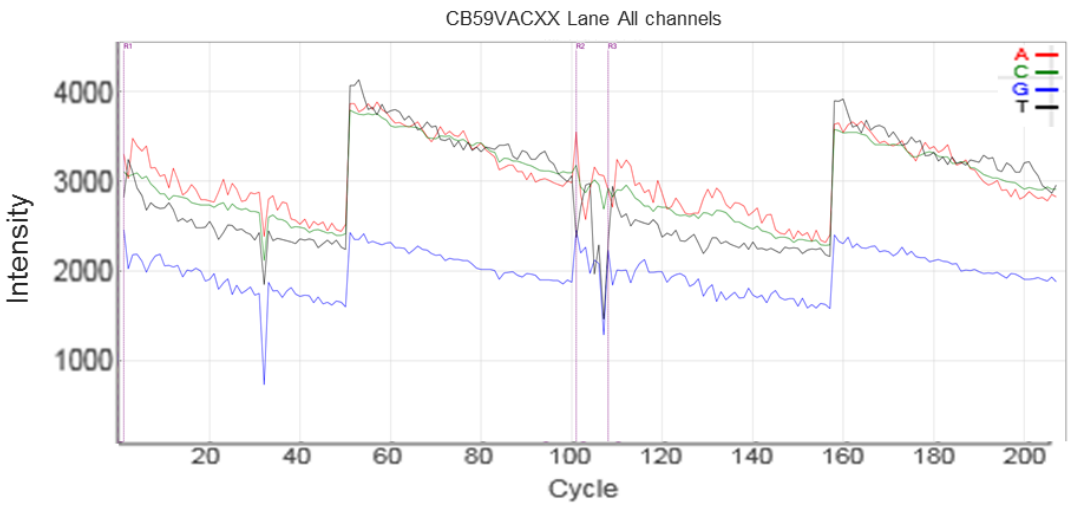

Figure 4.3. Signal intensity of recalled bases.
The number of sequencing cycles on X-axis and the signal intensity on Y-axis. Bases were visualized in different colors, A=red, C=green, G=Blue and T=black.

Cluster density is another key metric that impacts sequencing performance and the quality of the run, while under-clustering causes lower data output, over-clustering lowers the Q score due to introducing sequencing artefact (https://support.illumina.com/content/ 770-2014-038.pdf). Illumina has a so-called Chastity filter to measure the purity of the signal, and reads failing to pass the filter are considered less reliable and removed from the analysis. Therefore, the percentage of reads pass-filter (%PF) is an important quality indicator and over-clustering negatively impacts on the %PF causing its reduction. The study data in lane 1 (Figure 4.4) had cluster density (blue box) of about 700,000 clusters per mm^2, and they were overlapping with %PF quality filter (red box) indicating optimal generation of sequence data.

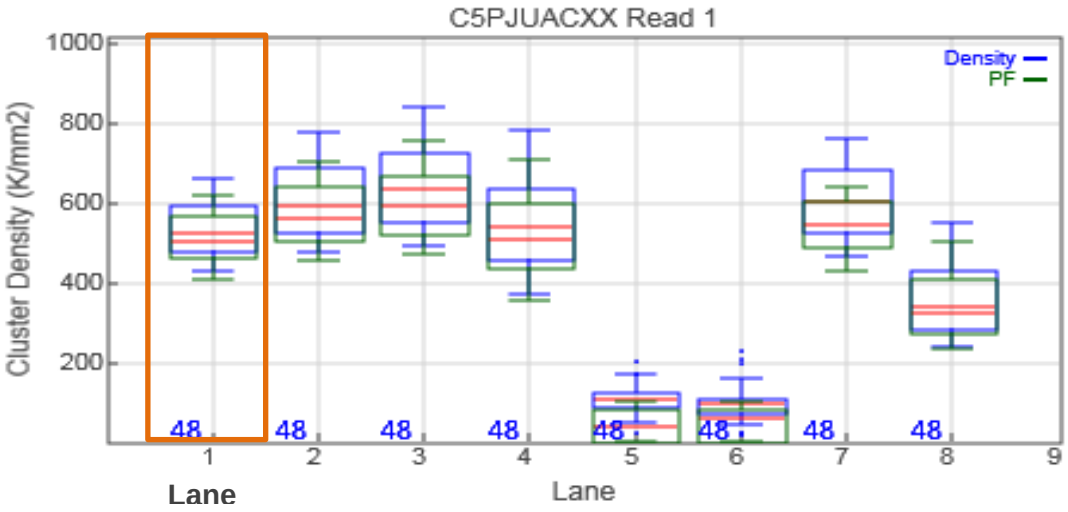

Figure 4.4. Cluster density and passing filter box plot quality control.
The lanes (1-8) in flow cell are represented on the X-axis. The cluster density is represented on the Y-axis. The samples were loaded on lane 1 (23 samples). Cluster density in the blue box and %PF in the green box and the median shown by a red line. The cluster density and %PF boxes are overlapping.

4.2.3. Primary analysis of TCR clonotype

The bioinformatics analysis was performed in collaboration with Dr. Afsaneh Maleki-Dizaji, a research fellow in computational biology, Department of Computer Science, University of Sheffield. Reads of the DNA sequence were paired endwise. The Illumina sequencer generated bcl files, which were converted to fastq files by the bcl2fastq program. An average of 7.7 million total raw reads were obtained from each sample, and 7 million reads that met the quality requirements after removal of low-quality reads were aligned to the TCRβ CDR3 human genome using the MIXCR pipeline (Table 4.3).

Table 4-3. Raw statistics of TCRβ sequences.

Sample ID	Total sequence read	Total of assembled	% of assembled reads
FAA26	6362770	6021783	95%
FAA32	7291450	5611589	77%
FAA33	9373820	6609669	71%
FAA34	3731882	3132306	84%
FAA43	3731882	3042128	82%
PAA7	8919572	8625223	97%
PAA10	13198354	12698016	96%
PAA13	17074228	16578466	97%
PAA21	7932050	7678520	97%
PAA22	11000178	10650348	97%
PAA24	5477294	5302667	97%
PAA26	9062926	8776243	97%
PAA27	5839794	5658942	97%
PAA28	8076702	7838701	97%
PAA29	5721290	5539912	97%
FHC01	3799472	3520331	93%
FHC15	4825830	3702722	77%
FHC16	2978560	2796238	94%
PHC01	2625519	2565593	98%
PHC03	13097328	12747960	97%
PHC13	8083120	7822527	97%
PHC15	5530536	5369027	97%
PHC16	3784520	3663315	97%
PHC17	6588222	6431118	98%
PHC18	24908242	24104445	97%
PHC01	2625519	2580114	98%

F=FACS, P=PBMC, HC=Healthy control, AA=alopecia areata patients.

MiXCR pipeline is a universal software developed by MiLaboratory (https://milaboratory.com/software/mixcr/) for fast analysis of Ig and TCR repertoires (Bolotin et al., 2015). It processes raw fastq sequences of immune data into quantitated clonotypes. It handles single-end and paired-ends reads, corrects PCR errors, considering sequence quality and identifies germline hypermutations. The pipeline (Figure 4.5) first aligns the sequence reads to V, D and J reference genes of TCR region, it then assembles the identical

sequences into clonotypes, and a correction step is performed by discarding low quality reads that result from PCR and sequencing errors, and finally exports them in human-readable format.

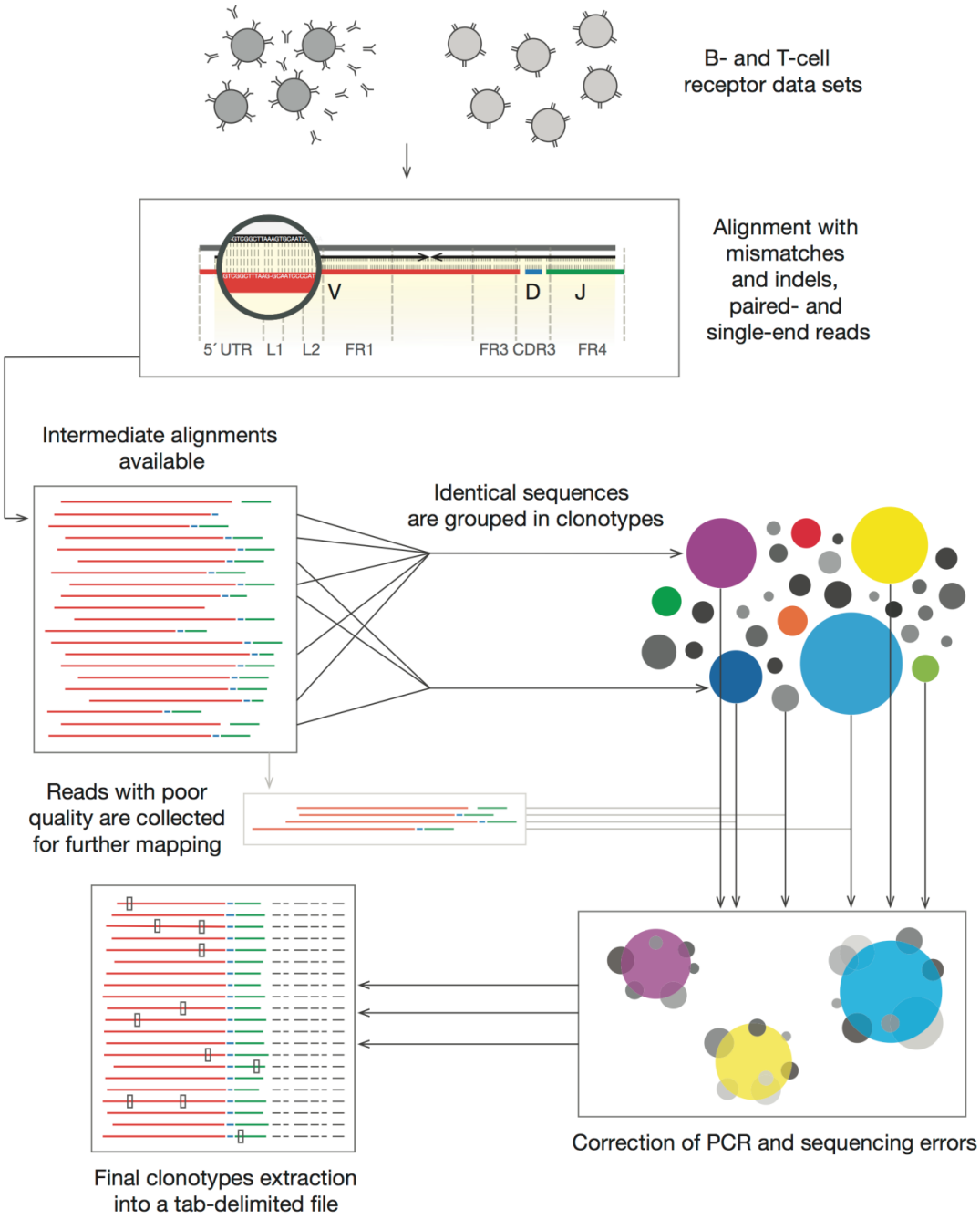

Figure 4.5. MiXCR workflow.
Raw Fastq file is uploaded to the software, alignment is then performed and identical sequences are assembled into clonotypes and exported into readable format after correction of PCR and sequencing errors. Figure was adopted from MiXCR website.

4.2.4. Secondary analysis of TCR clonotype data

The output of MiXCR was further analysed by complementary software called VDJtools (http://vdjtools-doc.readthedocs.io/en/latest/). It is a JAVA based framework which performs the post-analysis of TCR clonotypes and provides graphical representation of the data using TCR datasets (Shugay et al., 2015). The figures in this section were created by the researcher unless otherwise mentioned.

4.2.4.1. Estimating TCR repertoire diversity

The TCR repertoire can be described as a collection of different species, and the biodiversity is assessed by species richness calculating the frequencies of shared species in a given group (Robins et al., 2009, Joachims et al., 2016). Thus, in order to determine the impact of clonal expansion on the diversity of TCR repertoire in total lymphocytes and Tregs of AA patients, the biodiversity was assessed in each group using a choa1 normalised sample estimate, which is one of the most commonly used measures to calculate species richness (Colwell et al., 2012). It was crucial to use normalised sample measure for diversity where datasets are normalized to the same size because increasing sample size results in higher diversity (Lemos et al., 2011). Although the differences in Chao1 figures between the study groups did not reach statistical significance, it can be observed that the TCR repertoire of total lymphocytes from patients was slightly less diverse (chao1=3.2) compared to controls (chao1=3.4), which was likely due to the presence of dominant clonotypes. On the other hand, the Treg repertoire showed higher diversity in patients (chao1=2.4) when compared to HC (chao1=2.3) reflecting the limited heterogeneity and predominance of a few clonotypes of Treg cells in HC (Figure 4.6).

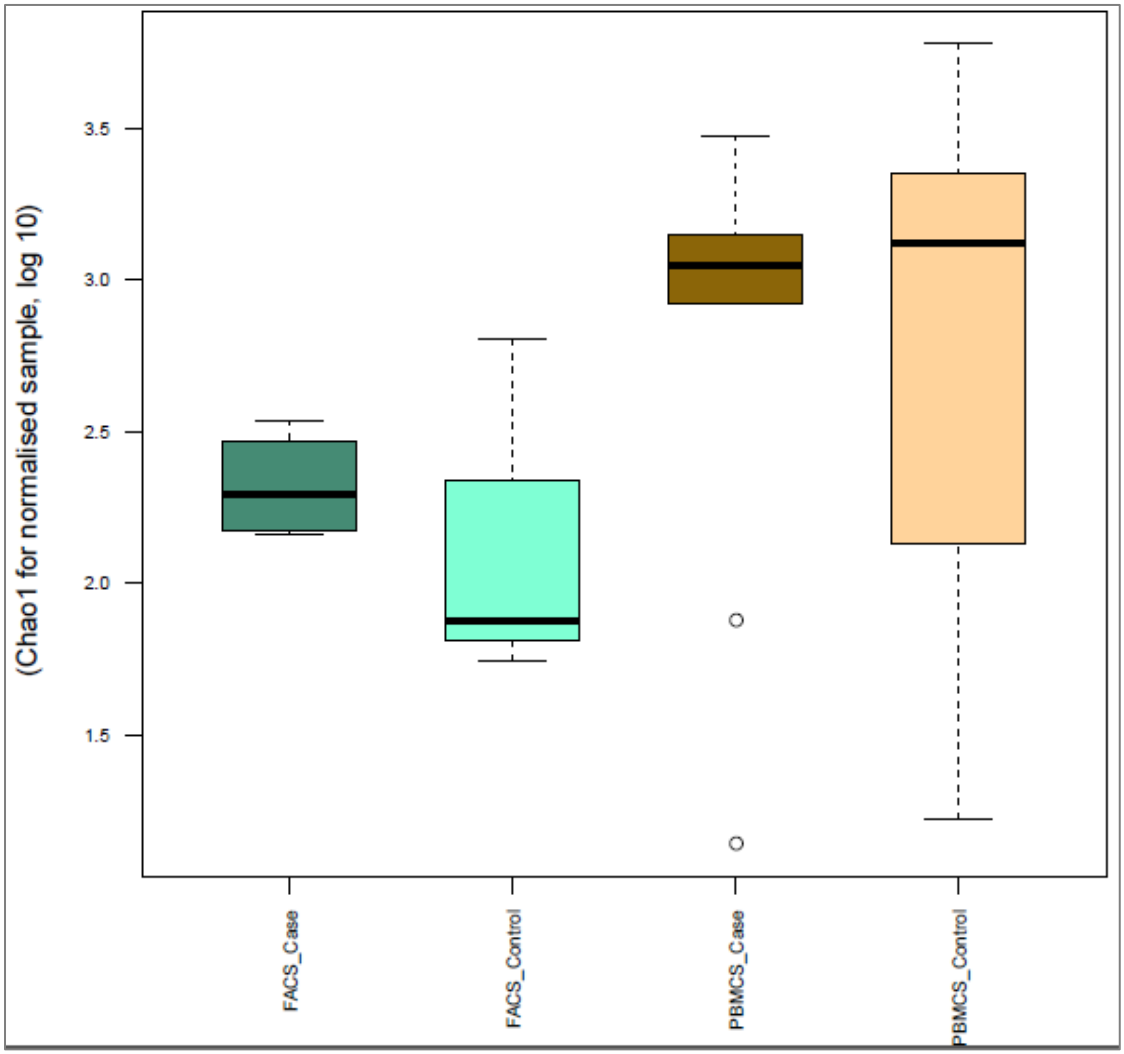

Figure 4.6. TCR Repertoire diversity estimation.
Boxplots of chao1 estimator for normalised datasets were used to assess the diversity of TCR repertoire in cases and controls. The figure was created by Dr. Afsaneh Maleki-Dizaji

4.2.4.2. Public sequence shared between individuals in each group

Unlimited numbers of antigens can be encountered during an individual's lifetime, and a huge number of diverse TCR regions can be detected in human blood. The observation of public TCR sequences shared by many individuals is therefore striking, suggesting immune-reactivity in those individuals to the same antigen. To investigate clonotype overlap, VDJtools produced pooled clonotype abundance table where the number of reads associated with public clonotypes was computed in each group as well as their frequency. Public clonotypes were

considered by the software as those having identical CDR3 nt sequences, VDJ arrangements and start and end locations of each segment. The most prevalent public clonotype in each group is presented in Figure 4.7.

CA*PGG*AS_GSYNEQFF and CASSLGTVYTEAFF were the most prevalent public clonotypes in all groups. Strikingly, there was clonal expansion of two CDR3 sequences; CASSYQGSTEAFF and CASSQDKGITNEKLFF in total lymphocytes from AA patients, and in relatively high frequency 0.005 and 0.004. Despite the enormous number of TCRβ chains, these clones are not present elsewhere within the sample set including total lymphocytes of HC and Tregs from patients or HCs. CASTKTKRQGPISRPFPTGELFF, CANSTRGS_PGNTIYF and CASSPTGPTEAFF sequences were more abundant in Tregs isolated from patients (with frequency of 0.02, 0.01 and 0.08 respectively) compared to controls (0.008, 0.002 and 0.003). On the other hand, some Treg clones were expanded in healthy individuals but not in patients. For instance, TCRβ sequences: CATSRDEGGLDEKLFF and CASRDGTGPSNYGYTF were found in Tregs of HCs at 0.003 and 0.002 frequencies but not in Tregs from AA patients. The top ten public sequences and their frequencies in each study group shown in appendix 4.

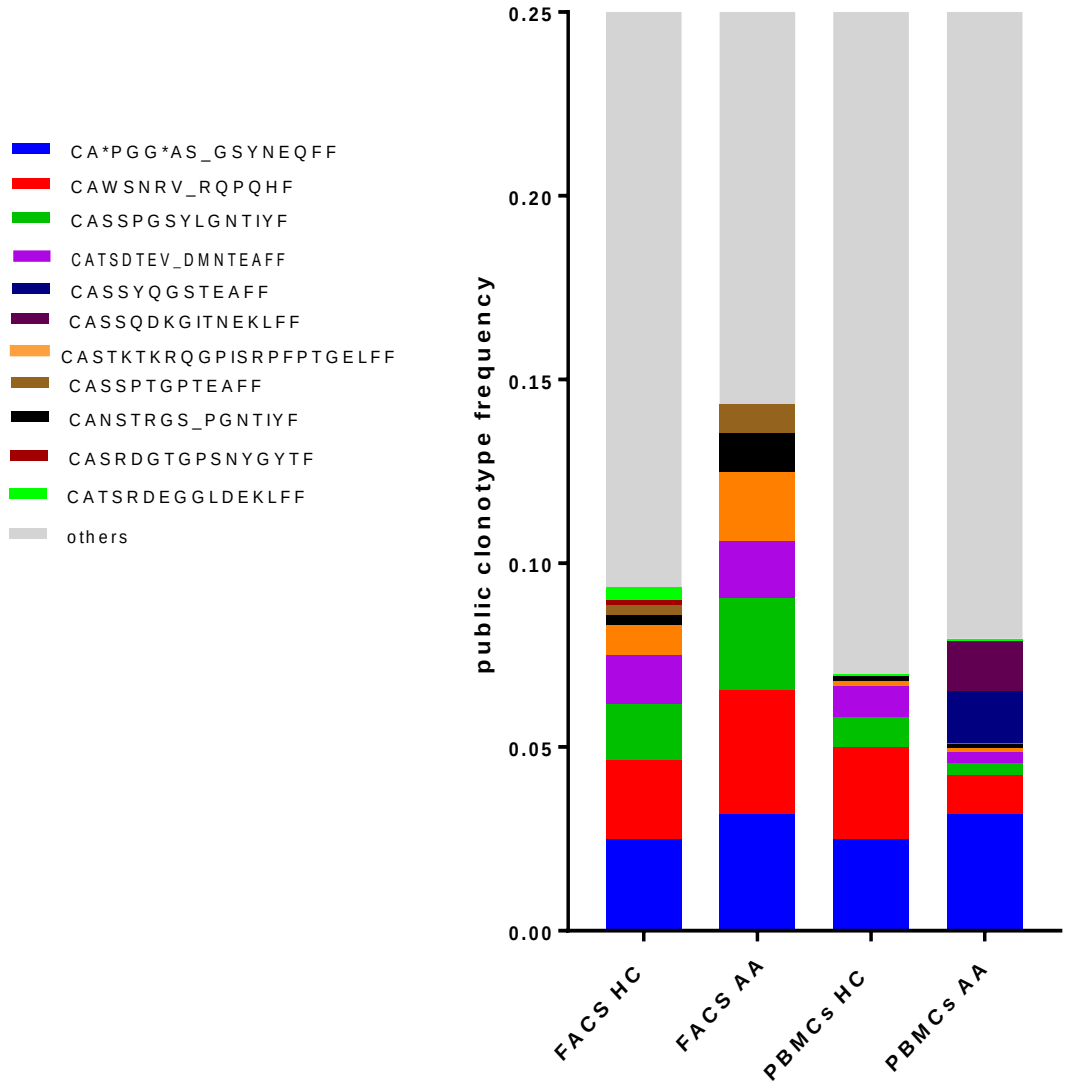

Figure 4.7. Distribution of public clonotypes in Tregs and total T-cells of patients and HCs.
The top most frequent sequences, as calculated by pooled clonotype abundance tool of VDJtools software, are shown in different colours while the others are in grey.

4.2.4.3. TCR segment usage analysis

To explore whether the usage of V and J segments is skewed in AA patients, a heatmap was generated demonstrating the weighted V and J segment usage profile of the TCR in each group. The heatmap reflects the frequency of associated reads for each of V/J segments present in each group.

Total lymphocytes

In total lymphocytes, the usage of V segments showed overall similarity between cases and controls with TRBV12-3 and TRBV24-1 the most frequently

used TRBV alleles (0.08% and 0.06% respectively) in both groups and TRBV11 and TRBV14 the least utilised V genes with approximately 0.001% frequency (Figure 4.8.A). The raw data of V and J frequencies is demonstrated in appendix 2. In comparison to controls, some differences were observed. For instance, TRBV19 and TRBV29-1 allels were relatively more frequently utilised in patients' cells than HCs'. Post-hoc analysis was performed to determine if there was any statistically significant difference in the usage of each V region between patients and controls. TRBV19 was the most utilised V segment by TCRβ chains of total lymphocytes of patients with 1.02 fold increase (P=0.001) compared to HC (Figure 4.8.B).

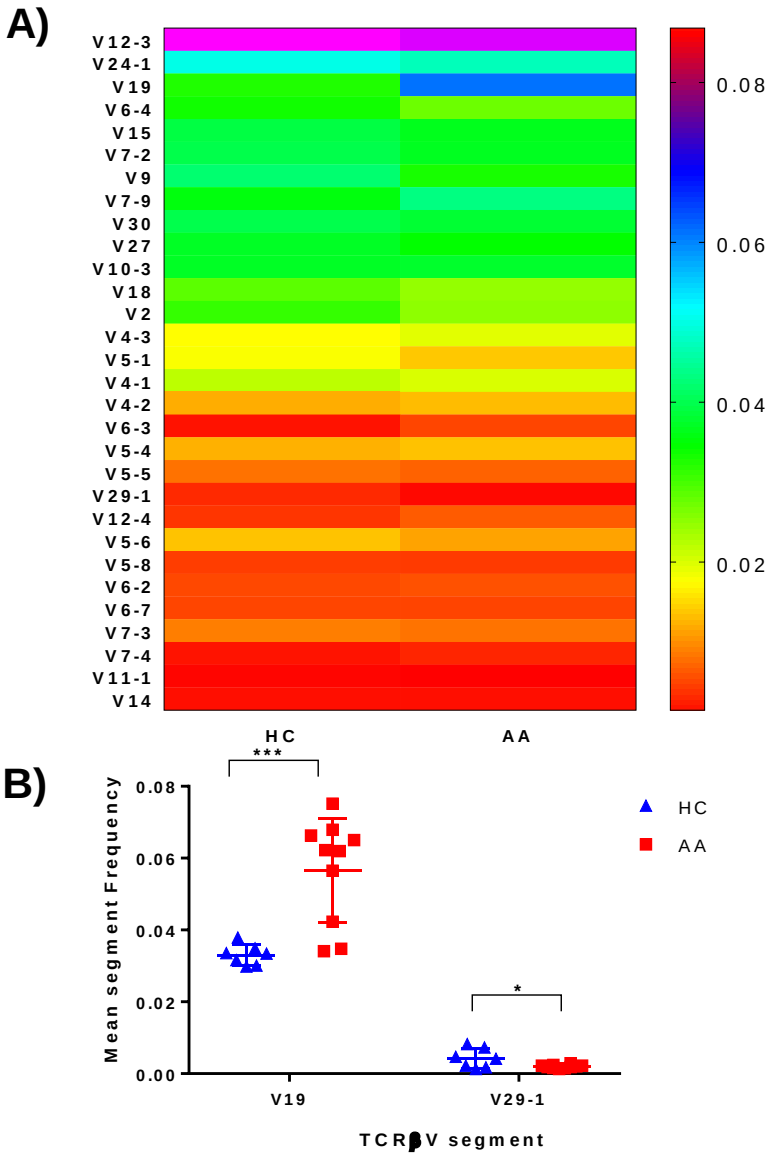

Figure 4.8. V gene segment usage in TCR repertoire of Treg cells.

A). The frequency of each V segment usage in healthy controls (HC) and AA patients, the data represented in the heatmap is the mean of seven HCs and ten AA patients. B) Changes in TCRβV segment usage between HC and AA where the difference was calculated by multiple t tests * $p \leq 0.05$. *** $p \leq 0.001$.

TRBJ usage in total lymphocytes showed no difference between cases and controls (Figure 4.9). TRBJ1-1 and TRBJ1-5 were highly abundant in both groups compared to all other J genes followed by TRBJ1-4, which was relatively more frequent in patients. TRBJ2-1 was more frequently utilised in controls,

however, no statistically significant difference in any J segment usage was observed using post-hoc analysis (Appendix 3).

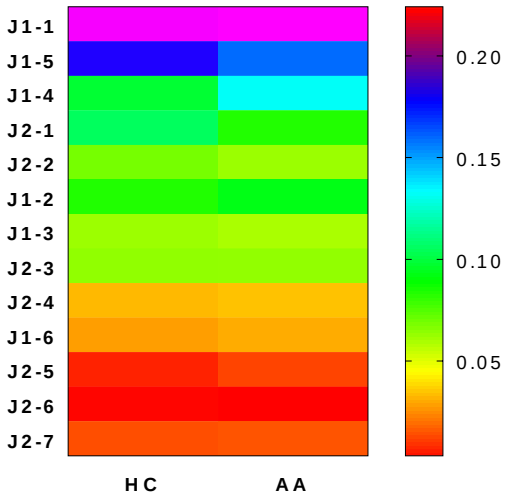

Figure 4.9. J gene segment usage in TCR of Treg cells.
Frequency of each J segment usage in controls (HC) and AA cases, the data represented in the heatmap is the mean frequency of each segment in seven HCs and ten AA patients.

Tregs

Regulatory T-cells showed a different V usage in their repertoire compared to total lymphocytes. TRBV12-4, 20-1 and 24-1 were more predominant in cases compared to controls, while other TRBV segments such as TRBV12-3, 2, 30 and 15 were more abundant in controls than cases (Figure 4.10. A). Applying post-hoc statistical analysis to these data, the frequency of the TRBV2 segment was significantly higher in controls compared to patients (P=0.01), on the other hand, TRBV 6-3 showed significantly increased frequency in Tregs of patients (P=0.005) (Figure 4.10. B).

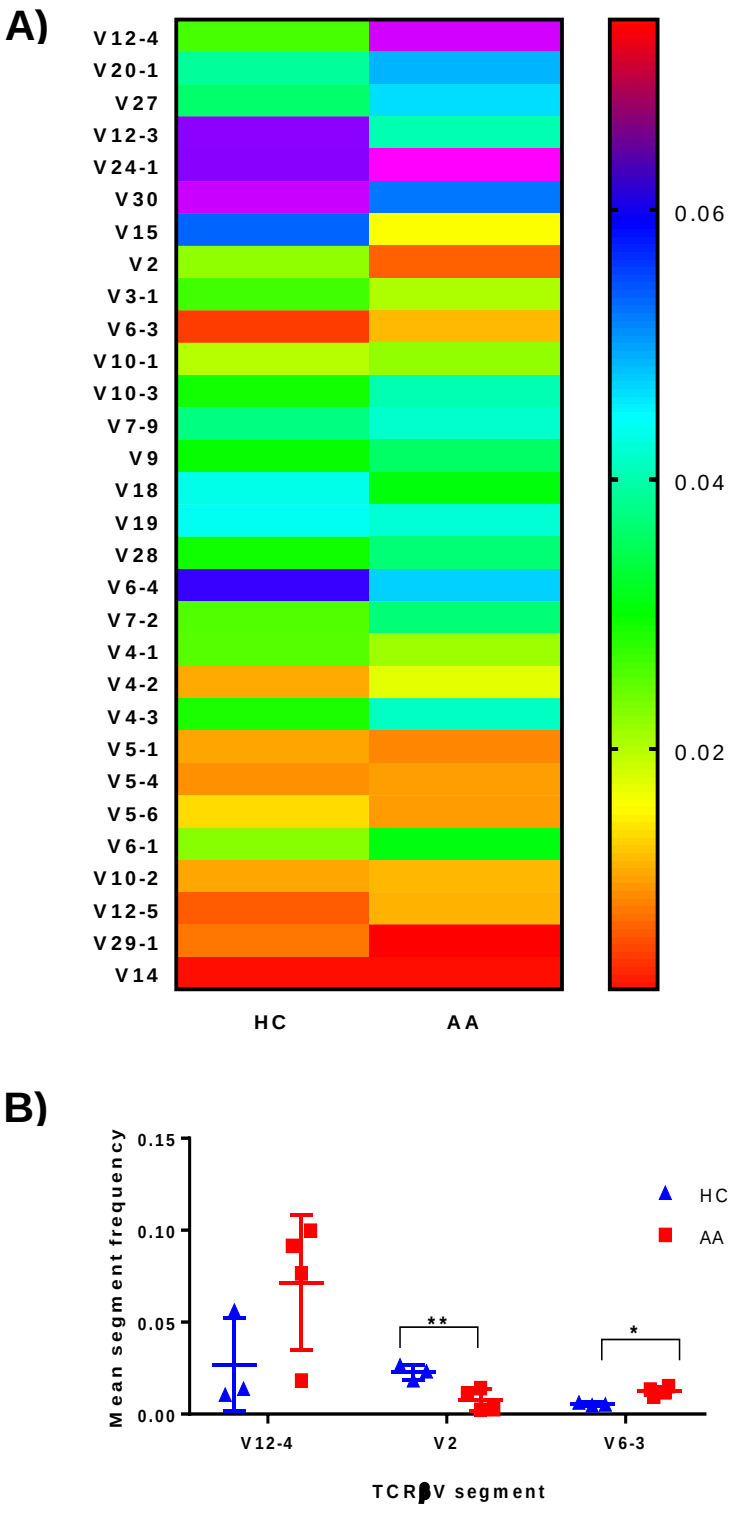

Figure 4.10. V gene segment usage in TCR of Treg cells.
A). frequency of each V segment usage in controls (HC) and AA cases, the data represented in the heatmap is the mean of three HCs and four AA patients. B). Changes in TCRβV segment usage between HC and AA where the difference was calculated by multiple t tests * $P \leq 0.05$.

Looking at J segment usage, TRBJ1-2 and to a lesser extent TRBJ2-5 and TRBJ2-4 were slightly more abundantly utilised in patients. HC have more abundant TRBJ2-2, 1-5, and 1-1 (Figure 4.11.A). Using post-hoc analysis, the frequency of TRBV 1-1 usage was significantly higher in HC (P=0.04), and TRBV2-5 is higher in patients (P=0.05) compared to patients (Figure 4.11.B).

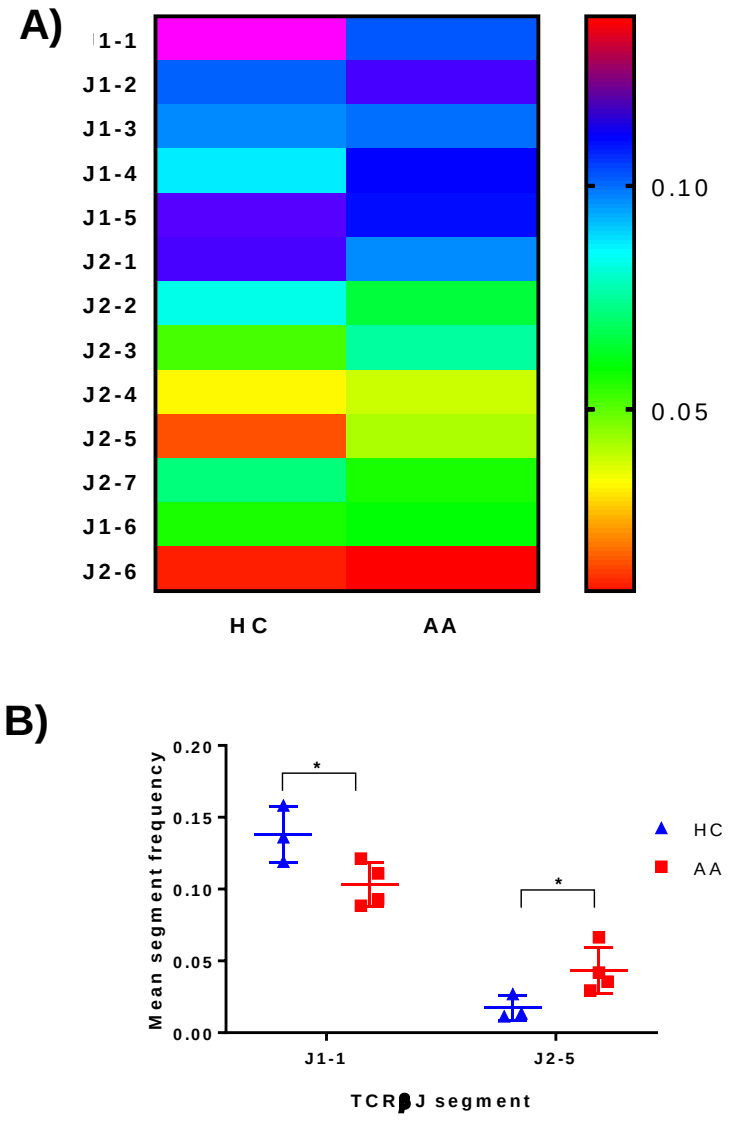

Figure 4.11. J gene segment usage in TCR of Treg cells.
A). Frequency of each V segment usage in controls (HC) and AA cases, the data represented in the heatmap is the mean of three HCs and four AA patients. B). Changes in TCRβJ segment usage between HC and AA where the difference was calculated by multiple t tests and * *P*≤0.05.

4.2.4.4. CDR3 length distribution

In addition to rearrangement of V, J and intervening D sequences, random insertion of nucleotides called N between these segments contributes to CDR3 structural diversity. In order to look at the intervening D segment and the inserts, VDJtools software provides data about CDR3 region bulk characteristics such as CDR3 nucleotide length, NDN length and insert size. Nucleotide length influences antigenic reactivity. The D region is located between the V and J segments and flanked by N nucleotides, so NDN represents the number of nucleotides that lie between V and J segment sequences in the CDR3 region. The software calculated the frequency of base addition and deletion, referred to as indel, at the V-D-J junction excluding the D region, yielding a representation of V-D and D-J insert size, which will be referred to as insert in the data presented here.

CDR3 nucleotide (nt) length ranges from 21 to 69nt, and the most frequently observed sizes are 39, 42, 45 and 48 nucleotides in TCRβ chains of total lymphocytes as well as Tregs in both patients and controls (Figure 4.12 A1 and 2). Similarly, the NDN nucleotide size distribution was identical in Tregs of patients and controls where the most frequently observed size was 13nt. In total lymphocytes, the NDN length showed the same bell-shaped distribution ranging from 0 to 40nt; however, the most frequent length in controls was 13nt while it was 9nt in patients.

On analysis of the insert between VD and VJ regions, a similar length distribution can be observed in total lymphocytes, where no insert (0nt) was the most commonly observed length in both study groups followed by 4nt length in patients and 7nt length in controls. In contrast, a marked difference can be seen in VD/VJ indel length in Treg cells; while no insert (0 nt) is the most frequent

distribution in patients, the inserts predominantly found in V-D/V-J region in controls with about 13nt indel the most commonly observed length, which might indicate the presence of a base deletion at the V-D/V-J junction in AA patients.

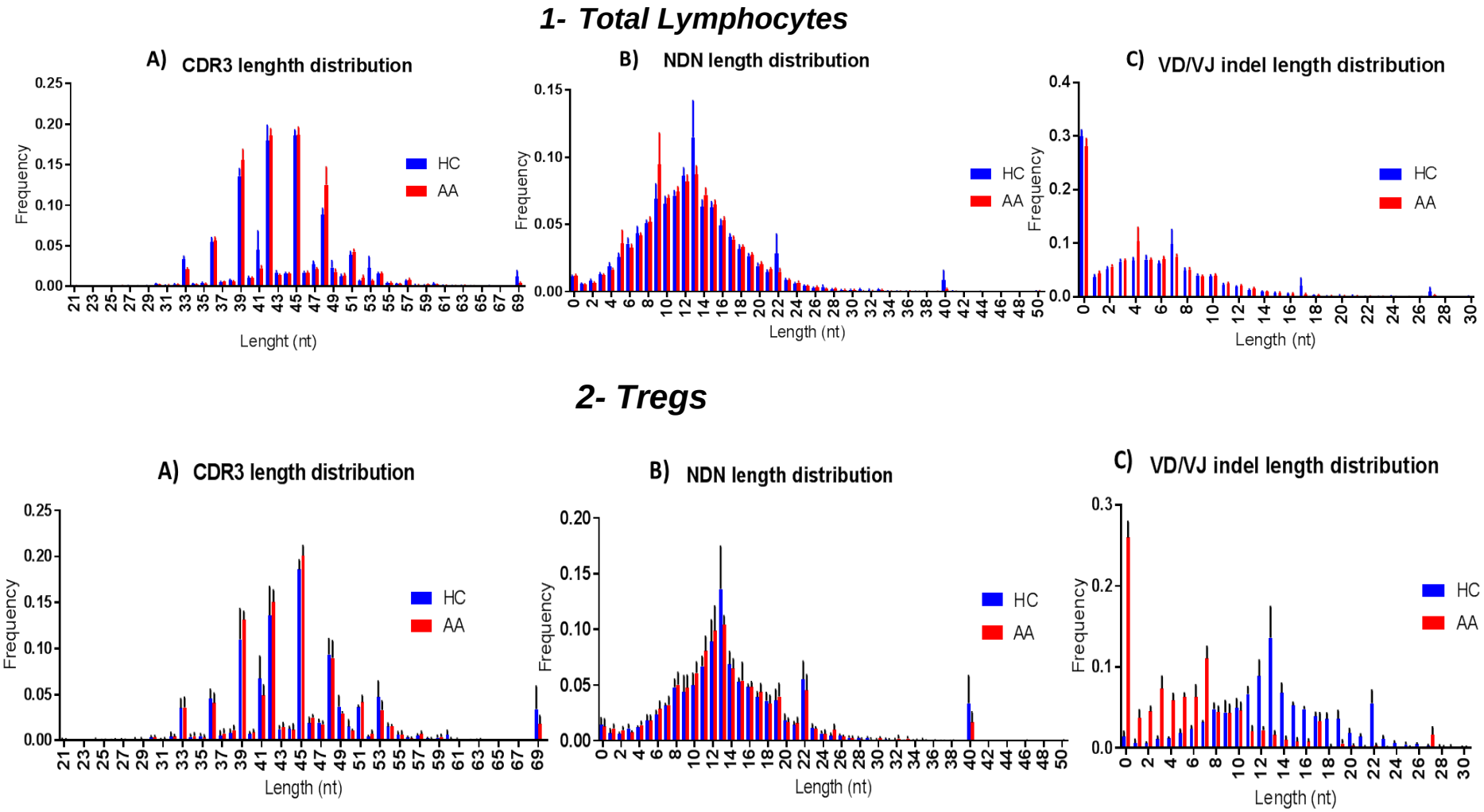

Figure 4.12. CDR3 bulk characteristics in total lymphocytes and Treg of AA patients, and healthy controls.
A). Nucleotide length of CDR3 segment B). NDN nucleotides size C). V-D and D-J indel size. NDN and CDR3 length in cases and controls showed the same distribution for Tregs and total lymphocytes. V-D/V-J indel size showed marked difference between patients and controls in Tregs with 13nt is the most commonly observed length in controls and no insert the most common nt length in patients.

4.3. Discussion

The imbalance between Teff and Treg in AA observed in this thesis suggested a need for further investigation of the molecular structure of the TCR of these cells to define clonally expanded T-cell populations. With a view to identify protective or pathogenic TCR clonotypes, CDR3 diversity is the main contributor to the huge number of clonotypes in TCR repertoires, and this region was therefore studied to determine the clonotypic dominance in AA. As highlighted previously, the CDR3 region is formed due to V (D)J gene segment rearrangements contributing to the high diversity of TCR receptors, and the diversity is further enhanced by the insertion or deletion of N nucleotides.

Interestingly, TCR repertoire analysis demonstrated a unique predominance of certain public clonotypes in total lymphocytes of AA patients, displaying a signature of antigenic selection in those individuals; where CASSYQGSTEAFF and CASSQDKGITNEKLFF were only found in the TCR repertoire of total lymphocytes of patients compared to other study groups (Tregs and total lymphocytes of HC). This was complemented by the TCR biodiversity data, with lymphocytes from AA patients showing less diversity (chao1=3.2) indicating the predominance of certain clones suggesting clonal expansion in response to specific antigen(s).

The two public sequences were searched for any potential match in the NCBI database. CASSYQGSTEAFF showed no matches of 100% similarity to any sequence in the database, but about 92% aa identity to CDR3 of CD8+ T-cell clone reactive to human tumour-associated antigen (Appendix 5. A), namely, tumour-associated human telomerase reverse transcriptase (Cole et al., 2017). Similarly, there was no 100% identical match for the CASSQDKGITNEKLFF sequence, but about 81% similarity was found with a

TCRb chain from auto-reactive CD8+ T-cells (Appendix 5. B) isolated from diabetic mice (Vincent et al., 2010). In contrast to the increased rates of additional autoimmune diseases such as thyroid disease and vitiligo found in AA, previous studies on the concurrence of AA with diabetes detected a negative association with type I diabetes mellitus found to be less common in AA patients although it is increased in frequency in their first degree relatives (Wang et al 1994, Noso et al 2015). This negative association may reflect differential HLA related susceptibilities to diabetes and AA. Nonetheless, it is noteworthy that the two public aa sequences showing identities to TCRβ chains were from CD8+ T-cells. In agreement with this, the VJ usage profile of lymphocytes was skewed toward the TRBV19 segment in patients with 0.06 frequency compared to 0.03 in HC (P=0.001). This particular Vβ gene segment has been associated with CD8+ T-cell response in many studies. For instance, the same pattern of TCR bias was seen in mice with Goodpasture disease, which is an autoimmune disease with autoantibodies against basement membrane of lung and kidney (Ooi et al., 2017). Preferential usage of TRBV19 was also found in insulin reactive CD8+ T-cells isolated from NOD mice (Pearson et al., 2016). Finding similar TCR sequences in unrelated patients suggests that these clones, probably of CD8+ T-cells may have an important functional contribution to the immunology of AA.

In this thesis, it has been proposed that Tregs are potential guardians of IP thereby preventing AA development and flow-cytomtery data showed a significant reduction in the suppressive Treg population in AA patients. Interestingly, the Treg repertoire showed limited heterogeneity in HC indicating the possible predominance of certain clones in unaffected individuals. The TCR repertoire of Tregs from these donors showed a bias toward two TCRβ clones

that were totally absent in other groups CATSRDEGGLDEKLFF (Appendix 5. C) and CASRDGTGPSNYGYTF (Appendix 5. D), which showed 69% and 76% aa identity to TCRβ of PBMCs from healthy donors on NCBI protein blast (Han et al., 2014) suggesting their role in maintaining normal immune haemostasis. These findings can be supported by looking at the VDJ composition of these public sequences; (V15 D1 J1-4) for the CATSRDEGGLDEKLFF sequence and (V2 D1 J1-2) for CASRDGTGPSNYGYTF revealing bias in V usage towards Vβ genes used in these public sequences. TRBV15 was more frequently utilised in controls 0.05 compared to 0.02 in patients. Similarly, there was preferential TRBV2 gene segment usage from 0.02 in HC to 0.007 in AA patients (P=0.01). Interestingly, the VD/DJ insert in the TCRβ chain of Tregs was markedly longer in controls with, typically 9 to 13nt insert compared to no insert in patients indicating probable base deletion in this junctional region of CDR3 in patients. Collectively, these data indicate a significant difference in the structure of the CDR3 region in Tregs from HC compared to patients, suggesting the presence of a particular clone of Tregs in HC that are deficient in AA patients, and raising the possibility of a role for these Treg clonotypes in preventing AA.

On the other hand, among the most utilised aa sequences by Treg of AA patients was CASTKTKRQGPISRPFPTGELFF, CANSTRGS_PGNTIYF and CASSPTGPTEAFF with frequencies of 0.02, 0.01 and 0.08 respectively compared to HC (0.008, 0.002 and 0.003). CASTKTKRQGPISRPFPTGELFF has no match to TCRβ chain in the database, but 80% aa identity to hypothetical protein from *Acidobacteria* bacterium (Appendix 5. E). CANSTRGS_PGNTIYF sequence has 72% aa identity (Appendix 5. F) to the TCRβ chain of CD4+ T-cells isolated from synovial fluid of rheumatoid arthritis (RA) patients (Striebich et al., 1998). CASSPTGPTEAFF has 72% aa identity (Appendix 5. G) to TCRβ

transcripts of CD4+CD45RA- T cells isolated from peripheral blood of Sjögren's syndrome (SS) patients (Joachims et al., 2016). Of note, the two matches were to CD4+ T-cells from autoimmune conditions. Predominance of these Treg clones supports the finding that Tregs are still present around HF in affected skin, however, with impaired suppressive function.

Identifying pathogenic or protective clones involved in AA pathogenesis is a vital discovery that can potentially lead to effective and specific therapeutic targeting of the disease. For instance, expanding a single clone of Tregs *in vitro* for treatment has been recently achieved with successful outcome reducing inflammation and neovascularisation in a mouse model of diabetic retinopathy (Deliyanti et al., 2017). Similarily, Vβ8 positive cells developed *in vivo* by immunizing mice with a peptide specific for EAE, and then injected as a vaccine in the animal model showed promosing effects against EAE develpoment (Vandenbark et al., 1989).

This novel TCR skewing pattern determined in this study requires further confirmatory experiments. First, that can be acehived by PCR analysis of patient and HC samples for the public clones, V and J regions found to be predominante in this work. Secondly, performing NGS on larger number of participants and stratifying by disease severity. Importnantly, generating antibodies to the public clonotype found in this work and perforeming immuno-staining to test AA lesional skin reactivity to these antibodies would be a feasible confirmatory test. Finally, studying the TCR repertoire of T-cells isolated from lesional and non-lesional skin would be ideal to determine the public TCRβ clonotype distribution in affected skin, howevere, it is challenging to perform due to the low number of T-cells in the skin, in particular Tregs.

Chapter 5 . EGCG is a potential therapy for AA

5.1. Introduction

As discussed in the previous two chapters, disruption of Treg-Teff balance is thought to be the key event in IP collapse and subsequent hair loss. The IP state is maintained by immunosuppressive molecules, such as α–MSH and TGF-β, where Tregs might contribute to this immunosuppressive microenvironment as proposed in this study. That maintains low expression of MHC class I and II, which guard privileged sites from an immune attack. IP collapse is induced mainly by IFN–γ secreted by Teff resulting in the up-regulation of MHC class I and II expression on the surface of keratinocytes in the proximal part of HF (René et al., 1998, Ito et al., 2004) leading to a lymphocytic attack towards the affected tissues. The IFN–γ signalling pathway, namely JAK-STAT, has been targeted by a chemical inhibitor (ruxolitinib) resulting in successful hair regrowth in nine patients of a small pilot study (Xing et al., 2014). However, the broad targeting of JAK1 and JAK2 by this chemical inhibitor mediates a wide range of side-effects (Tefferi and Pardanani, 2011). In this study, EGCG is proposed to target the same pathway with a higher specificity and a relatively superior safety profile. In addition to its STAT-1 inhibitory effect (Tedeschi et al., 2002), EGCG also has shown stimulatory effect on Treg differentiation from naïve CD4+ cells via inducing FOXP3 expression (Wong et al., 2011) and enhancing the naïve CD4+ differentiation toward the regulatory pole (Wang et al., 2013a). In this chapter, EGCG will be presented as

a theraputic molecule and its effect on key inflammatory and regulatory molecules invloved in AA pathoegensis will be investigated. The aim of the work presented in this chapter is to optimise EGCG dosage *in vitro*, construct an IFN-γ cellular model to induce the JAK-STAT pathway, and study the effect of EGCG on the IFN-γ signalling pathway (JAK-STAT) and regulatory molecules involved in AA pathogenesis.

5.2. Results

5.2.1. *In vitro* studies

5.2.1.1 Optimization of EGCG dosage

EGCG has been used topically at concentrations between 40-660μM without inducing dermal toxicity (Zhao et al., 2015), with doses of 50-75μM previously used in HaCat cells (Zhu et al., 2014) and 100μM in epidermal keratinocytes (Hsu et al., 2003). The first step in this study was to test the range of EGCG dosages that can be tolerated by the HaCat and Jurkat cell lines. 10, 20, 40, 60 and 100μM EGCG concentrations were used to treat these cell lines for 24 and 48hrs, with cell viability assayed by microscopic evaluation and by staining the dead cells with trypan blue to find the percentage of viable cells in each group.

5.2.1.1.1 Cell viability by Trypan blue

The effect of EGCG on cell viability was found to be dose-dependent, regardless of the duration of treatment. The viability of HaCat cells compared to untreated samples reduced slightly when treating the cells with 10μM EGCG and continued to drop gradually when increasing the dose of EGCG to 20, 40 and 60μM. However, this reduction was mild and not statistically significant. A significant sudden drop in cell viability was observed in samples treated with

100μM EGCG for 48hrs (P≤0.001), where it declines to about 50% (Figure 5.1). Data from 24hrs treated group can be found in appendix 6.

The same trend was seen in Jurkat cells, although a very significant toxic effect (P≤0.001) of EGCG was observed at a lower dose of EGCG (60μM) leading to approximately 30% reduction in cell viability, which dropped further by 50% when increasing the dose to 100μM. Therefore, it was concluded that 10, 20 and 40μM EGCG dosages do not show statistically significant adverse effects on cell viability in either cell line.

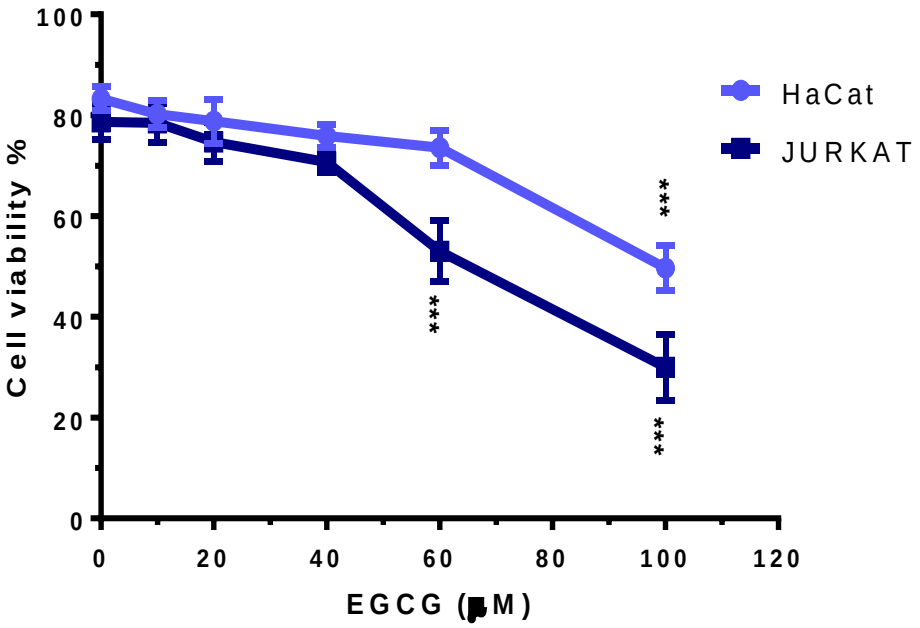

Figure 5.1. The effect of EGCG on cell viability of HaCat and Jurkat cells.
The mean percentage (%) of viable cells in HaCat and Jurkat cell lines after treatment with different concentrations of EGCG (10, 20, 40, 60 and 100μM) for 48hrs. Slight reduction in viability can be seen in both cell lines after treatment with lower doses of EGCG 10, 20, 40μM (not statistically significant) while a significant drop started to be seen at 100μM in HaCat cells and 60μM in Jurkat cells. The experiment was repeated three times and mean and SD were calculated. *** P≤0.001.

5.2.1.1.2. Microscopic assessment of cell viability

To confirm the viability assay results, microscopic assessment of HaCat and Jurkat cells was performed after 48hrs of treatment with EGCG. HaCat cells

treated with 10, 20 and 40μM EGCG displayed the same morphology as the untreated control group, where the cells proliferated in a compact monolayer in a relatively non-structured pattern. On the other hand, 60μM and 100μM EGCG treated cells showed marked disruption in the monolayer of cultured cells, and a reduction in cell density with adherent cells displaying a longer, stretched morphology (Figure 5.2). The Jurkat cells tend to be round and clump together to form grape-like colonies in untreated samples, and the same morphology can be seen for 10, 20 and 40μM EGCG treated samples (Figure 5.3). As with the HaCat cells, Jurkat cells cannot tolerate the higher doses of EGCG (60μM and 100μM) and the cells appeared as discrete entities with small particles floating in the media, which are probably apoptotic bodies when compared to the microscopic images by Ivan et al. (Ivan et al., 2014). These results indicate the adverse effect of EGCG on cell viability, and thus its toxicity at higher dosages.

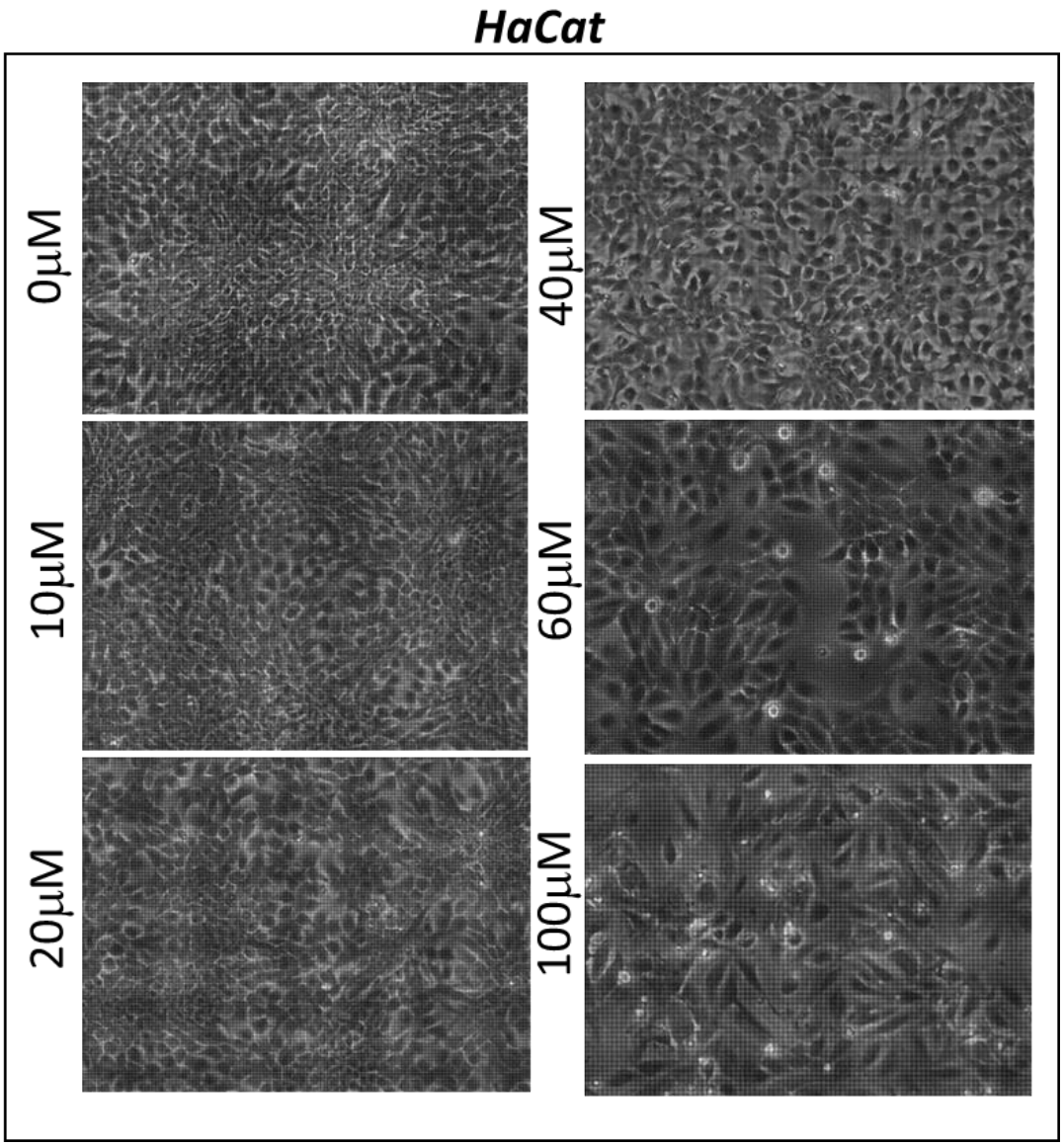

Figure 5.2. Morphological features of HaCat cells treated with EGCG.
Cells treated for 48hrs with 10, 20, 40, 60 or 100μM EGCG or left untreated as a conrol were examined under a light microscope at 10X magnification. The morphology in control versus 10, 20 , 40μM EGCG-treated cultures is relatively similar; however, 60 and 100μM EGCG alters the colony morphology forming less compact colonies.

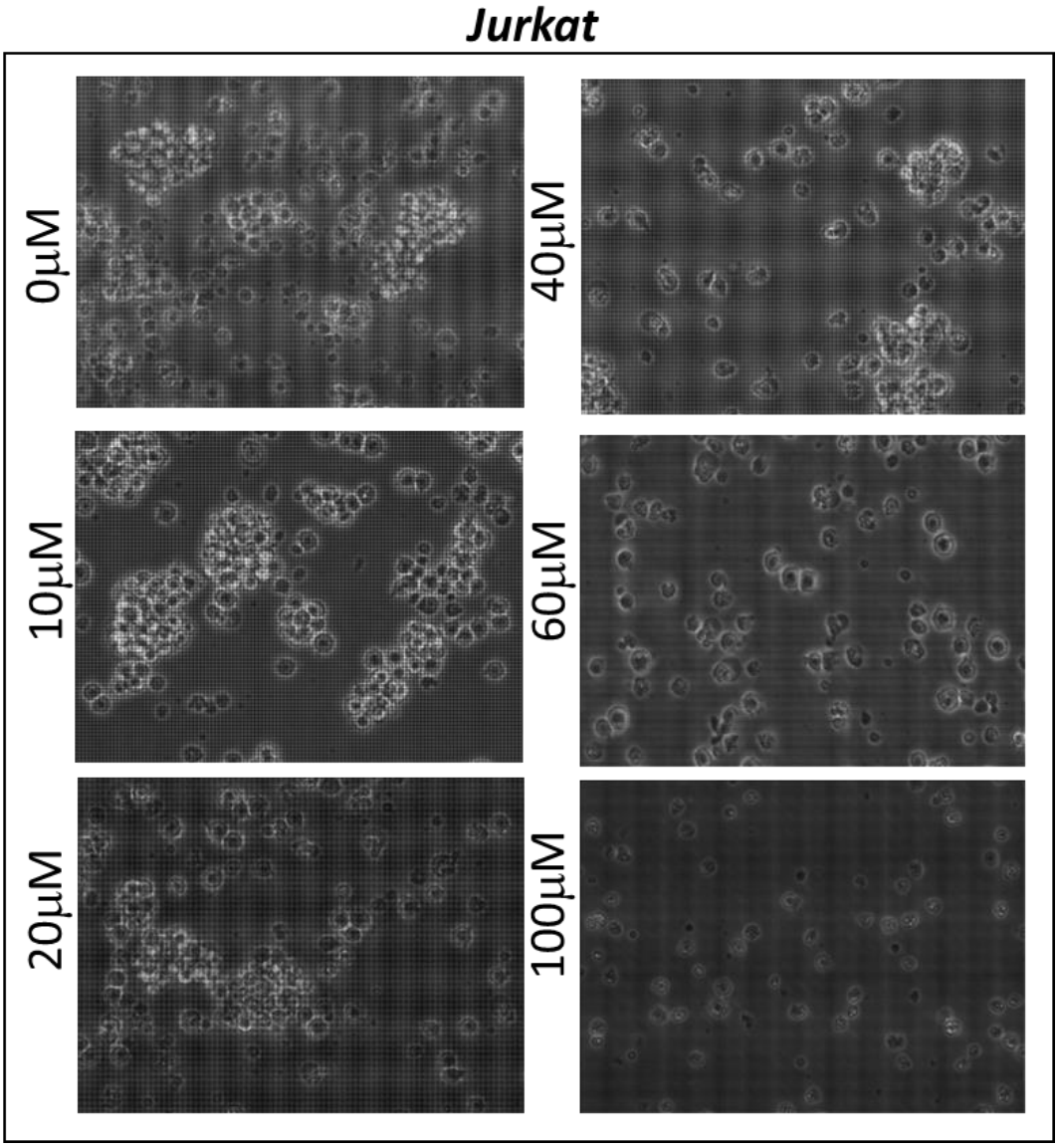

Figure 5.3. Morphological features of Jurkat cells treated with EGCG.
Cells treated for 48hrs with 10, 20, 40, 60 or 100μM EGCG or left untreated as a conrol were examined under a light microscope at 20X magnification. The morphology in control versus 10, 20 , 40μM EGCG-treated cultures is relatively similar with grape-like colonies; however, 60 and 100μM EGCG alters colony morphology forming less compact colonies with more discrete cells .

Based on the viability assay and microscopic findings, 40μM of EGCG was selected as an optimal dose that can be tolerated by HaCat and Jurkat cells without causing significant cell death. This dose was used in the subsequent experiments to investigate its effect on the expression of key molecules involved in JAK-STAT pathway.

5.2.1.2. Optimization of IFN-γ dose for the induced cellular model

In order to study the effect of EGCG on the JAK-STAT pathway, particularly STAT-1 phosphorylation, which is the key event in activating this pathway by IFN-γ, it was important to design a cellular model where the pathway is triggered to mimic the pathogenic state. However, it was important first to optimise the dose of IFN-γ that can induce the phosphorylation of STAT-1 protein without causing cell death.

5.2.1.2.1 Cell viability assay

Cell viability was measured by trypan blue assay in HaCat and Jurkat cells 48hrs following incubation with serial concentrations 25, 50, 100, 200IU/ ml of human rIFN-γ and compared to un-induced sample (media only). A slight decrease in cell viability (by 5 and 10%) when compared to an un-induced sample was observed in HaCat cells induced with 25IU/ ml and 50IU/ ml IFN-γ, respectively. The percentage of viable cells continued gradually to drop by increasing the dose of IFN-γ, until it is drastically decreased by approximately 25% in samples induced by 100IU/ ml IFN-γ and 40% in cells incubated with 200IU/ ml IFN-γ compared to the control group. The opposite effect on cell viability by IFN-γ can be seen in Jurkat cells where the viability was improved by activating the cells by IFN-γ in a dose-dependent manner. The percentage of viable cells recovered to a higher level by around 5% compared to the control group by 25 and 50IU/ml IFN-γ. Higher concentrations of IFN-γ showed a greater increase in cell viability with the percentage of viable cells increased by around 15% and 20% in samples incubated with 100 and 200IU/ ml IFN-γ compared to un-induced samples (Figure 5.4).

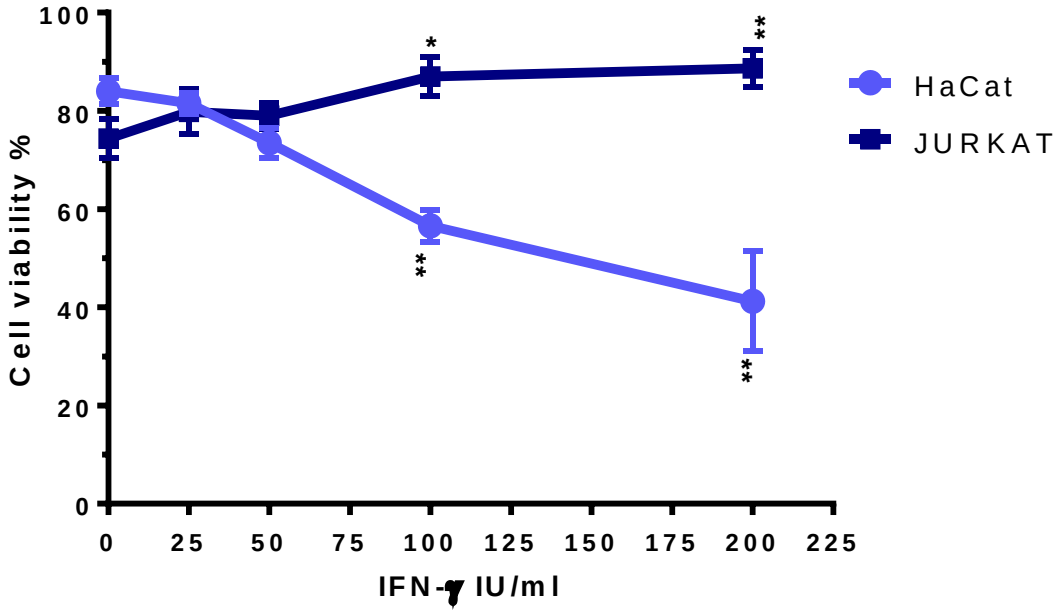

Figure 5.4. The effect of IFN-y on cell viability in HaCat and Jurkat cells.
Cells were incubated with serial concentrations of IFN-γ 25, 50, 100 and 200IU/ml for 48hrs and cell viability was measured by trypan blue assay. Slight reduction in viability can be seen in HaCat cells after treatment with 25IU.ml IFN-γ, and significant drop was caused by 200IU/ml concentration. Jurkat cells' viability was increased gradually by IFN-γ and 200IU/ml dose caused the most significant rise in the percentage of viable cells The data is the mean of three independent repeats and SD was calculated. Asterisks denote a significant reduction in cell viability, * P≤0.05, ** P≤0.01.

5.2.1.2.2 Microscopic assessment of cell viability

Microscopic evaluation of HaCat and Jurkat cells was performed to confirm the cell viability assay findings. A 25IU/ ml IFN-γ-induced sample cannot be differentiated from the control sample in terms of colony morphology which appeared as a monolayer with polygonal-shaped cells. A slight reduction in cell density was observed in a sample induced by a 50IU/ml dose making the colony more loose, but no change in cells phenotype was observed. The HaCat cell monolayer was markedly disrupted by higher concentrations of IFN-γ (100 and

200IU/ml) with a significant number of small rounded particles with increased refractivity, probably apoptotic bodies (Figure 5.5.A). In agreement with the cell viability assay data, no adverse effect on the colony morphology nor cell phenotype was observed in Jurkat cells by any of the IFN-γ doses used for induction. This was demonstrated by the microscopic images in cells induced with the highest dose 200IU/ml and control group after 48hrs in culture, which appeared as rounded cells clumped together forming grape-like colonies (Figure 5.5.B). Microscopic images of all groups of IFN-γ induced Jurkat cells are shown in appendix 7.

It was concluded from the viability assay and microscopic assessment of both cell lines that 50IU/ml of IFN-γ is the maximum dose that can be used for induction in HaCat cells before causing significant toxicity while all the tested doses (25, 50, 100 and 200IU/ml) can be used safely in Jurkat cells.

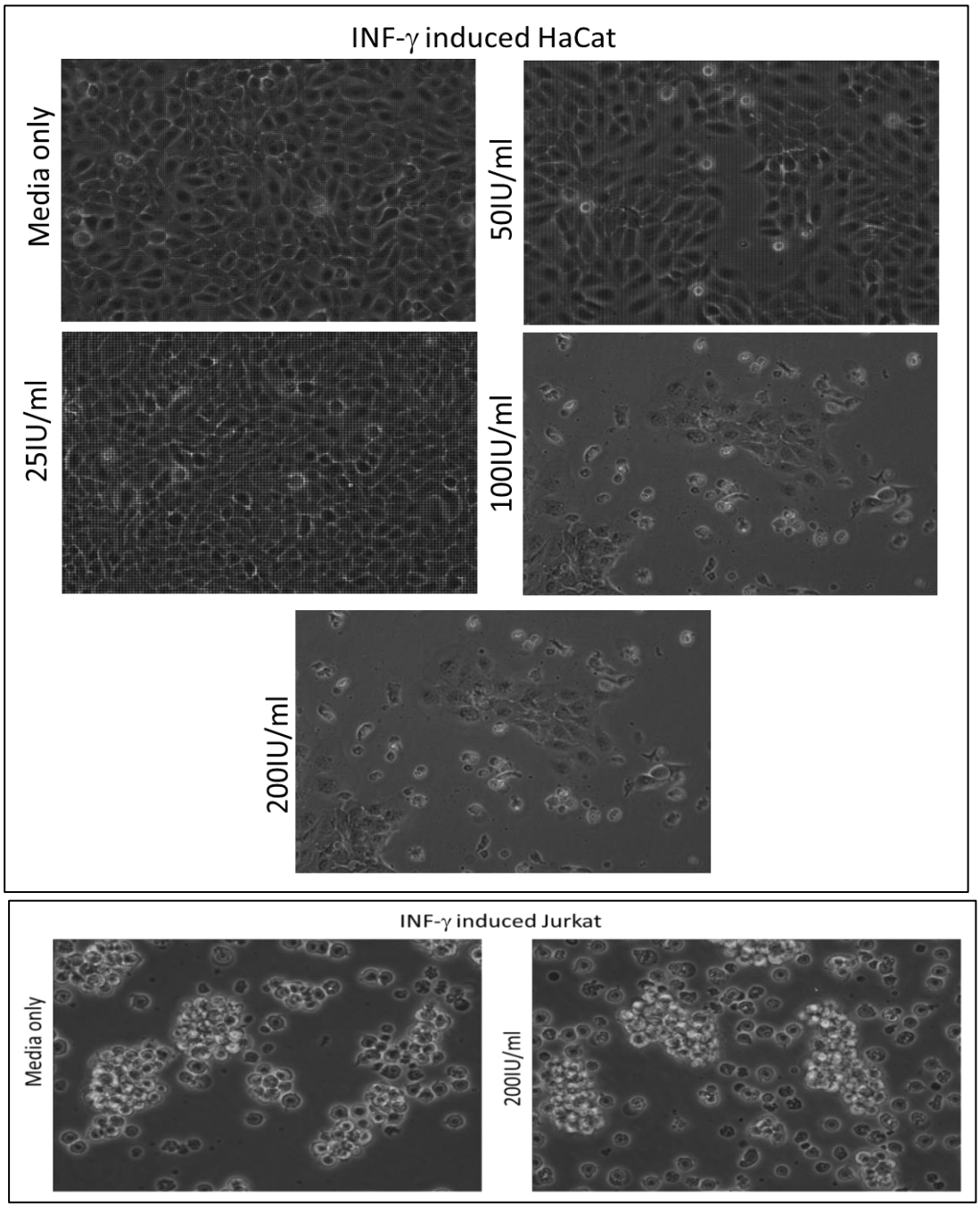

Figure 5.5. Microscopic evaluation of HaCat and Jurkat cells 48hrs following activation with serial concentrations of IFN-γ 25, 50, 100 or 200IU/ml.

A) Morphology of HaCat cells in un-induced, 25 or 50IU/ml groups is relatively similar. 100 and 200IU/ml caused significant reduction in cell density with presence of small rounded particles in the media indicating cell death.

B) Jurkat cell phenotype and colony morphology in 200IU/ml was not changed comapred to control group, and the other doses showed the same morphology (Appendix 7). Cells were examined under a light microscope at 10X magnification for HaCat and 20X for Jurkat.

5.2.1.2.3. Effect of IFN-γ on STAT-1 phosphorylation

p-STAT-1 is a key and specific regulator of the IFN-γ signalling pathway (Ivashkiv and Hu, 2004), therefore, HaCat and Jurkat cells were tested to identify the optimal dose of IFN-γ that can induce STAT-1 phosphorylation. Based on the viability assay, Jurkat cells were induced with 25, 50, 100 or 200IU/ml of IFN-γ, while HaCat cells were induced with 25 or 50IU/ml for 48hrs. Western blotting revealed that p-STAT-1 was not expressed by steady-state HaCat and Jurkat cells, and STAT-1 phosphorylation was induced by the minimum concentration of IFN-γ (25IU/ml) in both cell lines (Figure 5.6). However, a significant increase in phosphorylation was observed at 100IU/ml and 200IU/ml for Jurkat cells and 50IU/ml for HaCat cells ($P \leq 0.5$), when the band intensity was normalised against internal control (GAPDH). Therefore, 100IU/ml and 50IU/ml concentrations of IFN-γ were chosen for further experiments on Jurkat and HaCat cells, respectively.

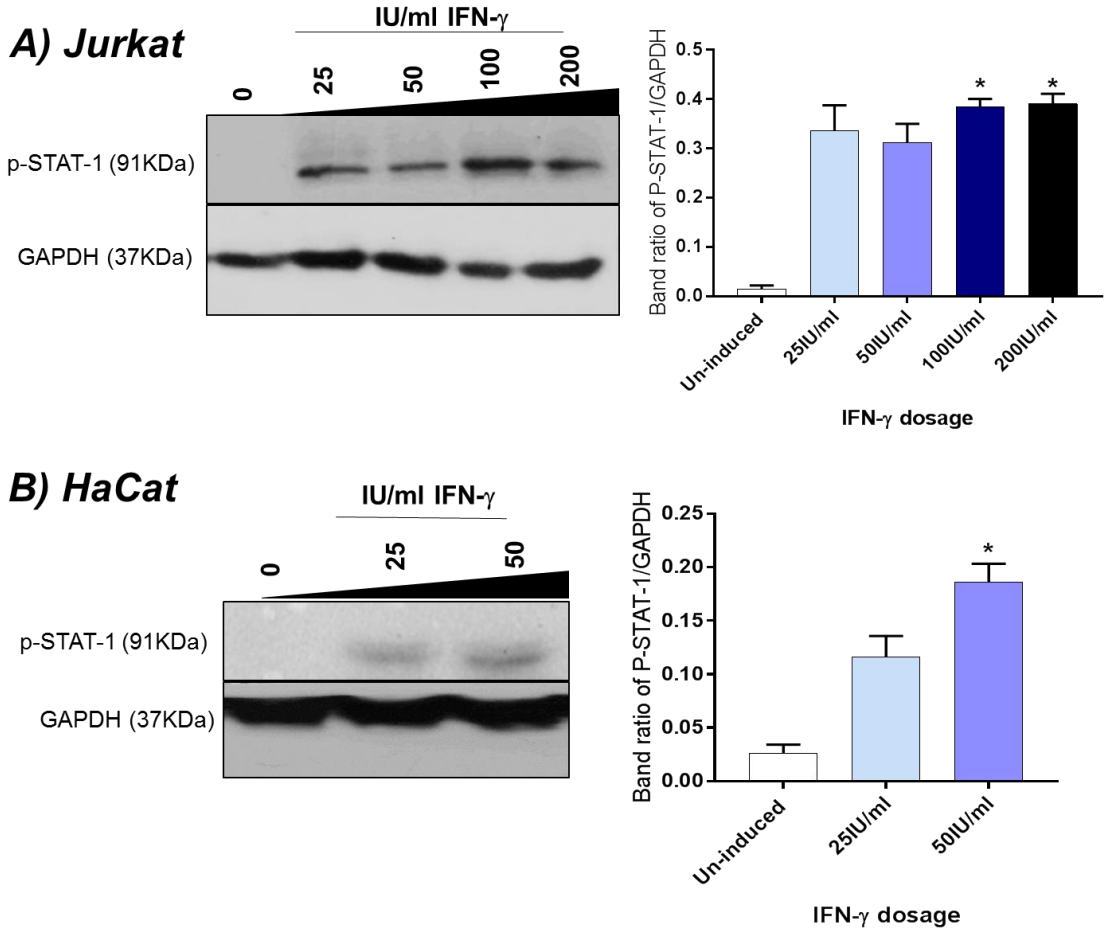

Figure 5.6. The effect of IFN-γ on STAT-1 phosphorylation.
Cell lysates of HaCat or Jurkat cells, incubated with serial concentrations of IFN-γ for 48hrs, were analysed with antibodies specific to the phosphorylated Tyr701 residue of STAT-1. A) STAT-1 phosphorylation in Jurkat cells was induced by all doses of INF-γ, but only significantly, by 100IU/ml and 200IU/ml. B) p-STAT-1 was induced significantly by 50IU/ml. A representative immunoblot is shown as well as a histogram representing the mean ± SD of p-STAT-1 band intensities relative to internal control (GAPDH) for each sample (n=3) calculated by ImagJ software; * P≤0.05.

5.2.1.3. The expression of p-STAT-1 is inhibited by EGCG treatment

p-STAT1 functions as a transcription factor in the JAK-STAT pathway, which activates the primary genes related to inflammatory responses. Therefore, the effect of EGCG on the activation of STAT1 in IFN-γ induced HaCat and Jurkat cells was investigated. Jurkat and HaCat cells were first incubated with

IFN-γ to induce STAT1 phosphorylation, then treated with EGCG at 20 or 40μM for 24 or 48h.

Analysis of p-STAT1 by western blot showed a 9% decrease in p-STAT1 expression after 24h of treatment with 20μM of EGCG in Jurkat cells. Further reduction of p-STAT1 expression up to 50% was achieved by increasing the concentration of EGCG from 20 to 40μM for 24hrs. Moreover, prolonged time of incubation to 48hrs at 20μM caused 30% drop. The percentage of reduction was based on the normalised band density relative to the internal control in each sample measured by densitometry (calculation in the appendix 8). The most marked reduction was observed in samples treated with 40μM dosage of EGCG for 48h where the p-STAT-1 protein level was about 80% less than the untreated samples (Figure 5.7.A). In HaCat cells, reduction in p-STAT-1 protein was observed starting from the 24hrs treated cells at both dosages (20 and 40μM), which continued to be the same in cells treated with EGCG for 48hrs with about 80% drop in protein levels (Figure 5.7.B). Therefore, it was concluded that 48hrs treatment duration is more effective in inhibiting STAT-1 phosphorylation than 24hrs in both cell lines, thus this longer treatment duration was used to look at the effect of EGCG on genes involved in IFN-γ signalling pathway and other regulatory genes involved in AA pathogenesis.

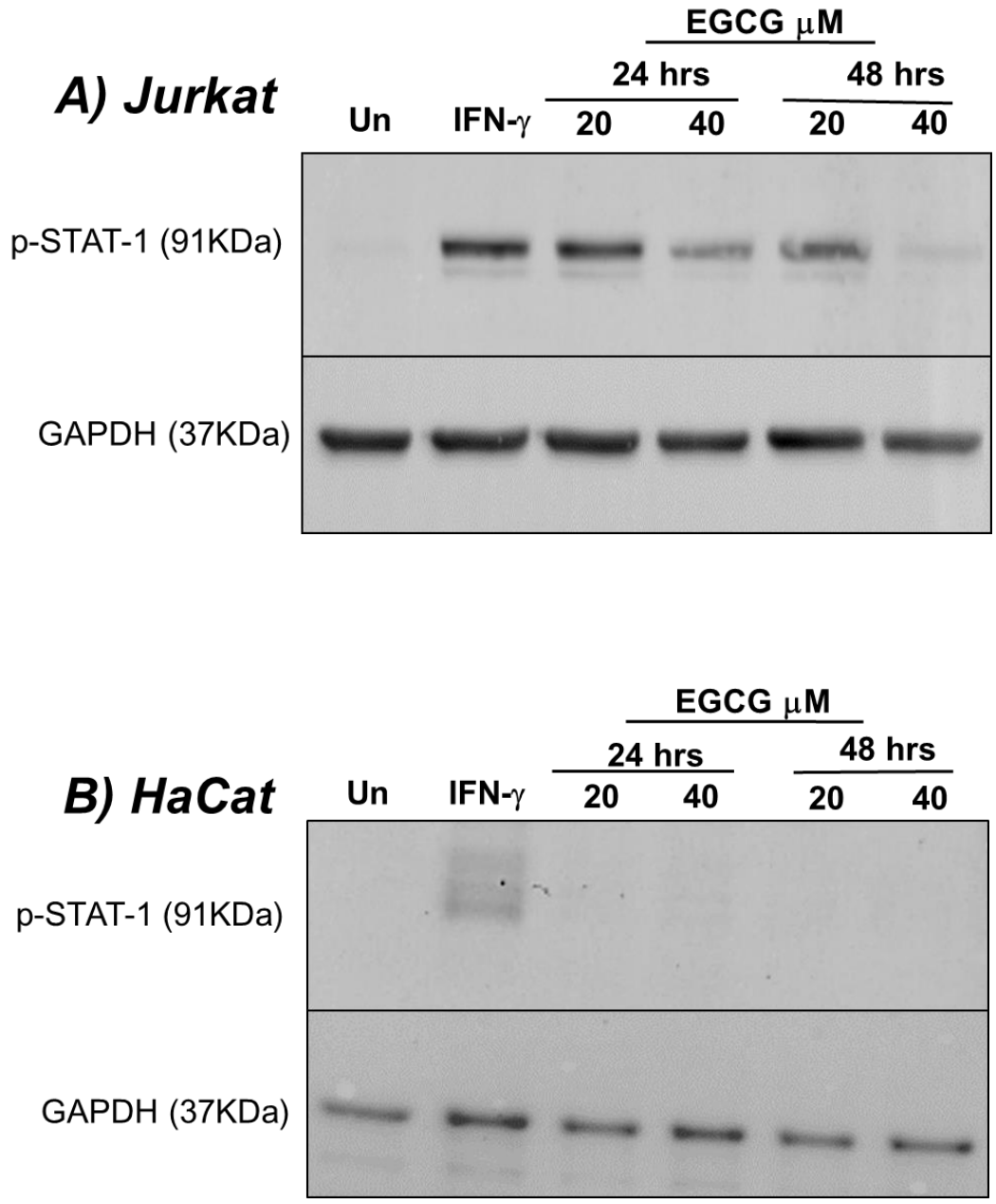

Figure 5.7. The effect of EGCG on p-STAT-1 protein in HaCat and Jurkat cells. STAT-1 phosphorylation was induced by treating the cells with IFN-γ for 48hrs. The cells were then treated with 20 and 40μM EGCG for 24 or 48hrs, with the protein levels determined by western blotting. A) Jurkat cells respond to EGCG treatment in a dose-dependent manner where 40μM dosage showed a more marked reduction in p-STAT-1 protein compared to 20μM. B) HaCat cells showed marked inhibition of STAT-1 phosphorylation at all doses and time points.

5.2.1.4. Effect of EGCG on IFN-γ downstream genes

To investigate whether inhibition of the key signalling molecule p-STAT-1 in the JAK-STAT pathway had an effect on IFN-γ downstream genes, q-PCR was used to quantify any changes in expression of a panel of INF-γ downstream genes. As explained in chapter 1, IFN-γ mediates its action via the JAK-STAT pathway (Horvath, 2004), where it binds to its receptors resulting in the activation of Janus kinase enzymes (JAK1 and JAK2). These kinases phosphorylate signal transducer and activator of transcription proteins such as STAT1, which translocates into the nucleus with subsequent activation of INF–γ dependent genes expression (Darnell et al., 1994). Interferon regulatory factor (IRF-1) is among the key genes regulated by IFN–γ that activates a group of genes that are involved in transcription of antigen presenting molecules namely TAP, HLA-B and HLA-DR (White et al., 1996).

HaCat and Jurkat cells were first induced by IFN-γ as described earlier then treated with 20 or 40μM EGCG for 48hrs or left untreated as a control. Data analysis showed that EGCG inhibited JAK-2 expression significantly in a dose-dependent manner in Jurkat cells (Figure 5.8). For instance, 20μM EGCG dosage reduced JAK-2 mRNA expression levels by 20% ($P \leq 0.05$) and to 50% in 40μM-treated samples ($P \leq 0.01$) compared to an untreated control. However, JAK-1 expression was not affected. As expected, EGCG also downregulated the expression of total STAT-1 significantly at 20 and 40μM by about 50% ($P \leq 0.05$), however, there was no significant change in the expression of STAT2 and STAT3 with any of EGCG concentrations. This inhibitory effect was reflected in the expression of a key downstream regulatory gene IRF-1, whose expression was dose-dependently inhibited by EGCG with significant reduction

(P≤0.05) to less than 50% of the expression level for the 40μM-treated group compared to untreated controls.

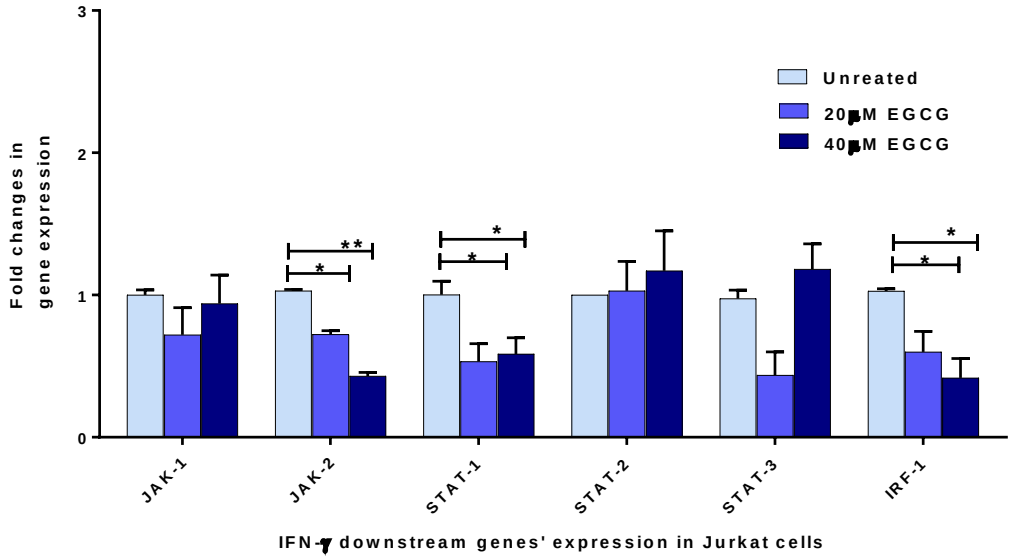

Figure 5.8. Effect of EGCG treatment on IFN-γ downstream genes in Jurkat cells. Following induction with IFN–γ, Jurkat cells were treated with 20 or 40μM EGCG for 48hrs and relative expression of IFN-γ downstream genes determined by q-PCR. CT values were normalised to GAPDH and differential expression (2^−ΔΔCT) of AA candidate genes in EGCG treated samples were calculated against untreated samples. Data represented as mean ± SEM (n = 4). Significant difference *$P \leq 0.05$. **$P \leq 0.01$.

A similar effect on the IFN-γ signalling pathway by EGCG was seen in HaCat cells (Figure 5.9). Significant inhibition of JAK-2 expression was observed (P≤0.05) in samples treated with 20 and 40μM EGCG, and an increase in JAK1 has been seen when cells were treated with 4 μM of EGCG but this was not significant. JAK-2 inhibition was associated with significant downregulation of STAT-1 expression levels to about 50% less than the untreated sample, while STAT-2 and STAT-3 did not show any significant changes with EGCG treatment. The expression of the downstream regulatory molecule (IRF-1) was also reduced significantly in dose-depended manner with about 75% reduction in

20μM EGCG treated samples (P≤0.05).and 80% drop in 40μM EGCG treated samples (P≤0.01).

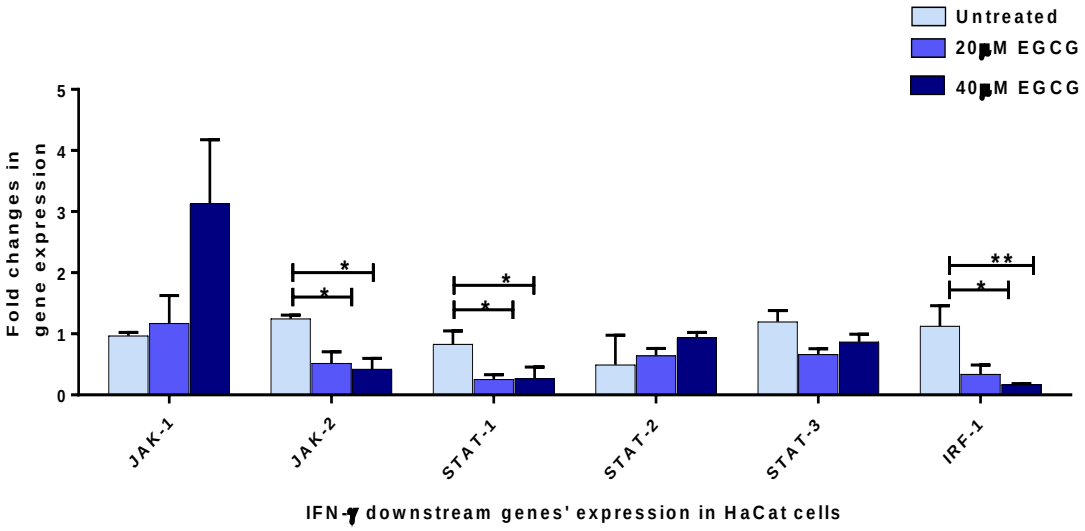

Figure 5.9. Effect of EGCG treatment on IFN-γ downstream genes in HaCat cells. Following induction with IFN–γ, HaCat or Jurkat cells were treated with 40μM EGCG for 48hrs and expression of IFN-γ downstream genes investigated by q-PCR. Significant dose-dependent reduction in the expression of JAK-2, STAT-1, IRF-1, HLA-B and HLA-DR by EGCG was observed. CT values were normalised to GAPDH and differential expression (2^−ΔΔCT) of AA candidate genes in EGCG treated samples was calculated against untreated samples. Data represented as mean ± SEM (n = 4). * Significant difference $P \leq 0.05$, ** $P \leq 0.01$.

5.2.1.5 Effect of EGCG on genes involved in IP molecules: HLA-DR and HLA-B

Because of the importance of HLA class I and class II in the IP being expressed by the keratinocytes of lower two-thirds of HF in IP collapse, it was essential to investigate whether EGCG also affects the expression of these molecules. Keratinocytes (HaCat) cells were first induced by IFN-γ as described earlier then treated with 20 or 40 μM EGCG for 24 or 48h or left untreated as a

control. The expression of HLA-B did not change after 48h of treatment of the cells with 20μM EGCG at mRNA level. However, a significant decrease ($p \leq 0.01$) in its expression of about 65% was observed with 40μM of EGCG treatment compared to untreated samples (Figure 5.10.A). In contrast, a significant reduction in HLA-DR expression was observed with the lower dose of EGCG (20μM), which continued with higher dose (40μM) with about 80% less expression of HLA-DR in those samples compared to untreated samples.

To confirm the q-PCR data, western blot was performed on total proteins extracted from treated and untreated cells, and proteins were hybridized with the HLA-DR or internal control (GAPDH) antibody. Induction with IFN-γ enhanced the expression of HLA-DR in HaCat cells. However, treatment with EGCG for 24h or 48h reduced the amount of HLA-DR proteins in the cells by more than 36% (Figure 5.10.B). Hybridization with HLA-B antibody showed no signal even after induction with IFN-γ due to the relatively low expression level of HLA-B in HaCat cells at mRNA level (data not shown).

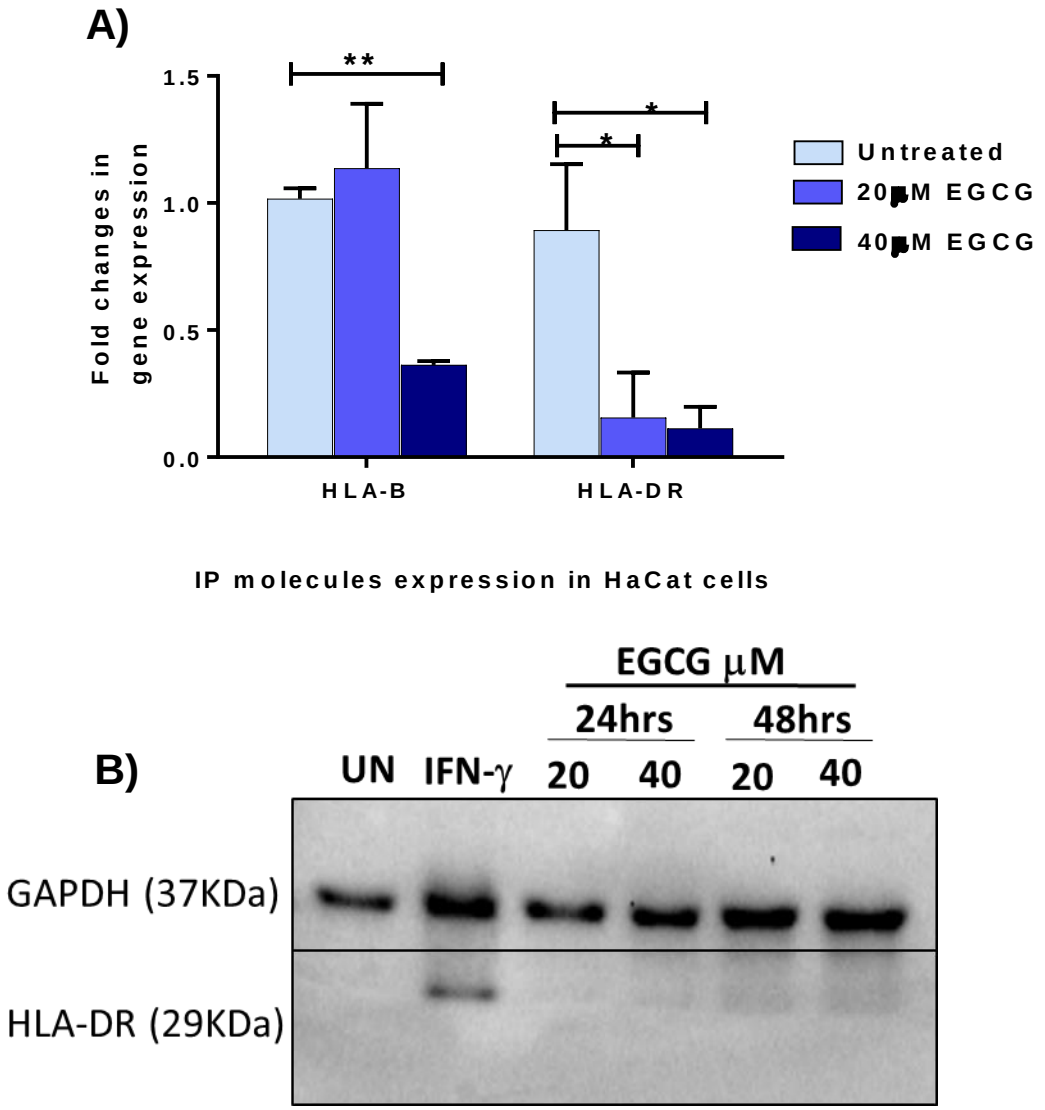

Figure 5.10. Expression of HLA-B and HLA-DR in HaCat cells treated with EGCG. HaCat cells were induced with IFN-γ for 48h then treated with 20 or 40µM EGCG for 24 or 48hrs. A). Expression of HLA-B and HLA-DR investigated by q-PCR. CT values were normalised to GAPDH and differential expression (2^−ΔΔCT) of HLA genes in EGCG-treated samples was calculated against untreated samples. Data represented as mean ± SEM (n = 4). Significant difference *P ≤ 0.05. **P ≤ 0.01. B). HLA-DR protein levels were analysed by western blot along with protein loading control (GAPDH).

5.2.1.6 The effect of EGCG on pro and anti-inflammatory cytokines

AA is the consequence of imbalance between inflammatory and regulatory arms of the immune system causing IP collapse. Therefore, the effect of EGCG on the expression of key inflammatory and regulatory candidate molecules involved in AA pathogenesis such as IL-17, CCL-5, TGF-β and

FOXP3 was investigated by q-PCR in Jurkat and HaCat cell lines treated with 20μm or 40μM EGCG for 48hrs. CCL-5 expression was significantly reduced ($P \leq 0.05$), and that was not statistically significant in HaCat cells. The Th17 marker (IL-17) was also significantly reduced by 20 or 40 μM EGCG ($P \leq 0.05$) in both cell lines. On the other hand, expression of the anti-inflammatory cytokine TGF-β was strongly enhanced in a dose-dependent manner (20μM and 40 μM with $P \leq 0.05$ and $P \leq 0.01$ respectively) in Jurkat cells while no significant effect was seen in HaCat cells. Expression of the Treg marker (FOXP3) was also increased but variation in the FOXP3 expression level did not reach statistical significance (Figure 5.11).

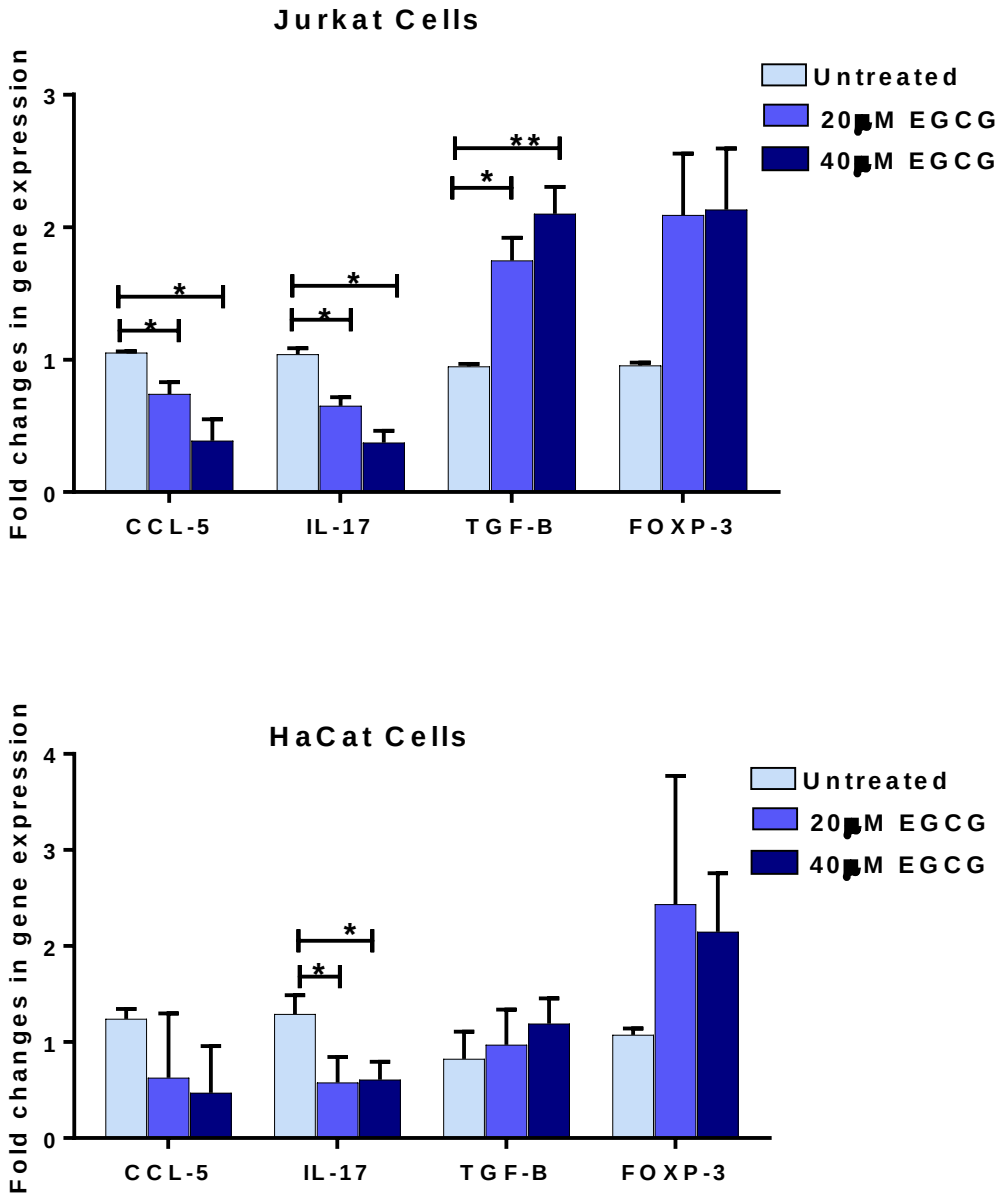

Figure 5.11. Effect of EGCG treatment on a group of inflammatory-regulatory genes involved in IP in HaCat and Jurkat cells.

Following induction with IFN–γ, HaCat or Jurkat cells were treated with 20 or 40μM EGCG for 48hrs and expression of IL-17, CCL-5, FOXP3 and TGF-β were investigated by q-PCR. CT values were normalised to GAPDH and differential expression (2^−ΔΔCT) of AA candidate genes in EGCG treated samples was calculated against untreated samples. Data represented as mean ± SEM (n = 4). Significant difference *P ≤ 0.05, **P ≤ 0.01, ***P ≤ 0.001.

5.2.2 *Ex-vivo* studies

To validate the *in vitro* data, an *ex-vivo* study was performed where lymphocytes (PBMCs) were isolated from the blood of patients (AA) and healthy (HC) donors using the ficoll method as described in section 2.2.2.

5.2.2.1. IFN-γ signalling pathway is a key in AA pathogenesis

The role of IFN-γ signalling in AA has been studied in lymphocytes isolated from regional lymph nodes (Xing et al., 2014). To investigate whether the same pathway is affected in circulating lymphocytes or specifically associated to skin, we looked at the level of IFN-γ protein produced by circulating lymphocytes in patients and HCs by ELISA after activating the cells with PMA/ ionomcyin. It was found that patient's PBMCs produced about seven times higher levels of IFN-γ ($P \leq 0.01$) compared to HC (Figure 5.12.A). To confirm these findings, the level of p-STAT-1 protein was tested by western blotting in naïve PBMCs that had not been activated, and interestingly, the expression of p-STAT-1 protein was markedly less in PBMCs isolated from HC compared to patients' blood (Figure 5.12.B).

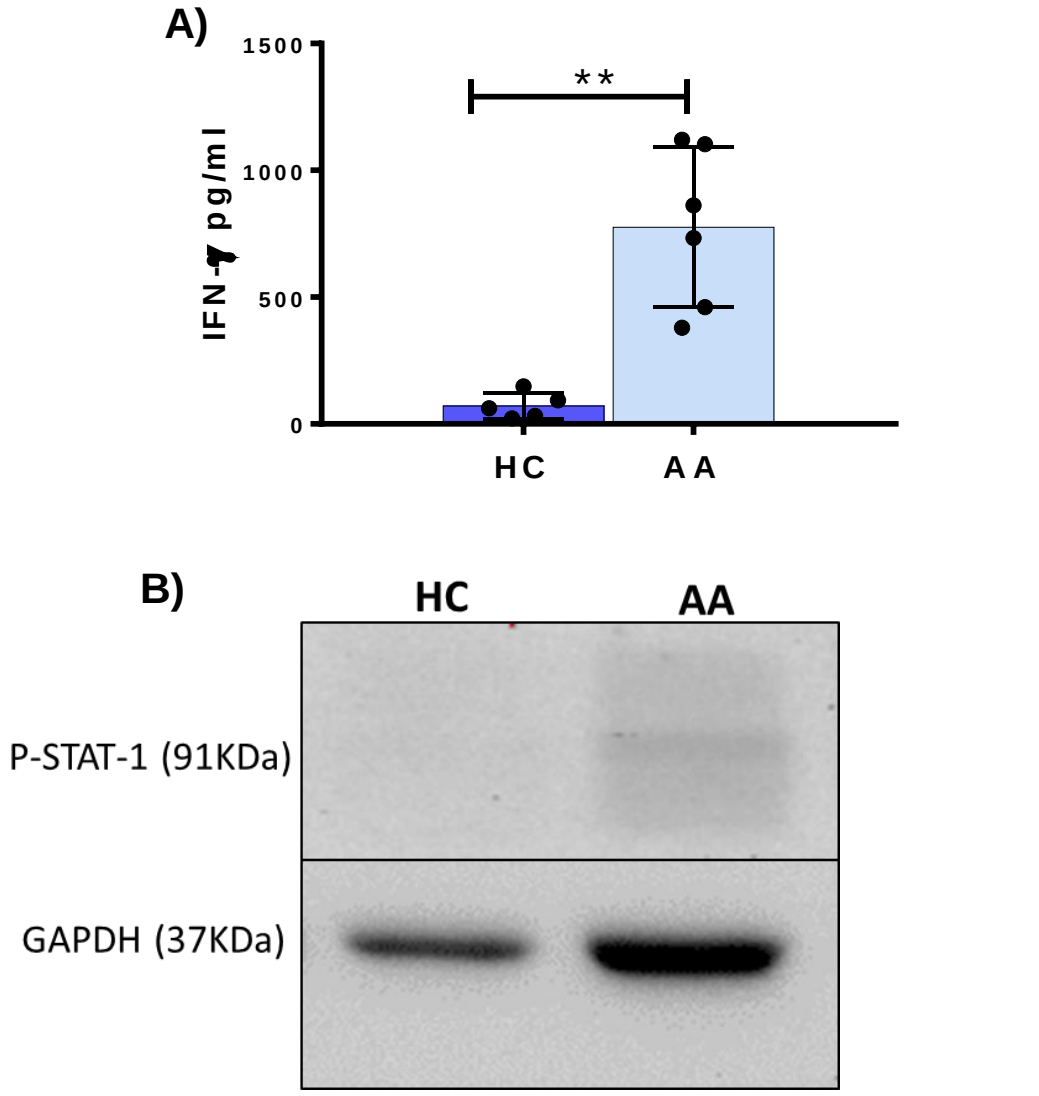

Figure 5.12. Involvement of the IFN-γ pathway in AA.

A) ELISA analysis of IFN-γ production (pg/ml) by PBMCs of patients (n=6) and HC (n=5) stimulated by PMA/ ionomycin for 3.5hrs. Individual data points and mean ± SD are shown. **P value≤0.01. B) Whole cell lysate probed against p-STAT-1 and GAPDH showing absence of p-STAT-1 expression in PMBCs of HC and its expression in those of patients. GAPDH used as protein loading control. To the left the molecular weights (kDa) are shown.

5.2.2.2. The effect of EGCG on STAT-1 phosphorylation

To investigate the effect of ECGC on the IFN-γ signalling pathway (JAK-STAT), PBMC were isolated from AA patients and treated with 40μM EGCG for 48h or left untreated as a control. At the end of the incubation period, the protein was extracted and the level of p-STAT-1 was detected by western blotting. As in Jurkat and HaCat cells, EGCG treatment markedly decreased p-STAT1 protein expression in PBMC to about 80% compared to the untreated group as calculated by densitometry (Figure 5.13).

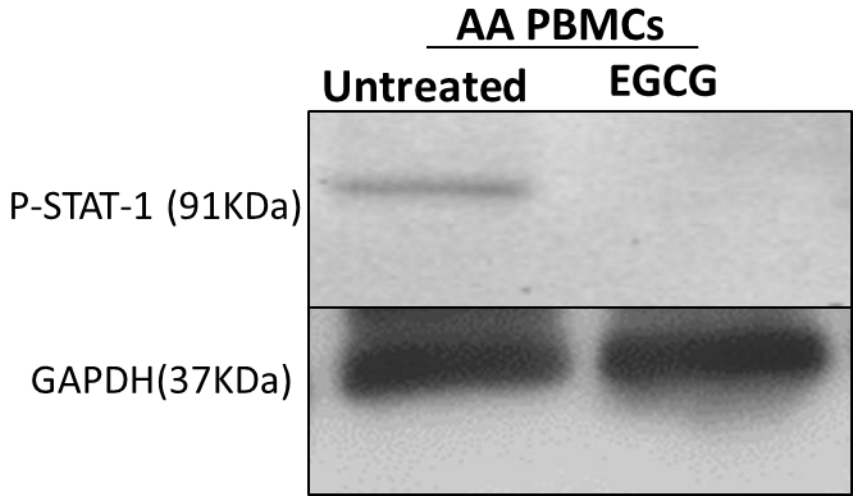

Figure 5.13. Effect of EGCG on p-STAT-1 and STAT-1 in AA subjects.
PBMC cell lysate probed against p-STAT-1 and GAPDH (loading control). There is reduction in the up-regulated p-STAT1 expression in PMBCs of patients by EGCG.

5.2.2.3. The effect of EGCG on Treg-Teff balance

As observed in chapter 3, there was imbalance in distribution of Treg and Teff in patient's peripheral blood where the proportion of Teff was high and suppressive Treg was low compared to HC. Therefore, it was sought to investigate the effect of EGCG on these T-cell subsets. PBMC from 3 patients were treated with 20μM EGC for 24hrs, and the panel of Teff and Treg was

analysed by Flow-cytometry as described in section 2.4. EGCG significantly reduced the proportion of Th1 cells by about 60% compared to untreated group ($P \leq 0.05$), with no effect on the proportion of Th2 population and insignificant increase in Th17 proportion (Figure 5.14. A). Interestingly, a significant reduction in the frequency of NKGD2+CD8+ T-cells was observed in EGCG treated samples ($P \leq 0.05$) by about 50% (Figure 5.14. B). Although no statistically significant effect can be seen on Treg cells and their subtypes, EGCG treated cells showed a slight increase in proportion of cells expressing TGF-β, IL-10 intracellular markers within the Treg population (Figure 5.14. C).

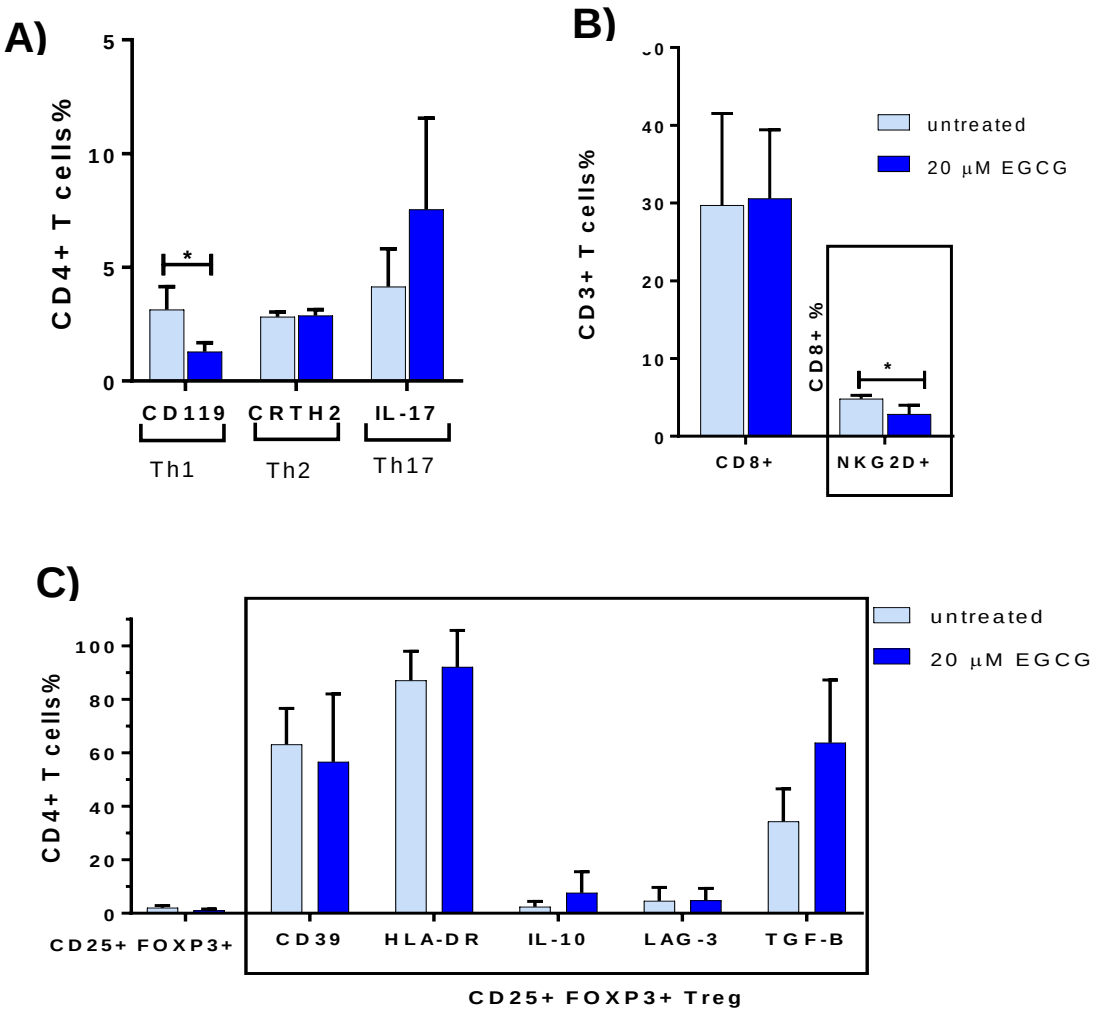

Figure 5.14. The effect of EGCG on Treg and Teff population in AA patients.
A) The frequencies of Th1, Th2 and Th17 calculated as a percentage out of total CD4+ T-cells. B) The frequency of CD8+ T-cells was calculated in the total lymphocyte population (CD3+), and the proportion of activated CD8+ T-cells subset (NKG2D+ cells) was found within CD8+ T-cells. C) Percentage of CD25+FOXP3+ Tregs within CD4+ T-cell population, and their suppressive subsets represented by CD39, HLA-DR, LAG3, IL-10 and TGF-β makers was calculated out of the total Treg pool. Data analysed by a two-tailed independent t-test, and the corrected t-test was used whenever the homogeneity of variance was violated. A 95% confidence interval was used where P≤ 0.05 is considered significant (*), P ≤ 0.01 (**). All bars plot depict mean with SEM in each study group. AA patients n=3

5.3. Discussion

IFN-γ is pivotal element in inducing IP collapse in the HF, and inhibiting its signalling pathway is the target of many therapeutic options. JAK inhibitors including ruxolitinib, tofacitinib and baricitinib were recently used in clinical trials of several inflammatory and autoimmune diseases including skin diseases such as psoriasis (Hsu and Armstrong, 2014) and AA (Xing *et al*., 2014). JAK inhibitors are efficient but have relatively high cost and present a range of significant potential side-effects (Shreberk-Hassidim et al., 2017). For instance, ruxolitinib is a broad JAK (1 and 2) inhibitor with potential to modulate the signalling pathway of cytokines including IL-6, IL-10, IL-22 and IL-3 (Murray, 2007). Ruxolitinib's side-effects include reactivation of tuberculosis, thrombocytopenia, anaemia and a risk of other unknown long-term side-effects (Tefferi and Pardanani, 2011).

In this thesis, EGCG was proposed as a potential therapeutic candidate for AA treatment mainly based on its anti-inflammatory properties and encouraged by its promising safety margin (Chow et al., 2003, Zhao et al., 2015). EGCG has an inhibitory effect on IFN-γ signalling via inhibiting STAT1 phosphorylation, which has been demonstrated by many studies (Tedeschi et al., 2002, Watson et al., 2004, Ogawa et al., 2012). It was therefore sought to establish whether EGCG acts directly on STAT1 and whether STAT1 inhibition can restore IP in HF.

As both JAK1 and JAK2 catalyse STAT1 phosphorylation at Tyr701 (Shuai et al., 1993), the effect of EGCG on JAK1 and JAK2 expression was analysed by q-PCR, and EGCG was found to specifically inhibit JAK2 expression by about 50% but not JAK1 in both HaCat and Jurkat cell lines. EGCG specifically blocks JAK2 and therefore will potentially be relatively safer and more efficient as the

broad JAK1/JAK2 inhibitors block the IFN-γ pathway as well as other pathways including IL-2, IL-6, IL-10, IL-23, and erythropoietin (Epo) (O'Shea and Plenge, 2012). The specificity of EGCG as a pure JAK2 inhibitor does not reduce its efficiency as this was accompanied by reduction in STAT1 phosphorylation at Tyr701 in both cell lines and PBMCs isolated from patients' blood as shown in this study. p-STAT1 interacts with IRF-1 which is a key regulator in IFN-γ signalling, and IFN-γ induced MHC I expression has been shown to be mediated by IRF-1 (Chang et al., 1992, Jarosinski and Massa, 2002). EGCG inhibitory effect on p-STAT1 lead to the significant reduction in IRF-1 expression observed in HaCat and JURKAT cells in keeping with the marked reduction in its protein level demonstrated in colonic epithelial cells (Watson et al., 2004).

It is well known that activation of IFN-γ/STAT1/IRF-1 signalling leads to the activation of HLA class I and class II genes, in particular HLA-B and HLA-DR (Girdlestone et al., 1993). Interestingly, we found that HLA-B expression was significantly reduced after treating HaCat cells with 40μM EGCG by about 66% when compared to untreated group. HLA-B expression is a major factor controlling immunological balance in tissues manifesting IP. For instance, low corneal HLA-B27 is an important contributor to ocular immune privilege (Lin et al., 2015). It has also been shown that MHC class I expression is very low in the proximal epithelium of healthy anagen HF (Harrist et al., 1983) but becomes highly expressed in AA lesional tissue (Gilhar et al., 2007). Interestingly, the current study also demonstrated the efficacy of EGCG to inhibit the expression of HLA-DR noticeably at mRNA and protein levels in HaCat cells treated with 20μM and 40μM EGCG by about 80% drop compared to untreated group. This effect adds to the value of EGCG as a potential treatment for AA. Aberrant expression of HLA-DR in the pre-cortical matrix and dermal papilla (DP) of

lesional anagen follicles was observed in AA (Messenger, 1984, Messenger and Bleehen, 1985, McDonagh et al., 1993). Therefore, it has been suggested that the treatment of AA with EGCG may have the same inhibitory effect on expression of HLA-B and HLA-DR in HF to enable IP restoration.

Another action of EGCG demonstrated in this study was its ability to reduce the expression of IL-17 at mRNA level (Figure 3.11). IL-17 is a key pro-inflammatory cytokine that has been found to be highly expressed in AA patients (Lew et al., 2012, Tembhre and Sharma, 2013, Aytekin et al., 2015). Targeting IL-17 by biological drugs such as secukinumab, ixekizumab and brodalumab has shown promising results in psoriasis (Wasilewska et al., 2016). Nonetheless, further experiments need to be performed to confirm EGCG effect on IL-17, particularly because flow-cytometric findings of Th17 cell frequency was not in keeping with q-PCR data on cell lines. EGCG can modulate immune function by enhancing the regulatory molecules. The current data show that EGCG was capable of enhancing the expression of FOXP3 and TGF-β in Jurkat cells by about 120% in cells treated with 40μM EGCG compared to untreated. These two molecules are markers for Tregs, which are guardians of IP in the HF. In agreement with that, EGCG-treated PBMC from AA patients showed increase in proportion of cells expressing IL-10 and TGF-β markers. Another encouraging effect of EGCG is its ability to reverse the Teff proportion seen in AA patients where Th1 and NKG2D+ CD8+ were csignificantly reduced by about 50% after 24hrs of treatment ($P \leq 0.05$).

In this study, it has been shown that 40μM EGCG which corresponds to a well-tolerated EGCG dose topically, would have multiple actions including inhibition of class I and class II HLA molecules through blocking STAT1 phosphorylation by JAK-2 blockade as well as enhancing the function of Tregs,

promoting re-establishment of IP in the HF (Figure 5.16). These findings support consideration of a clinical trial of EGCG in AA after confirming its proposed mechanism of action in HF organ culture model.

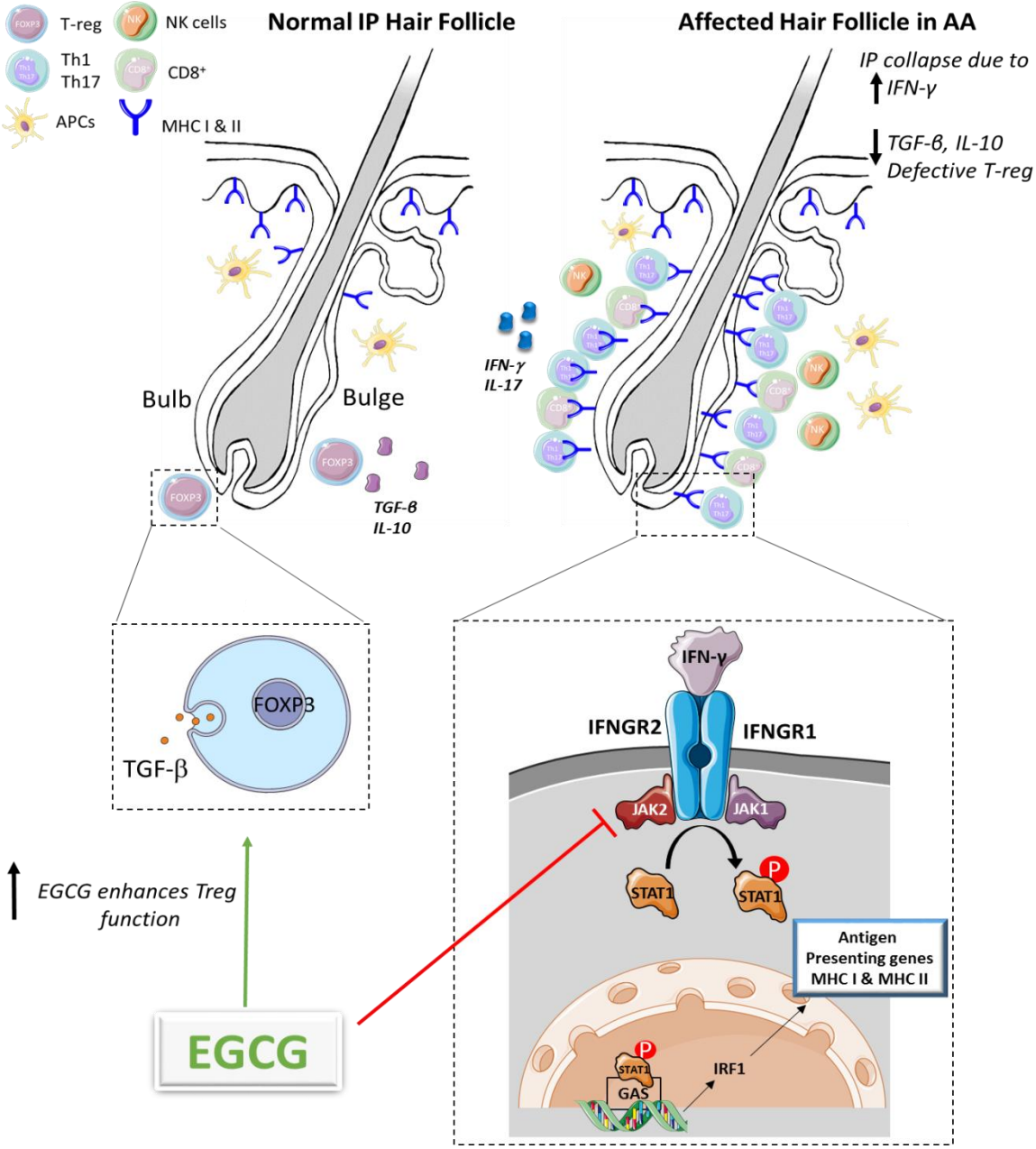

Figure 5.15. Schematic representation of proposed EGCG mechanism of action in AA. Normal HF has scant or no APCs and scant CD4+ T-cells in the bulbar and supra-bulbar region, which it is proposed to be mostly Treg secreting IL-10 and TGF–β maintaining the normal IP state of HF. Affected HF is infiltrated with APCS, NK, CD8+ (Tc) and Th1 and 17. We propose that antigen identification and processing results in IFN-γ production, which in turns up-regulates MHC class I with subsequent sequestration of Tc cells and further production of IFN-γ and up-regulation of MHC class II and sequestration of Th1 and Th17 resulting in HF damage. It is proposed in this study that EGCG down-regulates JAK2 resulting in inhibition STAT-1 phosphorylation, therefore, IFN-γ signalling pathway, and up-regulation of the regulatory arm acting on FOXP3 cells. Tools from Servier medical art were used to create the figure.

Chapter 6. Conclusion and future work

AA is a cosmetically disfiguring and psychologically disturbing skin disease, and poor mechanistic understanding of its pathogenesis has hampered the development of effective treatment. Many factors are thought to be involved in AA pathogenesis including IP collapse (Paus et al., 2003, Ito et al., 2004), where T-cells are thought to be the key mediators. For instance, T-cells are strongly associated with the histological picture of this disease (Todes-Taylor et al., 1984), and inflammatory T-cells mediate the disease progression in experimental models (Gilhar et al., 1999, Gilhar et al., 2002, Gilhar et al., 2003). Regulatory T-cells (Castela et al., 2014) and immunosuppressive molecules such as corticosteroids (Winter et al., 1976) and topical immunotherapy (Wiseman et al., 2001) limit AA progression in some patients. Therefore, imbalance in the T-cell compartments has been proposed in this thesis as a key mechanism in the pathogenesis. However, it was unknown which T-cell population is initially affected during AA pathogenesis and how these cells interact if more than one population involved.

To answer these questions, a comprehensive study of T-cell phenotype in 15 AA patients and 10 HCs was performed by flow-cytometry to define which subtype/s of T-cells mediate IP collapse or maintenance. This experiment demonstrated Treg-Teff balance disruption in AA where the proportion of inflammatory T-cells (Th1, Th17 and NKG2D+CD8+ T-cells) was significantly higher in peripheral blood of patients when compared to HCs. This was accompanied by marked reduction in the suppressive Treg population, which

showed impairment in CD39 and HLA-DR-mediated suppressive mechanisms. There was also a low proportion of CD39+ Tregs in AA affected skin compared to normal skin observed by Immunofluorescence IF analysis of these skin sections. Despite these novel findings, this work has limitations mainly due to the low number of participants in the study to gain a better statistical confidence. Additionally, increased numbers of subjects would allow stratification of the data according to disease severity providing more information about the role of T-cells in disease progression. The same is applied to IF data as the number of skin sections obtained was low. Although it is technically challenging to achieve, isolating T-cells from lesional and non-lesional skin for detailed phenotypic study would potentially allow better understanding of the pathology, and enable correlation of their tissue distribution to the changes in circulating lymphocytes observed in this thesis.

In the second part of this thesis, molecular analysis of the T-cell repertoire was performed by NGS. Interestingly, the TCRβ chain of total lymphocytes was skewed toward two public clonotypes that found to be more prevalent in patients compared to HC, CASSQDKGITNEKLFF and CASSYQGSTEAF, suggesting their expansion in response to unique antigenic recognition. These public clones were found in the literature to have over 80% amino acid identity to TCRβ sequence of CD8+ T-cells, indicating the importance of this T cell population in the pathogenesis. These CD8+ T-cells were isolated from diabetic mice (Vincent et al., 2010) suggesting a correlation between diabetes and AA, which has been proposed in previous studies (Karadag et al., 2013).

As these data are novel, more work is required to confirm TCR skewing pattern noticed in this study on larger number of participants. For instance, validating the NGS findings by q-PCR analysis or *in situ* immune-reactivity of AA

lesional skin sections to antibodies synthesised against these clones is essential to confirm the abundance of these public clones in patient samples (Fang and Cui, 2011). As the public TCR clones mediates the autoimmune susceptibility, another confirmatory test can be performed is testing the ability of the public clone found by this study to provoke AA in experimental animals (Zhao et al., 2016). Testing the reactivity of these clones to diabetes mellitus (DM) antigens such as insulin, tyrosine phosphatase-like proteins insulinoma antigen-2 (IA-2) and glutamate decarboxylase (GAD) (Roep and Peakman, 2012); as well as HF antigens such as hair-specific keratins (52, 50, 46 and 44KD) (Tobin et al., 1994), trichohyalin (Tobin, 2003) and melanocyte-associated proteins (Bystryn and Tobin, 1994, Paus et al., 1993) would elucidate which antigen these clones can recognise.

TCRβ analysis showed the prevalence of certain clonotypes in Tregs from HCs, CATSRDEGGLDEKLFF and CASRDGTGPSNYGYTF, which have high amino acid identity to CD4+ T-cells from healthy controls (Han et al., 2014). This was complemented with finding preferential usage of certain V segments by TCRβ of Tregs of HC such as TRBV2, and the observed deletion of the VD/DJ insert in the CDR3 region of TCRβ of Tregs of AA patients. Together, these data suggest the predominance of certain clones of Tregs in HC that are deficient in AA patient; therefore, their potential role in maintaining immune haemostasis. After validating these data by q-PCR or immune-assay, expanding these clones and injecting them as a therapy in an AA animal model would potentially confirm their role in maintaining IP. Applying this therapetutic approach in animal model to treat murine diabetic retinopathy facilitate its proposed use in AA animal model (Deliyanti et al., 2017).

Finally, it was sought to test the effect of EGCG on the key cells involved in AA as found by this study, namely CD8+ T-cells and Tregs. As CD8+ T-cells mainly secret IFN-γ, which mediates its effect via the JAK-STAT pathway, and due to the promising results from JAK inhibitor trials (Xing et al., 2014), targeting the JAK-STAT pathway by natural molecule was followed in this study. EGCG was proposed as a potential candidate in AA therapy, by virtue of its anti-inflammatory effect mediated by STAT-1 inhibition (Tedeschi et al., 2002) and its positive effect on enhancing Treg differentiation (Wong et al., 2011). Both *in vitro* work, using HaCat and Jurkat cells, and *ex vivo* work, using PBMCs isolated from AA patients, showed the efficiency of 40μM EGCG in reducing the levels of p-STAT-1 protein after 48hrs of treatment. This was accompanied by a significant reduction ($P \leq 0.05$) in expression of IFN-γ downstream genes including JAK-2, STAT-1 and IRF-1 in both cell lines, downregulation of CCL-5 and IL-17 with upregulation of FOXP3 and TGF-β expression in Jurkat cells. Downregulation of MHC class I and II genes in HaCat cells was also observed. These promising findings support EGCG as a candidate molecule for AA treatment especially as EGCG can be used topically with good penetration index (Scalia et al., 2014). This data would support the development of a clinical pilot study to measure the efficacy of EGCG in restoring IP to enhance hair re-growth in AA patients.

As this study was performed mainly in cell lines, more work is required to assess the efficiency of EGCG as a potential treatment of AA. Organ culture of human HF from healthy individuals and AA patients could be performed in the future where the effect of EGCG on the expression of MHC class I and II can be analysed. Similarly, intralesional T-cells could be analysed for the effect of EGCG on their phenotype, activation, and cytokine release. To sum up, the work

in this thesis has brought a number of novel findings to the field of AA research, and these should be taken forward to facilitate the development of more effective therapy for the disease.

References

ACHA-ORBEA, H., MITCHELL, D. J., TIMMERMANN, L., WRAITH, D. C., TAUSCH, G. S., WALDOR, M. K., ZAMVIL, S. S., MCDEVITT, H. O. & STEINMAN, L. 1988. Limited heterogeneity of T cell receptors from lymphocytes mediating autoimmune encephalomyelitis allows specific immune intervention. *Cell,* 54**,** 263-273.

AGHAEI, S., SAKI, N., DANESHMAND, E. & KARDEH, B. 2014. Prevalence of Psychological Disorders in Patients with Alopecia Areata in Comparison with Normal Subjects. *ISRN Dermatol.,* 2014**,** 304370.

AHMED, S. 2010. Green tea polyphenol epigallocatechin 3- gallate in arthritis: Progress and promise. *Arthritis Res & Ther,* 12**,** 208.

AKTAS, O., PROZOROVSKI, T., SMORODCHENKO, A., SAVASKAN, N. E., LAUSTER, R., KLOETZEL, P. M., INFANTE-DUARTE, C., BROCKE, S. & ZIPP, F. 2004. Green tea epigallocatechin-3- gallate mediates T cellular NF- kappa B inhibition and exerts neuroprotection in autoimmune encephalomyelitis. *J. Immunol.,* 173**,** 5794-5800.

ALKHALIFAH, A., ALSANTALI, A., WANG, E., MCELWEE, K. J. & SHAPIRO, J. 2010a. Alopecia areata update. Part I. Clinical picture, histopathology, and pathogenesis. *J Am Acad Dermatol,* 62**,** 177-188.

ALKHALIFAH, A., ALSANTALI, A., WANG, E., MCELWEE, K. J. & SHAPIRO, J. 2010b. Alopecia areata update: part II. Treatment. *J Am Acad Dermatol,* 62**,** 191.

ALLI, R., NGUYEN, P., BOYD, K., SUNDBERG, J. P. & GEIGER, T. L. 2012. A Mouse Model of Clonal CD8(+) T Lymphocyte- Mediated Alopecia Areata Progressing to Alopecia Universalis. *J. Immunol.,* 188**,** 477-486.

ALMEIDA, A. R. M., LEGRAND, N., PAPIERNIK, M. & FREITAS, A. A. 2002. Homeostasis of peripheral CD4(+) T cells: IL- 2R alpha and IL- 2 shape a population of regulatory cells that controls CD4(+) T cell numbers. *J. Immunol.,* 169**,** 4850-4860.

ALZOLIBANI, A. A. 2011. Epidemiologic and genetic characteristics of alopecia areata (part 1). *Acta Dermatoven APA,* 20**,** 191-198.

ANSELL, D., KLOEPPER, J., THOMASON, H., PAUS, R. & HARDMAN, M. 2010. Exploring the " Hair Growth– Wound Healing Connection": Anagen Phase Promotes Wound Re-Epithelialization. *J. Investig. Dermatol.,* 131**,** 518.

ANTONIOLI, L., PACHER, P., VIZI, E. S. & HASKÓ, G. 2013. CD39 and CD73 in immunity and inflammation. *Trends Mol. Med.,* 19**,** 355-367.

APTE, R. S. & NIEDERKORN, J. Y. 1996. Isolation and characterization of a unique natural killer cell inhibitory factor present in the anterior chamber of the eye. *J. Immunol.,* 156**,** 2667-2673.

ARDEN, B., CLARK, S., KABELITZ, D. & MAK, T. 1995. Human T- cell receptor variable gene segment families. *Immunogenetics,* 42**,** 455-500.

ASHLEY, C. W. & BAECHER-ALLAN, C. 2009. Cutting Edge: Responder T Cells Regulate Human DR+ Effector Regulatory T Cell Activity via Granzyme B. *J. Immunol.,* 183**,** 4843-4847.

ATWA, M. A., YOUSSEF, N. & BAYOUMY, N. M. 2016. T-helper 17 cytokines (interleukins 17, 21, 22, and 6, and tumor necrosis factor-alpha) in patients with alopecia areata: association with clinical type and severity. *Int. J. Dermatol.,* 55**,** 666-672.

AYTEKIN, N., AKCALI, C., PEHLIVAN, S., KIRTAK, N. & INALOZ, S. 2015. Investigation of interleukin- 12, interleukin- 17 and interleukin- 23 receptor gene polymorphisms in alopecia areata. *J. Int. Med. Res.,* 43**,** 526-534.

BAECHER-ALLAN, C., WOLF, E. & HALLER, D. A. 2006. MHC class II expression identifies functionally distinct human regulatory T cells. *J. Immunol.,* 176**,** 4622-4631.

BARAHMANI, N., DE ANDRADE, M., SLUSSER, J. P., ZHANG, Q. & DUVIC, M. 2006. Major histocompatibility complex class I chain- related gene a polymorphisms and extended haplotypes are associated with familial alopecia areata. *J Invest Dermatol,* 126**,** 74-78.

BASSING, C. H., SWAT, W. & ALT, F. W. 2002. The Mechanism and Regulation of Chromosomal V(D) J Recombination. *Cell,* 109**,** S45-S55.

BENTLEY, D. R. 2006. Whole-genome re-sequencing. *Curr. Opin. Genet. Dev.,* 16**,** 545-552.

BETTELLI, E., CARRIER, Y., GAO, W., KORN, T., STROM, T. B., OUKKA, M., WEINER, H. L. & KUCHROO, V. K. 2006. Reciprocal developmental pathways for the generation of pathogenic effector TH17 and regulatory T cells. *Nature,* 441**,** 235.

BETZ, R. C., PETUKHOVA, L., RIPKE, S., HUANG, H., MENELAOU, A., REDLER, S., BECKER, T., HEILMANN, S., YAMANY, T., DUVIC, M., HORDINSKY, M., NORRIS, D., PRICE, V. H., MACKAY-WIGGAN, J., DE JONG, A., DESTEFANO, G. M., MOEBUS, S., BOEHM, M., BLUME-PEYTAVI, U., WOLFF, H., LUTZ, G., KRUSE, R., BIAN, L., AMOS, C. I., LEE, A., GREGERSEN, P. K., BLAUMEISER, B., ALTSHULER, D., CLYNES, R., DE BAKKER, P. I. W., NOETHEN, M. M., DALY, M. J. & CHRISTIANO, A. M. 2015. Genome-wide meta-analysis in alopecia areata resolves HLA associations and reveals two new susceptibility loci. *Nat. Commun.,* 6**,** 5966.

BILLINGHAM, R. E. & SILVERS, W. K. 1971. Transplantation and cutaneous genetics. *J. Investig. Dermatol.,* 60**,** 509-515.

BODEMER, C., PEUCHMAUR, M., FRAITAIG, S., CHATENOUD, L., BROUSSE, N. & DE PROST, Y. 2000. Role of cytotoxic T cells in chronic alopecia areata. *J Invest Dermatol,* 114**,** 112-116.

BOLOTIN, D., POSLAVSKY, S., MITROPHANOV, I., SHUGAY, M., MAMEDOV, I., PUTINTSEVA, E. & CHUDAKOV, D. 2015. MiXCR: software for comprehensive adaptive immunity profiling. *Nat. Methods,* 12**,** 380.

BOS, J. D. & MEINARDI, M. M. H. M. 2000. The 500 Dalton rule for the skin penetration of chemical compounds and drugs. *Exp. Dermatol.,* 9**,** 165-169.

BRÖCKER, E. B., ECHTERNACHT-HAPPLE, K., HAMM, H., HAPPLE, R. & ECHTERNACHT-HAPPLE, K. 1987. Abnormal expression of class I and class II major histocompatibility antigens in alopecia areata: modulation by topical immunotherapy. *J Invest Dermatol,* 88**,** 564.

BYSTRYN, J. C. & TOBIN, D. J. 1994. ALOPECIA-AREATA IS ASSOCIATED WITH ANTIBODIES TO HAIR FOLLICLE MELANOCYTES. *J. Invest. Dermatol.,* 102**,** 532-532.

CABANIOLS, J.-P., FAZILLEAU, N., CASROUGE, A., KOURILSKY, P. & KANELLOPOULOS, J. M. 2001. Most α/β T Cell Receptor Diversity Is Due to Terminal Deoxynucleotidyl Transferase. *J. Exp. Med.,* 194**,** 1385-1390.

CACCIA, N., KRONENBERG, M., SAXE, D., HAARS, R., BRUNS, G. A. P., GOVERMAN, J., MALISSEN, M., WILLARD, H., YOSHIKAI, Y., SIMON, M., HOOD, L. & MAK, T. W. 1984. THE T-CELL RECEPTOR BETA-CHAIN GENES ARE LOCATED ON CHROMOSOME-6 IN MICE AND CHROMOSOME-7 IN HUMANS. *Cell,* 37**,** 1091-1099.

CAI, B., ZHANG, J., ZHANG, M., LI, L., FENG, W., AN, Z. & WANG, L. 2013. Micro-inflammation Characterized by Disturbed Treg/Teff Balance with Increasing sIL-2R in Patients with Type 2 Diabetes. *Exp. Clin. Endocrinol. Diabetes,* 121**,** 214-219.

CARROLL, J. M., MCELWEE, K. J., KING, L. E., BYRNE, M. C. & SUNDBERG, J. P. 2002. Gene array profiling and immunomodulation studies define a cell- mediated immune response underlying the pathogenesis of alopecia areata in a mouse model and humans. *J. Invest. Dermatol.,* 119**,** 392-402.

CARTER, D. M. & JEGASOTHY, B. V. 1976. Alopecia Areata and Down Syndrome. *Arch Dermatol.,* 112**,** 1397-1399.

CASTELA, E., LE DUFF, F., BUTORI, C., TICCHIONI, M., HOFMAN, P., BAHADORAN, P., LACOUR, J.-P. & PASSERON, T. 2014. Effects of Low-Dose Recombinant Interleukin 2 to Promote T-Regulatory Cells in Alopecia Areata. *Jama Dermatol.,* 150**,** 748-751.

CAVET, M. E., HARRINGTON, K., VOLLMER, T., WARD, K. & ZHANG, J. 2011. Anti- inflammatory and anti- oxidative effects of the green tea polyphenol epigallocatechin gallate in human corneal epithelial cells. *Mol. Vis.,* 17**,** 533-542.

CHANG, C.-H., HAMMER, J., LOH, J., FODOR, W. & FLAVELL, R. 1992. The activation of major histocompatibility complex class I genes by interferon regulatory factor- 1 (IRF- 1). *Immunogenetics,* 35**,** 378-384.

CHENG, C. W., SHIEH, P.C., LIN, Y.C., CHEN, Y.J., LIN, Y.H., KUO, D.H., LIU, J.Y., KAO, J.Y., KAO, M.C. & WAY, T.D. 2007. Indoleamine 2,3-dioxygenase, an immunomodulatory protein, is suppressed by (-)-epigallocatechin-3-gallate via blocking of gamma-interferon-induced JAK-PKC-delta-STAT1 signaling in human oral cancer cells. *Biochem Biophys Res Commun,* 354**,** 1004-9.

CHOW, H. H. S., CAI, Y., HAKIM, I. A., CROWELL, J. A., SHAHI, F., BROOKS, C. A., DORR, R. T., HARA, Y. & ALBERTS, D. S. 2003. Pharmacokinetics and safety of green tea polyphenols after multiple- dose administration of epigallocatechin gallate and Polyphenon E in healthy individuals. *Clin. Cancer Res.,* 9**,** 3312-3319.

CHRISTOPH, T., MULLER-ROVER, S., AUDRING, H., TOBIN, D. J., HERMES, B., COTSARELIS, G., RUCKERT, R. & PAUS, R. 2000. The human hair follicle immune system: cellular composition and immune privilege. *Br. J. Dermatol.,* 142**,** 862-873.

CHU, S. Y., CHEN, Y. J., TSENG, W. C., LIN, M. W., CHEN, T. J., HWANG, C. Y., CHEN, C. C., LEE, D. D., CHANG, Y. T., WANG, W. J. & LIU, H. N. 2012. Psychiatric comorbidities in patients with alopecia areata in Taiwan: a case-control study. *Br. J. Dermatol.,* 166**,** 525-531.

COLE, D. K., VAN DEN BERG, H. A., LLOYD, A., CROWTHER, M. D., BECK, K., EKERUCHE-MAKINDE, J., MILES, J. J., BULEK, A. M., DOLTON, G., SCHAUENBURG, A. J., WALL, A., FULLER, A., CLEMENT, M., LAUGEL, B., RIZKALLAH, P. J., WOOLDRIDGE, L. & SEWELL, A. K. 2017. Structural Mechanism Underpinning Cross- reactivity of a CD8+ T- cell Clone That Recognizes a Peptide Derived from Human Telomerase Reverse Transcriptase. *J. biol. chem.,* 292**,** 802.

COLLISON, L., W., WORKMAN, C., J., KUO, T., T., BOYD, K., WANG, Y., VIGNALI, K., M., CROSS, R., SEHY, D., BLUMBERG, R., S. & VIGNALI, D., A. A. 2007. The inhibitory cytokine IL-35 contributes to regulatory T- cell function. *Nature,* 450**,** 566-569.

COLOMBE, B. W., LOU, C. D. & PRICE, V. H. 1999. The genetic basis of alopecia areata: HLA associations with patchy alopecia areata versus alopecia totalis and alopecia universalis. *J. Invest. Dermatol. Symp. Proc.,* 4**,** 216-219.

COLOMBE, B. W., PRICE, V. H., KHOURY, E. L., GAROVOY, M. R. & LOU, C. D. 1995. HLA class- II antigen associations help to define 2 types of alopecia areata. *J. Am. Acad. Dermatol.,* 33**,** 757-764.

COLÓN, E. A., POPKIN, M. K., CALLIES, A. L., DESSERT, N. J. & HORDINSKY, M. K. 1991. Lifetime prevalence of psychiatric disorders in patients with alopecia areata. *Compr psychiatry,* 32**,** 245-51.

COLWELL, R. K., CHAO, A., GOTELLI, N. J., LIN, S.-Y., MAO, C. X., CHAZDON, R. L. & LONGINO, J. T. 2012. Models and estimators linking individual- based and sample- based rarefaction, extrapolation and comparison of assemblages. *J. Plant Ecol.,* 5**,** 3-21.

CUNLIFFE, W. J., HALL, R., STEVENSON, C. J. & WEIGHTMAN, D. 1969. Alopecia areata, thyroid disease and autoimmunity. *B. J. Dermatol.,* 81**,** 877-881.

DAL BELO, S. E., GASPAR, L. R., MAIA CAMPOS, P. M. B. G. & MARTY, J. P. 2009. Skin penetration of epigallocatechin-3-gallate and quercetin from green tea and Ginkgo biloba extracts vehiculated in cosmetic formulations. *Skin pharmacol. physiol.,* 22**,** 299-304.

DARNELL, J. E., KERR, I. M. & STARK, G. R. 1994. JAK- STAT PATHWAYS AND TRANSCRIPTIONAL ACTIVATION IN RESPONSE TO IFNS AND OTHER EXTRACELLULAR SIGNALING PROTEINS. *Science,* 264**,** 1415-1421.

DAVIS, M. M. & BJORKMAN, P. J. 1988. T-CELL ANTIGEN RECEPTOR GENES AND T-CELL RECOGNITION. *Nature,* 334**,** 395-402.

DE ANDRADE, M., JACKOW, C. M., DAHM, N., HORDINSKY, M., REVEILLE, J. D. & DUVIC, M. 1999. Alopecia areata in families: Association with the HLA locus. *J. Invest. Dermatol. Symp. Proc.,* 4**,** 220-223.

DEAGLIO, S., DWYER, K., GAO, W., FRIEDMAN, D., USHEVA, A., ERAT, A., CHEN, J.-F., ENJYOJI, K., LINDEN, J., OUKKA, M., KUCHROO, V., STROM, T. & ROBSON, S. 2007. Adenosine generation catalyzed by CD39 and CD73 expressed on regulatory T cells mediates immune suppression. *J. Exp. Med.,* 204**,** 1257-1265.

DEJACO, C., DUFTNER, C., GRUBECK‐LOEBENSTEIN, B. & SCHIRMER, M. 2006. Imbalance of regulatory T cells in human autoimmune diseases. *Immunology,* 117**,** 289-300.

DELAMERE, F. M., SLADDEN, M. M., DOBBINS, H. M. & LEONARDI-BEE, J. 2008. Interventions for alopecia areata. *Cochrane Database Syst. Rev.,* 2**,** CD004413.

DELIYANTI, D., TALIA, D., ZHU, T., MAXWELL, M., AGROTIS, A., JEROME, J., HARGREAVES, E., GERONDAKIS, S., HIBBS, M., MACKAY, F. & WILKINSON-BERKA, J. 2017. Foxp3+ Tregs are recruited to the retina to repair pathological angiogenesis. *Nat. Commun.,* 8**,** 1-12.

DEMPSEY, P., VAIDYA, S. & CHENG, G. 2003. The Art of War: Innate and adaptive immune responses. *Cell. Mol. Life Sci.,* 60**,** 2604-2621.

DRY, F. 1926. The coat of the mouse (Mus musculus). *Journ. of Gen.,* 16**,** 287-340.

DUBOIS, M., BAUMSTARCK-BARRAU, K., GAUDY-MARQUESTE, C., RICHARD, M. A., LOUNDOU, A., AUQUIER, P. & GROB, J. J. 2010. Quality of Life in Alopecia Areata: A Study of 60 Cases. *J. Invest. Dermatol.,* 130**,** 2830-2833.

DUVIC, M., HORDINSKY, M. K., FIEDLER, V. C., OBRIEN, W. R., YOUNG, R. & REVEILLE, J. D. 1991. HLA- D LOCUS ASSOCIATIONS IN ALOPECIA- AREATA - DRW52A MAY CONFER DISEASE RESISTANCE. *Arch. Dermatol.,* 127**,** 64-68.

DUVIC, M., NELSON, A. & DE ANDRADE, M. 2001. The genetics of alopecia areata. *Clin. Dermatol.,* 19**,** 135-139.

DVORAKOVA, K., DORR, R. T., VALCIC, S., TIMMERMANN, B. & ALBERTS, D. S. 1999. Pharmacokinetics of the green tea derivative, EGCG, by the topical route of administration in mouse and human skin. *Cancer Chemother. Pharmacol.,* 43**,** 331-335.

EDLING, A. E., GOMES, D., WEEDEN, T., DZURIS, J., STEFANO, J., PAN, C., WILLIAMS, J., KAPLAN, J. & PERRICONE, M. A. 2011. Immunosuppressive activity of a novel peptide analog of alpha- melanocyte stimulating hormone (α- MSH) in experimental autoimmune uveitis. *J. Neuroimmunol.,* 236**,** 1-9.

EHRENSTEIN, M. R., EVANS, J. G., SINGH, A., MOORE, S., WARNES, G., ISENBERG, D. A. & MAURI, C. 2004. Compromised function of regulatory T cells in rheumatoid arthritis and reversal by anti-TNFalpha therapy. *J. exp. med.,* 200**,** 277.

EL-MORSY, E. H., EID, A. A., GHONEIM, H. & AL‐TAMEEMI, K. A. 2016. Serum level of interleukin‐17A in patients with alopecia areata and its relationship to age. *Int. J. Dermatol.,* 55**,** 869-874.

ENK, A. H., JONULEIT, H., SALOGA, J. & KNOP, J. 1997. Dendritic cells as mediators of tumor-induced tolerance in metastatic melanoma. *Int. J. Cancer,* 73**,** 309-316.

ERIC, V., ELENA, T., MYRIAM, B., THIERRY, W. & SOPHIE, U. 2008. Functions of natural killer cells. *Nature Immunol.,* 9**,** 503.

FANG, Z. & CUI, X. 2011. Design and validation issues in RNA- seq experiments. *Brief. Bioinform.,* 12**,** 280-287.

FARRAR, M. A. & SCHREIBER, R. D. 1993. THE MOLECULAR CELL BIOLOGY OF INTERFERON-GAMMA AND ITS RECEPTOR. *Annu. Rev. Immunol.,* 11**,** 571-611.

FLETCHER, J. M., LONERGAN, R., COSTELLOE, L., KINSELLA, K., MORAN, B., O'FARRELLY, C., TUBRIDY, N. & MILLS, K. H. G. 2009. CD39(+)Foxp3(+) Regulatory T Cells Suppress

Pathogenic Th17 Cells and Are Impaired in Multiple Sclerosis. *J. Immunol.,* 183**,** 7602-7610.

FONTENOT, J., GAVIN, M. & RUDENSKY, A. 2003. Foxp3 programs the development and function of CD4+ CD25+ regulatory T cells. *Nat. Immunol.,* 4**,** 330-336.

FRAGALE, A., GABRIELE, L., STELLACCI, E., BORGHI, P., PERROTTI, E., ILARI, R., LANCIOTTI, A., REMOLI, A. L., VENDITTI, M., BELARDELLI, F. & BATTISTINI, A. 2008. IFN regulatory factor- 1 negatively regulates CD4 + CD25 + regulatory T cell differentiation by repressing Foxp3 expression. *J. Immunol.,* 181**,** 1673-1682.

FREYSCHMIDT-PAUL, P., MCELWEE, K. J., HOFFMANN, R., SUNDBERG, J. P., VITACOLONNA, M., KISSLING, S., ZÖLLER, M. & FREYSCHMIDT-PAUL, P. 2006. Interferon- gamma-deficient mice are resistant to the development of alopecia areata. *Br.J. Dermatol.,* 155**,** 515.

FRIDMAN, J. S., SCHERLE, P. A., COLLINS, R., BURN, T. C., LI, Y., LI, J., COVINGTON, M. B., THOMAS, B., COLLIER, P., FAVATA, M. F., WEN, X., SHI, J., MCGEE, R., HALEY, P. J., SHEPARD, S., RODGERS, J. D., YELESWARAM, S., HOLLIS, G., NEWTON, R. C., METCALF, B., FRIEDMAN, S. M. & VADDI, K. 2010. Selective inhibition of JAK1 and JAK2 is efficacious in rodent models of arthritis: preclinical characterization of INCB028050. *J. Immunol.,* 184**,** 5298.

FUJIMURA, T., OKUYAMA, R., ITO, Y. & AIBA, S. 2008. Profiles of Foxp3+ regulatory T cells in eczematous dermatitis, psoriasis vulgaris and mycosis fungoides. *Br. J. Dermatol.,* 158**,** 1256-1263.

FUKUHARA, K., OKUMURA, M., SHIONO, H., INOUE, M., KADOTA, Y., MIYOSHI, S. & MATSUDA, H. 2002. A study on CD45 isoform expression during T- cell development and selection events in the human thymus. *Human Immunol.,* 63**,** 394-404.

GARÍN, M. I., CHU, N.-C., GOLSHAYAN, D., LECHLER, R. I., CERNUDA-MOROLLÓN, E. & WAIT, R. 2007. Galectin- 1: A key effector of regulation mediated by CD4 + CD25 + T cells. *Blood,* 109**,** 2058-2065.

GHERSETICH, I., CAMPANILE, G. & LOTTI, T. 1996. Alopecia areata: Immunohistochemistry and ultrastructure of infiltrate and identification of adhesion molecule receptors. *Int. J. Dermatol.,* 35**,** 28-33.

GHORESCHI, K., LAURENCE, A., YANG, X. P., HIRAHARA, K. & SHEA, J. J. 2011. T helper 17 cell heterogeneity and pathogenicity in autoimmune disease. *Trends Immunol.,* 32**,** 395-401.

GILFILLAN, S., DIERICH, A., LEMEUR, M., BENOIST, C. & MATHIS, D. 1993. Mice Lacking TdT: Mature Animals with an Immature Lymphocyte Repertoire. *Science,* 261**,** 1175-1178.

GILHAR, A., ETZIONI, A., ASSAY, B. & EIDELMAN, S. 1993. Response of grafts from patients with alopecia areata transplanted onto nude mice, to administration of interferon-γ. *Clin. Immunol. Immunopathol.,* 66**,** 120-126.

GILHAR, A. & KALISH, R. S. 2006. Alopecia areata: A tissue specific autoimmune disease of the hair follicle. *Autoimmun. Rev.,* 5**,** 64-69.

GILHAR, A., KAM, Y., ASSY, B. & KALISH, R. S. 2005. Alopecia areata induced in C3H/ HeJ mice by interferon- gamma: evidence for loss of immune privilege. *J. investig. dermatol.,* 124**,** 288.

GILHAR, A., KEREN, A. & PAUS, R. 2013. A new humanized mouse model for alopecia areata. *J. Investig. Dermatol. Symp. proc.,* 16**,** 37.

GILHAR, A. & KRUEGER, G. G. 1987. Hair growth in scalp grafts from patients with alopecia areata and alopecia universalis grafted onto nude mice. *Arch. Dermatol.,* 123**,** 44-50.

GILHAR, A., LANDAU, M., ASSY, B., SHALAGINOV, R., SERAFIMOVICH, S. & KALISH, R. S. 2001. Melanocyte- associated T cell epitopes can function as autoantigens for transfer of alopecia areata to human scalp explants on Prkdc(scid) mice. *J. Invest. Dermatol.,* 117**,** 1357-1362.

GILHAR, A., LANDAU, M., ASSY, B., SHALAGINOV, R., SERAFIMOVICH, S. & KALISH, R. S. 2002. Mediation of alopecia areata by cooperation between CD4+ and CD8+ T lymphocytes: transfer to human scalp explants on Prkdc(scid) mice. *Arch. Dermatol.,* 138**,** 916.

GILHAR, A., LANDAU, M., ASSY, B., ULLMANN, Y., SHALAGINOV, R., SERAFIMOVICH, S. & KALISH, R. S. 2003. Transfer of alopecia areata in the human scalp graft/ Prkdc(scid) (SCID) mouse system is characterized by a TH1 response. *Clin. Immunol.,* 106**,** 181-187.

GILHAR, A., PAUS, R. & KALISH, R. S. 2007. Lymphocytes, neuropeptides, and genes involved in alopecia areata. *J Clin Invest.,* 117**,** 2019-27.

GILHAR, A., PILLAR, T., ASSAY, B. & DAVID, M. 1992. Failure of passive transfer of serum from patients with alopecia areata and alopecia universalis to inhibit hair growth in transplants of human scalp skin grafted on to nude mice. *British Journal of Dermatology,* 126**,** 166-171.

GILHAR, A., SHALAGINOV, R., ASSY, B., SERAFIMOVICH, S. & KALISH, R. S. 1999. Alopecia areata is a T- lymphocyte mediated autoimmune disease: Lesional human T-lymphocytes transfer alopecia areata to human skin grafts on SCID mice. *J. Invest. Dermatol. Symp. Proc.,* 4**,** 207-210.

GILHAR, A., ULLMANN, Y., BERKUTZKI, T., ASSY, B. & KALISH, R. S. 1998. Autoimmune hair loss (alopecia areata) transferred by T lymphocytes to human scalp explants on SCID mice. *J. clin. investig.,* 101**,** 62.

GILLIAM, A., KREMER, I., YUICHI, Y., STEVENS, S., TOOTELL, E., TEUNISSEN, M., HAMMERBERG, C. & COOPER, K. 1998. The Human Hair Follicle: A Reservoir of CD40+ B7- Deficient Langerhans Cells that Repopulate Epidermis After UVB Exposure. *J. Investig. Dermatol.,* 110**,** 422.

GIRDLESTONE, J., ISAMAT, M., GEWERT, D. & MILSTEIN, C. 1993. Transcriptional regulation of HLA-A and -B: differential binding of members of the Rel and IRF families of transcription factors. *Proc. Natl. Acad. Sci. U.S.A,* 90**,** 11568.

GOSEMANN, J. H., VAN GRIENSVEN, M., BARKHAUSEN, T., KOBBE, P., THOBE, B. M., HAASPER, C., PAPE, H. C., KRETTEK, C., HILDEBRAND, F. & FRINK, M. 2010. TLR4 influences the humoral and cellular immune response during polymicrobial sepsis. *Injury,* 41**,** 1060-1067.

GRABBE, S., BHARDWAJ, R. S., MAHNKE, K., SIMON, M. M., SCHWARZ, T. & LUGER, T. A. 1996. α- Melanocyte- stimulating hormone induces hapten- specific tolerance in mice. *J. Immunol.,* 156**,** 473-478.

GROSSMAN, W. J., VERBSKY, J. W., BARCHET, W., COLONNA, M., ATKINSON, J. P. & LEY, T. J. 2004. Human T Regulatory Cells Can Use the Perforin Pathway to Cause Autologous Target Cell Death. *Immunity,* 21**,** 589-601.

GRUSCHWITZ, M., MÜLLER, P. U., SEPP, N., HOFER, E., FONTANA, A. & WICK, G. 1990. Transcription and expression of transforming growth factor type beta in the skin of progressive systemic sclerosis: A mediator of fibrosis? *J. Investig. Dermatol.,* 94**,** 197-203.

GU, J., NI, X., PAN, X., LU, H., LU, Y., ZHAO, J., ZHENG, S. G., HIPPEN, K. L., WANG, X. & LU, L. 2017. Human CD39 hi regulatory T cells present stronger stability and function under inflammatory conditions. *Cell. Mol. Immunol.,* 14**,** 521-528.

GULERIA, I., KHOSROSHAHI, A., ANSARI, M. J., HABICHT, A., AZUMA, M., YAGITA, H., NOELLE, R. J., COYLE, A., MELLOR, A. L., KHOURY, S. J. & SAYEGH, M. H. 2005. A critical role for the programmed death ligand 1 in fetomaternal tolerance. *J. Experim. Med.,* 202**,** 231-237.

GUO, H. W., CHENG, Y. B., SHAPIRO, J. & MCELWEE, K. 2015. The role of lymphocytes in the development and treatment of alopecia areata. *Expert Rev. Clin. Immunol.,* 11**,** 1335-1351.

HACHAM-ZADEH, S., BRAUTBAR, C., COHEN, C. A. & COHEN, T. 1981. HLA and Alopecia areata in Jerusalem. *Tissue Antigens,* 18**,** 71-74.

HAIDA, Y., IKEDA, S., TAKAGI, A., KOMIYAMA, E., MABUCHI, T., OZAWA, A., KULSKI, J. K., INOKO, H. & OKA, A. 2013. Association analysis of the HLA- C gene in Japanese alopecia areata. *Immunogenetics,* 65**,** 553-557.

HAN, A., GLANVILLE, J., HANSMANN, L. & DAVIS, M. 2014. Linking T- cell receptor sequence to functional phenotype at the single- cell level. *Nat. Biotechnol.,* 32**,** 684-692.

HAN, Y. M., SHENG, Y. Y., XU, F., QI, S. S., LIU, X. J., HU, R. M., MIAO, Y., HUANG, G. Q. & YANG, Q. P. 2015. Imbalance of T‐helper 17 and regulatory T cells in patients with alopecia areata. *The Journal of dermatology,* 42**,** 981-988.

HAPPLE, R., HAUSEN, B. M. & WIESNER MENZEL, L. 1983. Diphencyprone in the treatment of alopecia areata. *Acta Derm. Venereol.,* 63**,** 49-52.

HARPAZ, I., ABUTBUL, S., NEMIROVSKY, A., GAL, R., COHEN, H. & MONSONEGO, A. 2013. Chronic exposure to stress predisposes to higher autoimmune susceptibility in C 57 BL / 6 mice: Glucocorticoids as a double‐edged sword. *European Journal of Immunology,* 43**,** 758-769.

HARRIST, T. J., RUITER, D. J., MIHM JR, M. C. & BHAN, A. K. 1983. Distribution of major histocompatibility antigens in normal skin. *Br. J. Dermatol.,* 109**,** 623-633.

HEAD, J. R. & BILLINGHAM, R. E. 1985. Immunologically privileged sites in transplantation immunology and oncology. *Perspect. Biol. Med.,* 29**,** 115-131.

HODGES, E., KRISHNA, M. T., PICKARD, C. & SMITH, J. L. 2003. Diagnostic role of tests for T cell receptor (TCR) genes. *J. Clin. Pathol.,* 56**,** 1-11.

HODKINSON, B. P. & GRICE, E. A. 2015. Next- Generation Sequencing: A Review of Technologies and Tools for Wound Microbiome Research. *Adv. Wound Care,* 4**,** 5-58.

HOORNSTRA, D., ANDERSSON, M. A., TEPLOVA, V. V., MIKKOLA, R., UOTILA, L. M., ANDERSSON, L. C., ROIVAINEN, M., GAHMBERG, C. G. & SALKINOJA-SALONEN, M. S. 2013. Potato crop as a source of emetic Bacillus cereus and cereulide- induced mammalian cell toxicity. *Appl. environ. microbiol.,* 79**,** 3534-43.

HORVATH, C. M. 2004. The Jak- STAT pathway stimulated by interferon gamma. *Sci. STKE,* 2004**,** tr8.

HOU, W. P., LI, S. Z., WU, Y. P., DU, X. & YUAN, F. H. 2009. Inhibition of indoleamine 2, 3-dioxygenase- mediated tryptophan catabolism accelerates crescentic glomerulonephritis. *Clin. Exp. Immunol.,* 156**,** 363-372.

HSU, L. & ARMSTRONG, A. W. 2014. JAK inhibitors: treatment efficacy and safety profile in patients with psoriasis. *J. Immunol. Res.,* 2014**,** 283617.

HSU, S., BOLLAG, W. B., LEWIS, J., HUANG, Q., SINGH, B., SHARAWY, M., YAMAMOTO, T. & SCHUSTER, G. 2003. Green tea polyphenols induce differentiation and proliferation in epidermal keratinocytes. *J. Pharmacol. Exp. Ther.,* 306**,** 29-34.

HU, J., BATTH, I. S., XIA, X. & LI, S. 2016. Regulation of NKG2D+ CD8+ T-cell-mediated antitumor immune surveillance: Identification of a novel CD28 activation-mediated, STAT3 phosphorylation-dependent mechanism. *Oncoimmunology,* 5**,** e1252012.

ITO, M., LIU, Y., YANG, Z., NGUYEN, J., LIANG, F., MORRIS, R. J. & COTSARELIS, G. 2005. Stem cells in the hair follicle bulge contribute to wound repair but not to homeostasis of the epidermis. *Nat. Med.,* 11**,** 1351-1354.

ITO, M. & SATO, Y. 1990. Dynamic ultrastructural changes of the connective tissue sheath of human hair follicles during hair cycle. *Arch. Dermatol. Res.,* 282**,** 434-441.

ITO, T., HASHIZUME, H., SHIMAUCHI, T., FUNAKOSHI, A., ITO, N., FUKAMIZU, H., TAKIGAWA, M. & TOKURA, Y. 2012. CXCL10 produced from hair follicles induces Th1 and Tc1 cell infiltration in the acute phase of alopecia areata followed by sustained Tc1 accumulation in the chronic phase. *J. Dermatol. Sci.,* 69**,** 140-147.

ITO, T., ITO, N., BETTERMANN, A., TOKURA, Y., TAKIGAWA, M. & PAUS, R. 2004. Collapse and Restoration of MHC Class- I- Dependent Immune Privilege: Exploiting the Human Hair Follicle as a Model. *Am. J. Pathol.,* 164**,** 623-634.

ITO, T., ITO, N., SAATOFF, M., HASHIZUME, H., FUKAMIZU, H., NICKOLOFF, B. J., TAKIGAWA, M. & PAUS, R. 2008. Maintenance of hair follicle immune privilege is linked to prevention of NK cell attack. *J. Invest. Dermatol.,* 128**,** 1196-1206.

IVAN, K. H. P., YU-HSIN, C., ALLISON, J. A., JASON, M. K., IGNACIO, J. J., DOUGLAS, A. B. & KODI, S. R. 2014. Unexpected link between an antibiotic, pannexin channels and apoptosis. *Nature,* 507**,** 329.

IVASHKIV, L. B. & HU, X. 2004. Signaling by STATs. *Arthritis Res.Ther,* 6**,** 159-168.

JABBARI, A., DAI, Z., XING, L., CERISE, J. E., RAMOT, Y., BERKUN, Y., SANCHEZ, G. A. M., GOLDBACH-MANSKY, R., CHRISTIANO, A. M., CLYNES, R. & ZLOTOGORSKI, A. 2015. Reversal of Alopecia Areata Following Treatment With the JAK1/ 2 Inhibitor Baricitinib. *EBioMedicine,* 2**,** 351-355.

JACKSON, K., KIDD, M., WANG, Y. & COLLINS, A. 2013. The shape of the lymphocyte receptor recepertoire: lessons from the B cell receptor. *Front. Immunol.,* 4**,** 263.

JANEWAY, C. A. 2001. *Immunobiology : the immune system in health and disease,* New York, New York : Garland, 2001.

JAROSINSKI, K. W. & MASSA, P. T. 2002. Interferon regulatory factor- 1 is required for interferon-γ- induced MHC class I genes in astrocytes. *J. Neuroimmunol.,* 122**,** 74-84.

JIMBOW, K., SATO, S. & KUKITA, A. 1969. Langerhans' cells of the normal human pilosebaceous system. An electron microscopic investigation. *J. Investig. Dermatol.,* 52**,** 177-180.

JOACHIMS, M. L., LEEHAN, K. M., LAWRENCE, C., PELIKAN, R. C., MOORE, J. S., PAN, Z., RASMUSSEN, A., RADFAR, L., LEWIS, D. M., GRUNDAHL, K. M., KELLY, J. A., WILEY, G. B., SHUGAY, M., CHUDAKOV, D. M., LESSARD, C. J., STONE, D. U., SCOFIELD, R. H., MONTGOMERY, C. G., SIVILS, K. L., THOMPSON, L. F. & FARRIS, A. D. 2016. Single-cell analysis of glandular T cell receptors in Sjogren's syndrome. *Jci Insight,* 1**,** e85609.

JONCKER, N. & RAULET, D. 2008. Regulation of NK cell responsiveness to achieve self-tolerance and maximal responses to diseased target cells. *Immunol. Rev.,* 224**,** 85-97.

JONULEIT, H. & SCHMITT, E. 2003. The regulatory T cell family: Distinct subsets and their interrelations. *J. Immunol.,* 171**,** 6323-6327.

KANELLOPOULOS-LANGEVIN, C., CAUCHETEUX, S. M., VERBEKE, P. & OJCIUS, D. M. 2003. Tolerance of the fetus by the maternal immune system: Role of inflammatory mediators at the feto- maternal interface. *Reprod. Biol. Endocrinol.,* 1**,** 121.

KANG, H., WU, W. Y., LO, B. K. K., YU, M., LEUNG, G., SHAPIRO, J. & MCELWEE, K. J. 2010. Hair Follicles from Alopecia Areata Patients Exhibit Alterations in Immune Privilege-Associated Gene Expression in Advance of Hair Loss. *J. Invest. Dermatol.,* 130**,** 2677-2680.

KARADAG, A. S., ERTUGRUL, D. T., BILGILI, S. G., TAKCI, Z., TUTAL, E. & YILMAZ, H. 2013. Insulin resistance is increased in alopecia areata patients. *Cutan. Ocul. Toxicol.,* 32**,** 102-106.

KATIYAR, S. K., MATSUI, M. S., ELMETS, C. A. & MUKHTAR, H. 1999. Polyphenolic antioxidant (-)-epigallocatechin- 3- gallate from green tea reduces UVB- induced inflammatory responses and infiltration of leukocytes in human skin. *Photochem. Photobiol.,* 69**,** 148-153.

KEMP, E. H., MCDONAGH, A. J. G., WENGRAF, D. A., MESSENGER, A. G., GAWKRODGER, D. J., CORK, M. J. & TAZI-AHNINI, R. 2006. The Non- Synonymous C1858T Substitution in the PTPN22 Gene is Associated with Susceptibility to the Severe Forms of Alopecia Areata. *Hum Immunol.,* 67**,** 535-539.

KENNEDY CRISPIN, M., KO, J. M., CRAIGLOW, B. G., LI, S., SHANKAR, G., URBAN, J. R., CHEN, J. C., CERISE, J. E., JABBARI, A., WINGE, M. C. G., MARINKOVICH, M. P., CHRISTIANO, A. M., ORO, A. E. & KING, B. A. 2016. Safety and efficacy of the JAK inhibitor tofacitinib citrate in patients with alopecia areata. *JCI insight,* 1**,** e89776.

KHOURY, E., L., PRICE, V., H. & GREENSPAN, J., S. 1988. HLA- DR Expression by Hair Follicle Keratinocytes in Alopecia Areata: Evidence That it Is Secondary to the Lymphoid Infiltration. *J. Investig. Dermatol.,* 90**,** 193.

KIANTO, U., REUNALA, T., KARVONEN, J., LASSUS, A. & TIILIKAINEN, A. 1977. HLA- B12 in alopecia areata. *Arch Dermatol.,* 113**,** 1716.

KITAICHI, N., NAMBA, K. & TAYLOR, A. W. 2005. Inducible immune regulation following autoimmune disease in the immune- privileged eye. *J. Leukoc. Biol.,* 77**,** 496-502.

KUBY, J. 1997. *Immunology,* New York, Freeman.

KUWANO, Y., FUJIMOTO, M., WATANABE, R., ISHIURA, N., NAKASHIMA, H., OHNO, Y., YANO, S., YAZAWA, N., OKOCHI, H. & TAMAKI, K. 2007. Serum chemokine profiles in patients with alopecia areata. *Br. J. Dermatol.,* 157**,** 466-473.

LAN, Q., FAN, H., QUESNIAUX, V., RYFFEL, B., LIU, Z. & GUO ZHENG, S. 2012. Induced Foxp3 + regulatory T cells: a potential new weapon to treat autoimmune and inflammatory diseases? *J Mol Cell Biol.,* 4**,** 22-28.

LAYDON, D. J., BANGHAM, C. R. M. & ASQUITH, B. 2015. Estimating T- cell repertoire diversity: limitations of classical estimators and a new approach. *Philos Trans R Soc Lond B Biol sci.,* 370**,** doi: 10.1098.

LECHLEITNER, S., GILLE, J., JOHNSON, D. R. & PETZELBAUER, P. 1998. Interferon enhances tumor necrosis factor- induced vascular cell adhesion molecule 1 (CD106) expression in human endothelial cells by an interferon- related factor 1- dependent pathway. *J. Exp. Med.,* 187**,** 2023-2030.

LEMOS, L. N., FULTHORPE, R. R., TRIPLETT, E. W. & ROESCH, L. F. W. 2011. Rethinking microbial diversity analysis in the high throughput sequencing era. *J Microbiol Methods,* 86**,** 42-51.

LEVINGS, M. K., BACCHETTA, R., SCHULZ, U. & RONCAROLO, M. G. 2002. The role of IL- 10 and TGF- beta in the differentiation and effector function of T regulatory cells.

LEW, B. L., CHO, H. R., HAW, S., KIM, H. J., CHUNG, J. H. & SIM, W. Y. 2012. Association between IL17A/ IL17RA Gene Polymorphisms and Susceptibility to Alopecia Areata in the Korean Population. *Ann. Dermatol.,* 24**,** 61-65.

LIANG, B., WORKMAN, C., LEE, J., CHEW, C., DALE, B., COLONNA, L., FLORES, M., LI, N., SCHWEIGHOFFER, E., GREENBERG, S., TYBULEWICZ, V., VIGNALI, D. & CLYNES, R. 2008. Regulatory T Cells Inhibit Dendritic Cells by Lymphocyte Activation Gene- 3 Engagement of MHC Class II. *J Immunol.,* 180**,** 5916-5926.

LIBERAL, R., GRANT, C. R., LONGHI, M. S., MIELI‐VERGANI, G. & VERGANI, D. 2015. Regulatory T cells: Mechanisms of suppression and impairment in autoimmune liver disease. 67**,** 88-97.

LIN, A., GUO, X., INMAN, R. D. & SIVAK, J. M. 2015. Ocular inflammation in HLA- B27 transgenic mice reveals a potential role for MHC class I in corneal immune privilege. *Mol vis,* 21**,** 131.

LIU, L. Y., CRAIGLOW, B. G., DAI, F. & KING, B. A. 2016. Tofacitinib for the treatment of severe alopecia areata and variants: A study of 90 patients. *J Am Acad Dermatol,* 76**,** 22-28.

LUCKAC, J., BUREK, B. & KUSIC, Z. 1993. Peripheral blood lymphocyte populations and phagocytic functions in patients with active alopecia areata. *Acta medica Croatica,* 47**,** 113-118.

MADANI, S. & SHAPIRO, J. 2000. Alopecia areata update. *J. Am. Acad. Dermatol.,* 42**,** 549-566.

MARGULIES, M., EGHOLM, M., ALTMAN, W. E., ATTIYA, S., BADER, J. S., BEMBEN, L. A., BERKA, J., BRAVERMAN, M. S., CHEN, Y. J., CHEN, Z., DEWELL, S. B., DE WINTER, A., DRAKE, J., DU, L., FIERRO, J. M., FORTE, R., GOMES, X. V., GODWIN, B. C., HE, W., HELGESEN, S., HO, C. H., HUTCHISON, S. K., IRZYK, G. P., JANDO, S. C., ALENQUER, M. L. I., JARVIE, T. P., JIRAGE, K. B., KIM, J. B., KNIGHT, J. R., LANZA, J. R., LEAMON, J. H., LEE, W. L., LEFKOWITZ, S. M., LEI, M., LI, J., LOHMAN, K. L., LU, H., MAKHIJANI, V. B., MCDADE, K. E., MCKENNA, M. P., MYERS, E. W., NICKERSON, E., NOBILE, J. R., PLANT, R., PUC, B. P., REIFLER, M., RONAN, M. T., ROTH, G. T., SARKIS, G. J., SIMONS, J. F.,

SIMPSON, J. W., SRINIVASAN, M., TARTARO, K. R., TOMASZ, A., VOGT, K. A., VOLKMER, G. A., WANG, S. H., WANG, Y., WEINER, M. P., WILLOUGHBY, D. A., YU, P., BEGLEY, R. F. & ROTHBERG, J. M. 2006. Genome sequencing in microfabricated high-density picolitre reactors. *Nature,* 437**,** 376-380.

MARKET, E. & PAPAVASILIOU, F. N. 2003. V(D) J Recombination and the Evolution of the Adaptive Immune System (Primer). *PLoS Biol.,* 1**,** e16.

MARTINEZ-MIR, A., ZLOTOGORSKI, A., GORDON, D., PETUKHOVA, L., MO, J., GILLIAM, T. C., LONDONO, D., HAYNES, C., OTT, J., HORDINSKY, M., NANOVA, K., NORRIS, D., PRICE, V., DUVIC, M. & CHRISTIANO, A. M. 2007. Genomewide scan for linkage reveals evidence of several susceptibility loci for alopecia areata. *Am J Hum Genet,* 80**,** 316-328.

MARZINEK, J., LIAN, G. P., MANTALARIS, A., PISTIKOPOULOS, E., ZHAO, Y., HAN, L., CHEN, L., BOND, P. & NORO, M. G. 2013. Molecular and Thermodynamic Basis for EGCG-Keratin Interaction-Part I: Molecular Dynamics Simulations. *AICHE J.,* 59**,** 4816-4823.

MATSUYAMA, T., KIMURA, T., KITAGAWA, M., PFEFFER, K., KAWAKAMI, T., WATANABE, N., KÜNDIG, T. M., AMAKAWA, R., KISHIHARA, K., WAKEHAM, A., POTTER, J., FURLONGER, C. L., NARENDRAN, A., SUZUKI, H., OHASHI, P. S., PAIGE, C. J., TANIGUCHI, T. & MAK, T. W. 1993. Targeted disruption of IRF- 1 or IRF- 2 results in abnormal type I IFN gene induction and aberrant lymphocyte development. *Cell,* 75**,** 83-97.

MATSUZAKI, T. & YOSHIZATO, K. 1998. Role of hair papilla cells on induction and regeneration processes of hair follicles. *Wound Repair Regen,* 6**,** 524-530.

MCBLANE, J. F., VAN GENT, D. C., RAMSDEN, D. A., ROMEO, C., CUOMO, C. A., GELLERT, M. & OETTINGER, M. A. 1995. Cleavage at a V(D) J recombination signal requires only RAG1 and RAG2 proteins and occurs in two steps. *Cell,* 83**,** 387-395.

MCDONAGH, A. J. G. & MESSENGER, A. G. 1996. The pathogenesis of alopecia areata. *Dermatol. Clin.,* 14**,** 661-670.

MCDONAGH, A. J. G., SNOWDEN, J. A., STIERLE, C., ELLIOTT, K. & MESSENGER, A. G. 1993. HLA and ICAM- 1 expression in alopecia areata in vivo and in vitro: The role of cytokines. *B. J. Dermatol.,* 129**,** 250-256.

MCELWEE, K., FREYSCHMIDT-PAUL, P., HOFFMANN, R., KISSLING, S., HUMMEL, S., VITACOLONNA, M. & ZÖLLER, M. 2005a. Transfer of CD8+ Cells Induces Localized Hair Loss Whereas CD4+/CD25− Cells Promote Systemic Alopecia Areata and CD4+/CD25+ Cells Blockade Disease Onset in the C3H/HeJ Mouse Model. *J Investig Dermatol,* 124**,** 947-957.

MCELWEE, K., ZOLLER, M., FREYSCHMIDT-PAUL, P. & HOFFMANN, R. 2005b. Regulatory T cells in autoimmune diseases and their potential. *J investig Dermatol Symp Proc,* 10**,** 280-281.

MCELWEE, K. J., BOGGESS, D., KING, L. E. & SUNDBERG, J. P. 1998. Experimental induction of alopecia areata- like hair loss in C3H/ HeJ mice using full- thickness skin grafts. *J. Invest. Dermatol.,* 111**,** 797-803.

MCELWEE, K. J. & HOFFMANN, R. 2002. Alopecia areata - animal models. *Clin Exp Dermatol,* 27**,** 410-7.

MCELWEE, K. J., PICKETT, P. & OLIVER, R. F. 1996. The DEBR rat, alopecia areata and autoantibodies to the hair follicle. *Br. J. Dermatol,* 134**,** 55-63.

MEDAWAR, P. B. 1948. Immunity to homologous grafted skin; the fate of skin homografts transplanted to the brain, to subcutaneous tissue, and to the anterior chamber of the eye. *Br J Exp pathol,* 29**,** 58-69.

MEGIORNI, F., PIZZUTI, A., MORA, B., RIZZUTI, A., GARELLI, V., MAXIA, C., CARLESIMO, M., FOTRUNA, M. C., DELLE CHIAIE, R., CAVAGGIONI, G. & ROSSI, A. 2011. Genetic association of HLA-DQB1 and HLA-DRB1 polymorphisms with alopecia areata in the Italian population. *Br. J. Dermatol.,* 165**,** 823-827.

MESSENGER, A. G. 1984. Alopecia areata: light and electron microscopic pathology of the regrowing white hair. *B. J. Dermatol.,* 110**,** 155-62.

MESSENGER, A. G. & BLEEHEN, S. S. 1985. Expression of HLA- DR by anagen hair follicles in alopecia areata. *J. Investig. Dermatol.,* 85**,** 569-572.

MESSENGER, A. G., MCKILLOP, J., FARRANT, P., MCDONAGH, A. J. & SLADDEN, M. 2012. British Association of Dermatologists' guidelines for the management of alopecia areata 2012. *Br. J. Dermatol.,* 166**,** 916-926.

MESSENGER, A. G., SLATER, D. N. & BLEEHEN, S. S. 1986. Alopecia areata: alterations in the hair growth cycle and correlation with the follicular pathology. *The British journal of dermatology,* 114**,** 337.

MICHIE, H. J., JAHODA, C. A. B., OLIVER, R. F. & JOHNSON, B. E. 1991. The DEBR rat: an animal model of human alopecia areata. *Br. J. Dermatol.,* 125**,** 94-100.

MILGRAUM, S. S., MITCHELL, A. J., BACON, G. E. & RASMUSSEN, J. E. 1987. Alopecia areata, endocrine function, and autoantibodies in patients 16 years of age or younger. *J. Am. Acad. Dermatol.,* 17**,** 57.

MILNER, Y., SUDNIK, J., FILIPPI, M., KIZOULIS, M., KASHGARIAN, M. & STENN, K. 2002. Exogen, shedding phase of the hair growth cycle: Characterization of a mouse model. *J. Invest. Dermatol.,* 119**,** 639-644.

MIRZOYEV, S. A., SCHRUM, A. G., DAVIS, M. D. P. & TORGERSON, R. R. 2014. Lifetime Incidence Risk of Alopecia Areata Estimated at 2.1% by Rochester Epidemiology Project, 1990– 2009. *J. Invest. Dermatol.,* 134**,** 1141-1142.

MIYARA, M., YOSHIOKA, Y., KITOH, A., SHIMA, T., WING, K., NIWA, A., PARIZOT, C., TAFLIN, C., HEIKE, T., VALEYRE, D., MATHIAN, A., NAKAHATA, T., YAMAGUCHI, T., NOMURA, T., ONO, M., AMOURA, Z., GOROCHOV, G. & SAKAGUCHI, S. 2009. Functional Delineation and Differentiation Dynamics of Human CD4+ T Cells Expressing the FoxP3 Transcription Factor. *Immunity,* 30**,** 899-911.

MONOD, M., GIUDICELLI, V., CHAUME, D. & LEFRANC, M. P. 2004. IMGT/Junction Analysis: the first tool for the analysis of the immunoglobulin and T cell receptor complex V- J and V- D- J JUNCTIONs. *Bioinformatics,* 20**,** 379-385.

MORESI, J. M. & HORN, T. D. 1997. Distribution of Langerhans cells in human hair follicle. *J. Cutan. Pathol.,* 24**,** 636-640.

MOROZOVA, O. & MARRA, M. A. 2008. Applications of next- generation sequencing technologies in functional genomics. *Genomics,* 92**,** 255-264.

MULLER-ROVER, S., HANDJISKI, B., VAN DER VEEN, C., EICHMULLER, S., FOITZIK, K., MCKAY, I. A., STENN, K. S. & PAUS, R. 2001. A comprehensive guide for the accurate classification of murine hair follicles in distinct hair cycle stages. *J. Invest. Dermatol.,* 117**,** 3-15.

MURAOKA, M., HASEGAWA, H., KOHNO, M., INOUE, A., MIYAZAKI, T., TERADA, M., NOSE, M. & YASUKAWA, M. 2006. IK cytokine ameliorates the progression of lupus nephritis in MRL/ lpr mice. *Arthritis Rheum.,* 54**,** 3591-3600.

MURRAY, P. J. 2007. The JAK- STAT signaling pathway: Input and output integration. *J. Immunol.,* 178**,** 2623-2629.

MUTYAMBIZI, K., BERGER, C. L. & EDELSON, R. L. 2009. The balance between immunity and tolerance: The role of Langerhans cells. *Cell. Mol. Life Sci.,* 66**,** 831-840.

NAGLE, D. G., FERREIRA, D. & ZHOU, Y. 2006. Epigallocatechin-3-gallate (EGCG): Chemical and biomedical perspectives. *Phytochemistry,* 67**,** 1849-1855.

NAKACHI, S., SUMITOMO, S., TSUCHIDA, Y., TSUCHIYA, H., KONO, M., KATO, R., SAKURAI, K., HANATA, N., NAGAFUCHI, Y., TATEISHI, S., KANDA, H., OKAMURA, T., YAMAMOTO, K. & FUJIO, K. 2017. Interleukin- 10- producing LAG3 + regulatory T cells are associated with disease activity and abatacept treatment in rheumatoid arthritis. *Arthritis Res Ther,* 19**,** 97.

NIEDERKORN, J. Y. 2003. Mechanisms of immune privilege in the eye and hair follicle. *J. Invest. Dermatol. Symp. Proc.,* 8**,** 168-172.

NOACK, M. & MIOSSEC, P. 2014. Th17 and regulatory T cell balance in autoimmune and inflammatory diseases. *Autoimmun Rev.,* 13**,** 668-677.

NOBLE, A., STAYNOV, D. Z. & KEMENY, D. M. 1993. Generation of rat Th2-like cells *in-vitro* is interleukin-4-dependent and inhibited by interferon-gamma. *Immunology,* 79**,** 562-567.

O'SHEA, J. & PLENGE, R. 2012. JAK and STAT Signaling Molecules in Immunoregulation and Immune- Mediated Disease. *Immunity,* 36**,** 542-550.

OGAWA, K., HARA, T., SHIMIZU, M., NAGANO, J., OHNO, T., HOSHI, M., ITO, H., TSURUMI, H., SAITO, K., SEISHIMA, M. & MORIWAKI, H. 2012. (-)-Epigallocatechin gallate inhibits the expression of indoleamine 2,3-dioxygenase in human colorectal cancer cells. *Oncol Lett.,* 4**,** 546-550.

OLDENHOVE, G., BOULADOUX, N., WOHLFERT, E. A., HALL, J. A., CHOU, D., DOS SANTOS, L., BRIEN, S., BLANK, R., LAMB, E., NATARAJAN, S., KASTENMAYER, R., HUNTER, C., GRIGG, M. E. & BELKAID, Y. 2009. Decrease of Foxp3+ Treg cell number and acquisition of effector cell phenotype during lethal infection. *Immunity,* 31**,** 772-782.

OLIVER, R. F., JAHODA, C. A. B., HORNE, K. A., MICHIE, H. J., POULTON, T. & JOHNSON, B. E. 1991. The DEBR rat model for Alopecia areata. *J. Invest. Dermatol.,* 96**,** 97S.

OOI, J., JAN, P., J., TAN, Y., HUYNH, M., WILLETT, Z., RAMARATHINAM, S., EGGENHUIZEN, P., LOH, K., WATSON, K., GAN, P., ALIKHAN, M., DUDEK, N., HANDEL, A., HUDSON, B., FUGGER, L., POWER, D., HOLT, S., COATES, P., GREGERSEN, J., PURCELL, A., HOLDSWORTH, S., LA GRUTA, L., REID, H., ROSSJOHN, J. & KITCHING, A. 2017. Dominant protection from HLA- linked autoimmunity by antigen- specific regulatory T cells. *Nature,* 545**,** 243-247.

ORAZIO, T. J. & NIEDERKORN, J. Y. 1998. A novel role for TGF- β and IL- 10 in the induction of immune privilege. *J. Immunol.,* 160**,** 2089-2098.

ORECCHIA, G. & RABBIOSI, G. 1985. Treatment of Alopecia areata with Diphencyprone. *Dermatologica,* 171**,** 193-196.

OSHIMA, H., ROCHAT, A., KEDZIA, C., KOBAYASHI, K. & BARRANDON, Y. 2001. Morphogenesis and Renewal of Hair Follicles from Adult Multipotent Stem Cells. *Cell,* 104**,** 233-245.

PAE, M., REN, Z. H., MEYDANI, M., SHANG, F., MEYDANI, S. N. & WU, D. Y. 2010. Epigallocatechin- 3- Gallate Directly Suppresses T Cell Proliferation through Impaired IL- 2 Utilization and Cell Cycle Progression. *J. Nutr.,* 140**,** 1509-1515.

PANDIYAN, P., ZHENG, L., ISHIHARA, S., REED, J. & LENARDO, M., J. 2007. CD4+ CD25+ Foxp3+ regulatory T cells induce cytokine deprivation– mediated apoptosis of effector CD4+ T cells. *Nat Immunol.,* 8**,** 1353-1362.

PANNETIER, C., COCHET, M., DARCHE, S., CASROUGE, A., ZOLLER, M. & KOURILSKY, P. 1993. The sizes of the CDR3 hypervariable regions of the murine T-cell receptor beta-chains vary as a function of the recombined germ-line segments. *Proc. Natl. Acad. Sci. U.S.A.,* 90**,** 4319-4323.

PARAKKAL, P. F. 1970. Morphogenesis of the hair follicle during catagen. *Z. Zellforsch. Mikrosk. Anat.,* 107**,** 174-186.

PAUS, R. & ARCK, P. 2009. Neuroendocrine Perspectives in Alopecia Areata: Does Stress Play a Role? *Journal of Investigative Dermatology,* 129**,** 1324.

PAUS, R., CHRISTOPH, T. & MULLER-ROVER, S. 1999a. Immunology of the hair follicle: A short journey into terra incognita. *J. Invest. Dermatol. Symp. Proc.,* 4**,** 226-234.

PAUS, R., COTSARELIS, G. & EPSTEIN, F. H. 1999b. The Biology of Hair Follicles. *N Engl J Med,* 341**,** 491-497.

PAUS, R., ITO, N., TAKIGAWA, M. & ITO, T. 2003. The hair follicle and immune privilege. *J. Invest. Dermatol. Symp. Proc.,* 8**,** 188-194.

PAUS, R., SLOMINSKI, A. & CZARNETZKI, B. M. 1993. IS ALOPECIA- AREATA AN AUTOIMMUNE-RESPONSE AGAINST MELANOGENESIS- RELATED PROTEINS, EXPOSED BY ABNORMAL MHC CLASS- I EXPRESSION IN THE ANAGEN HAIR BULB. *Yale J. Biol. Med.,* 66**,** 541-554.

PEARSON, J. A., THAYER, T. C., MCLAREN, J. E., LADELL, K., DE LEENHEER, E., PHILLIPS, A., DAVIES, J., KAKABADSE, D., MINERS, K., MORGAN, P., WEN, L., PRICE, D. A. & WONG, F. S. 2016. Proinsulin Expression Shapes the TCR Repertoire but Fails to Control the Development of Low- Avidity Insulin- Reactive CD8+ T Cells. *Diabetes,* 65**,** 1679.

PECKHAM, S. J., SLOAN, S. B. & ELSTON, D. M. 2011. Histologic features of alopecia areata other than peribulbar lymphocytic infiltrates. *J Am Acad Dermatol,* 65**,** 615-620.

PERRET, C., WIESNER MENZEL, L. & HAPPLE, R. 1984. Immunohistochemical analysis of T- cell subsets in the peribulbar and intrabulbar infiltrates of alopecia areata. *Acta Derm. Venereol.,* 64**,** 26-30.

PETERSON, R. A. 2012. Regulatory T- Cells: Diverse Phenotypes Integral to Immune Homeostasis and Suppression. *Toxicol Pathol,* 40**,** 186-204.

PETUKHOVA, L., DUVIC, M., HORDINSKY, M., NORRIS, D., PRICE, V., SHIMOMURA, Y., KIM, H., SINGH, P., LEE, A., CHEN, W. V., MEYER, K. C., PAUS, R., JAHODA, C. A. B., AMOS, C. I., GREGERSEN, P. K. & CHRISTIANO, A. M. 2010. Genome- wide association study in alopecia areata implicates both innate and adaptive immunity. *Nature,* 466**,** 113-U129.

PHILPOTT, M. P., SANDERS, D., WESTGATE, G. E. & KEALEY, T. 1994. Human hair growth in vitro: a model for the study of hair follicle biology. *J Dermatol. sci.,* 7**,** 55-72.

PRICE, V. H., GAROVOY, M. R., CARO, I., WHITING, D. A., HORDINSKY, M. K., OLSEN, E. A., ROBERTS, J. L., SIEGFRIED, E. C., RAFAL, E. S., KORMAN, N. J., ALTRABULSI, B. & LEUNG, H. M. 2008. Subcutaneous efalizumab is not effective in the treatment of alopecia areata. *J Am Acad Dermatol,* 58**,** 395-402.

QAZI, Y. & HAMRAH, P. 2013. Corneal Allograft Rejection: Immunopathogenesis to Therapeutics. *J clin cell immunol,* 2013**,** pii 006.

RAMIREZ, R. D., WRIGHT, W. E., SHAY, J. W. & TAYLOR, R. S. 1997. Telomerase activity concentrates in the mitotically active segments of human hair follicles. *J Invest Dermatol,* 108**,** 113-117.

REINHOLD, M. 1960. Relationship of Stress to the Development of Symptoms in Alopecia Areata and Chronic Urticaria. *British Medical Journal,* 1**,** 846.

RENCZ, F., GULÁCSI, L., PÉNTEK, M., WIKONKÁL, N., BAJI, P. & BRODSZKY, V. 2016. Alopecia areata and health‐related quality of life: a systematic review and meta‐analysis. *Br. J. Dermatol.,* 175**,** 561-571.

RENÉ, R., UDO, H., CARINA VAN DER, V., SILVIA, B.-P. & RALF, P. 1998. MHC Class I Expression in Murine Skin: Developmentally Controlled and Strikingly Restricted Intraepithelial Expression During Hair Follicle Morphogenesis and Cycling, and Response to Cytokine Treatment In Vivo. *J. Investig. Dermatol.,* 111**,** 25.

RISSIEK, A., BAUMANN, I., CUAPIO, A., MAUTNER, A., KOLSTER, M., ARCK, P. C., DODGE-KHATAMI, A., MITTRÜCKER, H.-W., KOCH-NOLTE, F., HAAG, F. & TOLOSA, E. 2015. The expression of CD39 on regulatory T cells is genetically driven and further upregulated at sites of inflammation. *J Autoimmun.,* 58**,** 12-20.

ROBINS, H. S., CAMPREGHER, P. V., SRIVASTAVA, S. K., WACHER, A., TURTLE, C. J., KAHSAI, O., RIDDELL, S. R., WARREN, E. H. & CARLSON, C. S. 2009. Comprehensive assessment of T-cell receptor β-chain diversity in αβ T cells. *Blood,* 114**,** 4099-4107.

ROEDERER, M. 2002. Compensation in flow cytometry. *Curr. protoc. cytom.,* Chapter 1**,** Unit 1.14.

ROEP, B. & PEAKMAN, M. 2012. Antigen Targets of Type 1 Diabetes Autoimmunity. *Cold Spring Harb. Perspect. Med.,* 2**,** a007781.

ROMAGNANI, P., ANNUNZIATO, F., PICCINNI, M. P., MAGGI, E. & ROMAGNANI, S. 2000. Th1/Th2 cells, their associated molecules and role in pathophysiology. *Eur. Cytokine Netw.,* 11**,** 510-511.

ROOK, A. H., KEHRL, J. H., WAKEFIELD, L. M., ROBERTS, A. B., SPORN, M. B., BURLINGTON, D. B., LANE, H. C. & FAUCI, A. S. 1986. Effects of transforming growth factor beta on the

functions of natural killer cells: depressed cytolytic activity and blunting of interferon responsiveness. *J. Immunol.,* 136**,** 3916-20.

ROSENBLUM, M. D., OLASZ, E. B., YANCEY, K. B., WOODLIFF, J. E., LAZAROVA, Z., GERBER, K. A. & TRUITT, R. L. 2004. Expression of CD200 on epithelial cells of the murine hair follicle: A role in tissue- specific immune tolerance? *J. Invest. Dermatol.,* 123**,** 880-887.

ROSENBLUM, M. D., WAY, S. S. & ABBAS, A. K. 2016. Regulatory T cell memory. *Nat. Rev. Immunol.,* 16**,** 90-101.

ROTH, D. B. & CRAIG, N. L. 1998. VDJ Recombination. *Cell,* 94**,** 411-414.

SAFAVI, K. H., MULLER, S. A., SUMAN, V. J., MOSHELL, A. N. & MELTON, L. J. 1995. INCIDENCE OF ALOPECIA- AREATA IN OLMSTED COUNTY, MINNESOTA, 1975 THROUGH 1989. *Mayo Clin. Proc.,* 70**,** 628-633.

SAKAGUCHI, S. 2004. Naturally arising CD4 + regulatory T cells for immunologic self- tolerance and negative control of immune responses. *Annu Rev Immunol.,* 22**,** 531-562.

SAKAGUCHI, S., SAKAGUCHI, N., ASANO, M., ITOH, M. & TODA, M. 1995. Immunologic self-tolerance maintained by activated T cells expressing IL- 2 receptor α- chains (CD25): Breakdown of a single mechanism of self- tolerance causes various autoimmune diseases. *J Immunol,* 155**,** 1151-1164.

SAKAGUCHI, S., SAKAGUCHI, N., ASANO, M., ITOH, M. & TODA, M. 2011. Immunologic Self-Tolerance Maintained by Activated T Cells Expressing IL- 2 Receptor alpha- Chains (CD25) Breakdown of a Single Mechanism of Self- Tolerance Causes Various Autoimmune Diseases. *J. Immunol.,* 186**,** 3808-3821.

SANCHEZ RODRIGUEZ, R., PAULI, M. L., NEUHAUS, I. M., YU, S. S., ARRON, S. T., HARRIS, H. W., YANG, S. H.-Y., ANTHONY, B. A., SVERDRUP, F. M., KROW-LUCAL, E., MACKENZIE, T. C., JOHNSON, D. S., MEYER, E. H., LÖHR, A., HSU, A., KOO, J., LIAO, W., GUPTA, R., DEBBANEH, M. G., BUTLER, D., HUYNH, M., LEVIN, E. C., LEON, A., HOFFMAN, W. Y., MCGRATH, M. H., ALVARADO, M. D., LUDWIG, C. H., TRUONG, H.-A., MAURANO, M. M., GRATZ, I. K., ABBAS, A. K., ROSENBLUM, M. D. & MACKENZIE, T. C. 2014. Memory regulatory T cells reside in human skin. *J Clin Invest.,* 124**,** 1027-36.

SANGER, F., NICKLEN, S. & COULSON, A. R. 1977. DNA sequencing with chain-terminating inhibitors. *Proc Natl Acad Sci U S A,* 74**,** 5463-5467.

SATO-KAWAMURA, M., AIBA, S. & TAGAMI, H. 2003. Strong expression of CD40, CD54 and HLA- DR antigen and lack of evidence for direct cellular cytotoxicity are unique immunohistopathological features in alopecia areata. *Arch. Dermatol. Res.,* 294**,** 536-543.

SCALBERT, A., MORAND, C., MANACH, C. & REMESY, C. 2002. Absorption and metabolism of polyphenols in the gut and impact on health. *Biomed Pharmacother.,* 56**,** 276-282.

SCALIA, S., TROTTA, V. & BIANCHI, A. 2014. In vivo human skin penetration of (-)-epigallocatechin-3-gallate from topical formulations. *Acta Pharm.,* 64**,** 257-265.

SCHMIDT, A., OBERLE, N. & KRAMMER, P. 2012. Molecular mechanisms of Treg- mediated T cell suppression. *Front. Immunol.,* 3**,** 51.

SCHMITT, E. & WILLIAMS, C. 2013. Generation and function of nducec regulatory T cells. *Front. Immunol.,* 19**,** 152.

SHELLOW, W. V. R., EDWARDS, J. E. & KOO, J. Y. M. 1992. Profile of Alopecia areata: A questionnaire analysis of patient and family. *Int. J Dermatol.,* 31**,** 186-189.

SHEVACH, E. M. 2006. From Vanilla to 28 Flavors: Multiple Varieties of T Regulatory Cells. *Immunity,* 25**,** 195-201.

SHIMIZU, T., HIZAWA, N., HONDA, A., ZHAO, Y., ABE, R., WATANABE, H., NISHIHIRA, J., NISHIMURA, M. & SHIMIZU, H. 2005. Promoter region polymorphism of macrophage migration inhibitory factor is strong risk factor for young onset of extensive alopecia areata. *Genes Immun.,* 6**,** 285-289.

SHIN, B. S., FURUHASHI, T., NAKAMURA, M., TORII, M. & MORITA, A. 2013. Impaired inhibitory function of circulating CD4(+) CD25(+) regulatory T cells in alopecia areata. *J. Dermatol. Sci.,* 70**,** 141-143.

SHREBERK-HASSIDIM, R., RAMOT, Y. & ZLOTOGORSKI, A. 2017. Janus kinase inhibitors in dermatology: A systematic review. *J Am Acad Dermatol.,* 76**,** 745-753.e19.

SHUAI, K., STARK, G. R., KERR, I. M. & DARNELL, J. E. 1993. A Single Phosphotyrosine Residue of Stat91 Required for Gene Activation by Interferon-γ. *Science,* 261**,** 1744-1746.

SHUGAY, M., BAGAEV, D. V., TURCHANINOVA, M. A., BOLOTIN, D. A., BRITANOVA, O. V., PUTINTSEVA, E. V., POGORELYY, M. V., NAZAROV, V. I., ZVYAGIN, I. V., KIRGIZOVA, V. I., KIRGIZOV, K. I., SKOROBOGATOVA, E. V. & CHUDAKOV, D. M. 2015. VDJtools: Unifying Post- analysis of T Cell Receptor Repertoires. *PLoS Comput Biol.,* 11**,** e1004503.

SIEBENHAAR, F., SHAROV, A., PETERS, E., SHAROVA, T. Y., SYSKA, W., MARDARYEV, A., FREYSCHMIDT-PAUL, P., SUNDBERG, J. P., MAURER, M. & BOTCHKAREV, V. B. 2007. Substance P as an Immunomodulatory Neuropeptide in a Mouse Model for Autoimmune Hair Loss (Alopecia Areata). *Journal of Investigative Dermatology,* 127**,** 1489.

SILVER, A. F. & CHASE, H. B. 1970. DNA synthesis in the adult hair germ during dormancy (telogen) and activation (early anagen). *Dev Biol.,* 21**,** 440-451.

SILVERSTEIN, A., M. 2002. The Clonal Selection Theory: what it really is and why modern challenges are misplaced. *Nat. Immunol.,* 3**,** 793.

SINGH, T. & KATIYAR, S. K. 2013. Green tea polyphenol, (-)-epigallocatechin-3-gallate, induces toxicity in human skin cancer cells by targeting β- catenin signaling. *Toxicol Appl Pharmacol.,* 273**,** 418-424.

SPERLING, L. C. 1991. HAIR ANATOMY FOR THE CLINICIAN. *J. Am. Acad. Dermatol.,* 25**,** 1-17.

STENN, K. S. & PAUS, R. 2001. Controls of hair follicle cycling. *Physiol. Rev.,* 81**,** 449-494.

STEVENS, D., KARPUS, W., GOULD, K. & SWANBORG, R. H. 1992. T- cell receptor peptide immunization protects Lewis rats against experimental autoimmune encephalomyelitis. *Faseb J.,* 6**,** A1685-A1685.

STRIEBICH, C., FALTA, M., WANG, Y., BILL, J. & KOTZIN, B. 1998. Selective Accumulation of Related CD4 super(+) T Cell Clones in the Synovial Fluid of Patients with Rheumatoid Arthritis. *J. Immunol.,* 161**,** 4428-4436.

STROBER, B. E., MENON, K., MCMICHAEL, A., HORDINSKY, M., KRUEGER, G., PANKO, J., SIU, K., LUSTGARTEN, J. L., ROSS, E. K. & SHAPIRO, J. 2009. Alefacept for Severe Alopecia Areata A Randomized, Double- blind, Placebo- Controlled Study. *Arch. Dermatol.,* 145**,** 1262-1266.

STROBER, B. E., SIU, K., ALEXIS, A. E., KIM, G., WASHENIK, K., SINHA, A. & SHUPACK, J. L. 2005. Etanercept does not effectively treat moderate to severe alopecia areata: An open-label study. *J. Am. Acad. Dermatol.,* 52**,** 1082-1084.

SUN, J., SILVA, K. A., MCELWEE, K. J., KING, L. E. & SUNDBERG, J. P. 2008. The C3H/ HeJ mouse and DEBR rat models for alopecia areata: review of preclinical drug screening approaches and results. *Exp. Dermatol.,* 17**,** 793-805.

SUN, Y., HUNG, W.-C., CHEN, F.-Y., LEE, C.-C. & HUANG, H. W. 2009. Interaction of Tea Catechin (−)-Epigallocatechin Gallate with Lipid Bilayers. *Biophys. J.,* 96**,** 452a-452a.

SUNDBERG, J., MCELWEE, K., BREHM, M., SU, L. & KING, J. L. 2015. Animal Models for Alopecia Areata: What and Where? *J. Investig. Dermatol. Symp. Proc.,* 17**,** 23-26.

SUNDBERG, J. P., CORDY, W. R. & KING, L. E. 1994. Alopecia areata in aging C3H/ HEJ mice. *J. Invest. Dermatol.,* 102**,** 847-856.

TANEMURA, A., OISO, N., NAKANO, M., ITOI, S., KAWADA, A. & KATAYAMA, I. 2013. Alopecia Areata: Infiltration of Th17 Cells in the Dermis, Particularly around Hair Follicles. *Dermatology,* 226**,** 333-336.

TAYLOR, A. W., STREILEIN, J. W. & COUSINS, S. W. 1992. Identification of alpha- melanocyte stimulating hormone as a potential immunosuppressive factor in aqueous- humor. *Curr. Eye Res.,* 11**,** 1199-1206.

TAYLOR, A. W., YEE, D. G., NISHIDA, T. & NAMBA, K. 2000. Neuropeptide regulation of immunity. The immunosuppressive activity of alpha- melanocyte- stimulating hormone (alpha- MSH). *Ann N Y Acad Sci,* 917**,** 239-247.

TAZI-AHNINI, R., CORK, M. J., GAWKRODGER, D. J., BIRCH, M. P., WENGRAF, D., MCDONAGH, A. J. G. & MESSENGER, A. G. 2002. Role of the Autoimmune Regulator (AIRE) gene in alopecia areata: Strong association of a potentially functional AIRE polymorphism with alopecia universalis. *Tissue Antigens,* 60**,** 489-495.

TAZI-AHNINI, R., CORK, M. J., WENGRAF, D., WILSON, A. G., GAWKRODGER, D. J., BIRCH, M. P., MESSENGER, A. G. & MCDONAGH, A. J. G. 2003. Notch4, a non-HLA gene in the MHC is strongly associated with the most severe form of alopecia areata. *Hum Genet,* 112**,** 400-403.

TEDESCHI, E., SUZUKI, H. & MENEGAZZI, M. 2002. Antiinflammatory action of EGCG, the main component of green tea, through STAT-1 inhibition. *Ann N Y Acad Sci,* 973**,** 435-437.

TEFFERI, A. & PARDANANI, A. 2011. Serious Adverse Events During Ruxolitinib Treatment Discontinuation in Patients With Myelofibrosis. *Mayo Clin. Proc.,* 86**,** 1188-1191.

TEMBHRE, M. K. & SHARMA, V. K. 2013. T- helper and regulatory T- cell cytokines in the peripheral blood of patients with active alopecia areata. *B. J. Dermatol.,* 169**,** 543-548.

TERAKI, Y., IMANISHI, K. & SHIOHARA, T. 1996. Cytokines in alopecia areata: Contrasting cytokine profiles in localized form and extensive form (alopecia universalis). *Acta Derm.-Venereol.,* 76**,** 421-423.

TOBIN, D. J. 2003. Characterization of hair follicle antigens targeted by the anti- hair follicle immune response. *J. Invest. Dermatol. Symp. Proc.,* 8**,** 176-181.

TOBIN, D. J., FENTON, D. A. & KENDALL, M. D. 1990. Ultrastructural study of exclamation - mark hair shafts in alopecia areata. *J Cutan Pathol,* 17**,** 348-354.

TOBIN, D. J., ORENTREICH, N., FENTON, D. A. & BYSTRYN, J. C. 1994. Antibodies to hair follicles in alopecia areata. *J Invest Dermatol.,* 102**,** 721-724.

TOBIN, D. J., SUNDBERG, J. P., KING, L. E., BOGGESS, D. & BYSTRYN, J. C. 1997. Autoantibodies to hair follicles in C3H/ HeJ mice with alopecia areata- like hair loss. *J. Invest. Dermatol.,* 109**,** 329-333.

TODES-TAYLOR, N., TURNER, R. & WOOD, G. S. 1984. T cell subpopulations in alopecia areata. *J. Am. Acad. Dermatol.,* 11**,** 216-223.

TOJO, G., FUJIMURA, T., KAWANO, M., OGASAWARA, K., KAMBAYASHI, Y., FURUDATE, S., MIZUASHI, M. & AIBA, S. 2013. Comparison of interleukin- 17- producing cells in different clinical types of alopecia areata. *Dermatology,* 227**,** 78-82.

TONEGAWA, S. 1983. Somatic generation of antibody diversity. *Nature,* 302**,** 575.

TOSTI, A., BELLAVISTA, S. & IORIZZO, M. 2006. Alopecia areata: a long term follow- up study of 191 patients. *J. Am. Acad. Dermatol.,* 55**,** 438-441.

TUNG, J. W., HEYDARI, K., TIROUVANZIAM, R., PARKS, D. R., HERZENBERG, L. A. & HERZENBERG, L. A. 2007. Modern flow cytometry: A practical approach. *Clin Lab Med.,* 27**,** 453-468.

ULLMANN, U., HALLER, J., DECOURT, J. P., GIRAULT, N., GIRAULT, J., RICHARD-CAUDRON, A. S., PINEAU, B. & WEBER, P. 2003. A Single Ascending Dose Study of Epigallocatechin Gallate in Healthy Volunteers. *J. Int. Med. Res.,* 31**,** 88-101.

VAN GENT, D., MIZUUCHI, K. & GELLERT, M. 1996. Similarities between initiation of V(D) J recombination and retroviral integration. *Science,* 271**,** 1592-1594.

VANDENBARK, A. A., HASHIM, G. & OFFNER, H. 1989. Immunization with a synthetic T-cell receptor V-region peptide protects against experimental autoimmune encephalomyelitis. *Nature,* 341**,** 541-544.

VANHECKE, D., LECLERCQ, G., PLUM, J. & VANDEKERCKHOVE, B. 1995. Characterization of distinct stages during the differentiation of human CD69 super(+)CD3 super(+) thymocytes and identification of thymic emigrants. *J. Immunol.,* 155**,** 1862-1872.

VERSTOVSEK, S., KANTARJIAN, H., MESA, R. A., PARDANANI, A. D., CORTES-FRANCO, J., THOMAS, D. A., ESTROV, Z., FRIDMAN, J. S., BRADLEY, E. C., ERICKSON-VIITANEN, S., VADDI, K., LEVY, R. & TEFFERI, A. 2010. Safety and Efficacy of INCB018424, a JAK1 and JAK2 Inhibitor, in Myelofibrosis. *N. Engl. J. Med.,* 363**,** 1117-1127.

VINCENT, B. G., YOUNG, E. F., BUNTZMAN, A. S., STEVENS, R., KEPLER, T. B., TISCH, R. M., FRELINGER, J. A. & HESS, P. R. 2010. Toxin- coupled MHC class I tetramers can specifically ablate autoreactive CD8+ T cells and delay diabetes in nonobese diabetic mice. *J. Immunol,* 184**,** 4196-204.

VON BOEHMER, H. 2005. Mechanisms of suppression by suppressor T cells. *Nat. Immunol.,* 6**,** 338-344.

WALKER, S. A. & ROTHMAN, S. 1950. A statistical study and consideration of endocrine influences. *J. Invest. Dermatol.,* 14**,** 403-413.

WANG, J., PAE, M., MEYDANI, S. N. & WU, D. 2013a. Green tea epigallocatechin- 3- gallate modulates differentiation of naïve CD4 + T cells into specific lineage effector cells. *J. Mol. Med.,* 91**,** 485-495.

WANG, W., SHAO, S., JIAO, Z., GUO, M., XU, H. & WANG, S. 2012a. The Th17/ Treg imbalance and cytokine environment in peripheral blood of patients with rheumatoid arthritis. *J. Clin. Exp. Inv.,* 32**,** 887-893.

WANG, X., MARR, A., BREITKOPF, T., LEUNG, G., WANG, E., HAO, J., MUI, A., WARNOCK, G., SHAPIRO, J. & MCELWEE, K. 2013b. Hair follicle- associated PD- L1 regulates T cell hyporesponsiveness: A potential mechanism of immune privilege. *J. Invest. Dermatol.,* 133**,** S83-S83.

WANG, X., SHI, Y., ZHOU, Q., LIU, X. M., XU, S. Z. & LEI, T. C. 2012b. Detailed histological structure of human hair follicle bulge region at different ages: A visible niche for nesting adult stem cells. *J. Huazhong Univ. Sci. Tech.-Med.,* 32**,** 648-656.

WASILEWSKA, A., WINIARSKA, M., OLSZEWSKA, M. & RUDNICKA, L. 2016. Interleukin- 17 inhibitors. A new era in treatment of psoriasis and other skin diseases. *Postep. Dermatol. Alergol.,* 33**,** 247-252.

WATSON, J. L., ANSARI, S., CAMERON, H., WANG, A., AKHTAR, M. & MCKAY, D. M. 2004. Green tea polyphenol (-)-epigallocatechin gallate blocks epithelial barrier dysfunction provoked by IFN-gamma but not by IL- 4. *Am J physiol. Gastrointest Liver physiol.,* 287**,** G954-961.

WESTGATE, G. E., CRAGGS, R. I. & GIBSON, W. T. 1991. IMMUNE PRIVILEGE IN HAIR-GROWTH. *J. Invest. Dermatol.,* 97**,** 417-420.

WHITE, L. C., WRIGHT, K. L., FELIX, N. J., RUFFNER, H., REIS, L. F. L., PINE, R. & TING, J. P. Y. 1996. Regulation of LMP2 and TAP1 genes by IRF- 1 explains the paucity of CD8 + T cells in IRF- 1(-/-) mice. *Immunity,* 5**,** 365-376.

WHITING, D. A. 1987. Structural abnormalities of the hair shaft. *J Am Acad Dermatol.,* 16**,** 1-25.

WHITING, D. A. 2001. The histopathology of alopecia areata in vertical and horizontal sections. *Dermatol. Ther.,* 14**,** 297-305.

WHITING, D. A. 2003. Histopathologic features of alopecia areata - A new look. *Arch. Dermatol.,* 139**,** 1555-1559.

WIEGAND, C. & HIPLER, U.-C. 2008. Methods for the measurement of cell and tissue compatibility including tissue regeneration processes. *GMS Krankenhaushygiene Interdisziplinar,* 3**,** 1-9.

WILBANKS, G. A. & STREILEIN, J. W. 1991. Studies on the induction of anterior chamber-associated immune deviation (ACAID).1. Evidence that an antigen-specific, ACAID-inducing, cell- associated signal exists in the peripheral blood. *J. Immunol.,* 146**,** 2610-2617.

WILLERFORD, D. M., SWAT, W. & ALT, F. W. 1996. Developmental regulation of V(D) J recombination and lymphocyte differentiation. *Curr. Opin. Genet. Dev.,* 6**,** 603-609.

WINTER, R. J., KERN, F. & BLIZZARD, R. M. 1976. Prednisone therapy for alopecia areata. A follow up report. *Arch. Dermatol.,* 112**,** 1549-1552.

WISEMAN, M. C., SHAPIRO, J., MACDONALD, N. & LUI, H. 2001. Predictive model for immunotherapy of alopecia areata with diphencyprone. *Arch. Dermatol.,* 137**,** 1063-1068.

WISUITIPROT, W., SOMSIRI, A., INGKANINAN, K. & WARANUCH, N. 2011. In vitro human skin permeation and cutaneous metabolism of catechins from green tea extract and green tea extract–loaded chitosan microparticles. *Int J Cosmet Sci.,* 33**,** 572-579.

WOLFRAM, S., RAEDERSTORFF, D., PRELLER, M., WANG, Y., TEIXEIRA, S. R., RIEGGER, C. & WEBER, P. 2006. Epigallocatechin gallate supplementation alleviates diabetes in rodents. *J. Nutr.,* 136**,** 2512-2518.

WONG, C. P., NGUYEN, L. P., NOH, S. K., BRAY, T. M., BRUNO, R. S. & HO, E. 2011. Induction of regulatory T cells by green tea polyphenol EGCG. *Immunol Lett.,* 139**,** 7-13.

WU, D., GUO, Z., REN, Z., GUO, W. & MEYDANI, S. N. 2009. Green tea EGCG suppresses T cell proliferation through impairment of IL- 2/ IL- 2 receptor signaling. *Free Radic. Biol. Med.,* 47**,** 636-643.

XIAO, F. L., YANG, S., YAN, K. L., CUI, Y., LIANG, Y. H., ZHOU, F. S., DU, W. H., GAO, M., SUN, L. D., FAN, X., CHEN, J. J., WANG, P. G., ZHU, Y. G., ZHOU, S. M. & ZHANG, X. J. 2006. Association of HLA class I alleles with aloplecia areata in Chinese Hans. *J. Dermatol. Sci.,* 41**,** 109-119.

XING, L. Z., DAI, Z. P., JABBARI, A., CERISE, J. E., HIGGINS, C. A., GONG, W. J., DE JONG, A., HAREL, S., DESTEFANO, G. M., ROTHMAN, L., SINGH, P., PETUKHOVA, L., MACKAY-WIGGAN, J., CHRISTIANO, A. M. & CLYNES, R. 2014. Alopecia areata is driven by cytotoxic T lymphocytes and is reversed by JAK inhibition. *Nat. Med.,* 20**,** 1043-1049.

YANG, C. S., MALIAKAL, P. & MENG, X. 2002. Inhibition of carcinogenesis by tea. *Annu. Rev. Pharmacol. Toxicol.,* 42**,** 25-54.

YANG, E.-J., LEE, J., LEE, S.-Y., KIM, E.-K., MOON, Y.-M., JUNG, Y., PARK, S.-H. & CHO, M.-L. 2014. EGCG Attenuates Autoimmune Arthritis by Inhibition of STAT3 and HIF-1 alpha with Th17/ Treg Control. *PLoS ONE,* 9**,** e86062.

YANG, L., LI, B., DANG, E., JIN, L., FAN, X. & WANG, G. 2016. Impaired function of regulatory T cells in patients with psoriasis is mediated by phosphorylation of STAT3. *J. Dermatol. Sci.,* 81**,** 85-92.

YANG, X. O., NURIEVA, R., MARTINEZ, G. J., KANG, H. S., CHUNG, Y., PAPPU, B. P., SHAH, B., CHANG, S. H., SCHLUNS, K. S., WATOWICH, S. S., FENG, X.-H., JETTEN, A. M. & DONG, C. 2008. Molecular Antagonism and Plasticity of Regulatory and Inflammatory T Cell Programs. *Immunity,* 29**,** 44-56.

YE, L., GOODALL, J., ZHANG, L., PUTINTSEVA, E., LAM, B., JIANG, L., LIU, W., YIN, J., LIN, L., TING, L., WU, X., YEO, G., SHUGAY, M., CHUDAKOV, D., GASTON, H. & XU, H. 2015. TCR usage, gene expression and function of two distinct FOXP3+ Treg subsets within CD4+ CD25hi T cells identified by expression of CD39 and CD45RO. *Immunol Cell Biol,* 94**,** 293-305.

YOON, J., KWON, H., MIN, S., THIBOUTOT, D. M. & SUH, D. 2013. Epigallocatechin-3-Gallate Improves Acne in Humans by Modulating Intracellular Molecular Targets and Inhibiting P. acnes. *J. Invest. Dermatol.,* 133**,** 429-440.

ZHANG, J. G. & OLIVER, R. F. 1994. Immunohistological study of the development of the cellular infiltrate in the pelage follicles of the DEBR model for alopecia areata. *Br. J. Dermatol.,* 130**,** 405-414.

ZHANG, L., WAN, F., SONG, J., TANG, K., ZHENG, F., GUO, J., GUO, D. & BI, H. 2016. Imbalance Between Th17 Cells and Regulatory T Cells During Monophasic Experimental Autoimmune Uveitis. *Inflammation,* 39**,** 113-122.

ZHANG, R., TIAN, A., ZHANG, H., ZHOU, Z., YU, H. & CHEN, L. 2011. Amelioration of experimental autoimmune encephalomyelitis by β- elemene treatment is associated with Th17 and Treg cell balance. *J. Mol. Neurosci.,* 44**,** 31-40.

ZHAO, H., ZHU, W., JIA, L., SUN, X., CHEN, G., ZHAO, X., LI, X., MENG, X., KONG, L., XING, L. & YU, J. 2015. Phase i study of topical epigallocatechin- 3- gallate (EGCG) in patients with breast cancer receiving adjuvant radiotherapy. *Br. J. Radiol.,* 89**,** 20150665

ZHAO, S., ZHU, W., XUE, S. & HAN, D. 2014. Testicular defense systems: immune privilege and innate immunity. *Cell. Mol. Immunol.,* 11**,** 428-437.

ZHAO, Y., NGUYEN, P., VOGEL, P., LI, B., JONES, L. & GEIGER, T. 2016. Autoimmune susceptibility imposed by public TCR beta chains. *Sci. Rep.,* 6**,** 37543.

ZHOU, L., LOPES, J. E., CHONG, M. M. W., IVANOV, I. I., MIN, R., VICTORA, G. D., SHEN, Y., DU, J., RUBTSOV, Y. P., RUDENSKY, A. Y., ZIEGLER, S. F. & LITTMAN, D. R. 2008. TGF-B-induced Foxp3 inhibits T H 17 cell differentiation by antagonizing RORγt function. *Nature,* 453**,** 236-240.

ZHU, J. F., YAMANE, H. & PAUL, W. E. 2010. Differentiation of Effector CD4 T Cell Populations. *Annu. Rev. Immunol.,* 28**,** 445-489.

ZHU, W., XU, J., GE, Y., CAO, H., GE, X., LUO, J., XUE, J., YANG, H., ZHANG, S. & CAO, J. 2014. Epigallocatechin- 3- gallate (EGCG) protects skin cells from ionizing radiation via heme oxygenase- 1 (HO- 1) overexpression. *J. Radiat. Res.,* 55**,** 1056-1065.

ZOLLER, M., MCELWEE, K. J., VITACOLONNA, M. & HOFFMANN, R. 2004. The progressive state, in contrast to the stable or regressive state of alopecia areata, is reflected in peripheral blood mononuclear cells. *Exp. Dermatol.,* 13**,** 435-444.

Appendix

Appendix 1. Multiplex PCR primer sequences for V and J segments (5' -> 3')

TRBV gene segment(s)	Primer sequence
TRBV2	TCAAATTTCACTCTGAAGATCCGGTCCACAA
TRBV3-1	GCTCACTTAAATCTTCACATCAATTCCCTGG
TRBV4-1	CTTAAACCTTCACCTACACGCCCTGC
TRBV(4-2, 4-3)	CTTATTCCTTCACCTACACACCCTGC
TRBV5-1	GCTCTGAGATGAATGTGAGCACCTTG
TRBV(5-4, 5-5, 5-6, 5-7, 5-8)	GCTCTGAGCTGAATGTGAACGCCTTG
TRBV(6-2, 6-3)	GCTGGGGTTGGAGTCGGCTG
TRBV6-4	CCCTCACGTTGGCGTCTGCTG
TRBV6-8	CACTCAGGCTGGTGTCGGCTG
TRBV6-9	CGCTCAGGCTGGAGTCAGCTG
TRBV7-2	CACTCTGACGATCCAGCGCACAC
TRBV7-3	CTCTACTCTGAAGATCCAGCGCACAG
TRBV7-4	CCACTCTGAAGATCCAGCGCACAG
TRBV7-7	CCACTCTGACGATTCAGCGCACAG
TRBV7-9	CACCTTGGAGATCCAGCGCACAG
TRBV9	GCACTCTGAACTAAACCTGAGCTCTCTG
TRBV10-1	CCCCTCACTCTGGAGTCTGCTG
TRBV10-2	CCCCCTCACTCTGGAGTCAGCTA
TRBV10-3	CCTCCTCACTCTGGAGTCCGCTA
TRBV(11-1,11-2, 11-3)	GAGGCTCAAAGGAGTAGACTCCACTCT
TRBV(11-1, 11-3)	CCACTCTCAAGATCCAGCCTGCAG
TRBV(12-3, 12-4, 12-5)	CCACTCTGAAGATCCAGCCCTCAG
TRBV13	CATTCTGAACTGAACATGAGCTCCTTGG
TRBV14	CTACTCTGAAGGTGCAGCCTGCAG
TRBV15	GATAACTTCCAATCCAGGAGGCCGAACA
TRBV16	CTGTAGCCTTGAGATCCAGGCTACGA
TRBV18	GCATCCTGAGGATCCAGCAGGTAG
TRBV19	CCTCTCACTGTGACATCGGCCC
TRBV20-1	CTTGTCCACTCTGACAGTGACCAGTG
TRBV24-1	CTCCCTGTCCCTAGAGTCTGCCAT
TRBV25-1	CCCTGACCCTGGAGTCTGCCA
TRBV27	CCCTGATCCTGGAGTCGCCCA
TRBV28	CTCCCTGATTCTGGAGTCCGCCA
TRBV29-1	CTAACATTCTCAACTCTGACTGTGAGCAACA
TRBV30	CGGCAGTTCATCCTGAGTTCTAAGAAGC

TRBJ gene segment	Primer sequence
TRBJ1-1	TTACCTACAACTGTGAGTCTGGTGCCTTGTCCAAA
TRBJ1-2	ACCTACAACGGTTAACCTGGTCCCCGAACCGAA
TRBJ1-3	ACCTACAACAGTGAGCCAACTTCCCTCTCCAAA
TRBJ1-4	CCAAGACAGAGAGCTGGGTTCCACTGCCAAA
TRBJ1-5	CTTACCTAGGATGGAGAGTCGAGTC
TRBJ1-6	CTGTCACAGTGAGCCTGGTCCCATTCCC
TRBJ2-1	CGGTGAGCCGTGTCCCTGGCCCGAA
TRBJ2-2	CCAGTACGGTCAGCCTAGAGCCTTCTCCAAA
TRBJ2-3	ACTGTCAGCCGGGTGCCTGGGCCAAA
TRBJ2-4	AGAGCCGGGTCCCGGCGCCGAA
TRBJ2-5	GGAGCCGCGTGCCTGGCCCGAA
TRBJ2-6	GTCAGCCTGCTGCCGGCCCCGAA
TRBJ2-7	GTGAGCCTGGTGCCCGGCCCGAA

Appendix 2. The frequency of V J usage by FACS and PBMCs from patients and HC.

sample_id	TRBJ1-1	TRBJ1-2	TRBJ1-3	TRBJ1-4	TRBJ1-5	TRBJ1-6	TRBJ2-1	TRBJ2-2	TRBJ2-3	TRBJ2-4	TRBJ2-5	TRBJ2-6	TRBJ2-7
PBMCS_HC15	0.244	0.091	0.058	0.118	0.173	0.032	0.107	0.061	0.057	0.030	0.005	0.006	0.016
PBMCS_HC18	0.202	0.085	0.069	0.095	0.189	0.036	0.109	0.071	0.068	0.043	0.012	0.006	0.016
PBMCS_HC01	0.219	0.048	0.081	0.058	0.253	0.019	0.161	0.075	0.030	0.028	0.003	0.001	0.021
PBMCS_HC03	0.202	0.107	0.065	0.116	0.142	0.030	0.103	0.070	0.098	0.033	0.013	0.005	0.016
PBMCS_HC13	0.192	0.097	0.061	0.111	0.174	0.034	0.093	0.074	0.089	0.042	0.014	0.006	0.013
PBMCS_HC16	0.281	0.080	0.062	0.103	0.167	0.037	0.074	0.078	0.045	0.037	0.007	0.002	0.025
PBMCS_HC17	0.218	0.094	0.056	0.100	0.199	0.026	0.105	0.069	0.077	0.033	0.010	0.004	0.010
PBMCS_AA7	0.153	0.131	0.065	0.107	0.190	0.031	0.103	0.061	0.091	0.051	0.014	0.002	0.001
PBMCS_AA10	0.166	0.118	0.060	0.103	0.199	0.029	0.103	0.068	0.059	0.043	0.015	0.006	0.031
PBMCS_AA13	0.329	0.079	0.063	0.120	0.122	0.029	0.069	0.086	0.055	0.026	0.008	0.002	0.012
PBMCS_AA21	0.203	0.092	0.072	0.098	0.191	0.038	0.100	0.069	0.078	0.037	0.010	0.003	0.008
PBMCS_AA22	0.214	0.112	0.058	0.118	0.148	0.041	0.097	0.064	0.070	0.038	0.017	0.004	0.018
PBMCS_AA24	0.171	0.062	0.044	0.341	0.112	0.022	0.082	0.050	0.048	0.019	0.040	0.003	0.007
PBMCS_AA26	0.237	0.093	0.075	0.101	0.177	0.043	0.071	0.073	0.072	0.036	0.011	0.003	0.008
PBMCS_AA27	0.274	0.107	0.071	0.153	0.187	0.035	0.037	0.048	0.038	0.035	0.006	0.001	0.008
PBMCS_AA28	0.230	0.082	0.057	0.110	0.144	0.033	0.104	0.073	0.083	0.042	0.016	0.006	0.019
PBMCS_AA29	0.262	0.076	0.057	0.095	0.144	0.029	0.091	0.056	0.068	0.041	0.012	0.003	0.065
FACS_AA26	0.121	0.076	0.067	0.095	0.158	0.032	0.116	0.068	0.137	0.037	0.066	0.015	0.010
FACS_HC01	0.136	0.065	0.119	0.082	0.142	0.050	0.125	0.116	0.052	0.057	0.013	0.010	0.031
FACS_HC15	0.119	0.182	0.077	0.068	0.073	0.078	0.103	0.034	0.063	0.004	0.027	0.015	0.156
FACS_HC16	0.158	0.059	0.099	0.114	0.147	0.046	0.129	0.102	0.046	0.043	0.011	0.012	0.032
FACS_AA32	0.088	0.127	0.114	0.130	0.098	0.069	0.081	0.073	0.053	0.055	0.036	0.004	0.073
FACS_AA33	0.111	0.140	0.110	0.116	0.093	0.074	0.103	0.056	0.059	0.027	0.042	0.005	0.065
FACS_AA34	0.093	0.133	0.114	0.107	0.095	0.068	0.092	0.070	0.058	0.042	0.029	0.013	0.085

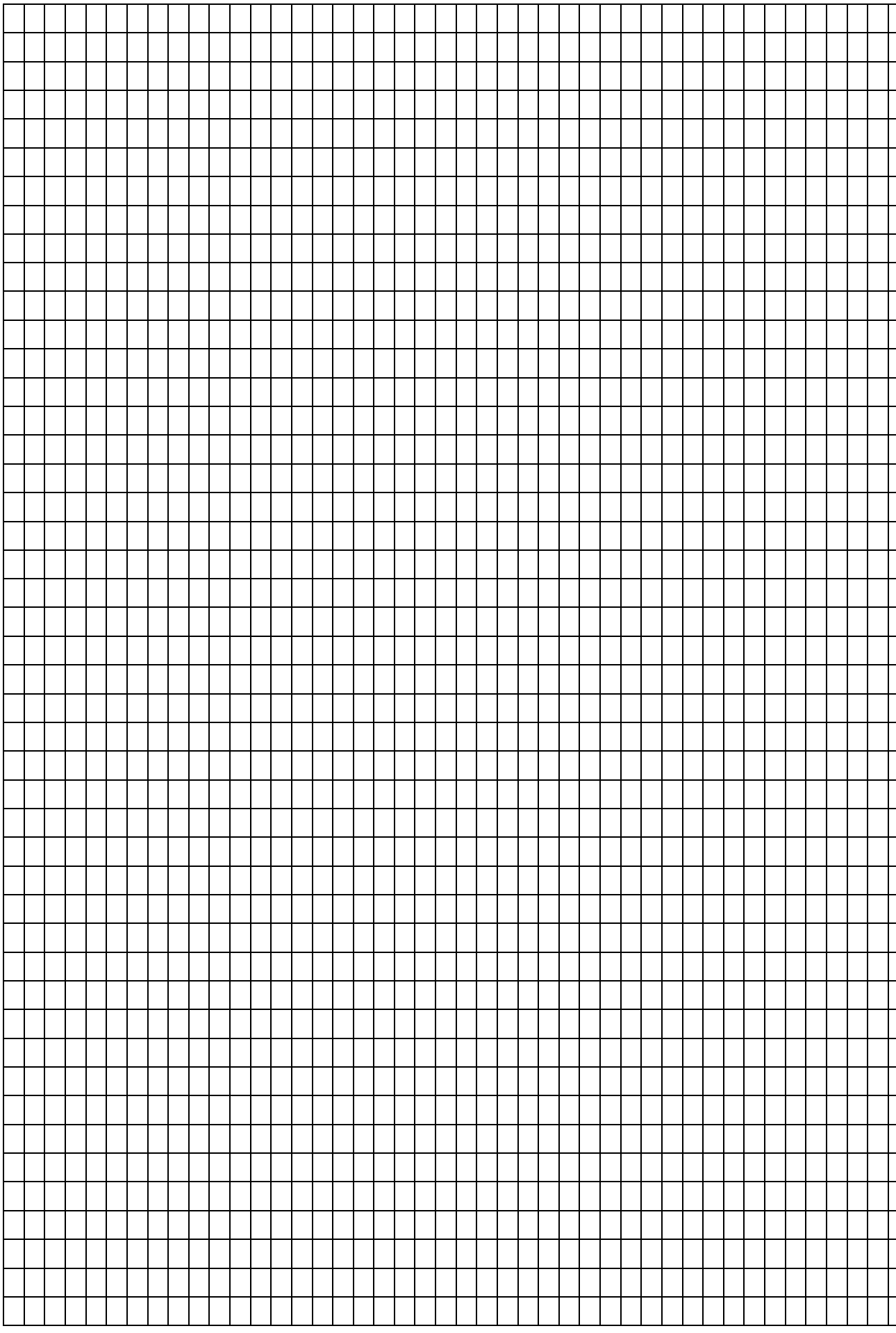

Appendix 3. Post hoc analysis of VJ segment usage

Calculating the fold changes in V or J segment frequency between healthy and patient samples.

V segments PBMC Samples	Fold Change	P
TRBV4.2	1.022	0.328
TRBV19	1.016	0.001
TRBV30	0.985	0.251
TRBV6.4	0.99	0.159
TRBV6.3	1.008	0.397
TRBV7.9	1.008	0.147
TRBV24.1	0.994	0.238
TRBV18	0.996	0.058
TRBV6.1	1.004	0.18
TRBV12.4	0.996	0.429
TRBV4.3	1.004	0.257
TRBV4.1	0.996	0.28
TRBV2	0.997	0.342
TRBV23.1	1.003	0.23

J segments PBMC Samples	Fold Change	P
TRBJ1.1	1	0.95
TRBJ1.2	1.01	0.37
TRBJ1.3	1	0.61
TRBJ1.4	1.02	0.26
TRBJ1.5	0.98	0.16
TRBJ1.6	1	0.47
TRBJ2.1	0.98	0.08
TRBJ2.2	1	0.19
TRBJ2.3	1	0.98
TRBJ2.4	1	0.69
TRBJ2.5	1	0.15
TRBJ2.6	1	0.36
TRBJ2.7	1	0.89

V segments in FACS samples	Fold Change	P
TRBV12.4	1.031362	0.122504
TRBV15	0.974515	0.237822
TRBV12.3	0.981623	0.320266
TRBV30	0.987527	0.136723
TRBV2	0.989532	0.01056
TRBV6.4	0.989735	0.080463
TRBV23.1	0.991213	0.074426
TRBV18	0.991401	0.199522
TRBV4.3	1.008597	0.091488
TRBV7.2	1.007843	0.224518
TRBV10.3	1.007612	0.143311
TRBV27	1.007165	0.22666
TRBV20.1	1.00693	0.31493
TRBV6.1	1.005858	0.172824
TRBV28	1.005183	0.56941
TRBV6.3	1.00489	0.003808
TRBV29.1	0.995428	0.172708
TRBV24.1	1.004588	0.204315
TRBV4.2	1.004421	0.187009
TRBV3.1	0.995767	0.047727

TRBV9	1.00413	0.167778

J segments in FACS samples	Fold Change	P
TRBJ1.1	-0.03447	0.97639
TRBJ2.5	0.026076	1.018239
TRBJ1.4	0.023731	1.016585
TRBJ2.3	0.022998	1.016069
TRBJ2.1	-0.02124	0.985388
TRBJ2.2	-0.01767	0.987826
TRBJ1.2	0.016845	1.011745
TRBJ2.7	-0.01488	0.989738
TRBJ2.4	0.005837	1.004054
TRBJ2.6	-0.00309	0.997862
TRBJ1.6	0.002904	1.002015
TRBJ1.3	0.002768	1.001921

Appendix 4. Frequency of top 10 public aa sequences in each study group

Group	Public AA sequence	Frequency
FACS AA	CAWSNRV_RQPQHF	0.03
	CA*PGG*AS_GSYNEQFF	0.03
	CASSPGSYLGNTIYF	0.02
	CASTKTKRQGPISRPFPTGELFF	0.01
	CATSDTEV_DMNTEAFF	0.01
	CAAQGNTEAFF	0.01
	CASSWGTGNGYTF	0.01
	CANSTRGS_PGNTIYF	0.01
	CASSPTGPTEAFF	0.008
	CASSLSDTQYF	0.006
	CASSDGSYQGNEQFF	0.007
FACS HC	CA*PGG*AS_GSYNEQFF	0.02
	CAWSNRV_RQPQHF	0.02
	CASSPGSYLGNTIYF	0.01
	CATSDTEV_DMNTEAFF	0.01
	CASTKTKRQGPISRPFPTGELFF	0.008
	CAAQGNTEAFF	0.008
	CASSWGTGNGYTF	0.005
	CASSLSDTQYF	0.005
	CASSDGSYQGNEQFF	0.004
	CASSPTGPTEAFF	0.002
	CATSRDEGGLDEKLFF	0.003
	CASRDGTGPSNYGYTF	0.002
PBMC AA	CASSYQGSTEAFF	0.01
	CASSQDKGITNEKLFF	0.01
	CAWSNRV_RQPQHF	0.01
	CARVPRAV_NTGELFF	0.005
	CASSQDGGVNTGELFF	0.004
	CASSPGGTANTEAFF	0.004
	CASSPGSYLGNTIYF	0.003
	CATSEGGLEAFF	0.003
	CA*PGG*AS_GSYNEQFF	0.001
	CATSDTEV_DMNTEAFF	0.002
PBMC HC	CAWSNRV_RQPQHF	0.02
	CA*PGG*AS_GSYNEQFF	0.01

	CATSDTEV_DMNTEAFF	0.008
	CASSPGSYLGNTIYF	0.008
	CARVPRAV_NTGELFF	0.007
	CASTKTKRQGPISRPFPTGELFF	0.004
	CASSLGTVYTEAFF	0.004
	CASSLDSQ_RNTEAFF	0.003
	CASSQEGRARF	0.003
	CAAQGNTEAFF	0.002
	CASSDGSYQGNEQFF	0.001

Appendix 5. NCBI search of public AA sequences identity

A- CASSYQGSTEAFF

Chain E, Human Leukocyte Antigen A02 Presenting Ilakflhwl, In Complex With Cognate T-cell Receptor

Sequence ID: 5MEN_ELength: 240Number of Matches: 1

Range 1: 90 to 101GenPeptGraphics

Alignment statistics for match #1				
Score	**Expect**	**Identities**	**Positives**	**Gaps**
37.5 bits(81)	0.070	12/13(92%)	12/13(92%)	1/13(7%)

```
Query  1    CASSYQGSTEAFF  13
           CASSYQG TEAFF
Sbjct  90   CASSYQG-TEAFF  101
```

B- CASSQDKGITNEKLFF

T-cell receptor beta chain, partial [Mus musculus]

Sequence ID: ADD98295.1Length: 43Number of Matches: 1

Range 1: 21 to 36

Alignment statistics for match #1				
Score	**Expect**	**Identities**	**Positives**	**Gaps**
42.2 bits(92)	0.002	13/16(81%)	13/16(81%)	0/16(0%)

```
Query  1   CASSQDKGITNEKLFF  16
           CASSQD GI NE LFF
Sbjct  21  CASSQDGGISNERLFF  36
```

C- CATSRDEGGLDEKLFF

T cell receptor beta, partial [Homo sapiens]

Sequence ID: AIE10719.1Length: 81Number of Matches: 1

Range 1: 31 to 46

Alignment statistics for match #1				
Score	**Expect**	**Identities**	**Positives**	**Gaps**
32.0 bits(68)	11	11/16(69%)	12/16(75%)	0/16(0%)

```
Query  1   CATSRDEGGLDEKLFF  16
           CA SRD G  +EKLFF
Sbjct  31  CASSRDLGATNEKLFF  46
```

D- CASRDGTGPSNYGYTF

T-cell receptor beta, partial [Homo sapiens]

Sequence ID: AIE10595.1Length: 77Number of Matches: 1

Range 1: 28 to 42

Alignment statistics for match #1

Score	Expect	Identities	Positives	Gaps
35.0 bits(75)	0.97	13/17(76%)	13/17(76%)	3/17(17%)

```
Query  1   CASRD-GTGPSNYGYTF  16
           CAS D GTG  NYGYTF
Sbjct  28  CASSDPGTG--NYGYTF  42
```

E- CASTKTKRQGPISRPFPTGELFF

hypothetical protein CO090_04760 [Acidobacteria bacterium CG_4_9_14_3_um_filter_49_7]

Sequence ID: PJB79852.1Length: 61Number of Matches: 1

Range 1: 33 to 44

Alignment statistics for match #1				
Score	Expect	Identities	Positives	Gaps
32.9 bits(70)	14	10/12(83%)	10/12(83%)	0/12(0%)

```
Query  8   RQGPISRPFPTG  19
           R GPI RPFPTG
Sbjct  33  RNGPIRRPFPTG  44
```

F- CANSTRGS_PGNTIYF

T cell receptor beta chain CDR3, partial [Homo sapiens]

Sequence ID: AAC72553.1Length: 28Number of Matches: 1

Range 1: 11 to 27

Alignment statistics for match #1				
Score	Expect	Identities	Positives	Gaps
34.1 bits(73)	1.0	13/18(72%)	13/18(72%)	4/18(22%)

```
Query  1   CANSTR---GSPGNTIYF  15
           CA STR   GS GNTIYF
Sbjct  11  CA-STRPGQGSSGNTIYF  27
```

G- CASSPTGPTEAFF

T-cell receptor beta chain variable region, partial [Homo sapiens]

Sequence ID: ANO54375.1Length: 53Number of Matches: 1

Range 1: 30 to 44

Alignment statistics for match #1				
Score	Expect	Identities	Positives	Gaps
35.0 bits(75)	0.59	12/15(80%)	12/15(80%)	2/15(13%)

```
Query  1   CASSP--TGPTEAFF  13
           CASSP  TG TEAFF
Sbjct  30  CASSPLPTGSTEAFF  44
```

H- CANSTRGSPGNTIYF

T-cell receptor beta chain variable region, partial [Homo sapiens]

Sequence ID: ANO55971.1Length: 33Number of Matches: 1

Range 1: 11 to 24GenPeptGraphics

Alignment statistics for match #1				
Score	Expect	Identities	Positives	Gaps
34.1 bits(73)	1.3	12/15(80%)	12/15(80%)	1/15(6%)

```
Query  1   CANSTRGSPGNTIYF  15
           CA S RGS GNTIYF
Sbjct  11  CASSLRGS-GNTIYF  24
```

Appendix 6 cell viability in 24hrs EGCG treated HaCat/Jurkat

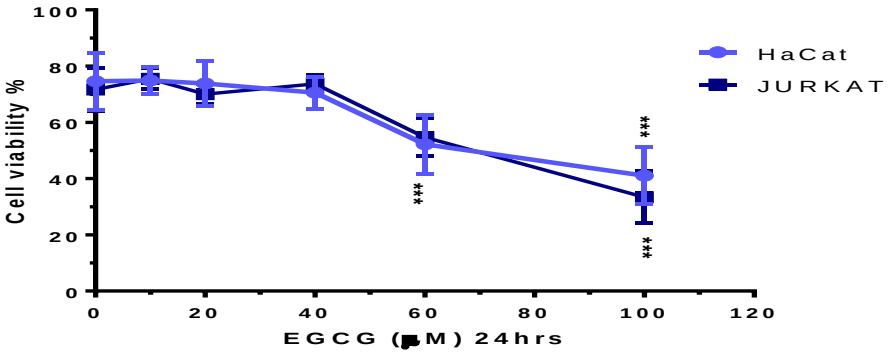

Figure 1. The mean percentage (%) of viable cells in HaCat and Jurkat cell lines after treatment with different concentrations of EGCG (10, 20, 40, 60 and 100µM) for 24hrs.

Slight reduction in viability can be seen in both cell lines after treatment with lower doses of EGCG 10, 20, 40µM (not statistically significant) while a significant drop started to be seen at 100µM in HaCat cells and 60µM in Jurkat cells. The experiment was repeated three times and mean and SD were calculated. Asterisks denote a significant reduction in cell viability, *** P≤0.001.

Appendix 7. 48hrs IFN-γ treatment in Jurkat.

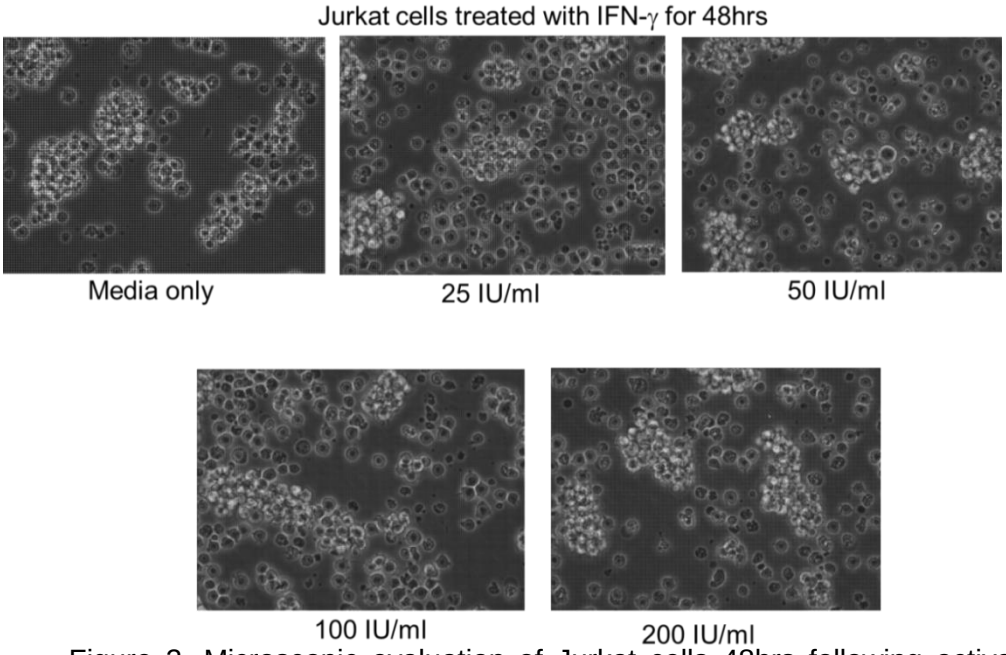

Figure 2. Microscopic evaluation of Jurkat cells 48hrs following activation with serial concentrations of IFN-γ 25, 50, 100 or 200IU/ml.

Jurkat cell phenotype and colony morphology in control versus all the tested doses of IFN-γ 200IU/ml is relatively similar; Cells were examined under a light microscope using 20X objective.

Appendix 8. Densitometric analysis of p-STAT1 band in Jurkat and HaCat cells treated with EGCG.

Jurkat	P-STAT-1	Inverted	net band	GAPDH	Inverted	net band	final ratio	% of reduction
Un	194.6	60.4	4.2	102.6	152.4	53.2	0.1	
Ind	140.9	114.1	57.9	102.4	152.6	53.4	1.1	
20-24hr	145.6	109.4	53.2	102.1	152.9	53.7	1.0	8.8
40-24hr	174.6	80.4	24.2	110.7	144.3	45.1	0.5	50.5
20-48hr	158.4	96.7	40.4	102.5	152.5	53.2	0.8	30.0
40-48hr	191.3	63.7	7.5	115.8	139.2	40.0	0.2	82.8
Background	198.8	56.2	0.0	155.8	99.2	0.0		

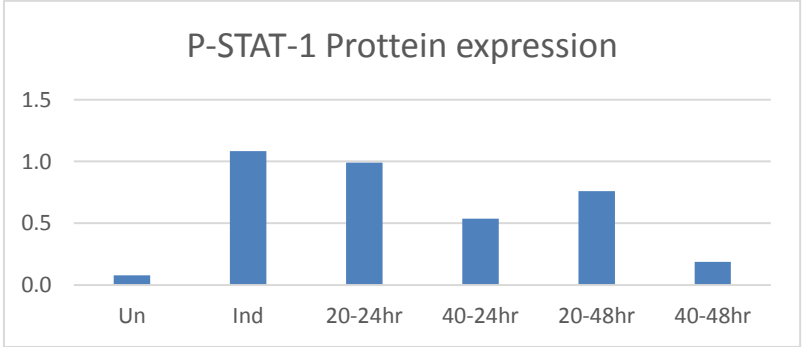

Figure 7.1. The effect of EGCG on p-STAT-1 protein in Jurkat cells.

The band intensity of WB (Figure 5.7.) was calculate by ImageJ software following the formula recommended by the software :

http://www.yorku.ca/yisheng/Internal/Protocols/ImageJ.pdf

The data showed in the table was plotted in the figure here showing dose-dependent reduction of p-STAT-1 protein levels in Jurkat cells treated with 20 and 40μM EGCG for 24hrs or 48hrs.

Samples	p-STAT-1	inverted	net band	GAPDH	inverted	net band	Final RATIO	% of reduction
UN	239.5	15.5	0.6	218.3	36.7	21.8	0.0	
Induced	213.7	41.3	26.5	199.5	55.5	40.6	0.7	
20-24hr	236.7	18.3	3.4	215.6	39.4	24.5	0.1	78.5
40-24hr	237.1	17.9	3.1	209.2	45.8	30.9	0.1	84.8
20-48hr	239.1	15.9	1.0	219.7	35.3	20.4	0.0	92.5
40-48hr	238.3	16.7	1.8	217.7	37.3	22.4	0.1	87.4
Background	240.113	14.887	0			0		

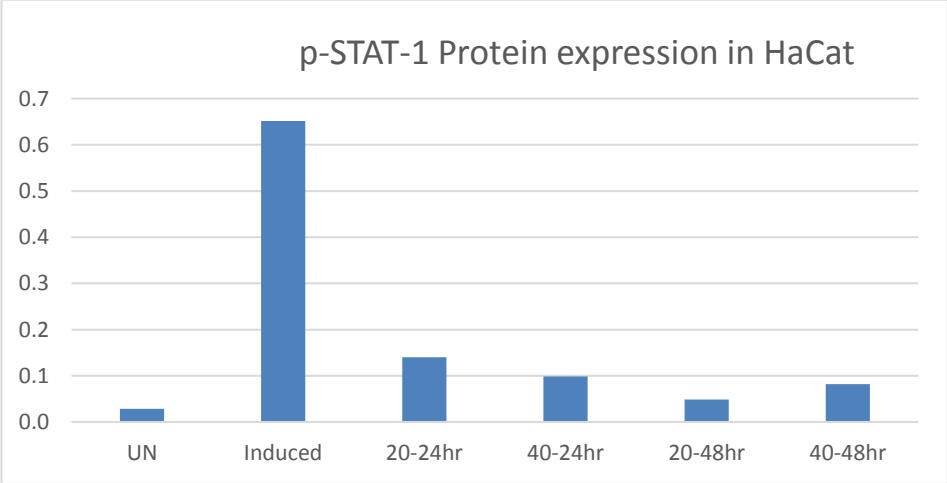

Figure 7.2. The effect of EGCG on p-STAT-1 protein in HaCat cells.

The band intensity of WB (Figure 5.7.) was calculate by ImageJ software following the formula recommended by the software :

http://www.yorku.ca/yisheng/Internal/Protocols/ImageJ.pdf

The data showed in the table was plotted in the figure here showing dose-dependent reduction of p-STAT-1 protein levels in HaCat cells treated with 20 and 40μM EGCG for 24hrs or 48hrs.

-Servier medical art used to create some images in this thesis (with permission) can be accessed via this link (http://smart.servier.com/image-set-download).